

Global Carbon Budget 2023

Pierre Friedlingstein [1,2](#), Michael O'Sullivan [1](#), Matthew W. Jones [3](#), Robbie M. Andrew [4](#), Dorothee C. E. Bakker [5](#), Judith Hauck [6](#), Peter Landschützer [7](#), Corinne Le Quéré [3](#), Ingrid T. Luijkx [8](#), Glen P. Peters [4](#), Wouter Peters [8,9](#), Julia Pongratz [10,11](#), Clemens Schwingshackl [10](#), Stephen Sitch [1](#), Josep G. Canadell [12](#), Philippe Ciais [13](#), Robert B. Jackson [14](#), Simone R. Alin [15](#), Peter Anthoni [16](#), Leticia Barbero [17](#), Nicholas R. Bates [18,19](#), Meike Becker [20,21](#), Nicolas Bellouin [22](#), Bertrand Decharme [23](#), Laurent Bopp [2](#), Ida Bagus Mandhara Brasika [1,24](#), Patricia Cadule [25](#), Matthew A. Chamberlain [26](#), Naveen Chandra [27](#), Thi-Tuyet-Trang Chau [13](#), Frédéric Chevallier [13](#), Louise P. Chini [28](#), Margot Cronin [29](#), Xinyu Dou [30](#), Kazutaka Enyo [31](#), Wiley Evans [32](#), Stefanie Falk [10](#), Richard A. Feely [15](#), Liang Feng [33,34](#), Daniel J. Ford [1](#), Thomas Gasser [35](#), Josefine Ghattas [13](#), Thanos Gkritzalis [7](#), Giacomo Grassi [36](#), Luke Gregor [37](#), Nicolas Gruber [38](#), Özgür Gürses [6](#), Ian Harris [39](#), Matthew Hefner [40](#), Jens Heinke [41](#), Richard A. Houghton [42](#), George C. Hurtt [43](#), Yosuke Iida [31](#), Tatiana Ilyina [11](#), Andrew R. Jacobson [44,45](#), Atul Jain [46](#), Tereza Jarníková [47](#), Annika Jersild [11](#), Fei Jiang [48](#), Zhe Jin [49,50](#), Fortunat Joos [51,52](#), Etsushi Kato [53](#), Ralph F. Keeling [54](#), Daniel Kennedy [55](#), Kees Klein Goldewijk [56](#), Jürgen Knauer [57,58](#), Jan Ivar Korsbakken [4](#), Arne Körtzinger [58](#), Xin Lan [44,45](#), Nathalie Lefèvre [59](#), Hongmei Li [11](#), Junjie Liu [60,61](#), Zhiqiang Liu [62](#), Lei Ma [28](#), Greg Marland [40,63](#), Nicolas Mayot [3](#), Patrick C. McGuire [64](#), G.A. McKinley [65](#), Gesa Meyer [66](#), Eric J. Morgan [54](#), David R. Munro [44,67](#), Shin-Ichiro Nakaoka [68](#), Yosuke Niwa [68](#), Kevin M. O'Brien [70,71](#), Are Olsen [20,21](#), Abdirahman M. Omar [71,72](#), Tsuneo Ono [72](#), Melf E. Paulsen [58](#), Denis Pierrot [73](#), Katie Pocock [74](#), Benjamin Poulter [75](#), Carter M. Powis [76](#), Gregor Rehder [77](#), Laure Resplandy [78](#), Eddy Robertson [79](#), Christian Rödenbeck [80](#), Thais M Rosan [1](#), Jörg Schwinger [21,81](#), Roland Séférian [82](#), T. Luke Smallman [33](#), Stephen M. Smith [76](#), Reinel Sospedra-Alfonso [83](#), Qing Sun [51,52](#), Adrienne J. Sutton [15](#), Colm Sweeney [45](#), Shintaro Takao [68](#), Pieter P. Tans [84](#), Hanqin Tian [85](#), Bronte Tilbrook [86,87](#), Hiroyuki Tsujino [88](#), Francesco Tubiello [89](#), Guido R. van der Werf [8](#), Erik van Ooijen [86](#), Rik Wanninkhof [73](#), Michio Watanabe [90](#), Cathy Wilmart-Rousseau [58](#), Dongxu Yang [91](#), Xiaojuan Yang [92](#), Wenping Yuan [93](#), Xu Yue [94](#), Sönke Zaehle [80](#), Jiye Zeng [68](#), Bo Zheng [95](#)

- 1 Faculty of Environment, Science and Economy, University of Exeter, Exeter EX4 4QF, UK
- 2 Laboratoire de Météorologie Dynamique / Institut Pierre-Simon Laplace, CNRS, Ecole Normale Supérieure / Université PSL, Sorbonne Université, Ecole Polytechnique, Paris, France
- 3 Tyndall Centre for Climate Change Research, School of Environmental Sciences, University of East Anglia, Norwich Research Park, Norwich NR4 7TJ, UK
- 4 CICERO Center for International Climate Research, Oslo 0349, Norway
- 5 School of Environmental Sciences, University of East Anglia, Norwich NR4 7TJ, UK
- 6 Alfred-Wegener-Institut, Helmholtz-Zentrum für Polar- und Meeresforschung, Am Handelshafen 12, 27570 Bremerhaven
- 7 VLIZ Flanders Marine Institute, Jacobsenstraat 1, 8400, Ostend, Belgium

Style Definition: Normal

Style Definition: Heading 1: Outline numbered + Level: 1 + Numbering Style: 1, 2, 3, ... + Start at: 1 + Alignment: Left + Aligned at: 0.63 cm + Indent at: 1.27 cm

Style Definition: Heading 2: Outline numbered + Level: 2 + Numbering Style: a, b, c, ... + Start at: 1 + Alignment: Left + Aligned at: 1.9 cm + Indent at: 2.54 cm

Style Definition: Heading 3: Outline numbered + Level: 3 + Numbering Style: i, ii, iii, ... + Start at: 1 + Alignment: Right + Aligned at: 3.49 cm + Indent at: 3.81 cm

Style Definition: Heading 4: Indent: Left: 0 cm, Hanging: 1.52 cm, Outline numbered + Level: 4 + Numbering Style: 1, 2, 3, ... + Start at: 1 + Alignment: Left + Aligned at: 4.44 cm + Indent at: 5.08 cm

Style Definition: Heading 5: Indent: Left: 0 cm, Hanging: 1.78 cm, Outline numbered + Level: 5 + Numbering Style: a, b, c, ... + Start at: 1 + Alignment: Left + Aligned at: 5.71 cm + Indent at: 6.35 cm

Style Definition: Heading 6: Indent: Left: 0 cm, Hanging: 2.03 cm, Outline numbered + Level: 6 + Numbering Style: i, ii, iii, ... + Start at: 1 + Alignment: Right + Aligned at: 7.3 cm + Indent at: 7.62 cm

Style Definition: Heading 7: Indent: Left: 0 cm, Hanging: 2.29 cm, Outline numbered + Level: 7 + Numbering Style: 1, 2, 3, ... + Start at: 1 + Alignment: Left + Aligned at: 8.25 cm + Indent at: 8.89 cm

Style Definition: Heading 8: Indent: Left: 0 cm, Hanging: 2.54 cm, Outline numbered + Level: 8 + Numbering Style: a, b, c, ... + Start at: 1 + Alignment: Left + Aligned at: 9.52 cm + Indent at: 10.16 cm

Style Definition: Heading 9: Indent: Left: 0 cm, Hanging: 2.79 cm, Outline numbered + Level: 9 + Numbering Style: i, ii, iii, ... + Start at: 1 + Alignment: Right + Aligned at: 11.11 cm + Indent at: 11.43 cm

Style Definition: Revision

Formatted

Deleted: ...2, Michael O'Sullivan [1](#), Matthew W. Jones [3](#), Robbie M. Andrew [4](#), Dorothee C. E. Bakker [5](#), Judith Hauck [6](#), Peter Landschützer [7](#), Corinne Le Quéré [3](#), Ingrid T. Luijkx [8](#), Glen P. Peters [4](#), Wouter Peters [8,9](#), Julia Pongratz [10,11](#), Clemens Schwingshackl [10](#), Stephen Sitch [1](#), Josep G. Canadell [12](#), Philippe Ciais [13](#), Robert B. Jackson [14](#), Simone R. Alin [15](#), Peter Anthoni [16](#), Leticia Barbero [17](#), Nicholas R. Bates [18,19](#), Meike Becker [20,21](#), Nicolas Bellouin [22](#), Bertrand Decharme [23](#), Laurent Bopp [2](#), Ida Bagus Mandhara Brasika [1,24](#), Patricia Cadule [25](#), Matthew A. Chamberlain [26](#), Naveen Chandra [27](#), Thi-Tuyet-Trang Chau [13](#), Frédéric Chevallier [13](#), Louise P. Chini [28](#), Margot Cronin [29](#), Xinyu Dou [30](#), Kazutaka Enyo [31](#), Wiley Evans [32](#), Stefanie Falk [10](#), Richard A. Feely [15](#), Liang Feng [33,34](#), Daniel J. Ford [1](#), Thomas Gasser [35](#), Josefine Ghattas [13](#), Thanos Gkritzalis [7](#), Giacomo Grassi [36](#), Luke Gregor [37](#), Nicolas Gruber [38](#), Özgür Gürses [6](#), Ian Harris [39](#), Matthew Hefner [40,41](#),...Jens Heinke [42](#)...41, Richard A. Houghton [43](#),... [21](#)

Formatted: Default Paragraph Font, Font colour: Black

Formatted ... 11

Formatted: Font colour: Black

- 169 [8](#) Wageningen University, Environmental Sciences Group, P.O. Box 47, 6700AA, Wageningen, The
 170 Netherlands
- 171 [9](#) University of Groningen, Centre for Isotope Research, Groningen, The Netherlands
- 172 [10](#) Ludwig-Maximilians-Universität München, Luisenstr. 37, 80333 München, Germany
- 173 [11](#) Max Planck Institute for Meteorology, Bundesstraße 53, 20146 Hamburg, Germany
- 174 [12](#) CSIRO Environment, Canberra, ACT 2101, Australia
- 175 [13](#) Laboratoire des Sciences du Climat et de l'Environnement, LSCE/IPSL, CEA-CNRS-UVSQ, Université
 176 Paris-Saclay, F-91198 Gif-sur-Yvette, France
- 177 [14](#) Department of Earth System Science, Woods Institute for the Environment, and Precourt Institute for
 178 Energy, Stanford University, Stanford, CA 94305-2210, United States of America
- 179 [15](#) National Oceanic and Atmospheric Administration, Pacific Marine Environmental Laboratory
 180 (NOAA/PMEL), 7600 Sand Point Way NE, Seattle, WA 98115, USA
- 181 [16](#) Karlsruhe Institute of Technology, Institute of Meteorology and Climate Research/Atmospheric
 182 Environmental Research, 82467 Garmisch-Partenkirchen, Germany
- 183 [17](#) Rosenstiel School of Marine Atmospheric and Earth Science, Cooperative Institute for Marine and
 184 Atmospheric Studies (CIMAS), University of Miami, 4600 Rickenbacker Causeway, Miami, FL, USA
- 185 [18](#) School of Ocean Futures, Julie Ann Wrigley Global Futures Laboratory, Arizona State University, Tempe,
 186 Arizona, AZ 85287-5502, USA
- 187 [19](#) Bermuda Institute of Ocean Sciences (BIOS), 17 Biological Lane, St. Georges, GE01, Bermuda
- 188 [20](#) Geophysical Institute, University of Bergen, Allégaten 70, 5007 Bergen, Norway
- 189 [21](#) Bjerknes Centre for Climate Research, Bergen, Norway
- 190 [22](#) Department of Meteorology, University of Reading, Reading, RG6 6BB, UK
- 191 [23](#) CNRM, Université de Toulouse, Météo-France, CNRS, Toulouse, France
- 192 [24](#) Faculty of Marine Science & Fisheries, University of Udayana, Bali 80361, Indonesia
- 193 [25](#) CNRS, Institut Pierre-Simon Laplace, Sorbonne Université, Paris, France
- 194 [26](#) CSIRO Environment, Hobart, TAS, Australia
- 195 [27](#) Research Institute for Global Change, JAMSTEC, 3173-25 Showa-machi, Kanazawa, Yokohama, 236-0001,
 196 Japan
- 197 [28](#) Department of Geographical Sciences, University of Maryland, College Park, MD 20742, USA
- 198 [29](#) Marine Institute, Rinville, Oranmore, Co Galway H91 R673, Ireland
- 199 [30](#) Department of Earth System Science, Tsinghua University, Beijing, China
- 200 [31](#) Japan Meteorological Agency, 3-6-9 Toranomon, Minato City, Tokyo 105-8431, Japan
- 201 [32](#) Hakai Institute, 1713 Hyacinthe Bay Rd, Heriot Bay, BC, V0P 1H0, Canada
- 202 [33](#) National Centre for Earth Observation, University of Edinburgh, Edinburgh, EH9 3FE, UK
- 203 [34](#) School of Geosciences, University of Edinburgh, UK
- 204 [35](#) International Institute for Applied Systems Analysis (IIASA), Schlossplatz 1,
 205 A-2361 Laxenburg, Austria
- 206 [36](#) European Commission, Joint Research Centre, 21027 Ispra (VA), Italy
- 207 [37](#) [ETH Zuerich](#)

Deleted: ,

Deleted: Zürich, Switzerland

Formatted: Default Paragraph Font, Font colour: Black

Formatted: Normal, Centred, Border: Top: (No border),
 Bottom: (No border), Left: (No border), Right: (No border),
 Between : (No border), Tab stops: 7.96 cm, Centred + 15.92
 cm, Right, Position: Horizontal: Left, Relative to: Column,
 Vertical: In line, Relative to: Margin, Wrap Around

Formatted: Font colour: Black

210 [38](#) Environmental Physics Group, [ETH Zürich](#), Institute of Biogeochemistry and Pollutant Dynamics and
 211 Center for Climate Systems Modeling (C2SM)
 212 [39](#) NCAS-Climate, Climatic Research Unit, School of Environmental Sciences, University of East Anglia,
 213 Norwich Research Park, Norwich, NR4 7TJ, UK
 214 [40](#) Research Institute for Environment, Energy, and Economics, Appalachian State University, Boone, North
 215 Carolina, USA
 216 [41](#) Potsdam Institute for Climate Impact Research (PIK), member,
 217 of the Leibniz Association, P.O. Box 60 12 03, 14412 Potsdam, Germany
 218 [42](#) Woodwell Climate Research Center, Falmouth, MA 02540, USA
 219 [43](#) Department of Geographical Sciences, University of Maryland, College Park, Maryland 20742, USA
 220 [44](#) Cooperative Institute for Research in Environmental Sciences (CIRES), University of Colorado, Boulder,
 221 CO 80305, USA
 222 [45](#) National Oceanic and Atmospheric Administration, Global Monitoring Laboratory (NOAA/GML), 325
 223 Broadway R/GML, Boulder, CO 80305, USA
 224 [46](#) Department of Atmospheric Sciences, University of Illinois, Urbana, IL 61821, USA
 225 [47](#) School of Environmental Sciences, University of East Anglia, Norwich Research Park, Norwich NR4 7TJ,
 226 UK
 227 [48](#) Jiangsu Provincial Key Laboratory of Geographic Information Science and Technology, International
 228 Institute for Earth System Science, Nanjing University, Nanjing, 210023, China
 229 [Nanjing University, Nanjing, China](#)
 230 [49](#) State Key Laboratory of Tibetan Plateau Earth System and Resource Environment, Institute of Tibetan
 231 Plateau Research, Chinese Academy of Sciences, Beijing 100101, China
 232 [50](#) Institute of Carbon Neutrality, Peking University, Beijing 100871, China
 233 [51](#) Climate and Environmental Physics, Physics Institute, University of Bern, Bern, Switzerland
 234 [52](#) Oeschger Centre for Climate Change Research, University of Bern, Bern, Switzerland
 235 [53](#) Institute of Applied Energy (IAE), Minato-ku, Tokyo 105-0003, Japan
 236 [54](#) University of California, San Diego, Scripps Institution of Oceanography, La Jolla, CA 92093-0244, USA
 237 [55](#) National Center for Atmospheric Research, Climate and Global Dynamics, Terrestrial Sciences Section,
 238 Boulder, CO 80305, USA
 239 [56](#) Utrecht University, Faculty of Geosciences, Department IMEW, Copernicus Institute of Sustainable
 240 Development, Heidelberglaan 2, P.O. Box 80115, 3508 TC, Utrecht, the Netherlands
 241 [57](#) Hawkesbury Institute for the Environment, Western Sydney University, Penrith, New South Wales,
 242 Australia
 243 [58](#) GEOMAR Helmholtz Centre for Ocean Research, Wischhofstr. 1-3, 24148 Kiel, Germany
 244 [59](#) LOCEAN/IPSL laboratory, Sorbonne Université, CNRS/IRD/MNHN, Paris, France
 245 [60](#) NASA JPL
 246 [61](#) Caltech
 247 [62](#) CMA Key Open Laboratory of Transforming Climate Resources to Economy, Chongqing Institute of
 248 Meteorological Sciences, Chongqing 401147, China

Deleted:), ETH Zürich, Switzerland

Deleted: 41 Department of Geological and Environmental Sciences, Appalachian State University, Boone, North Carolina, USA
42

Deleted:

Deleted: 43

Deleted: 44

Deleted: 45

Deleted: 46

Deleted: 47

Deleted: 48

Deleted: 49

Deleted: 50

Deleted: 51

Deleted: 52

Deleted: 53

Deleted: 54

Deleted: 55

Deleted: 56

Deleted: 57

Deleted: 58

Deleted: 59

Deleted: 60

Deleted: 61

Deleted: , USA

Deleted: 62

Deleted: , USA

Deleted: 63

Formatted: Default Paragraph Font, Font colour: Black

Formatted: Normal, Centred, Border: Top: (No border), Bottom: (No border), Left: (No border), Right: (No border), Between : (No border), Tab stops: 7.96 cm, Centred + 15.92 cm, Right, Position: Horizontal: Left, Relative to: Column, Vertical: In line, Relative to: Margin, Wrap Around

Formatted: Font colour: Black

- 278 [63 Department of Geological and Environmental Sciences, Appalachian State University, Boone, North](#)
 279 [Carolina, USA](#)
- 280 [64 Department of Meteorology & National Centre for Atmospheric Science \(NCAS\), University of Reading,](#)
 281 [Reading, United Kingdom](#)
- 282 [65 Columbia University,](#)
- 283 [66 Climate Research Division, Environment and Climate Change Canada, Victoria, BC, Canada](#)
- 284 [67 National Oceanic and Atmospheric Administration/Global Monitoring Laboratory \(NOAA/GML\), 325](#)
 285 [Broadway R/GML, Boulder, CO 80305, USA](#)
- 286 [68 Earth System Division, National Institute for Environmental Studies, 16-2 Onogawa, Tsukuba, Ibaraki, 305-](#)
 287 [8506 Japan](#)
- 288 [69 Department of Climate and Geochemistry Research, Meteorological Research Institute, 1-1 Nagamine,](#)
 289 [Tsukuba, Ibaraki 305-0052, Japan](#)
- 290 [70 Cooperative Institute for Climate, Ocean and Ecosystem Studies \(CICOES\), University of Washington,](#)
 291 [Seattle, WA 98105, USA](#)
- 292 [71 NORCE Norwegian Research Centre, Jahnebakken 5, 5007 Bergen, Norway](#)
- 293 [72 Marine Environment Division, Fisheries Resources Institute, Japan Fisheries Research and Education](#)
 294 [Agency, 2-12-4 Fukuura, Kanazawa-Ku, Yokohama 236-8648, Japan](#)
- 295 [73 National Oceanic & Atmospheric Administration, Atlantic Oceanographic & Meteorological Laboratory](#)
 296 [\(NOAA/AOML\), 4301 Rickenbacker Causeway, Miami, FL 33149, USA](#)
- 297 [74 Hakai Institute, 1713 Hyacinthe Bay Rd, Heriot Bay, BC, V0P 1H0, Canada](#)
- 298 [75 NASA Goddard Space Flight Center, Biospheric Sciences Laboratory, Greenbelt, Maryland 20771, USA](#)
- 299 [76 Smith School for Enterprise and the Environment, University of Oxford, Oxford, UK](#)
- 300 [77 Leibniz Institute for Baltic Sea Research Warnemünde \(IOW\), Seestrasse 15, 18119 Rostock, Germany](#)
- 301 [78 Princeton University, Department of Geosciences and Princeton Environmental Institute, Princeton, NJ,](#)
 302 [USA](#)
- 303 [79 Met Office Hadley Centre, FitzRoy Road, Exeter EX1 3PB, UK](#)
- 304 [80 Max Planck Institute for Biogeochemistry, P.O. Box 600164, Hans-Knöll-Str. 10, 07745 Jena, Germany](#)
- 305 [81 NORCE Climate & Environment, Jahnebakken 5, 5007 Bergen, Norway](#)
- 306 [82 CNRM \(Météo-France/CNRS\)-UMR 3589,](#)
- 307 [83 Canadian Centre for Climate Modelling and Analysis, Victoria BC, Canada](#)
- 308 [84 Institute of Arctic and Alpine Research, University of Colorado, Boulder, CO 80309, USA](#)
- 309 [85 Schiller Institute of Integrated Science and Society, Department of Earth and Environmental Sciences,](#)
 310 [Boston College, Chestnut Hill, MA 02467, USA](#)
- 311 [86 CSIRO Environment, Castray Esplanade, Hobart, Tasmania 7004, Australia](#)
- 312 [87 Australian Antarctic Partnership Program, University of Tasmania, Hobart, Australia](#)
- 313 [88 JMA Meteorological Research Institute, Japan](#)
- 314 [89 Statistics Division, Food and Agriculture Organization of the United Nations, Via Terme di Caracalla, Rome](#)
 315 [00153, Italy](#)

Deleted: 64 University of East Anglia, Norwich, UK
65

Deleted: 66

Deleted: , USA

Deleted: 67

Deleted: 68

Deleted: 69

Deleted: 70

Deleted: 71

Deleted: 72

Deleted: 73

Deleted: 74

Deleted: 75

Deleted: 76

Deleted: 77

Deleted: 78

Deleted: 79

Deleted: 80

Deleted: 81

Deleted: 82

Deleted: 83

Deleted: , Toulouse, France

Deleted: 84

Deleted: 85

Deleted: 86

Deleted: 87

Deleted: 88

Deleted: 89

Deleted: 90

Formatted: Default Paragraph Font, Font colour: Black

Formatted: Normal, Centred, Border: Top: (No border), Bottom: (No border), Left: (No border), Right: (No border), Between : (No border), Tab stops: 7.96 cm, Centred + 15.92 cm, Right, Position: Horizontal: Left, Relative to: Column, Vertical: In line, Relative to: Margin, Wrap Around

Formatted: Font colour: Black

345 [90](#) Japan Agency for Marine-Earth Science and Technology (JAMSTEC), 3173-25, Showa-machi, Kanazawa-
346 ku, Yokohama, 236-0001, Japan

Deleted: 91

347 [91](#) Institute of Atmospheric Physics, Chinese Academy of Sciences

Deleted: 92

348 [92](#) Environmental Sciences Division and Climate Change Science Institute, Oak Ridge National Laboratory,
349 Oak Ridge, TN, 37831, USA

Deleted: 93

350 [93](#) School of Atmospheric Sciences, Sun Yat-sen University, Zhuhai, Guangdong 510245, China

Deleted: 94

351 [94](#) School of Environmental Science and Engineering, Nanjing University of Information Science and
352 Technology (NUIST)

Deleted: 95

353 [95](#) Shenzhen Key Laboratory of Ecological Remediation and Carbon Sequestration, Institute of Environment
354 and Ecology, Tsinghua Shenzhen International Graduate School, Tsinghua University, Shenzhen 518055, China
355

Deleted: 96

356 *Correspondence to:* Pierre Friedlingstein (p.friedlingstein@exeter.ac.uk)

357 Abstract

Formatted: Indent: Left: 0 cm, First line: 0 cm

358 Accurate assessment of anthropogenic carbon dioxide (CO₂) emissions and their redistribution among the
359 atmosphere, ocean, and terrestrial biosphere in a changing climate is critical to better understand the global
360 carbon cycle, support the development of climate policies, and project future climate change. Here we describe
361 and synthesise data sets and methodology to quantify the five major components of the global carbon budget
362 and their uncertainties. Fossil CO₂ emissions (E_{FOS}) are based on energy statistics and cement production data,
363 while emissions from land-use change (E_{LUC}), mainly deforestation, are based on land-use and land-use change
364 data and bookkeeping models. Atmospheric CO₂ concentration is measured directly, and its growth rate (G_{ATM})
365 is computed from the annual changes in concentration. The ocean CO₂ sink (S_{OCEAN}) is estimated with global
366 ocean biogeochemistry models and observation-based *f*CO₂-products. The terrestrial CO₂ sink (S_{LAND}) is
367 estimated with dynamic global vegetation models. Additional lines of evidence on land and ocean sinks are
368 provided by atmospheric inversions, atmospheric oxygen measurements and Earth System Models. The
369 resulting carbon budget imbalance (B_{IM}), the difference between the estimated total emissions and the
370 estimated changes in the atmosphere, ocean, and terrestrial biosphere, is a measure of imperfect data and
371 [incomplete](#) understanding of the contemporary carbon cycle. All uncertainties are reported as ±1σ.

372 For the year 2022, E_{FOS} increased by [0.9%](#) relative to 2021, with fossil emissions at [9.9 ± 0.5 GtC yr⁻¹](#) (10.2 ±
373 0.5 GtC yr⁻¹ when the cement carbonation sink is [not](#) included), E_{LUC} was 1.2 ± 0.7 GtC yr⁻¹, for a total
374 anthropogenic CO₂ emission (including the cement carbonation sink) of 11.1 ± 0.8 GtC yr⁻¹ (40.7 ± 3.2 GtCO₂
375 yr⁻¹). Also, for 2022, G_{ATM} was 4.6 ± 0.2 GtC yr⁻¹ (2.18 ± 0.1 ppm yr⁻¹), S_{OCEAN} was 2.8 ± 0.4 GtC yr⁻¹ and
376 S_{LAND} was 3.8 ± 0.8 GtC yr⁻¹, with a B_{IM} of -0.1 GtC yr⁻¹ (i.e. total estimated sources marginally too low or
377 sinks [marginally](#) too high). The global atmospheric CO₂ concentration averaged over 2022 reached 417.1 ± 0.1
378 ppm. Preliminary data for 2023, suggest an increase in E_{FOS} relative to 2022 of +1 [.1%](#) (0 [.1%](#) to 2.2%) globally,
379 and atmospheric CO₂ concentration reaching 419 [.3](#) ppm, [.51%](#) above pre-industrial level (around 278 ppm in
380 1750). Overall, the mean and trend in the components of the global carbon budget are consistently estimated

Deleted: 1.

Deleted: (9.9 ± 0.5 GtC yr⁻¹

Deleted: 2

Deleted: 2

Deleted: 2

Deleted: more than 50

Formatted: Default Paragraph Font, Font colour: Black

Formatted: Normal, Centred, Border: Top: (No border),
Bottom: (No border), Left: (No border), Right: (No border),
Between : (No border), Tab stops: 7.96 cm, Centred + 15.92
cm, Right, Position: Horizontal: Left, Relative to: Column,
Vertical: In line, Relative to: Margin, Wrap Around

Formatted: Font colour: Black

393 over the period 1959-2022, with a near-zero overall budget imbalance, although discrepancies of up to around
394 1 GtC yr⁻¹ persist for the representation of annual to semi-decadal variability in CO₂ fluxes. Comparison of
395 estimates from multiple approaches and observations shows: (1) a persistent large uncertainty in the estimate of
396 land-use changes emissions, (2) a low agreement between the different methods on the magnitude of the land
397 CO₂ flux in the northern extra-tropics, and (3) a discrepancy between the different methods on the strength of
398 the ocean sink over the last decade.

399 This living data update documents changes in methods and data sets applied to this most-recent global carbon
400 budget as well as evolving community understanding of the global carbon cycle. The data presented in this
401 work are available at <https://doi.org/10.18160/GCP-2023> (Friedlingstein et al., 2023).

402

403 Executive Summary

404 **Global fossil CO₂ emissions (including cement carbonation) are expected to further increase in 2023, to**
405 **1.4% above their pre-COVID-19 pandemic 2019 level.** The 2022 emission increase was 0.09 GtC yr⁻¹ (0.33
406 GtCO₂ yr⁻¹) relative to 2021, bringing 2022 fossil CO₂ emissions to 9.9 ± 0.5 GtC yr⁻¹ (36.4 ± 1.8 GtCO₂ yr⁻¹),
407 virtually equal to the emissions level of 2019. Preliminary estimates based on data available suggest fossil CO₂
408 emissions to increase further in 2023, by 1.1% relative to 2022 (0.1% to 2.2%), bringing emissions to 10.0 GtC
409 yr⁻¹ (36.8 GtCO₂ yr⁻¹), 1.4% above the 2019 level.

410 Emissions from coal, oil, and gas in 2023 are all expected to be slightly above their 2022 levels (by 1.3%, 1.5%
411 and 0.2% respectively). Regionally, fossil emissions in 2022 are expected to decrease by 7.4% in the European
412 Union (0.7 GtC, 2.6 GtCO₂), and by 3.0% in the United States (1.3 GtC, 4.9 GtCO₂), but to increase by 4.0% in
413 China (3.2 GtC, 11.9 GtCO₂), 8.7% in India (0.8 GtC, 3.1 GtCO₂) and 0.5% for the rest of the world (4.2 GtC,
414 15.2 GtCO₂).

415 **Fossil CO₂ emissions decreased in 18 countries during the decade 2013-2022.** Altogether, these 18 countries
416 contribute about 1.9 GtC yr⁻¹ (7.1 GtCO₂) fossil fuel CO₂ emissions over the last decade, representing about
417 20% of world CO₂ fossil emissions.

418 **Global CO₂ emissions from land-use, land-use change, and forestry (LULUCF) averaged 1.3 ± 0.7 GtC yr⁻¹**
419 **(4.7 ± 2.6 GtCO₂ yr⁻¹) for the 2013-2022 period with a preliminary projection for 2023 of 1.1 ± 0.7 GtC**
420 **yr⁻¹ (4.0 ± 2.6 GtCO₂ yr⁻¹).** A small decrease over the past two decades is not robust given the large model
421 uncertainty. Emissions from deforestation, the main driver of global gross sources, remain high at around 1.9
422 GtC yr⁻¹ over the 2013-2022 period, highlighting the strong potential of halting deforestation for emissions
423 reductions. Sequestration of 1.3 GtC yr⁻¹ through re-/afforestation and forestry offsets two third of the
424 deforestation emissions. Emissions from other land-use transitions and from peat drainage and peat fire add
425 further, smaller contributions. The highest emitters during 2013-2022 in descending order were Brazil,
426 Indonesia, and the Democratic Republic of the Congo, with these 3 countries contributing more than half of
427 global land-use CO₂ emissions.

Deleted: the

Deleted: used in

Deleted: new

Formatted: Font: Roboto, 9 pt, Font colour: Custom Colour (RGB(31,31,31)), Highlight

Formatted: Font: Roboto, 9 pt, Font colour: Custom Colour (RGB(31,31,31)), Highlight

Formatted: Font: Roboto, 9 pt, Font colour: Custom Colour (RGB(31,31,31)), Highlight

Formatted: Font: Roboto, 9 pt, Font colour: Custom Colour (RGB(31,31,31)), Highlight

Deleted: and the progress in

Deleted: compared with previous publications of this data set...

Formatted: Font: Roboto, 9 pt, Font colour: Custom Colour (RGB(31,31,31)), Highlight

Formatted: Font: Roboto, 9 pt, Font colour: Custom Colour (RGB(31,31,31)), Highlight

Formatted: Indent: Left: 0 cm, First line: 0 cm

Deleted: 5

Deleted: 08

Deleted: 31

Deleted: 3

Deleted: 2

Deleted: 2

Deleted: 5

Deleted: %, 1.8

Deleted: 3

Deleted: 1

Deleted: 4

Deleted: 0

Deleted: 9

Deleted: LUC

Formatted: Default Paragraph Font, Font colour: Black

Formatted: Normal, Centred, Border: Top: (No border), Bottom: (No border), Left: (No border), Right: (No border), Between : (No border), Tab stops: 7.96 cm, Centred + 15.92 cm, Right, Position: Horizontal: Left, Relative to: Column, Vertical: In line, Relative to: Margin, Wrap Around

Formatted: Font colour: Black

448 **Total anthropogenic emissions were 11.1 GtC yr⁻¹ (40.7 GtCO₂ yr⁻¹) in 2022, with a similar preliminary**
449 **estimate of 11.2 GtC yr⁻¹ (40.9 GtCO₂ yr⁻¹) for 2023.**

Moved (insertion) [1]

Formatted: Font: Bold

450 **The remaining carbon budget for a 50% likelihood to limit global warming to 1.5°C, 1.7°C and 2°C has**
451 **respectively reduced to 75 GtC (275 GtCO₂), 175 GtC (625 GtCO₂) and 315 GtC (1150 GtCO₂) from the**
452 **beginning of 2024, equivalent to around 7, 15 and 28 years, assuming 2023 emissions levels.**

Moved up [1]: Total anthropogenic emissions were 11.1 GtC yr⁻¹ (40.7 GtCO₂ yr⁻¹) in 2022, with a similar preliminary estimate of 11.2 GtC yr⁻¹ (40.9 GtCO₂ yr⁻¹) for 2023.

Formatted: Font: Bold

453 **The concentration of CO₂ in the atmosphere is set to reach 419.3 ppm in 2023, 51% above pre-industrial**
454 **levels.** The atmospheric CO₂ growth was 5.2 ± 0.02 GtC yr⁻¹ during the decade 2013-2022 (47% of total CO₂
455 emissions) with a preliminary 2023 growth rate estimate of around 5.1 GtC (2.4 ppm).

Deleted: 2

Deleted: 4.0

Deleted: 1.89

456 **The ocean CO₂ sink resumed a more rapid growth in the past two decades after low or no growth during**
457 **the 1991-2002 period, overlaid with imprints of climate variability.** The estimates based on JCO₂-products
458 and models diverge with the growth of the ocean CO₂ sink in the past decade being a factor 2.5 larger than in the
459 models. This discrepancy in the trend originates from all latitudes but is largest in the Southern Ocean. The
460 ocean CO₂ sink was 2.9 ± 0.4 GtC yr⁻¹ during the decade 2013-2022 (26% of total CO₂ emissions), and did not
461 grow since 2019 due to a triple La Niña event. A similar value of 2.9 GtC yr⁻¹ is preliminarily estimated for
462 2023, which marks an increase in the sink compared to the last two years due to the transition from La Niña to
463 El Niño conditions in 2023.

464 **The land CO₂ sink continued to increase during the 2013-2022 period primarily in response to increased**
465 **atmospheric CO₂, albeit with large interannual variability.** The land CO₂ sink was 3.3 ± 0.8 GtC yr⁻¹ during
466 the 2013-2022 decade (31% of total CO₂ emissions), 0.4 GtC yr⁻¹ larger than during the previous decade (2000-
467 2009), with a preliminary 2023 estimate of around 2.9 GtC yr⁻¹, significantly lower than in 2022, and attributed
468 to the response of the land biosphere to the emerging El Niño in 2023. Year to year variability in the land sink is
469 about 1 GtC yr⁻¹ and dominates the year-to-year changes in the global atmospheric CO₂ concentration, implying
470 that small annual changes in anthropogenic emissions (such as the fossil fuel emission decrease in 2020) are
471 hard to detect in the atmospheric CO₂ observations.

Deleted: 3.0 GtC yr⁻¹.

Formatted: Font colour: Custom Colour (RGB(36,36,36))

Formatted: Default Paragraph Font, Font colour: Black

Formatted: Normal, Centred, Border: Top: (No border), Bottom: (No border), Left: (No border), Right: (No border), Between : (No border), Tab stops: 7.96 cm, Centred + 15.92 cm, Right, Position: Horizontal: Left, Relative to: Column, Vertical: In line, Relative to: Margin, Wrap Around

Formatted: Font colour: Black

480 **1 Introduction**

481 The concentration of carbon dioxide (CO₂) in the atmosphere has increased from approximately 278 parts per
482 million (ppm) in 1750 (Gulev et al., 2021), the beginning of the Industrial Era, to 417.1 ± 0.1 ppm in 2022 (Lan
483 et al., 2023; Figure 1). The atmospheric CO₂ increase above pre-industrial levels was, initially, primarily caused
484 by the release of carbon to the atmosphere from deforestation and other land-use change activities (Canadell et
485 al., 2021). While emissions from fossil fuels started before the Industrial Era, they became the dominant source
486 of anthropogenic emissions to the atmosphere from around 1950 and their relative share has continued to
487 increase until present. Anthropogenic emissions occur on top of an active natural carbon cycle that circulates
488 carbon between the reservoirs of the atmosphere, ocean, and terrestrial biosphere on time scales from sub-daily
489 to millennia, while exchanges with geologic reservoirs occur at longer timescales (Archer et al., 2009).

490 The global carbon budget (GCB) presented here refers to the mean, variations, and trends in the perturbation of
491 CO₂ in the environment, referenced to the beginning of the Industrial Era (defined here as 1750). This paper
492 describes the components of the global carbon cycle over the historical period with a stronger focus on the
493 recent period (since 1958, onset of robust atmospheric CO₂ measurements), the last decade (2013-2022), the last
494 year (2022) and the current year (2023). Finally, it provides cumulative emissions from fossil fuels and land-use
495 change since the year 1750 (the pre-industrial period), and since the year 1850 (the reference year for historical
496 simulations in IPCC AR6) (Eyring et al., 2016).

497 We quantify the input of CO₂ to the atmosphere by emissions from human activities, the growth rate of
498 atmospheric CO₂ concentration, and the resulting changes in the storage of carbon in the land and ocean
499 reservoirs in response to increasing atmospheric CO₂ levels, climate change and variability, and other
500 anthropogenic and natural changes (Figure 2). An understanding of this perturbation budget over time and the
501 underlying variability and trends of the natural carbon cycle is necessary to understand the response of natural
502 sinks to changes in climate, CO₂ and land-use change drivers, and to quantify emissions compatible with a given
503 climate stabilisation target.

504 The components of the CO₂ budget that are reported annually in this paper include separate and independent
505 estimates for the CO₂ emissions from (1) fossil fuel combustion and oxidation from all energy and industrial
506 processes; also including cement production and carbonation (E_{FOS} ; GtC yr⁻¹) and (2) the emissions resulting
507 from deliberate human activities on land, including those leading to land-use change (E_{LUC} ; GtC yr⁻¹); and their
508 partitioning among (3) the growth rate of atmospheric CO₂ concentration (G_{ATM} ; GtC yr⁻¹), and the uptake of
509 CO₂ (the ‘CO₂ sinks’) in (4) the ocean (S_{OCEAN} ; GtC yr⁻¹) and (5) on land (S_{LAND} ; GtC yr⁻¹). The CO₂ sinks as
510 defined here conceptually include the response of the land (including inland waters and estuaries) and ocean
511 (including coastal and marginal seas) to elevated CO₂ and changes in climate and other environmental
512 conditions, although in practice not all processes are fully accounted for (see Section 2.10). Global emissions
513 and their partitioning among the atmosphere, ocean and land are in balance in the real world. Due to the
514 combination of imperfect spatial and/or temporal data coverage, errors in each estimate, and smaller terms not
515 included in our budget estimate (discussed in Section 2.10), the independent estimates (1) to (5) above do not

Deleted:Page Break.....

Formatted: Default Paragraph Font, Font colour: Black

Formatted: Normal, Centred, Border: Top: (No border),
Bottom: (No border), Left: (No border), Right: (No border),
Between : (No border), Tab stops: 7.96 cm, Centred + 15.92
cm, Right, Position: Horizontal: Left, Relative to: Column,
Vertical: In line, Relative to: Margin, Wrap Around

Formatted: Font colour: Black

519 necessarily add up to zero. We therefore assess a set of additional lines of evidence derived from global
520 atmospheric inversion system results (Section 2.7), observed changes in oxygen concentration (Section 2.8) and
521 Earth System Models (ESMs) simulations (Section 2.9), all of which closing the global carbon balance. We also
522 estimate a budget imbalance (B_{IM}), which is a measure of the mismatch between the estimated emissions and the
523 estimated changes in the atmosphere, land and ocean, as follows:

$$524 \quad B_{IM} = E_{FOS} + E_{LUC} - (G_{ATM} + S_{OCEAN} + S_{LAND}) \quad (1)$$

525 G_{ATM} is usually reported in ppm yr⁻¹, which we convert to units of carbon mass per year, GtC yr⁻¹, using 1 ppm
526 = 2.124 GtC (Ballantyne et al., 2012; Table 1). All quantities are presented in units of gigatonnes of carbon
527 (GtC, 10¹⁵ gC), which is the same as petagrams of carbon (PgC; Table 1). Units of gigatonnes of CO₂ (or billion
528 tonnes of CO₂) used in policy are equal to 3.664 multiplied by the value in units of GtC.

529 We also quantify E_{FOS} and E_{LUC} by country, including both territorial and consumption-based accounting for
530 E_{FOS} (see Section 2), and discuss missing terms from sources other than the combustion of fossil fuels (see
531 Section 2.10, Supplement S1 and S2).

532 We now assess carbon dioxide removal (CDR) (see Sect. 2.2 and 2.3). Land-based CDR is significant, but
533 already accounted for in E_{LUC} in equation (1) (Sect 3.2.2). Other CDR methods, not based on vegetation, are
534 currently several orders of magnitude smaller than the other components of the budget (Sect. 3.3), hence these
535 are not included in equation (1), or in the global carbon budget tables or figures (with the exception of Figure 2
536 where CDR is shown primarily for illustrative purpose).

537 The global CO₂ budget has been assessed by the Intergovernmental Panel on Climate Change (IPCC) in all
538 assessment reports (Prentice et al., 2001; Schimel et al., 1995; Watson et al., 1990; Denman et al., 2007; Ciais et
539 al., 2013; Canadell et al., 2021), and by others (e.g. Ballantyne et al., 2012). The Global Carbon Project (GCP,
540 www.globalcarbonproject.org, last access: 9 November 2023) has coordinated this cooperative community
541 effort for the annual publication of global carbon budgets for the year 2005 (Raupach et al., 2007; including
542 fossil emissions only), year 2006 (Canadell et al., 2007), year 2007 (GCP, 2008), year 2008 (Le Quéré et al.,
543 2009), year 2009 (Friedlingstein et al., 2010), year 2010 (Peters et al., 2012a), year 2012 (Le Quéré et al., 2013;
544 Peters et al., 2013), year 2013 (Le Quéré et al., 2014), year 2014 (Le Quéré et al., 2015a; Friedlingstein et al.,
545 2014), year 2015 (Jackson et al., 2016; Le Quéré et al., 2015b), year 2016 (Le Quéré et al., 2016), year 2017 (Le
546 Quéré et al., 2018a; Peters et al., 2017), year 2018 (Le Quéré et al., 2018b; Jackson et al., 2018), year 2019
547 (Friedlingstein et al., 2019; Jackson et al., 2019; Peters et al., 2020), year 2020 (Friedlingstein et al., 2020; Le
548 Quéré et al., 2021), year 2021 (Friedlingstein et al., 2022a; Jackson et al., 2022) and most recently the year 2022
549 (Friedlingstein et al., 2022b). Each of these papers updated previous estimates with the latest available
550 information for the entire time series.

551 We adopt a range of ± 1 standard deviation (σ) to report the uncertainties in our global estimates, representing a
552 likelihood of 68% that the true value will be within the provided range if the errors have a gaussian distribution,
553 and no bias is assumed. This choice reflects the difficulty of characterising the uncertainty in the CO₂ fluxes

Deleted: 27 September

Formatted: Default Paragraph Font, Font colour: Black

Formatted: Normal, Centred, Border: Top: (No border),
Bottom: (No border), Left: (No border), Right: (No border),
Between : (No border), Tab stops: 7.96 cm, Centred + 15.92
cm, Right, Position: Horizontal: Left, Relative to: Column,
Vertical: In line, Relative to: Margin, Wrap Around

Formatted: Font colour: Black

555 between the atmosphere and the ocean and land reservoirs individually, particularly on an annual basis, as well
556 as the difficulty of updating the CO₂ emissions from land-use change. A likelihood of 68% provides an
557 indication of our current capability to quantify each term and its uncertainty given the available information.
558 The uncertainties reported here combine statistical analysis of the underlying data, assessments of uncertainties
559 in the generation of the data sets, and expert judgement of the likelihood of results lying outside this range. The
560 limitations of current information are discussed in the paper and have been examined in detail elsewhere
561 (Ballantyne et al., 2015; Zscheischler et al., 2017). We also use a qualitative assessment of confidence level to
562 characterise the annual estimates from each term based on the type, amount, quality, and consistency of the
563 different lines of evidence as defined by the IPCC (Stocker et al., 2013).

564 This paper provides a detailed description of the data sets and methodology used to compute the global carbon
565 budget estimates for the industrial period, from 1750 to 2023, and in more detail for the period since 1959. This
566 paper is updated every year using the format of 'living data' to keep a record of budget versions and the changes
567 in new data, revision of data, and changes in methodology that lead to changes in estimates of the carbon
568 budget. Additional materials associated with the release of each new version will be posted at the Global Carbon
569 Project (GCP) website (<http://www.globalcarbonproject.org/carbonbudget>, last access: 9 November 2023), with
570 fossil fuel emissions also available through the Global Carbon Atlas (<http://www.globalcarbonatlas.org>, last
571 access: 9 November 2023). All underlying data used to produce the budget can also be found at
572 <https://globalcarbonbudget.org/> (last access: 9 November 2023). With this approach, we aim to provide the
573 highest transparency and traceability in the reporting of CO₂, the key driver of climate change.

574 2 Methods

575 Multiple organisations and research groups around the world generated the original measurements and data used
576 to complete the global carbon budget. The effort presented here is thus mainly one of synthesis, where results
577 from individual groups are collated, analysed, and evaluated for consistency. We facilitate access to original
578 data with the understanding that primary data sets will be referenced in future work (see Table 2 for how to cite
579 the data sets, and Section on data availability). Descriptions of the measurements, models, and methodologies
580 follow below, with more detailed descriptions of each component provided as Supplementary Information (S1 to
581 S5).

582 This is the 18th version of the global carbon budget and the 12th revised version in the format of a living data
583 update in Earth System Science Data. It builds on the latest published global carbon budget of Friedlingstein et
584 al. (2022b). The main changes this year are: the inclusion of (1) data to year 2022 and a projection for the global
585 carbon budget for year 2023; (2) CO₂ uptake from Carbon Dioxide Removal (CDR); (3) land and ocean net
586 carbon fluxes estimates from changes in atmospheric oxygen concentration; (4) land and ocean net carbon
587 fluxes estimates from ESMs; and (5) revised method to estimate the current year (2023) atmospheric CO₂. The
588 main methodological differences between recent annual carbon budgets (2019 to 2023) are summarised in Table
589 3 and previous changes since 2006 are provided in Table S8.

Deleted: 27 September

Deleted: 27 September

Deleted: 27 September

Formatted: Outline numbered + Level: 1 + Numbering
Style: 1, 2, 3, ... + Start at: 1 + Alignment: Left + Aligned at:
0 cm + Indent at: 0.76 cm

Formatted: Default Paragraph Font, Font colour: Black

Formatted: Normal, Centred, Border: Top: (No border),
Bottom: (No border), Left: (No border), Right: (No border),
Between: (No border), Tab stops: 7.96 cm, Centred + 15.92
cm, Right, Position: Horizontal: Left, Relative to: Column,
Vertical: In line, Relative to: Margin, Wrap Around

Formatted: Font colour: Black

593 **2.1 Fossil CO₂ emissions (E_{FOS})**

594 **2.1.1 Historical period 1850-2022**

595 The estimates of global and national fossil CO₂ emissions (E_{FOS}) include the oxidation of fossil fuels through
596 both combustion (e.g., transport, heating) and chemical oxidation (e.g. carbon anode decomposition in
597 aluminium refining) activities, and the decomposition of carbonates in industrial processes (e.g. the production
598 of cement). We also include CO₂ uptake from the cement carbonation process. Several emissions sources are not
599 estimated or not fully covered: coverage of emissions from lime production are not global, and decomposition of
600 carbonates in glass and ceramic production are included only for the “Annex 1” countries of the United Nations
601 Framework Convention on Climate Change (UNFCCC) for lack of activity data. These omissions are
602 considered to be minor. Short-cycle carbon emissions - for example from combustion of biomass - are not
603 included here but are accounted for in the CO₂ emissions from land use (see Section 2.2).

604 Our estimates of fossil CO₂ emissions rely on data collection by many other parties. Our goal is to produce the
605 best estimate of this flux, and we therefore use a prioritisation framework to combine data from different
606 sources that have used different methods, while being careful to avoid double counting and undercounting of
607 emissions sources. The CDIAC-FF emissions dataset, derived largely from UN energy data, forms the
608 foundation, and we extend emissions to year Y-1 using energy growth rates reported by the Energy Institute (a
609 dataset formally produced by BP). We then proceed to replace estimates using data from what we consider to be
610 superior sources, for example Annex 1 countries’ official submissions to the UNFCCC. All data points are
611 potentially subject to revision, not just the latest year. For full details see Andrew and Peters (2022).

612 Other estimates of global fossil CO₂ emissions exist, and these are compared by Andrew (2020a). The most
613 common reason for differences in estimates of global fossil CO₂ emissions is a difference in which emissions
614 sources are included in the datasets. Datasets such as those published by the energy company BP, the US Energy
615 Information Administration, and the International Energy Agency’s ‘CO₂ emissions from fuel combustion’ are
616 all generally limited to emissions from combustion of fossil fuels. In contrast, datasets such as PRIMAP-hist,
617 CEDS, EDGAR, and GCP’s dataset aim to include all sources of fossil CO₂ emissions. See Andrew (2020a) for
618 detailed comparisons and discussion.

619 Cement absorbs CO₂ from the atmosphere over its lifetime, a process known as ‘cement carbonation’. We
620 estimate this CO₂ sink, from 1931, onwards as the average of two studies in the literature (Cao et al., 2020; Guo
621 et al., 2021). Both studies use the same model, developed by Xi et al. (2016), with different parameterisations
622 and input data, with the estimate of Guo and colleagues being a revision of Xi et al. (2016). The trends of the
623 two studies are very similar. Since carbonation is a function of both current and previous cement production, we
624 extend these estimates to 2022 by using the growth rate derived from the smoothed cement emissions (10-year
625 smoothing) fitted to the carbonation data. In the present budget, we always include the cement carbonation
626 carbon sink in the fossil CO₂ emission component (E_{FOS}).

Formatted: Outline numbered + Level: 2 + Numbering
Style: 1, 2, 3, ... + Start at: 1 + Alignment: Left + Aligned at:
0 cm + Indent at: 1.02 cm

Formatted: Outline numbered + Level: 3 + Numbering
Style: 1, 2, 3, ... + Start at: 1 + Alignment: Left + Aligned at:
0 cm + Indent at: 1.27 cm

Formatted: Default Paragraph Font, Font colour: Black

Formatted: Normal, Centred, Border: Top: (No border),
Bottom: (No border), Left: (No border), Right: (No border),
Between : (No border), Tab stops: 7.96 cm, Centred + 15.92
cm, Right, Position: Horizontal: Left, Relative to: Column,
Vertical: In line, Relative to: Margin, Wrap Around

Formatted: Font colour: Black

627 We use the Kaya Identity for a simple decomposition of CO₂ emissions into the key drivers (Raupach et al.,
628 2007). While there are variations (Peters et al., 2017), we focus here on a decomposition of CO₂ emissions into
629 population, GDP per person, energy use per GDP, and CO₂ emissions per energy. Multiplying these individual
630 components together returns the CO₂ emissions. Using the decomposition, it is possible to attribute the change
631 in CO₂ emissions to the change in each of the drivers. This method gives a first-order understanding of what
632 causes CO₂ emissions to change each year.

633 2.1.2 2023 projection

634 We provide a projection of global fossil CO₂ emissions in 2022 by combining separate projections for China,
635 USA, EU, India, and for all other countries combined. The methods are different for each of these. For China we
636 combine monthly fossil fuel production data from the National Bureau of Statistics and trade data from the
637 Customs Administration, giving us partial data for the growth rates to date of natural gas, petroleum, and
638 cement, and of the apparent consumption itself for raw coal. We then use a regression model to project full-year
639 emissions based on historical observations. For the USA our projection is taken directly from the Energy
640 Information Administration's (EIA) Short-Term Energy Outlook (EIA, 2023), combined with the year-to-date
641 growth rate of cement clinker production. For the EU we use monthly energy data from Eurostat to derive
642 estimates of monthly CO₂ emissions through July, with coal emissions extended through September using a
643 statistical relationship with reported electricity generation from coal and other factors. For natural gas we use
644 Holt-Winters to project the last four months of the year. EU emissions from oil are derived using the EIA's
645 projection of oil consumption for Europe. EU cement emissions are based on available year-to-date data from
646 three of the largest producers, Germany, Poland, and Spain. India's projected emissions are derived from
647 estimates through August (July for coal) using the methods of Andrew (2020b) and extrapolated assuming
648 seasonal patterns from before 2019. Emissions for the rest of the world are derived using projected growth in
649 economic production from the IMF (2023) combined with extrapolated changes in emissions intensity of
650 economic production. More details on the EFOS methodology and its 2023 projection can be found in
651 Supplement S.1.

652 2.2 CO₂ emissions from land-use, land-use change and forestry (ELUC)

653 2.2.1 Historical period 1850-2022

654 The net CO₂ flux from land-use, land-use change and forestry (ELUC, called land-use change emissions in the
655 rest of the text) includes CO₂ fluxes from deforestation, afforestation, logging and forest degradation (including
656 harvest activity), shifting cultivation (cycle of cutting forest for agriculture, then abandoning), and regrowth of
657 forests (following wood harvest or agriculture abandonment). Emissions from peat burning and peat drainage
658 are added from external datasets, peat drainage being averaged from three spatially explicit independent datasets
659 (see Supplement S.2.1).

660 Three bookkeeping approaches (updated estimates each of BLUE (Hansis et al., 2015), OSCAR (Gasser et al.,
661 2020), and H&C2023 (Houghton and Castanho, 2023)) were used to quantify gross emissions and gross

Formatted: Outline numbered + Level: 3 + Numbering
Style: 1, 2, 3, ... + Start at: 1 + Alignment: Left + Aligned at:
0 cm + Indent at: 1.27 cm

Formatted: Outline numbered + Level: 2 + Numbering
Style: 1, 2, 3, ... + Start at: 1 + Alignment: Left + Aligned at:
0 cm + Indent at: 1.02 cm

Formatted: Outline numbered + Level: 3 + Numbering
Style: 1, 2, 3, ... + Start at: 1 + Alignment: Left + Aligned at:
0 cm + Indent at: 1.27 cm

Formatted: Default Paragraph Font, Font colour: Black

Formatted: Normal, Centred, Border: Top: (No border),
Bottom: (No border), Left: (No border), Right: (No border),
Between : (No border), Tab stops: 7.96 cm, Centred + 15.92
cm, Right, Position: Horizontal: Left, Relative to: Column,
Vertical: In line, Relative to: Margin, Wrap Around

Formatted: Font colour: Black

662 removals and the resulting net E_{LUC} . Uncertainty estimates were derived from the Dynamic Global Vegetation
663 Models (DGVMs) ensemble for the time period prior to 1960, and using for the recent decades an uncertainty
664 range of $\pm 0.7 \text{ GtC yr}^{-1}$, which is a semi-quantitative measure for annual and decadal emissions and reflects our
665 best value judgement that there is at least 68% chance ($\pm 1\sigma$) that the true land-use change emission lies within
666 the given range, for the range of processes considered here.

667 Our E_{LUC} estimates follow the definition of global carbon cycle models of CO_2 fluxes related to land use and
668 land management and differ from IPCC definitions adopted in National GHG Inventories (NGHGI) for
669 reporting under the UNFCCC, which additionally generally include, through adoption of the IPCC so-called
670 managed land proxy approach, the terrestrial fluxes occurring on all land that countries define as managed. This
671 partly includes fluxes due to environmental change (e.g. atmospheric CO_2 increase), which are part of S_{LAND} in
672 our definition. This causes the global emission estimates to be smaller for NGHGI than for the global carbon
673 budget definition (Grassi et al., 2018). The same is the case for the Food Agriculture Organization (FAO)
674 estimates of carbon fluxes on forest land, which include both anthropogenic and natural sources on managed
675 land (Tubiello et al., 2021). We translate the two definitions to each other, to provide a comparison of the
676 anthropogenic carbon budget to the official country reporting to the climate convention.

677 E_{LUC} contains a range of fluxes that are related to Carbon Dioxide Removal (CDR). CDR can be defined as the
678 set of anthropogenic activities that remove CO_2 from the atmosphere and store it in durable form, such as in
679 forest biomass and soils, long-lived products, or in geological or ocean reservoirs. We quantify vegetation-based
680 CDR that is implicitly or explicitly captured by land-use fluxes consistent with our updated model estimates
681 (CDR not based on vegetation is discussed in Section 2.3; IPCC, 2023). We quantify re/afforestation from the
682 three bookkeeping estimates by separating forest regrowth in shifting cultivation cycles from permanent
683 increases in forest cover (see Supplement C.2.1). The latter count as CDR, but it should be noted that the
684 permanence of the storage under climate risks such as fire is increasingly questioned. Other CDR activities
685 contained in E_{LUC} include the transfer of carbon to harvested wood products (HWP), which is represented by the
686 bookkeeping models with varying details concerning product usage and their lifetimes; bioenergy with carbon
687 capture and storage (BECCS); and biochar production. Bookkeeping and TRENDY models currently only
688 represent BECCS and biochar with regard to the CO_2 removal through photosynthesis, but not for the durable
689 storage. HWP, BECCS, and biochar are typically counted as CDR when the transfer to the durable storage site
690 occurs and not when the CO_2 is removed from the atmosphere, which complicates a direct comparison to the
691 global carbon budgets approach to quantify annual fluxes to and from the atmosphere. Estimates for CDR
692 through HWP, BECCS, and biochar are thus not indicated in this budget, but can be found elsewhere (see
693 Section 3.2.2).

694 2.2.2 2023 Projection

695 We project the 2023 land-use emissions for BLUE, H&C2023, and OSCAR based on their E_{LUC} estimates for
696 2022 and adding the change in carbon emissions from peat fires and tropical deforestation and degradation fires
697 (2023 emissions relative to 2022 emissions) estimated using active fire data (MCD14ML; Giglio et al., 2016).

Formatted: Outline numbered + Level: 3 + Numbering
Style: 1, 2, 3, ... + Start at: 1 + Alignment: Left + Aligned at:
0 cm + Indent at: 1.27 cm

Formatted: Default Paragraph Font, Font colour: Black

Formatted: Normal, Centred, Border: Top: (No border),
Bottom: (No border), Left: (No border), Right: (No border),
Between: (No border), Tab stops: 7.96 cm, Centred + 15.92
cm, Right, Position: Horizontal: Left, Relative to: Column,
Vertical: In line, Relative to: Margin, Wrap Around

Formatted: Font colour: Black

698 Peat drainage is assumed to be unaltered as it has low interannual variability. More details on the ELUC
699 methodology can be found in Supplement S.2.

700 2.3 Carbon Dioxide Removal (CDR) not based on vegetation

701 CDR not based on terrestrial vegetation currently relies on enhanced rock weathering and Direct Air Carbon
702 Capture and Storage (DACCS) projects. The majority of this (58%) derives from a single project: Climeworks'
703 Orca DACCS plant based in Hellisheidi, Iceland. The remainder is generated by 13 small-scale projects
704 including, for example, 500 tons of carbon dioxide sequestered through the spreading of crushed olivine on
705 agricultural areas by Eion Carbon. We use data from the State of CDR Report (Smith et al., 2023), which
706 quantifies all currently deployed CDR methods, including the land-use related activities already covered by
707 Section 2.2. The State of CDR Report (Smith et al., 2023) combines estimates of carbon storage in managed
708 land derived from NGHGI data with project-by-project storage rates obtained through 20 extant CDR databases
709 and registries (status as of mid-year 2022) by Powis et al. (2023). They assessed the data quality on existing
710 CDR projects to be poor, suffering from fragmentation, different reporting standards, limited geographical
711 coverage, and inclusion of a number of pilot plants with uncertain lifespans. As a consequence, these numbers
712 could change substantially from year-to-year in the near-term.

713 2.4 Growth rate in atmospheric CO₂ concentration (G_{ATM})

714 2.4.1 Historical period 1850-2022

715 The rate of growth of the atmospheric CO₂ concentration is provided for years 1959-2022 by the US National
716 Oceanic and Atmospheric Administration Global Monitoring Laboratory (NOAA/GML; Lan et al., 2023),
717 which includes recent revisions to the calibration scale of atmospheric CO₂ measurements (Hall et al., 2021).
718 For the 1959-1979 period, the global growth rate is based on measurements of atmospheric CO₂ concentration
719 averaged from the Mauna Loa and South Pole stations, as observed by the CO₂ Program at Scripps Institution of
720 Oceanography (Keeling et al., 1976). For the 1980-2021 time period, the global growth rate is based on the
721 average of multiple stations selected from the marine boundary layer sites with well-mixed background air
722 (Ballantyne et al., 2012), after fitting a smooth curve through the data for each station as a function of time, and
723 averaging by latitude band (Masarie and Tans, 1995). The annual growth rate is estimated by Lan et al. (2023)
724 from atmospheric CO₂ concentration by taking the average of the most recent December-January months
725 corrected for the average seasonal cycle and subtracting this same average one year earlier. The growth rate in
726 units of ppm yr⁻¹ is converted to units of GtC yr⁻¹ by multiplying by a factor of 2.124 GtC per ppm, assuming
727 instantaneous mixing of CO₂ throughout the atmosphere (Ballantyne et al., 2012; Table 1).

728 Since 2020, NOAA/GML provides estimates of atmospheric CO₂ concentrations with respect to a new
729 calibration scale, referred to as WMO-CO₂-X2019, in line with a recalibration agreed by the World
730 Meteorological Organization (WMO) Global Atmosphere Watch (GAW) community (Hall et al., 2021). The
731 recalibrated data were first used to estimate G_{ATM} in the 2021 edition of the global carbon budget (Friedlingstein
732 et al., 2022a). Friedlingstein et al. (2022a) verified that the change of scales from WMO-CO₂-X2007 to WMO-

Formatted: Outline numbered + Level: 2 + Numbering
Style: 1, 2, 3, ... + Start at: 1 + Alignment: Left + Aligned at:
0 cm + Indent at: 1.02 cm

Formatted: Outline numbered + Level: 2 + Numbering
Style: 1, 2, 3, ... + Start at: 1 + Alignment: Left + Aligned at:
0 cm + Indent at: 1.02 cm

Formatted: Outline numbered + Level: 3 + Numbering
Style: 1, 2, 3, ... + Start at: 1 + Alignment: Left + Aligned at:
0 cm + Indent at: 1.27 cm

Deleted: is updated from Ballantyne et al. (2012) and

Formatted: Default Paragraph Font, Font colour: Black

Formatted: Normal, Centred, Border: Top: (No border),
Bottom: (No border), Left: (No border), Right: (No border),
Between : (No border), Tab stops: 7.96 cm, Centred + 15.92
cm, Right, Position: Horizontal: Left, Relative to: Column,
Vertical: In line, Relative to: Margin, Wrap Around

Formatted: Font colour: Black

734 CO2-X2019 made a negligible difference to the value of G_{ATM} ($-0.06 \text{ GtC yr}^{-1}$ during 2010-2019 and -0.01 GtC
735 yr^{-1} during 1959-2019, well within the uncertainty range reported below).

736 The uncertainty around the atmospheric growth rate is due to four main factors. First, the long-term
737 reproducibility of reference gas standards (around 0.03 ppm for 1σ from the 1980s; Lan et al., 2023). Second,
738 small unexplained systematic analytical errors that may have a duration of several months to two years come
739 and go. They have been simulated by randomising both the duration and the magnitude (determined from the
740 existing evidence) in a Monte Carlo procedure. Third, the network composition of the marine boundary layer
741 with some sites coming or going, gaps in the time series at each site, etc (Lan et al., 2023). The latter uncertainty
742 was estimated by NOAA/GML with a Monte Carlo method by constructing 100 "alternative" networks (Masarie
743 and Tans, 1995; NOAA/GML, 2019). The second and third uncertainties, summed in quadrature, add up to
744 0.085 ppm on average (Lan et al., 2023). Fourth, the uncertainty associated with using the average CO_2
745 concentration from a surface network to approximate the true atmospheric average CO_2 concentration (mass-
746 weighted, in 3 dimensions) as needed to assess the total atmospheric CO_2 burden. In reality, CO_2 variations
747 measured at the stations will not exactly track changes in total atmospheric burden, with offsets in magnitude
748 and phasing due to vertical and horizontal mixing. This effect must be very small on decadal and longer time
749 scales, when the atmosphere can be considered well mixed. The CO_2 increase in the stratosphere lags the
750 increase (meaning lower concentrations) that we observe in the marine boundary layer, while the continental
751 boundary layer (where most of the emissions take place) leads the marine boundary layer with higher
752 concentrations. These effects nearly cancel each other. In addition, the growth rate is nearly the same
753 everywhere (Ballantyne et al, 2012). We therefore maintain an uncertainty around the annual growth rate based
754 on the multiple stations data set ranges between 0.11 and 0.72 GtC yr^{-1} , with a mean of 0.61 GtC yr^{-1} for 1959-
755 1979 and 0.17 GtC yr^{-1} for 1980-2022, when a larger set of stations were available as provided by Lan et al.
756 (2023). We estimate the uncertainty of the decadal averaged growth rate after 1980 at 0.02 GtC yr^{-1} based on the
757 calibration and the annual growth rate uncertainty but stretched over a 10-year interval. For years prior to 1980,
758 we estimate the decadal averaged uncertainty to be 0.07 GtC yr^{-1} based on a factor proportional to the annual
759 uncertainty prior and after 1980 ($0.02 * [0.61/0.17] \text{ GtC yr}^{-1}$).

760 We assign a high confidence to the annual estimates of G_{ATM} because they are based on direct measurements
761 from multiple and consistent instruments and stations distributed around the world (Ballantyne et al., 2012; Hall
762 et al., 2021).

763 To estimate the total carbon accumulated in the atmosphere since 1750 or 1850, we use an atmospheric CO_2
764 concentration of $278.3 \pm 3 \text{ ppm}$ or $285.1 \pm 3 \text{ ppm}$, respectively (Gulev et al., 2021). For the construction of the
765 cumulative budget shown in Figure 3, we use the fitted estimates of CO_2 concentration from Joos and Spahni
766 (2008) to estimate the annual atmospheric growth rate using the conversion factors shown in Table 1. The
767 uncertainty of $\pm 3 \text{ ppm}$ (converted to $\pm 1\sigma$) is taken directly from the IPCC's AR5 assessment (Ciais et al., 2013).
768 Typical uncertainties in the growth rate in atmospheric CO_2 concentration from ice core data are equivalent to
769 $\pm 0.1\text{-}0.15 \text{ GtC yr}^{-1}$ as evaluated from the Law Dome data (Etheridge et al., 1996) for individual 20-year intervals
770 over the period from 1850 to 1960 (Bruno and Joos, 1997).

Formatted: Default Paragraph Font, Font colour: Black

Formatted: Normal, Centred, Border: Top: (No border),
Bottom: (No border), Left: (No border), Right: (No border),
Between : (No border), Tab stops: 7.96 cm, Centred + 15.92
cm, Right, Position: Horizontal: Left, Relative to: Column,
Vertical: In line, Relative to: Margin, Wrap Around

Formatted: Font colour: Black

771 **2.4.2 2023 projection**

772 We provide an assessment of G_{ATM} for 2023 as the average of two methods. [The GCB regression method](#)
773 [models monthly global-average atmospheric CO₂ concentrations and derives the increment and annual average](#)
774 [from these. The model uses lagged observations of concentration \(Lan et al., 2023\): both a 12-month lag, and](#)
775 [the lowest lag that will allow model prediction to produce an estimate for the following January, recalling that](#)
776 [the \$G_{ATM}\$ increment is derived from December/January pairs. The largest driver of interannual changes is the](#)
777 [ENSO signal \(Betts et al., 2016\), so the monthly ENSO 3.4 index \(Huang et al., 2023\) is included in the model.](#)
778 [Given the natural lag between sea-surface temperatures and effects on the biosphere, and in turn effects on](#)
779 [globally mixed atmospheric CO₂ concentration, a lagged ENSO index is used, and we use both a 5-month and a](#)
780 [6-month lag. The combination of the two lagged ENSO values helps reduce possible effects of noise in a single](#)
781 [month. To help characterise the seasonal variation, we add month as a categorical variable. Finally, we flag the](#)
782 [period affected by the Pinatubo eruption \(August 1991 - November 1993\) as a categorical variable. Note that](#)
783 [while emissions of CO₂ are the largest driver of the trend in atmospheric CO₂ concentration, our goal here is to](#)
784 [predict divergence from that trend. Because changes in emissions from year to year are relatively minor, this has](#)
785 [little effect on the variation of concentration from the trend line. Even the relatively large drop in emissions in](#)
786 [2020 due to the COVID-19 pandemic does not cause any problems for the model.](#)

787 For the first time this year, we also use the multi-model mean and uncertainty of the 2023 G_{ATM} estimated by the
788 ESMs prediction system (see Section 2.9). We then take the average of the [GCB regression](#) and ESMs G_{ATM}
789 estimates, with their respective uncertainty combined quadratically.

790 Similarly, the projection of the 2023 global average CO₂ concentration (in ppm), is calculated as the average of
791 the estimates from the two methods. For [the GCB regression](#) method, it is the annual average of global
792 concentration over the 12 months [of 2023](#); for the ESMs, it is the observed global average CO₂ concentration for
793 2022 plus the annual increase in 2023 [of the global average CO₂ concentration](#) predicted by the ESMs multi-
794 model mean.

795 **2.5 Ocean CO₂ sink**

796 **2.5.1 Historical period 1850-2022**

797 The reported estimate of the global ocean anthropogenic CO₂ sink S_{OCEAN} is derived as the average of two
798 estimates. The first estimate is derived as the mean over an ensemble of ten global ocean biogeochemistry
799 models (GOBMs, Table 4 and Table S2). The second estimate is obtained as the mean over an ensemble of
800 seven surface ocean fCO_2 -observation-based data-products (Table 4 and Table S3). An eighth fCO_2 -product
801 (Watson et al., 2020) is shown, but is not included in the ensemble average as it differs from the other products
802 by adjusting the flux to a cool, salty ocean surface skin (see Supplement S.3.1 for a discussion of the Watson
803 product). The GOBMs simulate both the natural and anthropogenic CO₂ cycles in the ocean. They constrain the
804 anthropogenic air-sea CO₂ flux (the dominant component of S_{OCEAN}) by the transport of carbon into the ocean
805 interior, which is also the controlling factor of present-day ocean carbon uptake in the real world. They cover

Formatted: Outline numbered + Level: 3 + Numbering Style: 1, 2, 3, ... + Start at: 1 + Alignment: Left + Aligned at: 0 cm + Indent at: 1.27 cm

Deleted: As in previous GCB releases, we use the observed monthly global atmospheric CO₂ concentration (GLO) through June 2023 (Lan et al., 2023), and the bias-adjusted Holt-Winters exponential smoothing with additive seasonality (Chatfield, 1978) to project to January 2024. The uncertainty is estimated from past variability using the standard deviation of the last 5 years' monthly growth rates.

Deleted: Holt-Winters

Deleted: Holt-Winters

Formatted: Outline numbered + Level: 2 + Numbering Style: 1, 2, 3, ... + Start at: 1 + Alignment: Left + Aligned at: 0 cm + Indent at: 1.02 cm

Formatted: Outline numbered + Level: 3 + Numbering Style: 1, 2, 3, ... + Start at: 1 + Alignment: Left + Aligned at: 0 cm + Indent at: 1.27 cm

Formatted: Default Paragraph Font, Font colour: Black

Formatted: Normal, Centred, Border: Top: (No border), Bottom: (No border), Left: (No border), Right: (No border), Between: (No border), Tab stops: 7.96 cm, Centred + 15.92 cm, Right, Position: Horizontal: Left, Relative to: Column, Vertical: In line, Relative to: Margin, Wrap Around

Formatted: Font colour: Black

815 the full globe and all seasons and were recently evaluated against surface ocean carbon observations, suggesting
816 they are suitable to estimate the annual ocean carbon sink (Hauck et al., 2020). The $f\text{CO}_2$ -products are tightly
817 linked to observations of $f\text{CO}_2$ (fugacity of CO_2 , which equals $p\text{CO}_2$ corrected for the non-ideal behaviour of the
818 gas; Pfeil et al., 2013), which carry imprints of temporal and spatial variability, but are also sensitive to
819 uncertainties in gas-exchange parameterizations and data-sparsity (Gloege et al., 2021, Hauck et al., 2023).
820 Their asset is the assessment of the mean spatial pattern of variability and its seasonality (Hauck et al., 2020,
821 Gloege et al. 2021, Hauck et al., 2023). We further use two diagnostic ocean models to estimate SO_{OCEAN} over the
822 industrial era (1781-1958).

823 The global $f\text{CO}_2$ -based flux estimates were adjusted to remove the pre-industrial ocean source of CO_2 to the
824 atmosphere of $0.65 \pm 0.3 \text{ GtC yr}^{-1}$ from river input to the ocean (Regnier et al., 2022), to satisfy our definition of
825 SO_{OCEAN} (Hauck et al., 2020). The river flux adjustment was distributed over the latitudinal bands using the
826 regional distribution of Lacroix et al. (2020; North: 0.14 GtC yr^{-1} , Tropics: 0.42 GtC yr^{-1} , South: 0.09 GtC yr^{-1}).
827 Acknowledging that this distribution is based on only one model, the advantage is that a gridded field is
828 available, and the river flux adjustment can be calculated for the three latitudinal bands and the RECCAP
829 regions (REgional Carbon Cycle Assessment and Processes (RECCAP2; Ciais et al., 2020, Poulter et al., 2022,
830 DeVries et al., 2023). This data set suggests that more of the riverine outgassing is located in the tropics than in
831 the Southern Ocean, and is thus opposed to the previously used data set of Aumont et al. (2001). Accordingly,
832 the regional distribution is associated with a major uncertainty in addition to the large uncertainty around the
833 global estimate (Crisp et al., 2022; Gruber et al., 2023). Anthropogenic perturbations of river carbon and
834 nutrient transport to the ocean are not considered (see Section 2.10 and Supplement S.6.3).

835 We derive SO_{OCEAN} from GOBMs by using a simulation (sim A) with historical forcing of climate and
836 atmospheric CO_2 , accounting for model biases and drift from a control simulation (sim B) with constant
837 atmospheric CO_2 and normal year climate forcing. A third simulation (sim C) with historical atmospheric CO_2
838 increase and normal year climate forcing is used to attribute the ocean sink to CO_2 (sim C minus sim B) and
839 climate (sim A minus sim C) effects. A fourth simulation (sim D; historical climate forcing and constant
840 atmospheric CO_2) is used to compare the change in anthropogenic carbon inventory in the interior ocean (sim A
841 minus sim D) to the observational estimate of Gruber et al. (2019) with the same flux components (steady state
842 and non-steady state anthropogenic carbon flux). The $f\text{CO}_2$ -products are adjusted with respect to their original
843 publications to represent the full ice-free ocean area, including coastal zones and marginal seas, when the area
844 coverage is below 99%. This is done by either area filling following Fay et al. (2021) or a simple scaling
845 approach. GOBMs and $f\text{CO}_2$ -products fall within the observational constraints over the 1990s ($2.2 \pm 0.7 \text{ GtC yr}^{-1}$,
846 Ciais et al., 2013) after applying adjustments.

847 SO_{OCEAN} is calculated as the average of the GOBM ensemble mean and the $f\text{CO}_2$ -product ensemble mean from
848 1990 onwards. Prior to 1990, it is calculated as the GOBM ensemble mean plus half of the offset between
849 GOBMs and $f\text{CO}_2$ -products ensemble means over 1990-2001.

850 We assign an uncertainty of $\pm 0.4 \text{ GtC yr}^{-1}$ to the ocean sink based on a combination of random (ensemble
851 standard deviation) and systematic uncertainties (GOBMs bias in anthropogenic carbon accumulation,

Deleted: 2020).

Deleted: ,

Formatted: Default Paragraph Font, Font colour: Black

Formatted: Normal, Centred, Border: Top: (No border),
Bottom: (No border), Left: (No border), Right: (No border),
Between : (No border), Tab stops: 7.96 cm, Centred + 15.92
cm, Right, Position: Horizontal: Left, Relative to: Column,
Vertical: In line, Relative to: Margin, Wrap Around

Formatted: Font colour: Black

854 previously reported uncertainties in $f\text{CO}_2$ -products; see Supplement S.3.4). We assess a medium confidence
855 level to the annual ocean CO_2 sink and its uncertainty because it is based on multiple lines of evidence, it is
856 consistent with ocean interior carbon estimates (Gruber et al., 2019, see Section 3.6.5) and the interannual
857 variability in the GOBMs and data-based estimates is largely consistent and can be explained by climate
858 variability. We refrain from assigning a high confidence because of the systematic deviation between the
859 GOBM and $f\text{CO}_2$ -product trends since around 2002. More details on the SO_{OCEAN} methodology can be found in
860 Supplement S.3.

861 2.5.2 2023 Projection

862 The ocean CO_2 sink forecast for the year 2023 is based on the annual historical (Lan et al., 2023) and our
863 estimated 2023 atmospheric CO_2 concentration growth rate, the historical and our estimated 2023 annual global
864 fossil fuel emissions from this year's carbon budget, and the spring (March, April, May) Oceanic Niño Index
865 (ONI) (NCEP, 2023). Using a non-linear regression approach, i.e., a feed-forward neural network, atmospheric
866 CO_2 , ONI, and the fossil fuel emissions are used as training data to best match the annual ocean CO_2 sink (i.e.
867 combined SO_{OCEAN} estimate from GOBMs and data products) from 1959 through 2022 from this year's carbon
868 budget. Using this relationship, the 2023 SO_{OCEAN} can then be estimated from the projected 2022 input data using
869 the non-linear relationship established during the network training. To avoid overfitting, the neural network was
870 trained with a variable number of hidden neurons (varying between 2-5) and 20% of the randomly selected
871 training data were withheld for independent internal testing. Based on the best output performance (tested using
872 the 20% withheld input data), the best performing number of neurons was selected. In a second step, we trained
873 the network 10 times using the best number of neurons identified in step 1 and different sets of randomly
874 selected training data. The mean of the 10 trainings is considered our best forecast, whereas the standard
875 deviation of the 10 ensembles provides a first order estimate of the forecast uncertainty. This uncertainty is then
876 combined with the SO_{OCEAN} uncertainty (0.4 GtC yr^{-1}) to estimate the overall uncertainty of the 2023 projection.
877 As an additional line of evidence, we also assess the 2023 atmosphere-ocean carbon flux from the ESM
878 prediction system (see Section 2.9).

879 2.6 Land CO_2 sink

880 2.6.1 Historical Period 1850-2022

881 The terrestrial land sink (S_{LAND}) is thought to be due to the combined effects of fertilisation by rising
882 atmospheric CO_2 and N inputs on plant growth, as well as the effects of climate change such as the lengthening
883 of the growing season in northern temperate and boreal areas. S_{LAND} does not include land sinks directly
884 resulting from land-use and land-use change (e.g., regrowth of vegetation) as these are part of the land-use flux
885 (E_{LUC}), although system boundaries make it difficult to attribute exactly CO_2 fluxes on land between S_{LAND} and
886 E_{LUC} (Erb et al., 2013).

887 S_{LAND} is estimated from the multi-model mean of 20 DGVMs (Table S1) with an additional comparison of
888 DGVMs with a data-driven, carbon data model framework (CARDAMOM) (Bloom and Williams, 2015; Bloom

Formatted: Outline numbered + Level: 3 + Numbering
Style: 1, 2, 3, ... + Start at: 1 + Alignment: Left + Aligned at:
0 cm + Indent at: 1.27 cm

Formatted: Outline numbered + Level: 2 + Numbering
Style: 1, 2, 3, ... + Start at: 1 + Alignment: Left + Aligned at:
0 cm + Indent at: 1.02 cm

Formatted: Outline numbered + Level: 3 + Numbering
Style: 1, 2, 3, ... + Start at: 1 + Alignment: Left + Aligned at:
0 cm + Indent at: 1.27 cm

Formatted: Default Paragraph Font, Font colour: Black

Formatted: Normal, Centred, Border: Top: (No border),
Bottom: (No border), Left: (No border), Right: (No border),
Between : (No border), Tab stops: 7.96 cm, Centred + 15.92
cm, Right, Position: Horizontal: Left, Relative to: Column,
Vertical: In line, Relative to: Margin, Wrap Around

Formatted: Font colour: Black

889 et al., 2016), see Supplement S4. DGVMs simulations include all climate variability and CO₂ effects over land.
890 In addition to the carbon cycle represented in all DGVMs, 14 models also account for the nitrogen cycle and
891 hence can include the effect of N inputs on S_{LAND}. The DGVMs estimate of S_{LAND} does not include the export of
892 carbon to aquatic systems or its historical perturbation, which is discussed in Supplement S.6.3. [DGVMs need to](#)
893 [meet several criteria to be included in this assessment](#). [In addition, we use the International Land Model](#)
894 [Benchmarking system \(ILAMB; Collier et al., 2018\) for the DGVMs evaluation \(see Supplement S.4.2\). The](#)
895 [uncertainty on S_{LAND} is taken from the GGVMs standard deviation \(see Supplement S.4.3\)](#). More details on the
896 S_{LAND} methodology can be found in Supplement S.4.

Deleted: See Supplement S.4.2 for DGVMs evaluation and uncertainty ...

Deleted: for S_{LAND}, using

897 2.6.2 2023 Projection

898 Like for the ocean forecast, the land CO₂ sink (S_{LAND}) forecast is based on the annual historical (Lan et al.,
899 2023) and our estimated 2023 atmospheric CO₂ concentration, [historical and our estimated 2023 annual global](#)
900 [fossil fuel emissions from this year's carbon budget, and the summer \(June, July, August\) ONI \(NCEP, 2022\)](#).
901 All training data are again used to best match S_{LAND} from 1959 through 2022 from this year's carbon budget
902 using a feed-forward neural network. To avoid overfitting, the neural network was trained with a variable
903 number of hidden neurons (varying between 2-15), larger than for Socean prediction due to the stronger land
904 carbon interannual variability. As done for Socean, a pre-training selects the optimal number of hidden neurons
905 based on 20% withheld input data, and in a second step, an ensemble of 10 forecasts is produced to provide the
906 mean forecast plus uncertainty. This uncertainty is then combined with the S_{LAND} uncertainty for 2022 (0.9 GtC
907 yr⁻¹) to estimate the overall uncertainty of the 2023 projection.

Formatted: Outline numbered + Level: 3 + Numbering Style: 1, 2, 3, ... + Start at: 1 + Alignment: Left + Aligned at: 0 cm + Indent at: 1.27 cm

Deleted:

908 2.7 Atmospheric inversion estimate

909 The world-wide network of in-situ atmospheric measurements and satellite derived atmospheric CO₂ column
910 (xCO₂) observations put a strong constraint on changes in the atmospheric abundance of CO₂. This is true
911 globally (hence our large confidence in G_{ATM}), but also regionally in regions with sufficient observational
912 density found mostly in the extra-tropics. This allows atmospheric inversion methods to constrain the magnitude
913 and location of the combined total surface CO₂ fluxes from all sources, including fossil and land-use change
914 emissions and land and ocean CO₂ fluxes. The inversions assume E_{FOS} to be well known, and they solve for the
915 spatial and temporal distribution of land and ocean fluxes from the residual gradients of CO₂ between stations
916 that are not explained by fossil fuel emissions. By design, such systems thus close the carbon balance (B_{IM} = 0)
917 and thus provide an additional perspective on the independent estimates of the ocean and land fluxes.

Formatted: Outline numbered + Level: 2 + Numbering Style: 1, 2, 3, ... + Start at: 1 + Alignment: Left + Aligned at: 0 cm + Indent at: 1.02 cm

918 This year's release includes fourteen inversion systems that are described in Table S4, of which thirteen are
919 included in the ensemble of inverse estimates presented in the text and figures. Each system is rooted in
920 Bayesian inversion principles but uses different methodologies. These differences concern the selection of
921 atmospheric CO₂ data or xCO₂, and the choice of a-priori fluxes to refine. They also differ in spatial and
922 temporal resolution, assumed correlation structures, and mathematical approach of the models (see references in
923 Table S4 for details). Importantly, the systems use a variety of transport models, which was demonstrated to be
924 a driving factor behind differences in atmospheric inversion-based flux estimates, and specifically their

Formatted: Default Paragraph Font, Font colour: Black

Formatted: Normal, Centred, Border: Top: (No border), Bottom: (No border), Left: (No border), Right: (No border), Between : (No border), Tab stops: 7.96 cm, Centred + 15.92 cm, Right, Position: Horizontal: Left, Relative to: Column, Vertical: In line, Relative to: Margin, Wrap Around

Formatted: Font colour: Black

929 distribution across latitudinal bands (Gaubert et al., 2019; Schuh et al., 2019). Six inversion systems (CAMS-
930 FT23r1, CMS-flux, GONGGA, THU, COLA, GCASv2) used satellite xCO₂ retrievals from GOSAT and/or
931 OCO-2, scaled to the WMO 2019 calibration scale. Two inversions this year (CMS-Flux, COLA) used these
932 xCO₂ datasets in addition to the in-situ observational CO₂ mole fraction records.

933 The original products delivered by the inverse modellers were modified to facilitate the comparison to the other
934 elements of the budget, specifically on two accounts: (1) global total fossil fuel emissions including cement
935 carbonation CO₂ uptake, and (2) riverine CO₂ transport. Details are given below. We note that with these
936 adjustments the inverse results no longer represent the net atmosphere-surface exchange over land/ocean areas
937 as sensed by atmospheric observations. Instead, for land, they become the net uptake of CO₂ by vegetation and
938 soils that is not exported by fluvial systems, similar to the DGVMs estimates. For oceans, they become the net
939 uptake of anthropogenic CO₂, similar to the GOBMs estimates.

940 The inversion systems prescribe global fossil fuel emissions based on e.g. the GCP's Gridded Fossil Emissions
941 Dataset versions 2023.1 (GCP-GridFED; Jones et al., 2023), which are updates to GCP-GridFEDv2021
942 presented by Jones et al. (2021b). GCP-GridFEDv2023 scales gridded estimates of CO₂ emissions from
943 EDGARv4.3.2 (Janssens-Maenhout et al., 2019) within national territories to match national emissions
944 estimates provided by the GCB for the years 1959-2022, which were compiled following the methodology
945 described in Section 2.1. Small differences between the systems due to for instance regridding to the transport
946 model resolution, or use of different fossil fuel emissions, are adjusted in the latitudinal partitioning we present,
947 to ensure agreement with the estimate of E_{FOS} in this budget. We also note that the ocean fluxes used as prior by
948 8 out of 14 inversions are part of the suite of the ocean process model or fCO₂-products listed in Section 2.5.
949 Although these fluxes are further adjusted by the atmospheric inversions, it makes the inversion estimates of the
950 ocean fluxes not completely independent of S_{OCEAN} assessed here.

951 To facilitate comparisons to the independent S_{OCEAN} and S_{LAND}, we used the same corrections for transport and
952 outgassing of carbon transported from land to ocean, as done for the observation-based estimates of S_{OCEAN} (see
953 Supplement S.3).

954 The atmospheric inversions are evaluated using vertical profiles of atmospheric CO₂ concentrations (Figure S4).
955 More than 30 aircraft programs over the globe, either regular programs or repeated surveys over at least 9
956 months (except for SH programs), have been used to assess system performance (with space-time observational
957 coverage sparse in the SH and tropics, and denser in NH mid-latitudes; Table S7). The fourteen systems are
958 compared to the independent aircraft CO₂ measurements between 2 and 7 km above sea level between 2001 and
959 2022. Results are shown in Figure S4 and discussed in Supplement S.5.2. One inversion was flagged for
960 concerns after quality control with these observations, as well as assessment of their global growth rate. This
961 makes the number of systems included in the ensemble to be N=13.

962 With a relatively small ensemble of systems that cover at least one full decade (N=9), and which moreover share
963 some a-priori fluxes used with one another, or with the process-based models, it is difficult to justify using their
964 mean and standard deviation as a metric for uncertainty across the ensemble. We therefore report their full range

Formatted: Default Paragraph Font, Font colour: Black

Formatted: Normal, Centred, Border: Top: (No border),
Bottom: (No border), Left: (No border), Right: (No border),
Between : (No border), Tab stops: 7.96 cm, Centred + 15.92
cm, Right, Position: Horizontal: Left, Relative to: Column,
Vertical: In line, Relative to: Margin, Wrap Around

Formatted: Font colour: Black

965 (min-max) without their mean. More details on the atmospheric inversions methodology can be found in
966 Supplement S.5.

967 2.8 Atmospheric oxygen based estimate

968 Long-term atmospheric O₂ and CO₂ observations allow estimation of the global ocean and land carbon sinks,
969 due to the coupling of O₂ and CO₂ with distinct exchange ratios for fossil fuel emissions and land uptake, and
970 uncoupled O₂ and CO₂ ocean exchange (Keeling and Manning, 2014). The global ocean and net land carbon
971 sinks were calculated following methods and constants used in Keeling and Manning (2014), modified to
972 include the effective O₂ source from metal refining (Battle et al., 2023), and using a value of 1.05 for the
973 exchange ratio of the net land sink, following Resplandy et al. (2019). Atmospheric O₂ is observed as $\delta(O_2/N_2)$
974 and combined with CO₂ mole fraction observations into Atmospheric Potential Oxygen (APO, Stephens et al.,
975 1998). The APO observations from 1990 to 2022 were taken from a weighted average of flask records from the
976 three stations in the Scripps O₂ program network (Alert, Canada (ALT), La Jolla, California (LJO), and Cape
977 Grim, Australia (CGO), weighted per Keeling and Manning (2014). Observed CO₂ was taken from the globally
978 averaged marine surface annual mean growth rate from the NOAA/GML Global Greenhouse Gas Reference
979 Network (Lan et al., 2023). The O₂ source from ocean warming is based on ocean heat content from updated
980 data from NOAA/NCEI (Levitus et al., 2012). The effective O₂ source from metal refining is based on
981 production data from Bray (2020), Flanagan (2021), and Tuck (2022). Uncertainty was determined through a
982 Monte Carlo approach with 5,000 iterations, using uncertainties prescribed in Keeling and Manning (2014),
983 including observational uncertainties from Keeling et al. (2007) and autoregressive errors in fossil fuel
984 emissions (Ballantyne et al., 2015). The reported uncertainty is 1 standard deviation of the ensemble.

985 2.9 Earth System Models estimate

986 Reconstructions and predictions from decadal prediction systems based on Earth system models (ESMs) provide
987 a novel line of evidence in assessing the atmosphere-land and atmosphere-ocean carbon fluxes in the past
988 decades and predicting their changes for the current year. The decadal prediction systems based on ESMs used
989 here consist of three sets of simulations: (i) uninitialized freely evolving historical simulations (1850-2014); (ii)
990 assimilation reconstruction incorporating observational data into the model (1980-2022); (iii) initialized
991 prediction simulations for the 1981-2023 period, starting every year from initial states obtained from the above
992 assimilation simulations. The assimilations are designed to reconstruct the actual evolution of the Earth system
993 by assimilating essential fields from data products. The assimilations' states, which are expected to be close to
994 observations, are used to start the initialized prediction simulations used for the current year (2023) global
995 carbon budget. Similar initialized prediction simulations starting every year (Nov. 1st or Jan. 1st) over the 1981-
996 2022 period (i.e., hindcasts) are also performed for predictive skill quantification and for bias correction. More
997 details on the illustration of a decadal prediction system based on an ESM can refer to Figure 1 of Li et al.
998 (2023).

999 By assimilating physical atmospheric and oceanic data products into the ESMs, the models are able to reproduce
1000 the historical variations of the atmosphere-sea CO₂ fluxes, atmosphere-land CO₂ fluxes, and atmospheric CO₂

Formatted: Outline numbered + Level: 2 + Numbering
Style: 1, 2, 3, ... + Start at: 1 + Alignment: Left + Aligned at:
0 cm + Indent at: 1.02 cm

Deleted: but

Deleted: also

Deleted: 2020

Deleted: ESRL

Deleted: one

Formatted: Outline numbered + Level: 2 + Numbering
Style: 1, 2, 3, ... + Start at: 1 + Alignment: Left + Aligned at:
0 cm + Indent at: 1.02 cm

Formatted: Default Paragraph Font, Font colour: Black

Formatted: Normal, Centred, Border: Top: (No border),
Bottom: (No border), Left: (No border), Right: (No border),
Between : (No border), Tab stops: 7.96 cm, Centred + 15.92
cm, Right, Position: Horizontal: Left, Relative to: Column,
Vertical: In line, Relative to: Margin, Wrap Around

Formatted: Font colour: Black

1006 growth rate (Li et al., 2016, 2019; Lovenduski et al., 2019a,b; Ilyina et al., 2021; Li et al., 2023). Furthermore,
1007 the ESM-based predictions have proven their skill in predicting the air-sea CO₂ fluxes for up to 6 years, the air-
1008 land CO₂ fluxes and atmospheric CO₂ growth for 2 years (Lovenduski et al., 2019a,b; Ilyina et al., 2021; Li et
1009 al., 2023). The reconstructions from the fully coupled model simulations ensure a closed budget within the Earth
1010 system, i.e., no budget imbalance term.

1011 Four ESMs, i.e., CanESM5 (Swart et al., 2019; Sospedra-Alfonso et al., 2021), IPSL-CM6A-CO2-LR (Boucher
1012 et al., 2020), MIROC-ES2L (Watanabe et al., 2020), and MPI-ESM1-2-LR (Mauritsen et al., 2019; Li et al., 2023),
1013 have performed the set of prediction simulations. Each ESM uses a different assimilation method and combination
1014 of data products incorporated in the system, more details on the models configuration can be found in Table 4.
1015 The ESMs use external forcings from the Coupled Model Intercomparison Project Phase 6 (CMIP6) historical
1016 (1980-2014) plus SSP2-4.5 baseline and CovidMIP two-year blip scenario (2015-2023) (Eyring et al., 2016; Jones
1017 et al., 2021a). The CO₂ emissions forcing from 2015-2023 are substituted by GCB-GridFED (v2023.1, Jones et
1018 al., 2023) to provide a more realistic forcing. Reconstructions of atmosphere-ocean CO₂ fluxes (SoCEAN) and
1019 atmosphere-land CO₂ fluxes (SLAND-ELUC) for the time period from 1980-2022 are assessed here. Predictions of
1020 the atmosphere-ocean CO₂ flux, atmosphere-land CO₂ flux, and atmospheric CO₂ growth for 2023 are calculated
1021 based on the predictions at a lead time of 1 year. The predictions are bias-corrected using the 1985-2014
1022 climatology mean of GCB2022 (Friedlingstein et al., 2022), more details on methods can be found in Boer et al.
1023 (2016) and Li et al. (2023). The ensemble size of initialized prediction simulations is 10, and the ensemble mean
1024 for each individual model is used here. The ESMs are used here to support the assessment of SoCEAN and net
1025 atmosphere-land CO₂ flux (SLAND - ELUC) over the 1980-2022 period, and to provide an estimate of the 2023
1026 projection of G_{ATM}.

1027 2.10 Processes not included in the global carbon budget

1028 The contribution of anthropogenic CO and CH₄ to the global carbon budget is not fully accounted for in Eq. (1)
1029 and is described in Supplement S.6.1. The contributions to CO₂ emissions of decomposition of carbonates not
1030 accounted for is described in Supplement S.6.2. The contribution of anthropogenic changes in river fluxes is
1031 conceptually included in Eq. (1) in SoCEAN and in SLAND, but it is not represented in the process models used to
1032 quantify these fluxes. This effect is discussed in Supplement S.6.3. Similarly, the loss of additional sink capacity
1033 from reduced forest cover is missing in the combination of approaches used here to estimate both land fluxes
1034 (ELUC and SLAND) and its potential effect is discussed and quantified in Supplement S.6.4.

1035 3 Results

1036 For each component of the global carbon budget, we present results for three different time periods: the full
1037 historical period, from 1850 to 2022, the decades in which we have atmospheric concentration records from
1038 Mauna Loa (1960-2022), a specific focus on last year (2022), and the projection for the current year (2023).
1039 Subsequently, we assess the estimates of the budget components of the last decades against the top-down
1040 constraints from inverse modelling of atmospheric observations, the land/ocean partitioning derived from the
1041 atmospheric O₂ measurements, and the budget components estimates from the ESMs assimilation simulations.

Deleted:

Formatted: Outline numbered + Level: 2 + Numbering
Style: 1, 2, 3, ... + Start at: 1 + Alignment: Left + Aligned at:
0 cm + Indent at: 1.02 cm

Formatted: Indent: Left: 0 cm, First line: 0 cm, Outline
numbered + Level: 1 + Numbering Style: 1, 2, 3, ... + Start
at: 1 + Alignment: Left + Aligned at: 0 cm + Indent at: 0.76
cm

Formatted: Default Paragraph Font, Font colour: Black

Formatted: Normal, Centred, Border: Top: (No border),
Bottom: (No border), Left: (No border), Right: (No border),
Between : (No border), Tab stops: 7.96 cm, Centred + 15.92
cm, Right, Position: Horizontal: Left, Relative to: Column,
Vertical: In line, Relative to: Margin, Wrap Around

Formatted: Font colour: Black

1043 Atmospheric inversions further allow for an assessment of the budget components with a regional breakdown of
1044 land and ocean sinks.

1045 3.1 Fossil CO₂ Emissions

1046 3.1.1 Historical period 1850-2022

1047 Cumulative fossil CO₂ emissions for 1850-2022 were 477 ± 25 GtC, including the cement carbonation sink
1048 (Figure 3, Table 8, with all cumulative numbers rounded to the nearest 5GtC). In this period, 46% of global
1049 fossil CO₂ emissions came from coal, 35% from oil, 15% from natural gas, 3% from decomposition of
1050 carbonates, and 1% from flaring. In 1850, the UK stood for 62% of global fossil CO₂ emissions. In 1891 the
1051 combined cumulative emissions of the current members of the European Union reached and subsequently
1052 surpassed the level of the UK. Since 1917 US cumulative emissions have been the largest. Over the entire
1053 period 1850-2022, US cumulative emissions amounted to 115GtC (24% of world total), the EU27's to 80 GtC
1054 (17%), China's to 70 GtC (15%), and India's to 15 GtC (3%).

1055 In addition to the estimates of fossil CO₂ emissions that we provide here (see Methods), there are three global
1056 datasets with long time series that include all sources of fossil CO₂ emissions: CDIAC-FF (Gilfillan and
1057 Marland, 2021), CEDS version v_2021_04_21 (Hoesly et al., 2018; O'Rourke et al., 2021) and PRIMAP-hist
1058 version 2.4.2 (Gütschow et al., 2016; Gütschow and Pflüger, 2023), although these datasets are not entirely
1059 independent from each other (Andrew, 2020a). CDIAC-FF has the lowest cumulative emissions over 1750-2018
1060 at 440 GtC, GCP has 444 GtC, CEDS 445 GtC, PRIMAP-hist TP 453 GtC, and PRIMAP-hist CR 452 GtC.
1061 CDIAC-FF excludes emissions from lime production. CEDS has higher emissions from international shipping
1062 in recent years, while PRIMAP-hist has higher fugitive emissions than the other datasets. However, in general
1063 these four datasets are in relative agreement as to total historical global emissions of fossil CO₂.

1064 3.1.2 Recent period 1960-2022

1065 Global fossil CO₂ emissions, E_{FOS} (including the cement carbonation sink), have increased every decade from an
1066 average of 3.0 ± 0.2 GtC yr⁻¹ for the decade of the 1960s to an average of 9.6 ± 0.5 GtC yr⁻¹ during 2013-2022
1067 (Table 7, Figure 2 and Figure 5). The growth rate in these emissions decreased between the 1960s and the
1068 1990s, from 4.3% yr⁻¹ in the 1960s (1960-1969), 3.2% yr⁻¹ in the 1970s (1970-1979), 1.6% yr⁻¹ in the 1980s
1069 (1980-1989), to 1.0% yr⁻¹ in the 1990s (1990-1999). After this period, the growth rate began increasing again in
1070 the 2000s at an average growth rate of 2.8% yr⁻¹, decreasing to 0.5% yr⁻¹ for the last decade (2013-2022).
1071 China's emissions increased by +1.6% yr⁻¹ on average over the last 10 years dominating the global trend, and
1072 India's emissions increased by +3.5% yr⁻¹, while emissions decreased in EU27 by -1.7% yr⁻¹, and in the USA
1073 by -1.0% yr⁻¹. Figure 6 illustrates the spatial distribution of fossil fuel emissions for the 2013-2022 period.

1074 E_{FOS} reported here includes the uptake of CO₂ by cement via carbonation which has increased with increasing
1075 stocks of cement products, from an average of 18 MtC yr⁻¹ (0.018 GtC yr⁻¹) in the 1960s to an average of 197
1076 MtC yr⁻¹ (0.197 GtC yr⁻¹) during 2013-2022 (Figure 5).

Formatted: Outline numbered + Level: 2 + Numbering
Style: 1, 2, 3, ... + Start at: 1 + Alignment: Left + Aligned at:
0 cm + Indent at: 1.02 cm

Formatted: Outline numbered + Level: 3 + Numbering
Style: 1, 2, 3, ... + Start at: 1 + Alignment: Left + Aligned at:
0 cm + Indent at: 1.27 cm

Deleted: EU's

Deleted: and

Formatted: Outline numbered + Level: 3 + Numbering
Style: 1, 2, 3, ... + Start at: 1 + Alignment: Left + Aligned at:
0 cm + Indent at: 1.27 cm

Deleted: 20

Deleted: 02

Deleted: 206

Deleted: 21

Formatted: Default Paragraph Font, Font colour: Black

Formatted: Normal, Centred, Border: Top: (No border),
Bottom: (No border), Left: (No border), Right: (No border),
Between : (No border), Tab stops: 7.96 cm, Centred + 15.92
cm, Right, Position: Horizontal: Left, Relative to: Column,
Vertical: In line, Relative to: Margin, Wrap Around

Formatted: Font colour: Black

1083 **3.1.3 Final year 2022**

1084 Global fossil CO₂ emissions were slightly higher, 0.92%, in 2022 than in 2021, with an increase of less than 0.1
1085 GtC to reach 9.9 ± 0.5 GtC (including the 0.2 GtC cement carbonation sink) in 2022 (Figure 5), distributed
1086 among coal (42%), oil (32%), natural gas (21%), cement (4%), flaring (1%), and others (<1%). Compared to the
1087 previous year, 2022 emissions from coal and oil increased by 1.6% and 3.2% respectively, while emissions from
1088 gas and cement respectively decreased by 2.2% and 5.1%. All growth rates presented are adjusted for the leap
1089 year, unless stated otherwise.

Formatted: Outline numbered + Level: 3 + Numbering
Style: 1, 2, 3, ... + Start at: 1 + Alignment: Left + Aligned at:
0 cm + Indent at: 1.27 cm

Deleted: 85...2%, in 2022 than in 2021, with an increase of less than 0.1 GtC to reach 9.9 ± 0.5 GtC (including the 0.2 GtC cement carbonation sink) in 2022 (Figure 5), distributed among coal (41...2%), oil (32%), natural gas (21%), cement (4%), flaring (1%), and others (...<1%). Compared to the previous year, 2022 emissions from coal and oil increased by 1.6% and 3.3...% respectively, while emissions from gas and cement respectively decreased by 2.2% and 5.7 (... [3])

1090 In 2022, the largest absolute contributions to global fossil CO₂ emissions were from China (31%), the USA
1091 (14%), India (8%), and the EU27 (7%). These four regions account for 59% of global fossil CO₂ emissions,
1092 while the rest of the world contributed 41%, including international aviation and marine bunker fuels (2.6% of
1093 the total). Growth rates for these countries from 2021 to 2022 were 0.5% (China), 0.5% (USA), -1.6% (EU27),
1094 and 5.8% (India), with +0.9% for the rest of the world. The per-capita fossil CO₂ emissions in 2022 were 1.3 tC
1095 person⁻¹ yr⁻¹ for the globe, and were 4.1 (USA), 2.2 (China), 1.7 (EU27) and 0.5 (India) tC person⁻¹ yr⁻¹ for the
1096 four highest emitters (Figure 5).

Deleted: 9...% (China), 1...5% (USA), -1.9...% (EU27), and 5.8% (India), with +0.6 (... [4])

1097 **3.1.4 Year 2023 Projection**

1098 Globally, we estimate that global fossil CO₂ emissions (including cement carbonation) will grow by 1.1% in
1099 2023 (0.1% to 2.2%) to 10.1 GtC (36.8 GtCO₂), exceeding the pre-COVID19 2019 emission levels of 9.9 GtC
1100 (36.3 GtCO₂). Global increase in 2023 emissions per fuel types are projected to be +1.3% (range 0.0% to 2.6%)
1101 for coal, +1.5% (range 0.5% to 2.5%) for oil, +0.2% (range -0.6% to 1.1%) for natural gas, and 1.4% (range -
1102 0.3% to 3.0%) for cement.

Formatted: Outline numbered + Level: 3 + Numbering
Style: 1, 2, 3, ... + Start at: 1 + Alignment: Left + Aligned at:
0 cm + Indent at: 1.27 cm

Deleted: 2...% in 2023 (0.2...% to 2.3...%) to 10.0... GtC (36.8 GtCO₂), exceeding the pre-COVID19 2019 emission levels of 9.9 GtC (36.3 GtCO₂). Global increase in 2023 emissions per fuel types are projected to be +1.1...% (range -0.2...% to 2.4...%) for coal, +1.8...% (range 0.8...% to 2.9...%) for oil, +0.3...% (range -0.6% to 1.3...%) for natural gas, and 1.8...% (range -0.2...% to 3.4 (... [5])

1103 For China, projected fossil emissions in 2023 are expected to increase by 4% (range 1.9% to 6.2%) compared
1104 with 2022 emissions, bringing 2023 emissions for China around 3.2 GtC yr⁻¹ (11.9 GtCO₂ yr⁻¹). Changes in fuel
1105 specific projections for China are 3.5% for coal, 7.7% for oil, 6.4% natural gas, and 0.2% for cement.

Deleted: 4...% (range -5.9...% to -1.0.9...) compared to 2022, bringing USA 2023 emissions to around 1.3 GtC yr⁻¹ (4.9 GtCO₂ yr⁻¹). This is based on separate projections for coal -19.9...8.3%, oil -0.7...%, natural gas +1.7...%, and cement -3.2... (... [6])

1106 For the USA, the Energy Information Administration (EIA) emissions projection for 2023 combined with
1107 cement clinker data from USGS gives an decrease of 3.0% (range -5.0% to -1.0%) compared to 2022, bringing
1108 USA 2023 emissions to around 1.3 GtC yr⁻¹ (4.9 GtCO₂ yr⁻¹). This is based on separate projections for coal -
1109 18.3%, oil -0.3%, natural gas +1.4%, and cement -4.0%.

Deleted: 1...% (range -9.6...% to -4.6...%) over 2022, with 2023 emissions around 0.7 GtC yr⁻¹ (2.6 GtCO₂ yr⁻¹). This is based on separate projections for coal of -19.6...8.8%, oil -0.9...5%, natural gas -6.6%, and cement unchanged. (... [7])

1110 For the European Union, our projection for 2023 is for a decrease of 7.4% (range -9.9% to -4.9%) over 2022,
1111 with 2023 emissions around 0.7 GtC yr⁻¹ (2.6 GtCO₂ yr⁻¹). This is based on separate projections for coal of -
1112 18.8%, oil -1.5%, natural gas -6.6%, and cement -8.7%.

Deleted: 9...% to 8.0...0.2%) over 2022, with 2023 emissions around 0.8 GtC yr⁻¹ (3.1 GtCO₂ yr⁻¹). This is based on separate projections for coal of +9.2...0.1%, oil +5.2...%, natural gas +4.4...6%, and cement +8.1 (... [8])

1113 For India, our projection for 2023 is an increase of 8.7% (range of 7.2% to 10.2%) over 2022, with 2023
1114 emissions around 0.8 GtC yr⁻¹ (3.1 GtCO₂ yr⁻¹). This is based on separate projections for coal of +10.1%, oil
1115 +5.3%, natural gas +5.6%, and cement +8.8%.

Formatted: Default Paragraph Font, Font colour: Black

Formatted: Normal, Centred, Border: Top: (No border), Bottom: (No border), Left: (No border), Right: (No border), Between : (No border), Tab stops: 7.96 cm, Centred + 15.92 cm, Right, Position: Horizontal: Left, Relative to: Column, Vertical: In line, Relative to: Margin, Wrap Around

Formatted: Font colour: Black

1190 For the rest of the world, the expected growth rate for 2023 is 0.5% (range -1.2% to 2.2%) with 2023 emissions
1191 around 4.2 GtC yr⁻¹ (15.2 GtCO₂ yr⁻¹). The fuel-specific projected 2023 growth rates for the rest of the world
1192 are: +0.8% for coal, +0.8% for oil, -0.4% for natural gas, +2.4% for cement.

1193 3.2 Emissions from Land Use Changes

1194 3.2.1 Historical period 1850-2022

1195 Cumulative CO₂ emissions from land-use changes (E_{LUC}) for 1850-2022 were 220 ± 65 GtC (Table 8; Figure 3;
1196 Figure 15). The cumulative emissions from E_{LUC} show a large spread among individual estimates of 150 GtC
1197 (H&C2023), 290 GtC (BLUE), and 215 GtC (OSCAR) for the three bookkeeping models and a similar wide
1198 estimate of 210 ± 65 GtC for the DGVMs (all cumulative numbers are rounded to the nearest 5 GtC). These
1199 estimates are broadly consistent with indirect constraints from vegetation biomass observations, giving
1200 cumulative emissions of 155 ± 50 GtC over the 1901-2012 period (Li et al., 2017). However, given the large
1201 spread, a best estimate is difficult to ascertain.

1202 3.2.2 Recent period 1960-2022

1203 In contrast to growing fossil emissions, CO₂ emissions from land-use, land-use change, and forestry remained
1204 relatively constant over the 1960-1999 period. Since the 1990s they have shown a slight decrease of about 0.1
1205 GtC per decade, reaching 1.3 ± 0.7 GtC yr⁻¹ for the 2013-2022 period (Table 7), but with large spread across
1206 estimates (Table 5, Figure 7). Different from the bookkeeping average, the DGVMs average grows slightly
1207 larger over the 1970-2022 period and shows no sign of decreasing emissions in the recent decades (Table 5,
1208 Figure 7). This is, however, expected as DGVM-based estimates include the loss of additional sink capacity,
1209 which grows with time, while the bookkeeping estimates do not (Supplement S.6.4).

1210 We separate net E_{LUC} into five component fluxes to gain further insight into the drivers of net emissions:
1211 deforestation, forest (re-)growth, wood harvest and other forest management, peat drainage and peat fires, and
1212 all other transitions (Figure 7c; Sec. C.2.1). We further decompose the deforestation and the forest (re-)growth
1213 term into contributions from shifting cultivation vs permanent forest cover changes (Figure 7d). Averaged over
1214 the 2013-2022 period and over the three bookkeeping estimates, fluxes from deforestation amount to 1.9 [1.5 to
1215 2.4] GtC yr⁻¹ (Table 5), of which 1.1 [1.0, 1.2] GtC yr⁻¹ are from permanent deforestation. Fluxes from forest
1216 (re-)growth amount to -1.3 [-1.5, -0.9] GtC yr⁻¹ (Table 5), of which -0.5 [-0.8 to -0.2] GtC yr⁻¹ are from
1217 re/afforestation and the remainder from forest regrowth in shifting cultivation cycles. Emissions from wood
1218 harvest and other forest management (0.2 [0.0, 0.6] GtC yr⁻¹), peat drainage and peat fires (0.3 [0.3, 0.3] GtC yr⁻¹)
1219 and the net flux from other transitions (0.1 [0.0, 0.3] GtC yr⁻¹) are substantially less important globally (Table
1220 5). However, the small net flux from wood harvest and other forest management contains substantial gross
1221 fluxes that largely compensate each other (see Figure S7): 1.3 [0.9, 2.0] GtC yr⁻¹ emissions result from the
1222 decomposition of slash and the decay of wood products and -1.1 [-1.3, -0.8] GtC yr⁻¹ removals result from
1223 regrowth after wood harvesting. This split into component fluxes clarifies the potentials for emission reduction
1224 and carbon dioxide removal: the emissions from permanent deforestation - the largest of our component fluxes -

Deleted: 9

Deleted: 0.8

Deleted: 6

Deleted: 1

Deleted: 1.5

Deleted: 3

Deleted: 6

Formatted: Outline numbered + Level: 2 + Numbering
Style: 1, 2, 3, ... + Start at: 1 + Alignment: Left + Aligned at:
0 cm + Indent at: 1.02 cm

Formatted: Outline numbered + Level: 3 + Numbering
Style: 1, 2, 3, ... + Start at: 1 + Alignment: Left + Aligned at:
0 cm + Indent at: 1.27 cm

Formatted: Outline numbered + Level: 3 + Numbering
Style: 1, 2, 3, ... + Start at: 1 + Alignment: Left + Aligned at:
0 cm + Indent at: 1.27 cm

Formatted: Default Paragraph Font, Font colour: Black

Formatted: Normal, Centred, Border: Top: (No border),
Bottom: (No border), Left: (No border), Right: (No border),
Between: (No border), Tab stops: 7.96 cm, Centred + 15.92
cm, Right, Position: Horizontal: Left, Relative to: Column,
Vertical: In line, Relative to: Margin, Wrap Around

Formatted: Font colour: Black

1232 could be halted (largely) without compromising carbon uptake by forests, contributing substantially to emissions
1233 reduction. By contrast, reducing wood harvesting would have limited potential to reduce emissions as it would
1234 be associated with less forest regrowth; removals and emissions cannot be decoupled here on long timescales. A
1235 similar conclusion applies to removals and emissions from shifting cultivation, which we have therefore
1236 separated out. Carbon Dioxide Removal (CDR) in forests could instead be increased by permanently increasing
1237 the forest cover through re/afforestation. Our estimate of about -0.5 [-0.8 , -0.2] GtC yr^{-1} (of which about two
1238 thirds are located in non-Annex-I countries, in particular in China) removed on average each year during 2013-
1239 2022 by re/afforestation is very similar to independent estimates that were derived from NGHGs for 2022.
1240 Re/afforestation constitutes the vast majority of all current CDR (Powis et al., 2023). Though they cannot be
1241 compared directly to annual fluxes from the atmosphere, CDR through transfers between non-atmospheric
1242 reservoirs such as in durable HWP, biochar or BECCS comprise much smaller amounts of carbon. 61 MtC yr^{-1}
1243 have been estimated to be transferred to HWP in 2022, and BECCS projects have been estimated to store 0.5
1244 MtC yr^{-1} in geological projects worldwide (Powis et al., 2023). “Blue carbon”, i.e. coastal wetland management
1245 such as restoration of mangrove forests, saltmarshes and seagrass meadows, though at the interface of land and
1246 ocean carbon fluxes, are counted towards the land-use sector as well. Currently, bookkeeping models do not
1247 include blue carbon; however, current CDR deployment in coastal wetlands is small globally, less than
1248 [0.003MtC yr⁻¹ \(Powis et al., 2023\).](#)

Deleted: .

1249 The small declining trend of E_{LUC} over the last three decades is a result of total deforestation emissions showing
1250 no clear trend, while forest regrowth has provided steadily increasing removals. Since the processes behind
1251 gross removals, foremost forest regrowth and soil recovery, are all slow, while gross emissions include a large
1252 instantaneous component, short-term changes in land-use dynamics, such as a temporary decrease in
1253 deforestation, influences gross emissions dynamics more than gross removals dynamics, which rather are a
1254 response to longer-term dynamics. Component fluxes often differ more across the three bookkeeping estimates
1255 than the net flux, which is expected due to different process representation; in particular, treatment of shifting
1256 cultivation, which increases both gross emissions and removals, differs across models, but also net and gross
1257 wood harvest fluxes show high uncertainty. By contrast, models agree relatively well for emissions from
1258 permanent deforestation emissions and removals by re/afforestation.

1259 Overall, highest land-use emissions occur in the tropical regions of all three continents. The top three emitters
1260 (both cumulatively 1959-2022 and on average over 2013-2022) are Brazil (in particular the Amazon Arc of
1261 Deforestation), Indonesia and the Democratic Republic of the Congo, with these 3 countries contributing 0.7
1262 GtC yr^{-1} or 55% of the global net land-use emissions (average over 2013-2022) (Figure 6b). This is related to
1263 massive expansion of cropland, particularly in the last few decades in Latin America, Southeast Asia, and sub-
1264 Saharan Africa (Hong et al., 2021), to a substantial part for export of agricultural products (Pendrill et al., 2019).
1265 Emission intensity is high in many tropical countries, particularly of Southeast Asia, due to high rates of land
1266 conversion in regions of carbon-dense and often still pristine, undegraded natural forests (Hong et al., 2021).
1267 Emissions are further increased by peat fires in equatorial Asia (GFED4s, van der Werf et al., 2017). Uptake due
1268 to land-use change occurs, particularly in Europe, partly related to expanding forest area as a consequence of the

Formatted: Default Paragraph Font, Font colour: Black

Formatted: Normal, Centred, Border: Top: (No border), Bottom: (No border), Left: (No border), Right: (No border), Between: (No border), Tab stops: 7.96 cm, Centred + 15.92 cm, Right, Position: Horizontal: Left, Relative to: Column, Vertical: In line, Relative to: Margin, Wrap Around

Formatted: Font colour: Black

1270 forest transition in the 19th and 20th century and subsequent regrowth of forest (Figure 6b) (Mather 2001;
1271 McGrath et al., 2015).

1272 While the mentioned patterns are robust and supported by independent literature, we acknowledge that model
1273 spread is substantially larger on regional than global levels, as has been shown for bookkeeping models (Bastos
1274 et al., 2021) as well as DGVMs (Obermeier et al., 2021). Assessments for individual regions will be performed
1275 as part of REgional Carbon Cycle Assessment and Processes (RECCAP2; Ciais et al., 2020, Poulter et al., 2022)
1276 or already exist for selected regions (e.g., for Europe by Petrescu et al., 2020, for Brazil by Rosan et al., 2021,
1277 for 8 selected countries/regions in comparison to inventory data by Schwingshackl et al., 2022).

1278 ~~As mentioned before, the NGHGI data under the LULUCF sector or data submitted by countries to FAOSTAT~~
1279 differ from the global models' definition of E_{LUC}. In the NGHGI reporting, the natural fluxes (S_{LAND}) are
1280 counted towards E_{LUC} when they occur on managed land (Grassi et al., 2018). ~~To compare our results to the~~
1281 NGHGI approach, we perform a translation of our E_{LUC} estimates by subtracting S_{LAND} in managed forest from
1282 the DGVMs simulations (following [the methodology described in](#) Grassi et al., 2023) from the bookkeeping
1283 E_{LUC} estimate (see Supplement S.2.3). For the 2013-2022 period, we estimate that 2.0 GtC yr⁻¹ of S_{LAND}
1284 occurred in managed forests. Subtracting this value from E_{LUC} changes E_{LUC} from being a source of 1.3 GtC yr⁻¹
1285 to a sink of 0.8 GtC yr⁻¹, very similar to the NGHGI estimate that yields a sink of 0.7 GtC yr⁻¹ (Table 9). The
1286 translation approach has been shown to be generally applicable also on country-level (Grassi et al., 2023;
1287 Schwingshackl et al., 2022). Country-level analysis suggests, e.g., that the bookkeeping method estimates higher
1288 deforestation emissions than the national report in Indonesia, but less CO₂ removal by afforestation than the
1289 national report in China. The fraction of the natural CO₂ sinks that the NGHGI estimates include differs
1290 substantially across countries, related to varying proportions of managed vs total forest areas (Schwingshackl et
1291 al., 2022). By comparing E_{LUC} and NGHGI on the basis of the component fluxes used above, we find that our
1292 estimates reproduce very closely the NGHGI estimates for emissions from permanent deforestation (1.1 GtC yr⁻¹
1293 averaged over 2013-2022). Forest fluxes, that is, (re-)growth from re/afforestation plus the net flux from wood
1294 harvesting and other forest management, constitute a large sink in the NGHGI (-1.9 GtC yr⁻¹ averaged over
1295 2013-2022), since they also include S_{LAND} in managed forests. Summing up the bookkeeping estimates of (re-
1296)growth from re/afforestation and the net flux from wood harvesting and other forest management and adding
1297 S_{LAND} in managed forests yields a flux of -2.3 GtC yr⁻¹ (averaged over 2013-2022), which compares well with
1298 the NGHGI estimate. Emissions from organic soils in NGHGI are similar to the estimates based on the
1299 bookkeeping approach and the external peat drainage and burning datasets. The net flux from other transitions is
1300 small in both NGHGI and bookkeeping estimates, but a difference in sign (small source in bookkeeping
1301 estimates, small sink in NGHGI) creates a notable difference between NGHGI and bookkeeping estimates.
1302 Though estimates between NGHGI, FAOSTAT and the translated budget estimates still differ in value and need
1303 further analysis, the approach suggested by Grassi et al. (2023), which we adopt here, provides a feasible way to
1304 relate the global models' and NGHGI approach to each other and thus link the anthropogenic carbon budget
1305 estimates of land CO₂ fluxes directly to the Global Stocktake, as part of UNFCCC Paris Agreement.

Deleted: National GHG inventory

Deleted: (NGHGI)

Deleted: In order to

Deleted: 2021

Formatted: Default Paragraph Font, Font colour: Black

Formatted: Normal, Centred, Border: Top: (No border),
Bottom: (No border), Left: (No border), Right: (No border),
Between : (No border), Tab stops: 7.96 cm, Centred + 15.92
cm, Right, Position: Horizontal: Left, Relative to: Column,
Vertical: In line, Relative to: Margin, Wrap Around

Formatted: Font colour: Black

1310 **3.2.3 Final year 2022**

1311 The global CO₂ emissions from land-use change are estimated as 1.2 ± 0.7 GtC in 2022, similar to the 2020 and
1312 2021 estimates. However, confidence in the annual change remains low. Effects of the COVID-19 pandemic on
1313 land-use change have turned out to be country-specific as global market mechanisms, national economics and
1314 changes in household income all could act to curb or enhance deforestation (Wunder et al., 2021). Concerns
1315 about enhanced deforestation due to weakened environmental protection and monitoring in tropical countries
1316 (Brancalion et al., 2020, Vale et al., 2021) have been confirmed only for some countries (Cespedes et al., 2023).
1317 For example, a recent study suggests slightly increased deforestation rates for the Democratic Republic of
1318 Congo linked in particular to post-pandemic economic recovery in the mining sector, while deforestation trends
1319 in Brazil seem to have been unaffected. Land use dynamics may be further altered by the Russian invasion of
1320 Ukraine, but scientific evidence related to international dependencies (like a shift to tropical palm oil to alleviate
1321 dependencies on sunflower oil) so far is very limited and recent changes will not be reflected by the land-use
1322 forcing applied in the global models. High food prices, which preceded but were exacerbated by the war (FAO,
1323 2022), are generally linked to higher deforestation (Angelsen and Kaimowitz, 1999). A new wave of cropland
1324 abandonment in the conflict region may increase the substantial Eastern European carbon sink due to land-use
1325 changes, but sanctions being placed on trade may also incentivise domestic agricultural production, thus leading
1326 to recultivation of abandoned areas in Russia (Winkler et al., 2023).

Formatted: Outline numbered + Level: 3 + Numbering
Style: 1, 2, 3, ... + Start at: 1 + Alignment: Left + Aligned at:
0 cm + Indent at: 1.27 cm

1327 **3.2.4 Year 2023 Projection**

1328 In Indonesia, peat fire emissions are below average (12 Tg C through September 29 2023) despite El Niño
1329 conditions, which in general lead to more fires. Tropical deforestation and degradation fires in Indonesia are
1330 around average (13 Tg C through September 29 2023), but higher than in the previous year, which had a
1331 relatively wet dry season (GFED4.1s, van der Werf et al., 2017; see also
1332 https://www.geo.vu.nl/~gwerf/GFED/GFED4/tables/GFED4.1s_C.txt). In South America, emissions from
1333 tropical deforestation and degradation fires are among the lowest over the last decades (64 Tg C through
1334 September 29 2023). Effects of the El Niño in the Amazon, such as droughts, are not expected before 2024.
1335 Disentangling the degree to which interannual variability in rainfall patterns and stronger environmental
1336 protection measures in both Indonesia after their 2015 high fire season and in Brazil after the change in
1337 government in Brazil play a role in this is an important research topic. Cumulative fire emission estimates
1338 through September 29 2023 are 155 Tg C for global deforestation and degradation fires and 12 Tg C for
1339 peatland fires in Indonesia (https://www.geo.vu.nl/~gwerf/GFED/GFED4/tables/GFED4.1s_C.txt).

Formatted: Outline numbered + Level: 3 + Numbering
Style: 1, 2, 3, ... + Start at: 1 + Alignment: Left + Aligned at:
0 cm + Indent at: 1.27 cm

1340 Based on these estimates, we expect E_{LUC} emissions of around 1.1 GtC (4.1 GtCO₂) in 2023. Our preliminary
1341 estimate of E_{LUC} for 2023 is substantially lower than the 2013-2022 average, which saw years of anomalously
1342 dry conditions in Indonesia and high deforestation fires in South America (Friedlingstein et al., 2022b). Note
1343 that although our extrapolation includes tropical deforestation and degradation fires, degradation attributable to
1344 selective logging, edge-effects or fragmentation is not captured. Further, deforestation and fires in deforestation
1345 zones may become more disconnected, partly due to changes in legislation in some regions. For example, Van

Formatted: Default Paragraph Font, Font colour: Black

Formatted: Normal, Centred, Border: Top: (No border),
Bottom: (No border), Left: (No border), Right: (No border),
Between : (No border), Tab stops: 7.96 cm, Centred + 15.92
cm, Right, Position: Horizontal: Left, Relative to: Column,
Vertical: In line, Relative to: Margin, Wrap Around

Formatted: Font colour: Black

1346 Wees et al. (2021) found that the contribution from fires to forest loss decreased in the Amazon and in Indonesia
1347 over the period of 2003-2018.

1348 3.3 CDR not based on vegetation

1349 Besides the CDR through land-use (Sec. 3.2), the atmosphere to geosphere flux of carbon resulting from carbon
1350 dioxide removal (CDR) activity is currently 0.003 MtC/yr, with 0.002 MtC/yr of DACCS and 0.001 MtC/yr of
1351 enhanced weathering projects. This represents an offset of about 0.03% of current fossil fuel emissions.

1352 3.4 Total anthropogenic emissions

1353 Cumulative anthropogenic CO₂ emissions for 1850-2022 totalled 695 ± 70 GtC (2550 ± 260 GtCO₂), of which
1354 70% (485 GtC) occurred since 1960 and 33% (235 GtC) since 2000 (Table 7 and 8). Total anthropogenic
1355 emissions more than doubled over the last 60 years, from 4.6 ± 0.7 GtC yr⁻¹ for the decade of the 1960s to an
1356 average of 10.9 ± 0.8 GtC yr⁻¹ during 2013-2022, and reaching 11.1 ± 0.9 GtC (40.7 ± 3.3 GtCO₂) in 2022. For
1357 2023, we project global total anthropogenic CO₂ emissions from fossil and land use changes to be also around
1358 11.2 GtC (40.9 GtCO₂). All values here include the cement carbonation sink (currently about 0.2 GtC yr⁻¹).

1359 During the historical period 1850-2022, 31% of historical emissions were from land use change and 69% from
1360 fossil emissions. However, fossil emissions have grown significantly since 1960 while land use changes have
1361 not, and consequently the contributions of land use change to total anthropogenic emissions were smaller during
1362 recent periods (18% during the period 1960-2022 and down to 12% over the 2013-2022 period).

1363 3.5 Atmospheric CO₂

1364 3.5.1 Historical period 1850-2022

1365 Atmospheric CO₂ concentration was approximately 278 parts per million (ppm) in 1750, reaching 300 ppm in
1366 the 1910s, 350 ppm in the late 1980s, and reaching 417.07 ± 0.1 ppm in 2022 (Lan et al., 2023; Figure 1). The
1367 mass of carbon in the atmosphere increased by 48% from 590 GtC in 1750 to 886 GtC in 2022. Current CO₂
1368 concentrations in the atmosphere are unprecedented in the last 2 million years and the current rate of
1369 atmospheric CO₂ increase is at least 10 times faster than at any other time during the last 800,000 years
1370 (Canadell et al., 2021).

1371 3.5.2 Recent period 1960-2022

1372 The growth rate in atmospheric CO₂ level increased from 1.7 ± 0.07 GtC yr⁻¹ in the 1960s to 5.2 ± 0.02 GtC yr⁻¹
1373 during 2013-2022 with important decadal variations (Table 7, Figure 3 and Figure 4). During the last decade
1374 (2013-2022), the growth rate in atmospheric CO₂ concentration continued to increase, albeit with large
1375 interannual variability (Figure 4).

Formatted: Outline numbered + Level: 2 + Numbering
Style: 1, 2, 3, ... + Start at: 1 + Alignment: Left + Aligned at:
0 cm + Indent at: 1.02 cm

Formatted: Outline numbered + Level: 2 + Numbering
Style: 1, 2, 3, ... + Start at: 1 + Alignment: Left + Aligned at:
0 cm + Indent at: 1.02 cm

Deleted: ,

Formatted: Indent: Left: 0 cm, First line: 0 cm, Outline
numbered + Level: 2 + Numbering Style: 1, 2, 3, ... + Start
at: 1 + Alignment: Left + Aligned at: 0 cm + Indent at: 1.02
cm

Formatted: Outline numbered + Level: 3 + Numbering
Style: 1, 2, 3, ... + Start at: 1 + Alignment: Left + Aligned at:
0 cm + Indent at: 1.27 cm

Formatted: Outline numbered + Level: 3 + Numbering
Style: 1, 2, 3, ... + Start at: 1 + Alignment: Left + Aligned at:
0 cm + Indent at: 1.27 cm

Formatted: Default Paragraph Font, Font colour: Black

Formatted: Normal, Centred, Border: Top: (No border),
Bottom: (No border), Left: (No border), Right: (No border),
Between: (No border), Tab stops: 7.96 cm, Centred + 15.92
cm, Right, Position: Horizontal: Left, Relative to: Column,
Vertical: In line, Relative to: Margin, Wrap Around

Formatted: Font colour: Black

1377 The airborne fraction (AF), defined as the ratio of atmospheric CO₂ growth rate to total anthropogenic
1378 emissions:

$$1379 \quad AF = G_{ATM} / (E_{FOS} + E_{LUC}) \quad (2)$$

1380 provides a diagnostic of the relative strength of the land and ocean carbon sinks in removing part of the
1381 anthropogenic CO₂ perturbation. The evolution of AF over the last 60 years shows no significant trend,
1382 remaining at around 44%, albeit showing a large interannual and decadal variability driven by the year-to-year
1383 variability in G_{ATM} (Figure 9). The observed stability of the airborne fraction over the 1960-2020 period
1384 indicates that the ocean and land CO₂ sinks have been removing on average about 56% of the anthropogenic
1385 emissions (see Sections 3.6.2 and 3.7.2).

1386 3.5.3 Final year 2022

1387 The growth rate in atmospheric CO₂ concentration was 4.6 ± 0.2 GtC (2.18 ± 0.08 ppm) in 2022 (Figure 4; Lan
1388 et al., 2023), below the 2021 growth rate (5.2 ± 0.2 GtC) or the 2013-2022 average (5.2 ± 0.02 GtC).

1389 3.5.4 Year 2023 Projection

1390 The 2023 growth in atmospheric CO₂ concentration (G_{ATM}) is projected to be about 5.1 GtC (2.4 ppm). This is
1391 the average of the GCB regression method (5.07 GtC, 2.39 ppm) and ESMs the multi-model mean (5.11 GtC,
1392 2.41 ppm). The 2023 atmospheric CO₂ concentration, averaged over the year, is expected to reach the level of
1393 419.3 ppm, 51% over the pre-industrial level.

1394 3.6 Ocean Sink

1395 3.6.1 Historical period 1850-2022

1396 Cumulated since 1850, the ocean sink adds up to 180 ± 35 GtC, with more than two thirds of this amount (125
1397 GtC) being taken up by the global ocean since 1960. Over the historical period, the ocean sink increased in pace
1398 with the anthropogenic emissions exponential increase (Figure 3). Since 1850, the ocean has removed 26% of
1399 total anthropogenic emissions.

1400 3.6.2 Recent period 1960-2022

1401 The ocean CO₂ sink increased from 1.1 ± 0.4 GtC yr⁻¹ in the 1960s to 2.8 ± 0.4 GtC yr⁻¹ during 2013-2022
1402 (Table 7), with interannual variations of the order of a few tenths of GtC yr⁻¹ (Figure 10). The ocean-borne
1403 fraction (S_{OCEAN}/(E_{FOS}+E_{LUC})) has been remarkably constant around 25% on average (Figure 9c), with variations
1404 around this mean illustrating the decadal variability of the ocean carbon sink. So far, there is no indication of a
1405 decrease in the ocean-borne fraction from 1960 to 2022. The increase of the ocean sink is primarily driven by
1406 the increased atmospheric CO₂ concentration, with the strongest CO₂ induced signal in the North Atlantic and
1407 the Southern Ocean (Figure 11a). The effect of climate change is much weaker, reducing the ocean sink globally

Formatted: Outline numbered + Level: 3 + Numbering
Style: 1, 2, 3, ... + Start at: 1 + Alignment: Left + Aligned at:
0 cm + Indent at: 1.27 cm

Formatted: Outline numbered + Level: 3 + Numbering
Style: 1, 2, 3, ... + Start at: 1 + Alignment: Left + Aligned at:
0 cm + Indent at: 1.27 cm

Deleted: 4.0

Deleted: 1.89

Deleted: Holt-Winters

Deleted: 3.7

Deleted: 1.73

Deleted: 4.4

Deleted: 05

Deleted: 2

Formatted: Indent: Left: 0 cm, First line: 0 cm, Outline
numbered + Level: 2 + Numbering Style: 1, 2, 3, ... + Start
at: 1 + Alignment: Left + Aligned at: 0 cm + Indent at: 1.02
cm

Formatted: Outline numbered + Level: 3 + Numbering
Style: 1, 2, 3, ... + Start at: 1 + Alignment: Left + Aligned at:
0 cm + Indent at: 1.27 cm

Formatted: Outline numbered + Level: 3 + Numbering
Style: 1, 2, 3, ... + Start at: 1 + Alignment: Left + Aligned at:
0 cm + Indent at: 1.27 cm

Formatted: Default Paragraph Font, Font colour: Black

Formatted: Normal, Centred, Border: Top: (No border),
Bottom: (No border), Left: (No border), Right: (No border),
Between : (No border), Tab stops: 7.96 cm, Centred + 15.92
cm, Right, Position: Horizontal: Left, Relative to: Column,
Vertical: In line, Relative to: Margin, Wrap Around

Formatted: Font colour: Black

1416 by $0.16 \pm 0.04 \text{ GtC yr}^{-1}$ (-6.7% of SOCEAN) during 2013-2022 (all models simulate a weakening of the ocean sink
1417 by climate change, range -4.3 to -10.3%), and does not show clear spatial patterns across the GOBMs ensemble
1418 (Figure 11b). This is the combined effect of change and variability in all atmospheric forcing fields, previously
1419 attributed, in one model, to wind and temperature changes (LeQuéré et al., 2010).

1420 The global net air-sea CO_2 flux is a residual of large natural and anthropogenic CO_2 fluxes into and out of the
1421 ocean with distinct regional and seasonal variations (Figure 6 and B1). Natural fluxes dominate on regional
1422 scales, but largely cancel out when integrated globally (Gruber et al., 2009). Mid-latitudes in all basins and the
1423 high-latitude North Atlantic dominate the ocean CO_2 uptake where low temperatures and high wind speeds
1424 facilitate CO_2 uptake at the surface (Takahashi et al., 2009). In these regions, formation of mode, intermediate
1425 and deep-water masses transport anthropogenic carbon into the ocean interior, thus allowing for continued CO_2
1426 uptake at the surface. Outgassing of natural CO_2 occurs mostly in the tropics, especially in the equatorial
1427 upwelling region, and to a lesser extent in the North Pacific and polar Southern Ocean, mirroring a well-
1428 established understanding of regional patterns of air-sea CO_2 exchange (e.g., Takahashi et al., 2009, Gruber et
1429 al., 2009). These patterns are also noticeable in the Surface Ocean CO_2 Atlas (SOCAT) dataset, where an ocean
1430 $f\text{CO}_2$ value above the atmospheric level indicates outgassing (Figure S1). This map further illustrates the data-
1431 sparsity in the Indian Ocean and the southern hemisphere in general.

1432 Interannual variability of the ocean carbon sink is driven by climate variability with a first-order effect from a
1433 stronger ocean sink during large El Niño events (e.g., 1997-1998) (Figure 10; Rödenbeck et al., 2014, Hauck et
1434 al., 2020; McKinley et al. 2017). The GOBMs show the same patterns of decadal variability as the mean of the
1435 $f\text{CO}_2$ -products, with a stagnation of the ocean sink in the 1990s and a strengthening since the early 2000s
1436 (Figure 10; Le Quéré et al., 2007; Landschützer et al., 2015, 2016; DeVries et al., 2017; Hauck et al., 2020;
1437 McKinley et al., 2020, Gruber et al., 2023). Different explanations have been proposed for this decadal
1438 variability, ranging from the ocean's response to changes in atmospheric wind and pressure systems (e.g., Le
1439 Quéré et al., 2007, Keppeler and Landschützer, 2019), including variations in upper ocean overturning circulation
1440 (DeVries et al., 2017) to the eruption of Mount Pinatubo and its effects on sea surface temperature and slowed
1441 atmospheric CO_2 growth rate in the 1990s (McKinley et al., 2020). The main origin of the decadal variability is
1442 a matter of debate with a number of studies initially pointing to the Southern Ocean (see review in Canadell et
1443 al., 2021), but also contributions from the North Atlantic and North Pacific (Landschützer et al., 2016, DeVries
1444 et al., 2019), or a global signal (McKinley et al., 2020) were proposed.

1445 Although all individual GOBMs and $f\text{CO}_2$ -products fall within the observational constraint, the ensemble means
1446 of GOBMs, and $f\text{CO}_2$ -products adjusted for the riverine flux diverge over time with a mean offset increasing
1447 from 0.30 GtC yr^{-1} in the 1990s to 0.57 GtC yr^{-1} in the decade 2013-2022 and reaching 0.61 GtC yr^{-1} in 2022.
1448 The SOCEAN positive trend over time diverges by a factor two since 2002 (GOBMs: $0.24 \pm 0.07 \text{ GtC yr}^{-1}$ per
1449 decade, $f\text{CO}_2$ -products: $0.48 \pm 0.11 \text{ GtC yr}^{-1}$ per decade, SOCEAN : 0.36 GtC yr^{-1} per decade) and by a factor of 2.5
1450 since 2010 (GOBMs: $0.16 \pm 0.15 \text{ GtC yr}^{-1}$ per decade, $f\text{CO}_2$ -products: $0.42 \pm 0.18 \text{ GtC yr}^{-1}$ per decade, SOCEAN :
1451 0.29 GtC yr^{-1} per decade). The $f\text{CO}_2$ -product estimate is slightly different compared to Friedlingstein et al.

Formatted: Default Paragraph Font, Font colour: Black

Formatted: Normal, Centred, Border: Top: (No border),
Bottom: (No border), Left: (No border), Right: (No border),
Between : (No border), Tab stops: 7.96 cm, Centred + 15.92
cm, Right, Position: Horizontal: Left, Relative to: Column,
Vertical: In line, Relative to: Margin, Wrap Around

Formatted: Font colour: Black

1452 (2022b) as a result of an updated submission of the NIES-ML3 product (previously NIES-NN), however the
1453 difference in the integrated mean flux is small.

1454 The discrepancy between the two types of estimates stems from a larger S_{OCEAN} trend in the northern and
1455 southern extra-tropics since around 2002 (Figure 13). Note that the discrepancy in the mean flux, which was
1456 located in the Southern Ocean in previous versions of the GCB, has been reduced due to the choice of the
1457 regional river flux adjustment (Lacroix et al., 2020 instead of Aumont et al., 2001). This comes at the expense of
1458 a new discrepancy in the mean S_{OCEAN} of about 0.2 GtC yr^{-1} in the tropics. Likely explanations for the
1459 discrepancy in the trends in the high-latitudes are data sparsity and uneven data distribution (Bushinsky et al.,
1460 2019, Gloege et al., 2021, Hauck et al., 2023). In particular, two fCO_2 -products that are part of the GCB
1461 ensemble were shown to overestimate the Southern Ocean CO_2 flux trend by 50 and 130% based on current
1462 sampling in a model subsampling experiment (Hauck et al., 2023). Another likely contributor to the discrepancy
1463 between GOBMs and fCO_2 -products are model biases (as indicated by the large model spread in the South,
1464 Figure 13, and the larger model-data fCO_2 mismatch, Figure S2).

1465 In previous GCB releases, the ocean sink 1959-1989 was only estimated by GOBMs due to the absence of fCO_2
1466 observations. Now, the first data-based estimates extending back to 1957/58 are becoming available (Jena-MLS,
1467 Rödenbeck et al., 2022, LDEO-HPD, Bennington et al., 2022; Gloege et al., 2022). These are based on a multi-
1468 linear regression of pCO_2 with environmental predictors (Rödenbeck et al., 2022) or on model-data pCO_2 misfits
1469 and their relation to environmental predictors (Bennington et al., 2022). The Jena-MLS and LDEO-HPD
1470 estimates fall well within the range of GOBM estimates and have a correlation of 0.99 and 0.98 respectively
1471 with S_{OCEAN} for the period 1959-2022 (and 0.98 and 0.97 for the 1959-1989 period). They agree well on the
1472 mean S_{OCEAN} estimate since 1977 with a slightly higher amplitude of variability (Figure 10). Until 1976, Jena-
1473 MLS and LDEO-HPD are respectively about 0.25 GtCyr^{-1} and about 0.1 GtCyr^{-1} below the central S_{OCEAN}
1474 estimate. The agreement especially on phasing of variability is impressive in both products, and the
1475 discrepancies in the mean flux 1959-1976 could be explained by an overestimated trend of Jena-MLS
1476 (Rödenbeck et al., 2022). Bennington et al. (2022) report a larger flux into the pre-1990 ocean than in Jena-
1477 MLS, although lower than S_{OCEAN} .

1478 The reported S_{OCEAN} estimate from GOBMs and fCO_2 -products is $2.2 \pm 0.4 \text{ GtC yr}^{-1}$ over the period 1994 to
1479 2007, which is in excellent agreement with the ocean interior estimate of $2.2 \pm 0.4 \text{ GtC yr}^{-1}$, which accounts for
1480 the climate effect on the natural CO_2 flux of $-0.4 \pm 0.24 \text{ GtC yr}^{-1}$ (Gruber et al., 2019) to match the
1481 definition of S_{OCEAN} used here (Hauck et al., 2020). This comparison depends critically on the estimate of the
1482 climate effect on the natural CO_2 flux, which is smaller from the GOBMs (-0.1 GtC yr^{-1}) than in Gruber et al.
1483 (2019). Uncertainties of these two estimates would also overlap when using the GOBM estimate of the climate
1484 effect on the natural CO_2 flux.

1485 During 2010-2016, the ocean CO_2 sink appears to have intensified in line with the expected increase from
1486 atmospheric CO_2 (McKinley et al., 2020). This effect is slightly stronger in the fCO_2 -products (Figure 10, ocean
1487 sink 2016 minus 2010, GOBMs: $+0.42 \pm 0.10 \text{ GtC yr}^{-1}$, fCO_2 -products: $+0.48 \pm 0.10 \text{ GtC yr}^{-1}$). The reduction of

Formatted: Font: Gungsuh

Formatted: Font: Gungsuh

Formatted: Font: Gungsuh

Formatted: Default Paragraph Font, Font colour: Black

Formatted: Normal, Centred, Border: Top: (No border),
Bottom: (No border), Left: (No border), Right: (No border),
Between : (No border), Tab stops: 7.96 cm, Centred + 15.92
cm, Right, Position: Horizontal: Left, Relative to: Column,
Vertical: In line, Relative to: Margin, Wrap Around

Formatted: Font colour: Black

1488 -0.14 GtC yr⁻¹ (range: -0.39 to +0.01 GtC yr⁻¹) in the ocean CO₂ sink in 2017 is consistent with the return to
1489 normal conditions after the El Niño in 2015/16, which caused an enhanced sink in previous years. After an
1490 increasing S_{ocean} in 2018 and 2019, 2017, the GOBM and fCO₂-product ensemble means suggest a decrease of
1491 S_{ocean}, related to the triple La Niña event 2020-2023.

1492 3.6.3 Final year 2022

1493 The estimated ocean CO₂ sink is 2.8 ± 0.4 GtC for 2022. This is a small decrease of 0.05 GtC compared to 2021,
1494 in line with the expected sink weakening from persistent La Niña conditions. GOBM and fCO₂-product
1495 estimates consistently result in a near-stagnation of S_{ocean} (GOBMs: -0.01 ± 0.05 GtC, fCO₂-products: -0.09
1496 ± 0.10 GtC). Four models and six fCO₂-products show a decrease in S_{ocean} (GOBMs down to -0.09 GtC, fCO₂-
1497 products down to -0.25 GtC), while one model shows no change and five models and two fCO₂-products show
1498 an increase in S_{ocean} (GOBMs up to 0.07 GtC, fCO₂-products up to 0.15 GtC; Figure 10). The fCO₂-products
1499 have a larger uncertainty at the end of the reconstructed time series (tail effect, e.g., Watson et al., 2020).
1500 Specifically, the fCO₂-products' estimate of the last year is regularly adjusted in the following release owing to
1501 the tail effect and an incrementally increasing data availability. While the monthly grid cells covered may have a
1502 lag of only about a year (Figure 10 inset), the values within grid cells may change with 1-5 years lag (see
1503 absolute number of observations plotted in previous GCB releases).

1504 3.6.4 Year 2023 Projection

1505 Using a feed-forward neural network method (see Section 2.5.2) we project an ocean sink of 2.9 GtC for 2023.
1506 This is slightly higher than for the year 2022 (2.8 GtC) and could mark a reversal of the slight decrease of
1507 S_{ocean} sink since 2019, due to the transition from persisting La Niña conditions to emerging El Niño conditions
1508 in 2023. The new set of ESMs predictions support this estimate with a 2023 ocean sink of around 3.1 [2.9, 3.2]
1509 GtC.

1510 3.6.5 Ocean Models Evaluation

1511 The process-based model evaluation draws a generally positive picture with GOBMs scattered around the
1512 observational values for Southern Ocean sea-surface salinity, Southern Ocean stratification index and surface
1513 ocean Revelle factor (Section C3.3 and Table S10). However, the Atlantic Meridional Overturning Circulation
1514 at 26°N is underestimated by 8 out of 10 GOBMs. It is planned to derive skill scores for the GOBMs in future
1515 releases based on these metrics.

1516 The model simulations allow to separate the anthropogenic carbon component (steady state and non-steady
1517 state, sim D - sim A) and to compare the model flux and DIC inventory change directly to the interior ocean
1518 estimate of Gruber et al. (2019) without further assumptions (Table S10). The GOBMs ensemble average of
1519 anthropogenic carbon inventory changes 1994-2007 amounts to 2.4 GtC yr⁻¹ and is thus lower than the 2.6 ± 0.3
1520 GtC yr⁻¹ estimated by Gruber et al. (2019) although within the uncertainty. Only four models with the highest
1521 sink estimate fall within the range reported by Gruber et al. (2019). This suggests that the majority of the

Formatted: Outline numbered + Level: 3 + Numbering
Style: 1, 2, 3, ... + Start at: 1 + Alignment: Left + Aligned at:
0 cm + Indent at: 1.27 cm

Formatted: Outline numbered + Level: 3 + Numbering
Style: 1, 2, 3, ... + Start at: 1 + Alignment: Left + Aligned at:
0 cm + Indent at: 1.27 cm

Deleted: decreasing

Deleted: trend of the past three years

Formatted: Outline numbered + Level: 3 + Numbering
Style: 1, 2, 3, ... + Start at: 1 + Alignment: Left + Aligned at:
0 cm + Indent at: 1.27 cm

Formatted: Default Paragraph Font, Font colour: Black

Formatted: Normal, Centred, Border: Top: (No border),
Bottom: (No border), Left: (No border), Right: (No border),
Between: (No border), Tab stops: 7.96 cm, Centred + 15.92
cm, Right, Position: Horizontal: Left, Relative to: Column,
Vertical: In line, Relative to: Margin, Wrap Around

Formatted: Font colour: Black

1524 GOBMs underestimate anthropogenic carbon uptake by 10-20%. Analysis of Earth System Models indicate that
1525 an underestimation by about 10% may be due to biases in ocean carbon transport and mixing from the surface
1526 mixed layer to the ocean interior (Goris et al., 2018, Terhaar et al., 2021, Bourgeois et al., 2022, Terhaar et al.,
1527 2022), biases in the chemical buffer capacity (Revelle factor) of the ocean (Vaittinada Ayar et al., 2022; Terhaar
1528 et al., 2022) and partly due to a late starting date of the simulations (mirrored in atmospheric CO₂ chosen for the
1529 preindustrial control simulation, Table S2, Bronselaer et al., 2017, Terhaar et al., 2022). Interestingly, and in
1530 contrast to the uncertainties in the surface CO₂ flux, we find the largest mismatch in interior ocean carbon
1531 accumulation in the tropics (96% of the mismatch), with minor contributions from the north (3%) and the south
1532 (<1%). These numbers deviate slightly from GCB2021 because of submission of the ACCESS model with a
1533 high anthropogenic carbon accumulation, particularly in the Southern Ocean. The large discrepancy in
1534 accumulation in the tropics highlights the role of interior ocean carbon redistribution for those inventories
1535 (Khatiwala et al., 2009, DeVries et al., 2023).

1536 The evaluation of the ocean estimates with the *f*CO₂ observations from the SOCAT v2023 dataset for the period
1537 1990-2022 shows an RMSE from annually detrended data of 0.4 to 2.4 μatm for the seven *f*CO₂-products over
1538 the globe (Figure S2). The GOBMs RMSEs are larger and range from 2.9 to 5.4 μatm. The RMSEs are
1539 generally larger at high latitudes compared to the tropics, for both the *f*CO₂-products and the GOBMs. The
1540 *f*CO₂-products have RMSEs of 0.3 to 2.8 μatm in the tropics, 0.7 to 2.3 μatm in the north, and 0.7 to 2.8 μatm in
1541 the south. Note that the *f*CO₂-products are based on the SOCAT v2023 database, hence the SOCAT is not an
1542 independent dataset for the evaluation of the *f*CO₂-products. The GOBMs RMSEs are more spread across
1543 regions, ranging from 2.5 to 5.0 μatm in the tropics, 3.0 to 7.2 μatm in the North, and 3.7 to 8.5 μatm in the
1544 South. The higher RMSEs occur in regions with stronger climate variability, such as the northern and southern
1545 high latitudes (poleward of the subtropical gyres). The upper range of the model RMSEs have increased
1546 somewhat relative to Friedlingstein et al. (2022b).

1547 3.7 Land Sink

1548 3.7.1 Historical period 1850-2022

1549 Cumulated since 1850, the terrestrial CO₂ sink amounts to 225 ± 55 GtC, 32% of total anthropogenic emissions.
1550 Over the historical period, the sink increased in pace with the anthropogenic emissions exponential increase
1551 (Figure 3).

1552 3.7.2 Recent period 1960-2022

1553 The terrestrial CO₂ sink *S*_{LAND} increased from 1.3 ± 0.5 GtC yr⁻¹ in the 1960s to 3.3 ± 0.8 GtC yr⁻¹ during 2013-
1554 2022, with important interannual variations of up to 2 GtC yr⁻¹ generally showing a decreased land sink during
1555 El Niño events (Figure 8), responsible for the corresponding enhanced growth rate in atmospheric CO₂
1556 concentration. The larger land CO₂ sink during 2013-2022 compared to the 1960s is reproduced by all the
1557 DGVMs in response to the increase in both atmospheric CO₂, nitrogen deposition, and the changes in climate,
1558 and is consistent with constraints from the other budget terms (Table 5).

Formatted: Outline numbered + Level: 2 + Numbering
Style: 1, 2, 3, ... + Start at: 1 + Alignment: Left + Aligned at:
0 cm + Indent at: 1.02 cm

Formatted: Outline numbered + Level: 3 + Numbering
Style: 1, 2, 3, ... + Start at: 1 + Alignment: Left + Aligned at:
0 cm + Indent at: 1.27 cm

Formatted: Outline numbered + Level: 3 + Numbering
Style: 1, 2, 3, ... + Start at: 1 + Alignment: Left + Aligned at:
0 cm + Indent at: 1.27 cm

Formatted: Default Paragraph Font, Font colour: Black

Formatted: Normal, Centred, Border: Top: (No border),
Bottom: (No border), Left: (No border), Right: (No border),
Between: (No border), Tab stops: 7.96 cm, Centred + 15.92
cm, Right, Position: Horizontal: Left, Relative to: Column,
Vertical: In line, Relative to: Margin, Wrap Around

Formatted: Font colour: Black

1559 Over the period 1960 to present the increase in the global terrestrial CO₂ sink is largely attributed to the CO₂
1560 fertilisation effect (Prentice et al., 2001, Piao et al., 2009, Schimel et al., 2015) and increased nitrogen
1561 deposition (Huntzinger et al., 2017, O’Sullivan et al., 2019), directly stimulating plant photosynthesis and
1562 increased plant water use in water limited systems, with a small negative contribution of climate change (Figure
1563 11). There is a range of evidence to support a positive terrestrial carbon sink in response to increasing
1564 atmospheric CO₂, albeit with uncertain magnitude (Walker et al., 2021). As expected from theory, the greatest
1565 CO₂ effect is simulated in the tropical forest regions, associated with warm temperatures and long growing
1566 seasons (Hickler et al., 2008) (Figure 11a). However, evidence from tropical intact forest plots indicate an
1567 overall decline in the land sink across Amazonia (1985-2011), attributed to enhanced mortality offsetting
1568 productivity gains (Brienen et al., 2015, Hubau et al., 2020). During 2013-2022 the land sink is positive in all
1569 regions (Figure 6) with the exception of eastern Brazil, Bolivia, Paraguay, northern Venezuela, Southwest USA,
1570 central Europe and Central Asia, North and South Africa, and eastern Australia, where the negative effects of
1571 climate variability and change (i.e. reduced rainfall and/or increased temperature) counterbalance CO₂ effects.
1572 This is clearly visible on Figure 11 where the effects of CO₂ (Figure 11a) and climate (Figure 11b) as simulated
1573 by the DGVMs are isolated. The negative effect of climate is the strongest in most of South America, Central
1574 America, Southwest US, Central Europe, western Sahel, southern Africa, Southeast Asia and southern China,
1575 and eastern Australia (Figure 11b). Globally, over the 2013-2022 period, climate change reduces the land sink
1576 by $0.68 \pm 0.62 \text{ GtC yr}^{-1}$ (20% of S_{LAND}).

1577 Most DGVMs have similar S_{LAND} averaged over 2013-2022, and 14/20 models fall within the 1σ range of the
1578 residual land sink [$2.0\text{-}3.8 \text{ GtC yr}^{-1}$] (see Table 5), and all but one model are within the 2σ range [$1.1\text{-}4.7 \text{ GtC yr}^{-1}$].
1579 The ED model is an outlier, with a land sink estimate of 5.7 GtC yr^{-1} , driven by a strong CO₂ fertilisation
1580 effect (6.6 GtC yr^{-1} in the CO₂ only (S1) simulation), that is offset by correspondingly high land-use emissions.
1581 There are no direct global observations of the land sink, or the CO₂ fertilisation effect, and so we are not yet in a
1582 position to rule out models based on component fluxes if the net land sink ($S_{\text{LAND-ELUC}}$) is within the
1583 observational uncertainty provided by atmospheric O₂ measurements (Table 5). Overall, therefore the spread
1584 among models for the estimate of S_{LAND} over the last decade has increased this year (0.8 GtC yr^{-1}) compared to
1585 GCB2022 (0.6 GtC yr^{-1}).

1586 Furthermore, DGVMs were compared against a data-constrained intermediate complexity model of the land
1587 carbon cycle (CARDAMOM) (Bloom and Williams, 2015; Bloom et al., 2016). Results suggest good
1588 correspondence between approaches at the interannual timescales, but divergence in the recent trend with
1589 CARDAMOM simulating a stronger trend than the DGVMs (Figure S8).

1590 Since 2020 the globe has experienced La Niña conditions which would be expected to lead to an increased land
1591 carbon sink. A clear peak in the global land sink is not evident in S_{LAND} , and we find that a La Niña- driven
1592 increase in tropical land sink is offset by a reduced high latitude extra-tropical land sink, which may be linked to
1593 the land response to recent climate extremes. A notable difference from GCB2022 (2012-2021 S_{LAND} mean) is
1594 the reduced carbon losses across tropical drylands. Further, central Europe has switched from a sink of carbon to
1595 a source, with the summer heatwave of 2022 (and associated drought and wildfire) causing widespread losses

Formatted: Default Paragraph Font, Font colour: Black

Formatted: Normal, Centred, Border: Top: (No border),
Bottom: (No border), Left: (No border), Right: (No border),
Between : (No border), Tab stops: 7.96 cm, Centred + 15.92
cm, Right, Position: Horizontal: Left, Relative to: Column,
Vertical: In line, Relative to: Margin, Wrap Around

Formatted: Font colour: Black

1596 (Peters et al., 2023). In the past years several regions experienced record-setting fire events. While global
1597 burned area has declined over the past decades mostly due to declining fire activity in savannas (Andela et al.,
1598 2017), forest fire emissions are rising and have the potential to counter the negative fire trend in savannas
1599 (Zheng et al., 2021). Noteworthy events include the 2019-2020 Black Summer event in Australia (emissions of
1600 roughly 0.2 GtC; van der Velde et al., 2021) and Siberia in 2021 where emissions approached 0.4 GtC or three
1601 times the 1997-2020 average according to GFED4s. While other regions, including Western US and
1602 Mediterranean Europe, also experienced intense fire seasons in 2021 their emissions are substantially lower.

1603 Despite these regional negative effects of climate change on S_{LAND} , the efficiency of land to remove
1604 anthropogenic CO_2 emissions has remained broadly constant over the last six decades, with a land-borne
1605 fraction ($S_{LAND}/(E_{FOS}+E_{LUC})$) of around 30% (Figure 9b).

1606 3.7.3 Final year 2022

1607 The terrestrial CO_2 sink from the DGVMs ensemble was 3.8 ± 0.8 GtC in 2022, above the decadal average of
1608 3.3 ± 0.8 GtC yr^{-1} (Figure 4, Table 7), and slightly above the 2021 sink of 3.5 ± 1.0 GtC, likely driven by the
1609 persistent La Niña conditions. We note that the DGVMs estimate for 2022 is similar to the 3.7 ± 1.0 GtC yr^{-1}
1610 estimate from the residual sink from the global budget ($E_{FOS}+E_{LUC}-G_{ATM}-S_{OCEAN}$) (Table 5).

1611 3.7.4 Year 2023 Projection

1612 Using a feed-forward neural network method we project a land sink of 2.9 GtC for 2023, 0.9 GtC smaller than
1613 the 2022 estimate. As for the ocean sink, we attribute this to the emerging El Niño conditions in 2023, leading to
1614 a reduced land sink. The ESMs do not provide an additional estimate of S_{LAND} as they only simulate the net
1615 atmosphere-land carbon flux ($S_{LAND}-E_{LUC}$).

1616 3.7.5 Land Models Evaluation

1617 The evaluation of the DGVMs shows generally high skill scores across models for runoff, and to a lesser extent
1618 for vegetation biomass, GPP, and ecosystem respiration. These conclusions are supported by a more
1619 comprehensive analysis of DGVM performance in comparison with benchmark data (Seiler et al., 2022). A
1620 relative comparison of DGVM performance (Figure S3) suggests several DGVMs (CABLE-POP, CLASSIC,
1621 OCN, ORCHIDEE) may outperform others at multiple carbon and water cycle benchmarks. However, results
1622 from Seiler et al., 2022, also show how DGVM differences are often of similar magnitude compared with the
1623 range across observational datasets. [All models score high enough over the metrics tests to support their use](#)
1624 [here. There are a few anomalously low scores for individual metrics from a single model, and these can direct](#)
1625 [the effort to improve models for use in future budgets.](#)

Formatted: Outline numbered + Level: 3 + Numbering
Style: 1, 2, 3, ... + Start at: 1 + Alignment: Left + Aligned at:
0 cm + Indent at: 1.27 cm

Formatted: Outline numbered + Level: 3 + Numbering
Style: 1, 2, 3, ... + Start at: 1 + Alignment: Left + Aligned at:
0 cm + Indent at: 1.27 cm

Deleted: 3.0

Deleted: 8

Formatted: Outline numbered + Level: 3 + Numbering
Style: 1, 2, 3, ... + Start at: 1 + Alignment: Left + Aligned at:
0 cm + Indent at: 1.27 cm

Formatted: Font colour: Auto

Formatted: Default Paragraph Font, Font colour: Black

Formatted: Normal, Centred, Border: Top: (No border),
Bottom: (No border), Left: (No border), Right: (No border),
Between: (No border), Tab stops: 7.96 cm, Centred + 15.92
cm, Right, Position: Horizontal: Left, Relative to: Column,
Vertical: In line, Relative to: Margin, Wrap Around

Formatted: Font colour: Black

1628 **3.8 Partitioning the carbon sinks**

1629 **3.8.1 Global sinks and spread of estimates**

1630 In the period 2013-2022, the bottom-up view of global net ocean and land carbon sinks provided by the GCB,
1631 SOCEAN for the ocean and SLAND-ELUC for the land, agrees closely with the top-down global carbon sinks
1632 delivered by the atmospheric inversions. This is shown in Figure 12, which visualises the individual decadal
1633 mean atmosphere-land and atmosphere-ocean fluxes from each, along with the constraints on their sum offered
1634 by the global fossil CO₂ emissions flux minus the atmospheric growth rate (E_{FOS} - G_{ATM}, 4.5 ± 0.5 Gt C yr⁻¹,
1635 Table 7, shown as diagonal line on Figure 12). The GCB estimate for net atmosphere-to-surface flux (SOCEAN +
1636 SLAND - ELUC) during 2013-2022 is 4.9 ± 1.2 Gt C yr⁻¹ (Table 7), with the difference to the diagonal representing
1637 the budget imbalance (B_M) of 0.4 GtC yr⁻¹ discussed in Section 3.9. By virtue of the inversion methodology, the
1638 imbalance of the top-down estimates is < 0.1 GtC yr⁻¹ and thus scatter across the diagonal, inverse models
1639 trading land for ocean fluxes in their solution. The independent constraint on the net atmosphere-to-surface flux
1640 based on atmospheric O₂ is 4.5 ± 1.0 GtC yr⁻¹ over the 2013-2022 period (orange symbol on Figure 12), while
1641 the ESMs estimate for the net atmosphere-to-surface flux over that period is 5.0 [4.2, 5.5] Gt C yr⁻¹, consistent
1642 with the GCB estimate (Tables 5 and 6).

1643 The distributions based on the individual models and data products reveal substantial spread but converge near
1644 the decadal means quoted in Tables 5 to 7. Sink estimates for SOCEAN and from inverse systems are mostly non-
1645 Gaussian, while the ensemble of DGVMs appears more normally distributed justifying the use of a multi-model
1646 mean and standard deviation for their errors in the budget. Noteworthy is that the tails of the distributions
1647 provided by the land and ocean bottom-up estimates would not agree with the global constraint provided by the
1648 fossil fuel emissions and the observed atmospheric CO₂ growth rate. This illustrates the power of the
1649 atmospheric joint constraint from G_{ATM} and the global CO₂ observation network it derives from.

1650 **3.8.1.1 Net atmosphere-to-land fluxes**

1651 The GCB net atmosphere-to-land fluxes (SLAND - ELUC), calculated as the difference between SLAND from the
1652 DGVMs and ELUC from the bookkeeping models, amounts to a 2.1 ± 1.1 GtC yr⁻¹ sink during 2013-2022 (Table
1653 5). Estimates of net atmosphere-to-land fluxes (SLAND - ELUC) from the DGVMs alone (1.7 ± 0.6 GtC yr⁻¹, Table
1654 5, green symbol on Figure 12) are slightly lower, within the uncertainty of the GCB estimate and also with the
1655 global carbon budget constraint from the ocean sink (E_{FOS} - G_{ATM} - SOCEAN, 1.6 ± 0.6 GtC yr⁻¹; Table 7). For the
1656 last decade (2013-2022), the inversions estimate the net atmosphere-to-land uptake to be 1.6 [0.5, 2.3] GtC yr⁻¹,
1657 similar to the DGVMs estimates (purple symbol on Figure 12). The ESMs estimate for the net atmosphere-to-
1658 land uptake during 2013-2022 is 2.4 [1.8, 3.3] GtC yr⁻¹, consistent with the GCB and DGVMs estimates of
1659 SLAND - ELUC (Figure 13 top row). The independent constraint based on atmospheric O₂ is significantly lower,
1660 1.2 ± 0.8 GtC yr⁻¹, although its relatively high uncertainty range overlaps with the central estimates from other
1661 approaches.

Formatted: Outline numbered + Level: 2 + Numbering Style: 1, 2, 3, ... + Start at: 1 + Alignment: Left + Aligned at: 0 cm + Indent at: 1.02 cm

Formatted: Indent: Left: 0 cm, First line: 0 cm, Outline numbered + Level: 3 + Numbering Style: 1, 2, 3, ... + Start at: 1 + Alignment: Left + Aligned at: 0 cm + Indent at: 1.27 cm

Deleted: 4

Deleted: 4

Formatted: Indent: Left: 0 cm, First line: 0 cm, Outline numbered + Level: 4 + Numbering Style: 1, 2, 3, ... + Start at: 1 + Alignment: Left + Aligned at: 0 cm + Indent at: 1.52 cm

Deleted: 1 ± 1.3

Formatted: Default Paragraph Font, Font colour: Black

Formatted: Normal, Centred, Border: Top: (No border), Bottom: (No border), Left: (No border), Right: (No border), Between: (No border), Tab stops: 7.96 cm, Centred + 15.92 cm, Right, Position: Horizontal: Left, Relative to: Column, Vertical: In line, Relative to: Margin, Wrap Around

Formatted: Font colour: Black

1665 **3.8.1.2 Net atmosphere-to-ocean fluxes**

1666 For the 2013-2022 period, the GOBMs ($2.6 \pm 0.4 \text{ GtC yr}^{-1}$) produce a lower estimate for the ocean sink than the
1667 $f\text{CO}_2$ -products ($3.1 [2.6, 3.3] \text{ GtC yr}^{-1}$), which shows up in Figure 12 as separate peaks in the distribution from
1668 the GOBMs (dark blue symbols) and from the $f\text{CO}_2$ -products (light blue symbols). Atmospheric inversions (3.0
1669 $[2.4, 4.1] \text{ GtC yr}^{-1}$) suggest an ocean uptake more in line with the $f\text{CO}_2$ -products for the recent decade (Table 7),
1670 although the inversions range includes both the GOBMs and $f\text{CO}_2$ -products estimates (Figure 13 top row). The
1671 ESMs $2.6 [2.2, 3.4] \text{ GtC yr}^{-1}$ suggest a moderate estimate for the ocean carbon sink, comparable to the GOBMs
1672 estimate with regard to mean and spread. Conversely, the independent constraint based on atmospheric O_2
1673 suggests a larger ocean sink ($3.3 \pm 0.5 \text{ GtC yr}^{-1}$), more consistent with the $f\text{CO}_2$ -products and atmospheric
1674 inversions. We caution that the riverine transport of carbon taken up on land and outgassing from the ocean is a
1675 substantial ($0.65 \pm 0.3 \text{ GtC yr}^{-1}$) and uncertain term (Crisp et al., 2022; Gruber et al., 2023; DeVries et al., 2023)
1676 that separates the GOBMs, ESMs and oxygen-based estimates on the one hand from the $f\text{CO}_2$ -products and
1677 atmospheric inversions on the other hand. However, the high ocean sink estimate based on atmospheric oxygen
1678 that is not subject to river flux adjustment, provides another line of evidence that most GOBMs and ESMs
1679 underestimate the ocean sink.

Formatted: Indent: Left: 0 cm, First line: 0 cm, Outline numbered + Level: 4 + Numbering Style: 1, 2, 3, ... + Start at: 1 + Alignment: Left + Aligned at: 0 cm + Indent at: 1.52 cm

Deleted: 6

1680 **3.8.2 Regional partitioning**

1681 Figure 13 shows the latitudinal partitioning of the global atmosphere-to-ocean (S_{OCEAN}), atmosphere-to-land
1682 ($S_{\text{LAND}} - E_{\text{LUC}}$), and their sum ($S_{\text{OCEAN}} + S_{\text{LAND}} - E_{\text{LUC}}$) according to the estimates from GOBMs and ocean
1683 $f\text{CO}_2$ -products (S_{OCEAN}), DGVMs ($S_{\text{LAND}} - E_{\text{LUC}}$), and from atmospheric inversions (S_{OCEAN} and $S_{\text{LAND}} - E_{\text{LUC}}$).

Formatted: Indent: Left: 0 cm, First line: 0 cm, Outline numbered + Level: 3 + Numbering Style: 1, 2, 3, ... + Start at: 1 + Alignment: Left + Aligned at: 0 cm + Indent at: 1.27 cm

1684 **3.8.2.1 North**

1685 Despite being one of the most densely observed and studied regions of our globe, annual mean carbon sink
1686 estimates in the northern extra-tropics (north of 30°N) continue to differ. The atmospheric inversions suggest an
1687 atmosphere-to-surface sink ($S_{\text{OCEAN}} + S_{\text{LAND}} - E_{\text{LUC}}$) for 2013-2022 of $2.8 [1.7 \text{ to } 3.3] \text{ GtC yr}^{-1}$, which is higher
1688 than the process models' estimate of $2.2 \pm 0.4 \text{ GtC yr}^{-1}$ (Figure 13). The GOBMs ($1.2 \pm 0.2 \text{ GtC yr}^{-1}$), $f\text{CO}_2$ -
1689 products ($1.3 [1.2-1.4] \text{ GtC yr}^{-1}$), and inversion systems ($1.2 [0.7 \text{ to } 1.4] \text{ GtC yr}^{-1}$) produce consistent estimates of
1690 the ocean sink. Thus, the difference mainly arises from the net land flux ($S_{\text{LAND}} - E_{\text{LUC}}$) estimate, which is $1.0 \pm$
1691 0.4 GtC yr^{-1} in the DGVMs compared to $1.6 [0.4 \text{ to } 2.6] \text{ GtC yr}^{-1}$ in the atmospheric inversions (Figure 13,
1692 second row). We note that the range among inversions driven by OCO-2 satellite data is smaller though ($1.6 -$
1693 $2.2 \text{ GtC yr}^{-1} \text{ N}=6$), supporting the notion that northern extra-tropics land uptake was larger than suggested by the
1694 DGVMs at least in the 2015-2022 period covered by this data product.

Formatted: Indent: Left: 0 cm, First line: 0 cm, Outline numbered + Level: 4 + Numbering Style: 1, 2, 3, ... + Start at: 1 + Alignment: Left + Aligned at: 0 cm + Indent at: 1.52 cm

1695 Discrepancies in the northern land fluxes conforms with persistent issues surrounding the quantification of the
1696 drivers of the global net land CO_2 flux (Armeth et al., 2017; Huntzinger et al., 2017; O'Sullivan et al., 2022) and
1697 the distribution of atmosphere-to-land fluxes between the tropics and high northern latitudes (Baccini et al.,
1698 2017; Schimel et al., 2015; Stephens et al., 2007; Ciais et al., 2019; Gaubert et al., 2019).

Formatted: Default Paragraph Font, Font colour: Black

Formatted: Normal, Centred, Border: Top: (No border), Bottom: (No border), Left: (No border), Right: (No border), Between : (No border), Tab stops: 7.96 cm, Centred + 15.92 cm, Right, Position: Horizontal: Left, Relative to: Column, Vertical: In line, Relative to: Margin, Wrap Around

Formatted: Font colour: Black

1700 In the northern extra-tropics, the process models, inversions, and $f\text{CO}_2$ -products consistently suggest that most
1701 of the variability stems from the land (Figure 13). Inversions generally estimate similar interannual variations
1702 (IAV) over land to DGVMs (0.28-0.35 vs 0.8-0.64 GtC yr^{-1} , averaged over 1990-2022), and they have higher
1703 IAV in ocean fluxes (0.05-0.10 GtC yr^{-1}) relative to GOBMs (0.02-0.06 GtC yr^{-1} , Figure S2), and $f\text{CO}_2$ -
1704 products (0.03-0.10 GtC yr^{-1}).

1705 3.8.2.2 Tropics

1706 In the tropics (30°S-30°N), both the atmospheric inversions and process models estimate a net carbon balance
1707 ($S_{\text{OCEAN}} + S_{\text{LAND}} - E_{\text{LUC}}$) that is close to neutral over the past decade. The GOBMs ($-0.03 \pm 0.24 \text{ GtC yr}^{-1}$), $f\text{CO}_2$ -
1708 products (0.2 [0.2, 0.3] GtC yr^{-1}), and inversion systems ($-0.3 [-0.1, 0.8] \text{ GtC yr}^{-1}$) all indicate an approximately
1709 neutral tropical ocean flux (see Figure S1 for spatial patterns). DGVMs indicate a net land sink ($S_{\text{LAND}} - E_{\text{LUC}}$) of
1710 $0.6 \pm 0.4 \text{ GtC yr}^{-1}$, whereas the inversion systems indicate a net land flux of $0.03 [-0.8, 1.1] \text{ GtC yr}^{-1}$, though with
1711 high uncertainty (Figure 13, third row).

1712 The tropical lands are the origin of most of the atmospheric CO_2 interannual variability (Ahlström et al., 2015),
1713 consistently among the process models and inversions (Figure 13). The interannual variability in the tropics is
1714 similar among the ocean $f\text{CO}_2$ -products (0.07-0.16 GtC yr^{-1}) and the GOBMs (0.07-0.16 GtC yr^{-1} ,
1715 Figure S2), which is the highest ocean sink variability of all regions. The DGVMs and inversions indicate that
1716 atmosphere-to-land CO_2 fluxes are more variable than atmosphere-to-ocean CO_2 fluxes in the tropics, with
1717 interannual variability of 0.35 to 1.61 and 0.77-0.92 GtC yr^{-1} for DGVMs and inversions, respectively.

1718 3.8.2.3 South

1719 In the southern extra-tropics (south of 30°S), the atmospheric inversions suggest a net atmosphere-to-surface
1720 sink ($S_{\text{OCEAN}} + S_{\text{LAND}} - E_{\text{LUC}}$) for 2013-2022 of 1.5 [1.2, 1.9] GtC yr^{-1} , slightly higher than the process models'
1721 estimate of $1.5 \pm 0.4 \text{ GtC yr}^{-1}$ (Figure 13). An approximately neutral net land flux ($S_{\text{LAND}} - E_{\text{LUC}}$) for the southern
1722 extra-tropics is estimated by both the DGVMs ($0.05 \pm 0.07 \text{ GtC yr}^{-1}$) and the inversion systems (sink of 0.02 [-
1723 0.2, 0.2] GtC yr^{-1}). This means nearly all carbon uptake is due to oceanic sinks south of 30°S. The Southern
1724 Ocean flux in the $f\text{CO}_2$ -products (1.6 [1.3, 1.7] GtC yr^{-1}) and inversion estimates (1.5 [1.3, 1.9] GtC yr^{-1}) is
1725 slightly higher than in the GOBMs ($1.4 \pm 0.3 \text{ GtC yr}^{-1}$) (Figure 13, bottom row). This discrepancy in the mean
1726 flux is smaller this year than in previous releases due to the change in data set of the regional distribution of the
1727 river flux adjustment applied to $f\text{CO}_2$ -products and inverse systems to isolate the anthropogenic S_{OCEAN} flux.
1728 The data set used (Lacroix et al., 2020) has less river-induced carbon outgassing in the Southern Ocean than the
1729 previously used data set (Aumont et al., 2001). Nevertheless, the time-series of atmospheric inversions and
1730 $f\text{CO}_2$ -products diverge from the GOBMs. A substantial overestimation of the trends in the $f\text{CO}_2$ -products could
1731 be explained by sparse and unevenly distributed observations, especially in wintertime (Figure S1; Hauck et al.,
1732 2023; Gloege et al., 2021). Model biases may contribute as well, with biases in mode water formation,
1733 stratification, and the chemical buffer capacity known to play a role in Earth System Models (Terhaar et al.,
1734 2021, Bourgeois et al., 2022, Terhaar et al., 2022).

Formatted: Indent: Left: 0 cm, First line: 0 cm, Outline numbered + Level: 4 + Numbering Style: 1, 2, 3, ... + Start at: 1 + Alignment: Left + Aligned at: 0 cm + Indent at: 1.52 cm

Formatted: Indent: Left: -0.08 cm, Hanging: 0.08 cm, Outline numbered + Level: 4 + Numbering Style: 1, 2, 3, ... + Start at: 1 + Alignment: Left + Aligned at: 0 cm + Indent at: 1.52 cm

Formatted: Default Paragraph Font, Font colour: Black

Formatted: Normal, Centred, Border: Top: (No border), Bottom: (No border), Left: (No border), Right: (No border), Between: (No border), Tab stops: 7.96 cm, Centred + 15.92 cm, Right, Position: Horizontal: Left, Relative to: Column, Vertical: In line, Relative to: Margin, Wrap Around

Formatted: Font colour: Black

1735 The interannual variability in the southern extra-tropics is low because of the dominance of ocean areas with
1736 low variability compared to land areas. The split between land ($S_{LAND-ELUC}$) and ocean (S_{OCEAN}) shows a
1737 substantial contribution to variability in the south coming from the land, with no consistency between the
1738 DGVMs and the inversions or among inversions. This is expected due to the difficulty of separating exactly the
1739 land and oceanic fluxes when viewed from atmospheric observations alone. The S_{OCEAN} interannual variability
1740 was found to be higher in the fCO_2 -products ($0.04-0.18 \text{ GtC yr}^{-1}$) compared to GOBMs (0.03 to 0.06 GtC yr^{-1})
1741 in 1990-2022 (Figure S2). Model subsampling experiments recently illustrated that fCO_2 -products may
1742 overestimate decadal variability in the Southern Ocean carbon sink by 30% and the trend since 2000 by 50-
1743 130% due to data sparsity, based on one and two fCO_2 -products with strong variability (Gloege et al., 2021,
1744 Hauck et al., 2023).

1745 3.8.2.4 RECCAP2 regions

1746 Aligning with the RECCAP-2 initiative (Ciais et al., 2022; Poulter et al., 2022; DeVries et al., 2023), we
1747 provide a breakdown of this GCB paper estimate of the E_{LUC} , S_{LAND} , Net land ($S_{LAND} - E_{LUC}$), and S_{OCEAN} fluxes
1748 over the 10 land, and 5 ocean RECCAP-2 regions, averaged over the period 2013-2022. The DGVMs and
1749 inversions suggest a positive net land sink in all regions, except for South America and Africa, where the
1750 inversions indicate a small net source of respectively $-0.1 [-0.5, 0.3] \text{ GtC yr}^{-1}$ and $-0.3 [-0.6, -0.1] \text{ GtC yr}^{-1}$,
1751 compared to a small sink of $0.1 \pm 0.3 \text{ GtC yr}^{-1}$ and $0.3 \pm 0.2 \text{ GtC yr}^{-1}$ for the DGVMs. However, for South
1752 America, there is substantial uncertainty in both products (ensembles span zero). For the DGVMs, this is driven
1753 by uncertainty in both S_{LAND} ($0.6 \pm 0.5 \text{ GtC yr}^{-1}$) and E_{LUC} ($0.4 \pm 0.2 \text{ GtC yr}^{-1}$). The bookkeeping models also
1754 suggest an E_{LUC} source of around 0.4 GtC yr^{-1} in South America and Africa, in line with the DGVMs estimates.
1755 Bookkeeping models and DGVMs similarly estimate a source of 0.4 GtC yr^{-1} in Southeast Asia, with DGVMs
1756 suggesting a near neutral net land sink ($0.03 \pm 0.12 \text{ GtC yr}^{-1}$). This contrasts with the inversion estimate of a 0.2
1757 $[-0.3, 0.6] \text{ GtC yr}^{-1}$ sink, although the inversions spread is substantial. The inversions suggest the largest net
1758 land sinks are located in North America ($0.5 [-0.1, 0.8] \text{ GtC yr}^{-1}$), Russia ($0.7 [0.5, 1.1] \text{ GtC yr}^{-1}$), and East Asia
1759 ($0.3 [0.0, 0.9] \text{ GtC yr}^{-1}$). This agrees well with the DGVMs in North America ($0.4 \pm 0.2 \text{ GtC yr}^{-1}$), which
1760 indicate a large natural land sink (S_{LAND}) of $0.6 \pm 0.2 \text{ GtC yr}^{-1}$, being slightly reduced by land-use related carbon
1761 losses ($0.2 \pm 0.1 \text{ GtC yr}^{-1}$). The DGVMs suggest a smaller net land sink in Russia compared to inversions
1762 ($0.4 \pm 0.2 \text{ GtC yr}^{-1}$), and a similar net sink in East Asia ($0.2 \pm 0.1 \text{ GtC yr}^{-1}$).

1763 There is generally a higher level of agreement in the estimates of regional S_{OCEAN} between the different data
1764 streams (GOBMs, fCO_2 -products and atmospheric inversions) on decadal scale, compared to the agreement
1765 between the different land flux estimates. All data streams agree that the largest contribution to S_{OCEAN} stems
1766 from the Southern Ocean, due to a combination of high flux density and large surface area, but with important
1767 contributions also from the Atlantic (high flux density) and Pacific (large area) basins. In the Southern Ocean,
1768 GOBMs suggest a sink of $1.0 \pm 0.3 \text{ GtC yr}^{-1}$, in line with the fCO_2 -products ($1.1 [0.9, 1.2] \text{ GtC yr}^{-1}$) and
1769 atmospheric inversions ($1.0 [0.8, 1.4] \text{ GtC yr}^{-1}$). There is similar agreement in the Pacific Ocean, with GOBMs,

Formatted: Indent: Left: 0 cm, First line: 0 cm, Outline numbered + Level: 4 + Numbering Style: 1, 2, 3, ... + Start at: 1 + Alignment: Left + Aligned at: 0 cm + Indent at: 1.52 cm

Deleted: an overview of

Deleted: for

Deleted: regions

Deleted: loss

Deleted: ensemble

Deleted: estimates

Formatted: Font colour: Custom Colour (RGB(31,31,31)), Highlight

Deleted: ,

Formatted: Font colour: Custom Colour (RGB(31,31,31)), Highlight

Deleted: vast ocean basins in the

Deleted: oceans.

Formatted: Font colour: Custom Colour (RGB(31,31,31)), Highlight

Formatted: Font colour: Custom Colour (RGB(31,31,31)), Highlight

Deleted: ocean

Formatted: Default Paragraph Font, Font colour: Black

Formatted: Normal, Centred, Border: Top: (No border), Bottom: (No border), Left: (No border), Right: (No border), Between: (No border), Tab stops: 7.96 cm, Centred + 15.92 cm, Right, Position: Horizontal: Left, Relative to: Column, Vertical: In line, Relative to: Margin, Wrap Around

Formatted: Font colour: Black

1780 $f\text{CO}_2$ -products, and atmospheric inversions indicating a sink of $0.5 \pm 0.1 \text{ GtC yr}^{-1}$, $0.7 [0.5, 0.9] \text{ GtC yr}^{-1}$, and
1781 $0.6 [0.2, 1.0] \text{ GtC yr}^{-1}$, respectively. However, in the Atlantic [Ocean](#), GOBMs simulate a sink of $0.5 \pm 0.1 \text{ GtC}$
1782 yr^{-1} , noticeably lower than both the $f\text{CO}_2$ -products ($0.8 [0.7, 0.9] \text{ GtC yr}^{-1}$) and atmospheric inversions (0.8
1783 $[0.5, 1.2] \text{ GtC yr}^{-1}$). It is important to note the $f\text{CO}_2$ -products and atmospheric inversions have a substantial and
1784 uncertain river flux adjustment in the Atlantic [Ocean](#) (0.3 GtC yr^{-1}) that also leads to a mean offset between
1785 GOBMs and $f\text{CO}_2$ -products/inversions in the latitude band of the tropics (Figure 13). The Indian Ocean due to its
1786 smaller size and the Arctic Ocean due to its size and sea-ice cover that prevents air-sea gas-exchange are
1787 responsible for smaller but non negligible SOCEAN fluxes (Indian Ocean: $0.3 [0.2, 0.4] \text{ GtC yr}^{-1}$, $0.3 [0.3, 0.4]$
1788 GtC yr^{-1} , and $0.4 [0.3, 0.6] \text{ GtC yr}^{-1}$ for GOBMs, $f\text{CO}_2$ -products, and atmospheric inversions, respectively, and
1789 Arctic Ocean: $0.1 [0.1, 0.1] \text{ GtC yr}^{-1}$, $0.2 [0.2, 0.2] \text{ GtC yr}^{-1}$, and $0.1 [0.1, 0.1] \text{ GtC yr}^{-1}$ for GOBMs, $f\text{CO}_2$ -
1790 products, and atmospheric inversions, respectively). Note that the SOCEAN numbers presented here deviate from
1791 numbers reported in RECCAP-2 where the net air-sea CO_2 flux is reported (i.e. without river flux adjustment for
1792 $f\text{CO}_2$ -products and inversions, and with river flux adjustment subtracted from GOBMs in most chapters, or
1793 comparing unadjusted data sets with discussion of uncertain regional riverine fluxes as major uncertainty, e.g.
1794 Sarma et al., 2023, DeVries et al., 2023).

Deleted: ocean

Deleted: ocean

1795 3.8.2.5 Tropical vs northern land uptake

1796 A continuing conundrum is the partitioning of the global atmosphere-land flux between the northern hemisphere
1797 land and the tropical land (Stephens et al., 2017; Pan et al., 2011; Gaubert et al., 2019). It is of importance
1798 because each region has its own history of land-use change, climate drivers, and impact of increasing
1799 atmospheric CO_2 and nitrogen deposition. Quantifying the magnitude of each sink is a prerequisite to
1800 understanding how each individual driver impacts the tropical and mid/high-latitude carbon balance.

Formatted: Indent: Left: 0 cm, First line: 0 cm, Outline numbered + Level: 4 + Numbering Style: 1, 2, 3, ... + Start at: 1 + Alignment: Left + Aligned at: 0 cm + Indent at: 1.52 cm

1801 We define the North-South (N-S) difference as net atmosphere-land flux north of 30°N minus the net
1802 atmosphere-land flux south of 30°N . For the inversions, the N-S difference ranges from -0.5 GtC yr^{-1} to $+3.0$
1803 GtC yr^{-1} across this year's inversion ensemble, but with a clear cluster of solutions driven by the OCO-2 satellite
1804 product with a NH land sink of $1.6\text{-}2.2 \text{ GtC yr}^{-1}$, along with a tropical land flux of -0.6 to $+0.2 \text{ GtC yr}^{-1}$, and a
1805 dipole between $+1.4$ and $+2.8 \text{ GtC yr}^{-1}$ for the period 2015-2022. Whether this tighter clustering relative to the
1806 surface-observation based inversions is driven by (a) additional information on tropical fluxes delivered by
1807 tropical retrievals contained in OCO-2, (b) a tighter constraint on the NH land sink from that same product, or
1808 (c) a reduced sensitivity to vertical transport differences between models when using CO_2 column integrals,
1809 requires further investigation.

1810 In the ensemble of DGVMs the N-S difference is $0.5 \pm 0.6 \text{ GtC yr}^{-1}$, a much narrower range than the one from
1811 atmospheric inversions. Five DGVMs have a N-S difference larger than 1.0 GtC yr^{-1} , compared to only two
1812 from last year's ensemble. This is still only 25% of DGVMs, compared to most inversion systems simulating a
1813 difference at least this large. The smaller spread across DGVMs than across inversions is to be expected as there
1814 is no correlation between Northern and Tropical land sinks in the DGVMs as opposed to the inversions where

Formatted: Default Paragraph Font, Font colour: Black

Formatted: Normal, Centred, Border: Top: (No border), Bottom: (No border), Left: (No border), Right: (No border), Between: (No border), Tab stops: 7.96 cm, Centred + 15.92 cm, Right, Position: Horizontal: Left, Relative to: Column, Vertical: In line, Relative to: Margin, Wrap Around

Formatted: Font colour: Black

1817 the sum of the two regions being well-constrained by atmospheric observations leads to an anti-correlation
1818 between these two regions. This atmospheric N-S gradient could be used as an additional way to evaluate
1819 tropical and NH uptake in DGVMs, if their fluxes were combined with multiple transport models. Vice versa,
1820 the much smaller spread in the N-S difference between the DGVMs could help to scrutinise the inverse systems
1821 further. For example, a large northern land sink and a tropical land source in an inversion would suggest a large
1822 sensitivity to CO₂ fertilisation (the dominant factor driving the land sinks) for Northern ecosystems, which
1823 would be not mirrored by tropical ecosystems. Such a combination could be hard to reconcile with the process
1824 understanding gained from the DGVM ensembles and independent measurements (e.g. Free Air CO₂
1825 Enrichment experiments).

1826 3.8.3 Fire Emissions in 2023

1827 Fire emissions so far in 2023 have been above the average of recent decades, due to an extreme wildfire season
1828 in North America. Figure S9 shows global and regional emissions estimates for the period 1st Jan-30th
1829 September in each year 2003-2023. Estimates derive from two global fire emissions products: the global fire
1830 emissions database (GFED, version 4.1s; van der Werf et al., 2017), and the global fire assimilation system
1831 (GFAS, operated by the Copernicus Atmosphere Service; Di Giuseppe et al., 2018). The two products estimate
1832 that global emissions from fires were 1.9-2.3 GtC yr⁻¹ during January-October 2023. These estimates are 19-
1833 33% above the 2013-2022 average for the same months (1.6-1.7 GtC yr⁻¹) and 10-28% above the 2003-2022
1834 average (1.8 GtC yr⁻¹ in both products).

1835 The above-average global fire emissions during January-October 2023 have occurred despite below-average fire
1836 emissions from major source regions. On average during 2013-2022, 75-80% of global fire emissions through
1837 October occur in the tropics (1.2-1.4 GtC yr⁻¹) and around 41-48% of global fire emissions through October
1838 occur in Africa (0.7-0.8 GtC yr⁻¹). This year, through October, fire emissions in the tropics were approximately
1839 equal to the 2013-2022 average and 7-9% below the 2003-2022 average, while in Africa the fire emissions were
1840 approximately equal to the 2013-2022 average and 4-13% below the 2003-2022 average.

1841 In contrast, fire emissions from the Northern extra-tropics so far in 2023 have exceeded the values of all
1842 previous years. Northern extra-tropical fire emissions during January-October 2023 (0.7-0.9 GtC yr⁻¹) were 84-
1843 183% above the average for the same months in 2013-2022 (0.3-0.4 GtC yr⁻¹) and 76-190% above the average
1844 for the same months in 2003-2022 (0.3-0.4 GtC yr⁻¹). Fire emissions in North America alone (0.5-0.8 GtC yr⁻¹)
1845 were 239-438% above the average of 2013-2022 (0.2 GtC yr⁻¹ for both products) and 215-410% above the
1846 average for 2003-2022 (0.2 GtC yr⁻¹ for both products). Extreme fires in Canada were the largest contributor to
1847 the anomaly in 2023, with emissions reaching 0.5-0.8 GtC yr⁻¹ or 527-874% above the 2013-2022 average (0.1
1848 GtC yr⁻¹ in both products) and 450-709% above the 2003-2022 average (0.1 GtC yr⁻¹ in both products).

1849 While the fire emission fluxes presented above point towards a highly unusual Northern Hemisphere fire season
1850 so far in 2023, we caution that the fluxes presented should not be compared directly with other fluxes of the
1851 budget (e.g. S_{LAND} or E_{LUC}) due to incompatibilities between the observable fire emission fluxes and what is
1852 quantified in the S_{LAND} and E_{LUC} components of the budget. The fire emission estimates from global fire

- Deleted: Forest Fires
- Formatted ... [10]
- Deleted: ;
- Deleted: 5-1.8
- Deleted: September
- Deleted: 13-15
- Deleted: 3
- Deleted: 6
- Deleted: 7-9
- Deleted: 4-1.6
- Deleted: September
- Deleted: 72-79
- Deleted: September
- Deleted: 0.9-
- Deleted: 3
- Deleted: half
- Deleted: September
- Deleted: 6
- Deleted: September
- Deleted: (0.7-0.9 GtC yr⁻¹)
- Deleted: 7-23% below
- Deleted: in Africa (0.5-0.7 GtC yr⁻¹)
- Deleted: 7-17% below
- Deleted: 2003-2022
- Deleted: September
- Deleted: 6
- Deleted: 8
- Deleted: 80-160
- Deleted: the past decade
- Deleted:
- Deleted: both global fire emissions products).
- Deleted: 7
- Deleted: 220-380
- Deleted: the past decade (0.1
- Deleted: In
- Deleted: , North America was the only RECCAP2 reg... [11]
- Deleted: -
- Deleted: fire
- Deleted: emissions for January-September
- Deleted: 2023.
- Formatted: Default Paragraph Font, Font colour: Black
- Formatted ... [9]
- Formatted: Font colour: Black

1894 products relate to all fire types that can be observed in Earth Observations (Giglio et al., 2018; Randerson et al.,
1895 2012; Kaiser et al., 2012), including (i) fires occurring as part of natural disturbance-recovery cycles that would
1896 also have occurred in the pre-industrial period (Yue et al., 2016; Keeley and Pausas, 2019; Zou et al., 2019), (ii)
1897 fires occurring above and beyond natural disturbance-recovery cycle due to changes in climate, CO₂ and N
1898 fertilisation and to an increased frequency of extreme drought and heatwave events (Abatzoglou et al., 2019;
1899 Jones et al., 2022; Zheng et al., 2021; Burton et al., 2023), and (iii) fires occurring in relation to land use and
1900 land use change, such as deforestation fires and agricultural fires (van der Werf et al., 2010; Magi et al., 2012).
1901 In the context of the global carbon budget, only the portion of fire emissions associated with (ii) should be
1902 included in the S_{LAND} component, and fire emissions associated with (iii) should already be accounted for in the
1903 E_{LUC} component. Emissions associated with (i) should not be included in the global carbon budget. It is not
1904 currently possible to derive specific estimates for fluxes (i), (ii), and (iii) using global fire emission products
1905 such as GFED or GFAS. In addition, the fire emissions estimates from global fire emissions products represent
1906 a gross flux of carbon to the atmosphere, whereas the S_{LAND} component of the budget is a net flux that should
1907 also include post-fire recovery fluxes. Even if emissions from fires of type (ii) could be separated from those of
1908 type (i), these fluxes may be partially or wholly offset in subsequent years by post-fire fluxes as vegetation
1909 recovers, sequestering carbon from the atmosphere to the terrestrial biosphere (Yue et al., 2016).

1910 3.9 Closing the Global Carbon Cycle

1911 3.9.1 Partitioning of Cumulative Emissions and Sink Fluxes

1912 The global carbon budget over the historical period (1850-2021) is shown in Figure 3.

1913 Emissions during the period 1850-2022 amounted to 695 ± 70 GtC and were partitioned among the atmosphere
1914 (280 ± 5 GtC; 40%), ocean (180 ± 35 GtC; 26%), and land (225 ± 55 GtC; 32%). The cumulative land sink is
1915 almost equal to the cumulative land-use emissions (220 ± 70 GtC), making the global land nearly neutral over
1916 the whole 1850-2022 period.

1917 The use of nearly independent estimates for the individual terms of the global carbon budget shows a cumulative
1918 budget imbalance of 15 GtC (2% of total emissions) during 1850-2022 (Figure 3, Table 8), which, if correct,
1919 suggests that emissions could be slightly too high by the same proportion (2%) or that the combined land and
1920 ocean sinks are slightly underestimated (by about 3%), although these are well within the uncertainty range of
1921 each component of the budget. Nevertheless, part of the imbalance could originate from the estimation of
1922 significant increase in E_{FOS} and E_{LUC} between the mid 1920s and the mid 1960s which is unmatched by a similar
1923 growth in atmospheric CO₂ concentration as recorded in ice cores (Figure 3). However, the known loss of
1924 additional sink capacity of 30-40 GtC (over the 1850-2020 period) due to reduced forest cover has not been
1925 accounted for in our method and would exacerbate the budget imbalance (see Section 2.10 and Supplement
1926 S.6.4).

1927 For the more recent 1960-2022 period where direct atmospheric CO₂ measurements are available, total
1928 emissions (E_{FOS} + E_{LUC}) amounted to 485 ± 50 GtC, of which 395 ± 20 GtC (82%) were caused by fossil CO₂

Formatted: Outline numbered + Level: 2 + Numbering
Style: 1, 2, 3, ... + Start at: 1 + Alignment: Left + Aligned at:
0 cm + Indent at: 1.02 cm

Formatted: Outline numbered + Level: 3 + Numbering
Style: 1, 2, 3, ... + Start at: 1 + Alignment: Left + Aligned at:
0 cm + Indent at: 1.27 cm

Formatted: Default Paragraph Font, Font colour: Black

Formatted: Normal, Centred, Border: Top: (No border),
Bottom: (No border), Left: (No border), Right: (No border),
Between : (No border), Tab stops: 7.96 cm, Centred + 15.92
cm, Right, Position: Horizontal: Left, Relative to: Column,
Vertical: In line, Relative to: Margin, Wrap Around

Formatted: Font colour: Black

1929 emissions, and 90 ± 45 GtC (18%) by land-use change (Table 8). The total emissions were partitioned among
1930 the atmosphere (215 ± 5 GtC; 44%), ocean (125 ± 25 GtC; 25%), and the land (150 ± 35 GtC; 31%), with a near
1931 zero (-5 GtC) unattributed budget imbalance. All components except land-use change emissions have
1932 significantly grown since 1960, with important interannual variability in the growth rate in atmospheric CO₂
1933 concentration and in the land CO₂ sink (Figure 4), and some decadal variability in all terms (Table 7).
1934 Differences with previous budget releases are documented in Figure S5.

1935 The global carbon budget averaged over the last decade (2013-2022) is shown in Figure 2, Figure 14 (right
1936 panel) and Table 7. For this period, 88% of the total emissions ($E_{\text{FOS}} + E_{\text{LUC}}$) were from fossil CO₂ emissions
1937 (E_{FOS}), and 12% from land-use change (E_{LUC}). The total emissions were partitioned among the atmosphere
1938 (47%), ocean (26%) and land (31%), with a small unattributed budget imbalance ($\sim 4\%$). For single years, the
1939 budget imbalance can be larger (Figure 4). For 2022, the combination of our estimated sources (11.1 ± 0.9 GtC
1940 yr^{-1}) and sinks (11.2 ± 0.9 GtC yr^{-1}) leads to a B_{IM} of -0.09 GtC, suggesting a near closure of the global carbon
1941 budget, although there is relatively high uncertainty on B_{IM} (± 1.3 GtC for 2022) as this is calculated as the
1942 residual of the five budget terms.

1943 3.9.2 Trend and Variability in the Carbon Budget Imbalance

1944 The carbon budget imbalance (B_{IM} ; Eq. 1, Figure 4) quantifies the mismatch between the estimated total
1945 emissions and the estimated changes in the atmosphere, land, and ocean reservoirs. The budget imbalance from
1946 1960 to 2022 is very small (-3.0 GtC over the period, i.e. average of 0.05 GtC yr^{-1}) and shows no trend over the
1947 full time series (Figure 4e). The process models (GOBMs and DGVMs) and data-products have been selected to
1948 match observational constraints in the 1990s, but no further constraints have been applied to their representation
1949 of trend and variability. Therefore, the near-zero mean and trend in the budget imbalance is seen as evidence of
1950 a coherent community understanding of the emissions and their partitioning on those time scales (Figure 4).
1951 However, the budget imbalance shows substantial variability of the order of ± 1 GtC yr^{-1} , particularly over semi-
1952 decadal time scales, although most of the variability is within the uncertainty of the estimates. The positive
1953 carbon imbalance during the 1960s, and early 1990s, indicates that either the emissions were overestimated, or
1954 the sinks were underestimated during these periods. The reverse is true for the 1970s, and to a lesser extent for
1955 the 1980s and 2013-2022 period (Figure 4, Table 7).

1956 We cannot attribute the cause of the variability in the budget imbalance with our analysis, we only note that the
1957 budget imbalance is unlikely to be explained by errors or biases in the emissions alone because of its large semi-
1958 decadal variability component, a variability that is atypical of emissions and has not changed in the past 60 years
1959 despite a near tripling in emissions (Figure 4). Errors in S_{LAND} and S_{OCEAN} are more likely to be the main cause
1960 for the budget imbalance, especially on interannual to semi-decadal timescales. For example, underestimation of
1961 the S_{LAND} by DGVMs has been reported following the eruption of Mount Pinatubo in 1991 possibly due to
1962 missing responses to changes in diffuse radiation (Mercado et al., 2009). Although since GCB2021 we
1963 accounted for aerosol effects on solar radiation quantity and quality (diffuse vs direct), most DGVMs only used
1964 the former as input (i.e., total solar radiation) (Table S1). Thus, the ensemble mean may not capture the full

Formatted: Outline numbered + Level: 3 + Numbering
Style: 1, 2, 3, ... + Start at: 1 + Alignment: Left + Aligned at:
0 cm + Indent at: 1.27 cm

Formatted: Default Paragraph Font, Font colour: Black

Formatted: Normal, Centred, Border: Top: (No border),
Bottom: (No border), Left: (No border), Right: (No border),
Between: (No border), Tab stops: 7.96 cm, Centred + 15.92
cm, Right, Position: Horizontal: Left, Relative to: Column,
Vertical: In line, Relative to: Margin, Wrap Around

Formatted: Font colour: Black

1965 effects of volcanic eruptions, i.e. associated with high light scattering sulphate aerosols, on the land carbon sink
1966 (O’Sullivan et al., 2021). DGVMs are suspected to overestimate the land sink in response to the wet decade of
1967 the 1970s (Sitch et al., 2008). Quasi-decadal variability in the ocean sink has also been reported, with all
1968 methods agreeing on a smaller than expected ocean CO₂ sink in the 1990s and a larger than expected sink in the
1969 2000s (Figure 10; Landschützer et al., 2016, DeVries et al., 2019, Hauck et al., 2020, McKinley et al., 2020,
1970 Gruber et al., 2023) and the climate-driven variability could be substantial but is not well constrained (DeVries
1971 et al., 2023, Müller et al., 2023). Errors in sink estimates could also be driven by errors in the climatic forcing
1972 data, particularly precipitation for S_{LAND} and wind for S_{OCEAN}. Also, the B_{IM} shows substantial departure from
1973 zero on yearly time scales (Figure 4e), highlighting unresolved variability of the carbon cycle, likely in the land
1974 sink (S_{LAND}), given its large year to year variability (Figure 4d and 8).

1975 Both the budget imbalance (B_{IM}, Table 7) and the residual land sink from the global budget (E_{FOS}+E_{ELUC}-G_{ATM}-
1976 S_{OCEAN}, Table 5) include an error term due to the inconsistencies that arises from combining E_{ELUC} from
1977 bookkeeping models with S_{LAND} from DGVMs, most notably the loss of additional sink capacity (see Section
1978 2.10 and Supplement S.6.4). Other differences include a better accounting of land use changes practices and
1979 processes in bookkeeping models than in DGVMs, or the bookkeeping models error of having present-day
1980 observed carbon densities fixed in the past. That the budget imbalance shows no clear trend towards larger
1981 values over time is an indication that these inconsistencies probably play a minor role compared to other errors
1982 in S_{LAND} or S_{OCEAN}.

1983 Although the budget imbalance is near zero for the recent decades, it could be due to a compensation of errors.
1984 We cannot exclude an overestimation of CO₂ emissions, particularly from land-use change, given their large
1985 uncertainty, as has been suggested elsewhere (Piao et al., 2018), and/or an underestimate of the sinks. A larger
1986 DGVM estimate of the atmosphere-land CO₂ flux (S_{LAND}-E_{ELUC}) over the extra-tropics would reconcile model
1987 results with inversion estimates for fluxes in the total land during the past decade (Figure 13; Table 5).
1988 Likewise, a larger S_{OCEAN} is also possible given the higher estimates from the *f*/CO₂-products (see Section 3.6.2,
1989 Figure 10 and Figure 13), the underestimation of interior ocean anthropogenic carbon accumulation in the
1990 GOBMs (Section 3.6.5), and the recently suggested upward adjustments of the ocean carbon sink in Earth
1991 System Models (Terhaar et al., 2022), and in *f*/CO₂-products, here related to a potential temperature bias and skin
1992 effects (Watson et al., 2020; Dong et al., 2022; Figure 10). If S_{OCEAN} were to be based on *f*/CO₂-products alone,
1993 with all *f*/CO₂-products including this adjustment, this would result in a 2013-2022 S_{OCEAN} of 3.7 GtC yr⁻¹ (Dong
1994 et al., 2022) or >3.9 GtC yr⁻¹ (Watson et al., 2020), i.e., outside of the range supported by the atmospheric
1995 inversions and with an implied negative B_{IM} of more than -1 GtC yr⁻¹ indicating that a closure of the budget
1996 could only be achieved with either anthropogenic emissions being significantly larger and/or the net land sink
1997 being substantially smaller than estimated here. A recent model study suggests that the skin effect is smaller
1998 (about 0.1 GtC yr⁻¹ or 5%) due to feedbacks with surface carbon concentration (Bellenger et al., 2023), which
1999 would nevertheless lead to a larger S_{OCEAN} even in the GOBMs. More integrated use of observations in the
2000 Global Carbon Budget, either on their own or for further constraining model results, should help resolve some of
2001 the budget imbalance (Peters et al., 2017).

Deleted: combined with

Formatted: Default Paragraph Font, Font colour: Black

Formatted: Normal, Centred, Border: Top: (No border),
Bottom: (No border), Left: (No border), Right: (No border),
Between : (No border), Tab stops: 7.96 cm, Centred + 15.92
cm, Right, Position: Horizontal: Left, Relative to: Column,
Vertical: In line, Relative to: Margin, Wrap Around

Formatted: Font colour: Black

2003 **4 Tracking progress towards mitigation targets**

2004 The average growth in global fossil CO₂ emissions peaked at nearly +3% per year during the 2000s, driven by
2005 the rapid growth in emissions in China. In the last decade, however, the global growth rate has slowly declined,
2006 reaching a low +0.5% per year over 2013-2022. While this slowdown in global fossil CO₂ emissions growth is
2007 welcome, global fossil CO₂ emissions continue to grow, far from the rapid emission decreases needed to be
2008 consistent with the temperature goals of the Paris Agreement.

2009 Since the 1990s, the average growth rate of fossil CO₂ emissions has continuously declined across the group of
2010 developed countries of the Organisation for Economic Co-operation and Development (OECD), with emissions
2011 peaking in around 2005 and now declining at around 1% yr⁻¹ (Le Quéré et al., 2021). In the decade 2013-2022,
2012 territorial fossil CO₂ emissions decreased significantly (at the 95% confidence level) in 26 countries/economies
2013 whose economies grew significantly ; Belgium, Brazil, Czechia, Denmark, Estonia, Finland, France, Germany,
2014 Greece, Hong Kong, Israel, Italy, Jamaica, Japan, Luxembourg, Netherlands, Norway, Portugal, Romania,
2015 Slovenia, South Africa, Sweden, Switzerland, United Kingdom, USA, Zimbabwe (updated from Le Quéré et al.,
2016 2019). Altogether, these 26 countries emitted 2.7 GtC yr⁻¹ (10.0 GtCO₂ yr⁻¹) on average over the last decade,
2017 about 28% of world CO₂ fossil emissions. For comparison, 22 countries showed a significant decrease in
2018 territorial fossil CO₂ emissions over the previous decade (2003-2012). Figure 16 shows that the emission
2019 declines in the USA and the EU27 are primarily driven by slightly weaker economic growth in the last decade
2020 compared to the 1990s, sustained declines in energy per GDP (though, weakening in the USA), and sustained
2021 declines in CO₂ emissions per unit energy (decarbonisation) with a slight acceleration in the USA in the last
2022 decade.

2023 In contrast, fossil CO₂ emissions continue to grow in non-OECD countries, although the growth rate has slowed
2024 from more than 6% yr⁻¹ during the 2000s to less than 2% yr⁻¹ in the last decade. Representing 47% of non-
2025 OECD emissions in 2022, a large part of this slowdown is due to China, which has seen emissions growth
2026 decline from 9% yr⁻¹ in the 2000s to 1.6% yr⁻¹ in the last decade. Excluding China, non-OECD emissions grew
2027 at 3.1% yr⁻¹ in the 2000s compared to 1.5% yr⁻¹ in the last decade. China has had weaker economic growth in
2028 the 2000s compared to the 2010s and a higher decarbonisation rate from 2005 to 2015 comparable to the highs
2029 in the 1990s, though the decarbonisation rate has slowed considerably since 2016 (Figure 16). India and the rest
2030 of the world have strong economic growth that is not offset by decarbonisation or declines in energy per GDP,
2031 driving up fossil CO₂ emissions. Despite the high deployment of renewables in some countries (e.g., India),
2032 fossil energy sources continue to grow to meet growing energy demand (Le Quéré et al., 2019).

2033 Globally, fossil CO₂ emissions growth is slowing, and this is due in part to the emergence of climate policy
2034 (Eskander and Fankhauser 2020; Le Quere et al 2019) and technological change, which is leading to a shift from
2035 coal to gas and growth in renewable energies, and reduced expansion of coal capacity. At the aggregated global
2036 level, decarbonisation shows a strong and growing signal in the last decade, with smaller contributions from
2037 lower economic growth and declines in energy per GDP. Altogether, global emissions are still growing (average

Formatted: Outline numbered + Level: 1 + Numbering
Style: 1, 2, 3, ... + Start at: 1 + Alignment: Left + Aligned at:
0 cm + Indent at: 0.76 cm

Deleted: 18

Deleted: (also at the 95% confidence level):

Deleted: , Croatia

Deleted: 18

Deleted: 1.9

Deleted: 7.1

Deleted: 20

Deleted: US

Deleted: almost

Deleted: 2.2

Deleted: Figure 16 shows that

Deleted: .

Deleted: Despite the slowing growth in

Deleted: fossil CO₂ emissions,

Deleted: ,

Formatted: Default Paragraph Font, Font colour: Black

Formatted: Normal, Centred, Border: Top: (No border),
Bottom: (No border), Left: (No border), Right: (No border),
Between : (No border), Tab stops: 7.96 cm, Centred + 15.92
cm, Right, Position: Horizontal: Left, Relative to: Column,
Vertical: In line, Relative to: Margin, Wrap Around

Formatted: Font colour: Black

2053 of 0.5% per year over the 2013-2022 decade), far from the reductions needed to meet the ambitious climate
2054 goals of the UNFCCC Paris agreement.

2055 This year we updated the remaining carbon budget (RCB) based on two studies, the IPCC AR6 (Canadell et al,
2056 2021) as used in GCB2022, and a recent revision of the IPCC AR6 estimates (Forster et al 2023, [Lamboll et al.,
2057 2023](#)). We update the RCB assessed by the IPCC AR6 (Canadell et al., 2021), accounting for the 2020 to 2023
2058 estimated emissions from fossil fuel combustion (E_{FOS}) and land use changes (E_{LUC}). From January 2024, the
2059 IPCC AR6 RCB (50% likelihood) for limiting global warming to 1.5°C, 1.7°C and 2°C is estimated to amount
2060 to 95, 190, and 325 GtC (340, 690, 1190 GtCO₂). The Forster et al. (2023) study proposed a significantly lower
2061 RCB than IPCC AR6, with the largest reduction being due to an update of the climate emulator (MAGICC)
2062 used to estimate the warming contribution of non-CO₂ agents, and to the warming (i.e. emissions) that occurred
2063 over the 2020-2022 period. We update the Forster et al., budget accounting for the 2023 estimated emissions
2064 from fossil fuel combustion (E_{FOS}) and land use changes (E_{LUC}). From January 2024, the Forster et al., (2023)
2065 RCB (50% likelihood) for limiting global warming to 1.5°C, 1.7°C and 2°C is estimated to amount to 55, 155,
2066 and 305 GtC (210, 560, 1110 GtCO₂), significantly smaller than the updated IPCC AR6 estimate. Both the
2067 original IPCC AR6 and Forster et al. (2023) estimates include an uncertainty due to the climate response to
2068 cumulative CO₂ emissions, which is reflected through the percent likelihood of exceeding the given temperature
2069 threshold, an additional uncertainty of 220GtCO₂ due to alternative non-CO₂ emission scenarios, and other
2070 sources of uncertainties (see Canadell et al., 2021). The two sets of estimates overlap when considering all
2071 uncertainties. The IPCC AR6 estimates have the advantage of a consensus building approach, while the Forster
2072 et al. (2023) estimates include significant update estimates but without the backing of the IPCC yet. Here, we
2073 take the average of our update of both IPCC AR6 and Forster et al. (2023) estimates, giving a remaining carbon
2074 (50% likelihood) for limiting global warming to 1.5°C, 1.7°C and 2°C of respectively 75, 175, and 315 GtC
2075 (275, 625, 1150 GtCO₂) starting from January 2024. We emphasise the large uncertainties, particularly when
2076 close to the global warming limit of 1.5°C. These 1.5°C, 1.7°C and 2°C average remaining carbon budgets
2077 correspond respectively to about 7, 15 and 28 years from the beginning of 2024, at the 2023 level of total
2078 anthropogenic CO₂ emissions. Reaching net-zero CO₂ emissions by 2050 entails cutting total anthropogenic
2079 CO₂ emissions by about 0.4 GtC (1.5 GtCO₂) each year on average, comparable to the decrease in E_{FOS}
2080 observed in 2020 during the COVID-19 pandemic. However, this would lead to cumulative emissions over
2081 2024-2050 of 150 GtC (550 GtCO₂), well above the remaining carbon budget of 75 GtC to limit global warming
2082 to 1.5°C, but still below the remaining budget of 175 GtC to limit warming to 1.7°C (in phase with the “well
2083 below 2°C” ambition of the Paris Agreement). Even reaching net zero CO₂ globally by 2040, which would
2084 require annual emissions cuts of 0.7 GtC (2.4 GtCO₂) on average, would still exceed the remaining carbon
2085 budget, with 95 GtC (350 GtCO₂) cumulative emissions over 2024-2050, unless the global emissions trajectory
2086 becomes net negative (i.e. more anthropogenic CO₂ sinks than emissions) after 2040.

2087 5 Discussion

2088 Each year when the global carbon budget is published, each flux component is updated for all previous years to
2089 consider corrections that are the result of further scrutiny and verification of the underlying data in the primary

Deleted:).

Formatted: Indent: Left: 0 cm, First line: 0 cm, Outline numbered + Level: 1 + Numbering Style: 1, 2, 3, ... + Start at: 1 + Alignment: Left + Aligned at: 0 cm + Indent at: 0.76 cm

Formatted: Default Paragraph Font, Font colour: Black

Formatted: Normal, Centred, Border: Top: (No border), Bottom: (No border), Left: (No border), Right: (No border), Between : (No border), Tab stops: 7.96 cm, Centred + 15.92 cm, Right, Position: Horizontal: Left, Relative to: Column, Vertical: In line, Relative to: Margin, Wrap Around

Formatted: Font colour: Black

2091 input data sets. Annual estimates may be updated with improvements in data quality and timeliness (e.g., to
2092 eliminate the need for extrapolation of forcing data such as land-use). Of all terms in the global budget, only the
2093 fossil CO₂ emissions and the growth rate in atmospheric CO₂ concentration are based primarily on empirical
2094 inputs supporting annual estimates in this carbon budget. The carbon budget imbalance, yet an imperfect
2095 measure, provides a strong indication of the limitations in observations, in understanding and representing
2096 processes in models, and/or in the integration of the carbon budget components.

2097 The persistent unexplained variability in the carbon budget imbalance limits our ability to verify reported
2098 emissions (Peters et al., 2017) and suggests we do not yet have a complete understanding of the underlying
2099 carbon cycle dynamics on annual to decadal timescales. Resolving most of this unexplained variability should
2100 be possible through different and complementary approaches. First, as intended with our annual updates, the
2101 imbalance as an error term should be reduced by improvements of individual components of the global carbon
2102 budget that follow from improving the underlying data and statistics and by improving the models through the
2103 resolution of some of the key uncertainties detailed in Table 10. Second, additional clues to the origin and
2104 processes responsible for the variability in the budget imbalance could be obtained through a closer scrutiny of
2105 carbon variability in light of other Earth system data (e.g., heat balance, water balance), and the use of a wider
2106 range of biogeochemical observations to better understand the land-ocean partitioning of the carbon imbalance
2107 such as the constraint from atmospheric oxygen included this year. Finally, additional information could also be
2108 obtained through better inclusion of process knowledge at the regional level, and through the introduction of
2109 inferred fluxes such as those based on satellite xCO₂ retrievals. The limit of the resolution of the carbon budget
2110 imbalance is yet unclear, but most certainly not yet reached given the possibilities for improvements that lie
2111 ahead.

2112 Estimates of global fossil CO₂ emissions from different datasets are in relatively good agreement when the
2113 different system boundaries of these datasets are considered (Andrew, 2020a). But while estimates of E_{FOS} are
2114 derived from reported activity data requiring much fewer complex transformations than some other components
2115 of the budget, uncertainties remain, and one reason for the apparently low variation between datasets is precisely
2116 the reliance on the same underlying reported energy data. The budget excludes some sources of fossil CO₂
2117 emissions, which available evidence suggests are relatively small (<1%). We have added emissions from lime
2118 production in China and the US, but these are still absent in most other non-Annex I countries, and before 1990
2119 in other Annex I countries.

2120 Estimates of E_{LUC} suffer from a range of intertwined issues, including the poor quality of historical land-cover
2121 and land-use change maps, the rudimentary representation of management processes in most models, and the
2122 confusion in methodologies and boundary conditions used across methods (e.g., Arneeth et al., 2017; Pongratz et
2123 al., 2014, see also Supplement S.6.4 on the loss of sink capacity; Bastos et al., 2021). Uncertainties in current
2124 and historical carbon stocks in soils and vegetation also add uncertainty in the E_{LUC} estimates. Unless a major
2125 effort to resolve these issues is made, little progress is expected in the resolution of E_{LUC}. This is particularly
2126 concerning given the growing importance of E_{LUC} for climate mitigation strategies, and the large issues in the
2127 quantification of the cumulative emissions over the historical period that arise from large uncertainties in E_{LUC}.

Formatted: Default Paragraph Font, Font colour: Black

Formatted: Normal, Centred, Border: Top: (No border),
Bottom: (No border), Left: (No border), Right: (No border),
Between : (No border), Tab stops: 7.96 cm, Centred + 15.92
cm, Right, Position: Horizontal: Left, Relative to: Column,
Vertical: In line, Relative to: Margin, Wrap Around

Formatted: Font colour: Black

2128 By adding the DGVMs estimates of CO₂ fluxes due to environmental change from countries' managed forest
2129 areas (part of S_{LAND} in this budget) to the budget E_{LUC} estimate, we successfully reconciled the large gap
2130 between our E_{LUC} estimate and the land use flux from NGHGs using the approach described in Grassi et al.
2131 (2021) for future scenarios and in Grassi et al. (2023) using data from the Global Carbon Budget 2021. The
2132 updated data presented here can be used as potential adjustment in the policy context, e.g., to help assess the
2133 collective countries' progress towards the goal of the Paris Agreement and avoiding double-accounting for the
2134 sink in managed forests. In the absence of this adjustment, collective progress would hence appear better than it
2135 is (Grassi et al., 2021). The application of this adjustment is also recommended in the UNFCCC Synthesis
2136 report for the first Global Stocktake (UNFCCC, 2022) whenever a comparison between LULUCF fluxes
2137 reported by countries and the global emission estimates of the IPCC is conducted. However, this adjustment
2138 should be seen as a short-term and pragmatic fix based on existing data, rather than a definitive solution to
2139 bridge the differences between global models and national inventories. Additional steps are needed to
2140 understand and reconcile the remaining differences, some of which are relevant at the country level (Grassi, et
2141 al., 2023, Schwingshackl, et al., 2022).

2142 The comparison of GOBMs, *f*CO₂-products, and inversions highlights substantial discrepancy in the temporal
2143 evolution of S_{OCEAN} in the Southern Ocean and northern high-latitudes (Figure 13, Hauck et al., 2023) and in the
2144 mean S_{OCEAN} in the tropics. A large part of the uncertainty in the mean fluxes stems from the regional
2145 distribution of the river flux adjustment term. The current distribution simulates the largest share of the
2146 outgassing to occur in the tropics (Lacroix et al., 2020) in contrast to the regional distribution previously used
2147 with the largest riverine outgassing flux south of 20°S (Aumont et al., 2001). The long-standing sparse data
2148 coverage of *f*CO₂ observations in the Southern compared to the Northern Hemisphere (e.g., Takahashi et al.,
2149 2009) continues to exist (Bakker et al., 2016, 2022, Figure S1) and to lead to substantially higher uncertainty in
2150 the S_{OCEAN} estimate for the Southern Hemisphere (Watson et al., 2020, Gloege et al., 2021, Hauck et al., 2023).
2151 This discrepancy, which also hampers model improvement, points to the need for increased high-quality *f*CO₂
2152 observations especially in the Southern Ocean. At the same time, model uncertainty is illustrated by the large
2153 spread of individual GOBM estimates (indicated by shading in Figure 13) and highlights the need for model
2154 improvement. The diverging trends in S_{OCEAN} from different methods is a matter of concern. Recent and on-
2155 going work suggests that the *f*CO₂-products may overestimate the trend (Hauck et al., 2023), though many
2156 products remain to be tested, whereas evidence is accumulating that GOBMs likely underestimate the mean flux
2157 (Section 3.6.2, Terhaar et al., 2022, DeVries et al., 2023, Müller et al., 2023). The independent constraint from
2158 atmospheric oxygen measurements is consistent within errors with the relatively larger ocean sink in the *f*CO₂-
2159 products. The assessment of the net land-atmosphere exchange from DGVMs and atmospheric inversions also
2160 shows substantial discrepancy, particularly for the estimate of the net land flux over the northern extra-tropic.
2161 This discrepancy highlights the difficulty to quantify complex processes (CO₂ fertilisation, nitrogen deposition
2162 and fertilisers, climate change and variability, land management, etc.) that collectively determine the net land
2163 CO₂ flux. Resolving the differences in the Northern Hemisphere land sink will require the consideration and
2164 inclusion of larger volumes of observations.

Formatted: Default Paragraph Font, Font colour: Black

Formatted: Normal, Centred, Border: Top: (No border),
Bottom: (No border), Left: (No border), Right: (No border),
Between : (No border), Tab stops: 7.96 cm, Centred + 15.92
cm, Right, Position: Horizontal: Left, Relative to: Column,
Vertical: In line, Relative to: Margin, Wrap Around

Formatted: Font colour: Black

2165 We provide metrics for the evaluation of the ocean and land models and the atmospheric inversions (Figures B2
2166 to B4, Table S10). These metrics expand the use of observations in the global carbon budget, helping 1) to
2167 support improvements in the ocean and land carbon models that produce the sink estimates, and 2) to constrain
2168 the representation of key underlying processes in the models and to allocate the regional partitioning of the CO₂
2169 fluxes. The introduction of process-based metrics targeted to evaluate the simulation of Socean in the ocean
2170 biogeochemistry models is an important addition to the evaluation based on ocean carbon observations. This is
2171 an initial step towards the introduction of a broader range of observations and more stringent model evaluation
2172 that we hope will support continued improvements in the annual estimates of the global carbon budget.

2173 We assessed before that a sustained decrease of -1% in global emissions could be detected at the 66%
2174 likelihood level after a decade only (Peters et al., 2017). Similarly, a change in behaviour of the land and/or
2175 ocean carbon sink would take as long to detect, and much longer if it emerges more slowly. To continue
2176 reducing the carbon imbalance on annual to decadal time scales, regionalising the carbon budget, and integrating
2177 multiple variables are powerful ways to shorten the detection limit and ensure the research community can
2178 rapidly identify issues of concern in the evolution of the global carbon cycle under the current rapid and
2179 unprecedented changing environmental conditions.

2180 6 Conclusions

2181 The estimation of global CO₂ emissions and sinks is a major effort by the carbon cycle research community that
2182 requires a careful compilation and synthesis of measurements, statistical estimates, and model results. The
2183 delivery of an annual carbon budget serves two purposes. First, there is a large demand for up-to-date
2184 information on the state of the anthropogenic perturbation of the climate system and its underpinning causes. A
2185 broad stakeholder community relies on the data sets associated with the annual carbon budget including
2186 scientists, policy makers, businesses, journalists, and non-governmental organisations engaged in adapting to
2187 and mitigating human-driven climate change. Second, over the last decades we have seen unprecedented
2188 changes in the human and biophysical environments (e.g., changes in the growth of fossil fuel emissions, impact
2189 of COVID-19 pandemic, Earth's warming, and strength of the carbon sinks), which call for frequent
2190 assessments of the state of the planet, a better quantification of the causes of changes in the contemporary global
2191 carbon cycle, and an improved capacity to anticipate its evolution in the future. Building this scientific
2192 understanding to meet the extraordinary climate mitigation challenge requires frequent, robust, transparent, and
2193 traceable data sets and methods that can be scrutinised and replicated. This paper via 'living data' helps to keep
2194 track of new budget updates.

2195 Data availability

2196 The data presented here are made available in the belief that their wide dissemination will lead to greater
2197 understanding and new scientific insights of how the carbon cycle works, how humans are altering it, and how
2198 we can mitigate the resulting human-driven climate change. Full contact details and information on how to cite
2199 the data shown here are given at the top of each page in the accompanying database and summarised in Table 2.

Formatted: Indent: Left: 0 cm, First line: 0 cm, Outline numbered + Level: 1 + Numbering Style: 1, 2, 3, ... + Start at: 1 + Alignment: Left + Aligned at: 0 cm + Indent at: 0.76 cm

Formatted: Default Paragraph Font, Font colour: Black

Formatted: Normal, Centred, Border: Top: (No border), Bottom: (No border), Left: (No border), Right: (No border), Between: (No border), Tab stops: 7.96 cm, Centred + 15.92 cm, Right, Position: Horizontal: Left, Relative to: Column, Vertical: In line, Relative to: Margin, Wrap Around

Formatted: Font colour: Black

2200 The accompanying database includes three Excel files organised in the following spreadsheets:

2201 File Global_Carbon_Budget_2023v1.0.xlsx includes the following:

Deleted: 2023v0.1

- 2202 1. Summary
- 2203 2. The global carbon budget (1959-2022);
- 2204 3. The historical global carbon budget (1750-2022);
- 2205 4. Global CO₂ emissions from fossil fuels and cement production by fuel type, and the per-capita emissions (1850-2022);
- 2206
- 2207 5. CO₂ emissions from land-use change from the individual bookkeeping models (1959-2022);
- 2208 6. Ocean CO₂ sink from the individual global ocean biogeochemistry models and fCO₂-products (1959-2022);
- 2209
- 2210 7. Terrestrial CO₂ sink from the individual DGVMs (1959-2022);
- 2211 8. Cement carbonation CO₂ sink (1959-2022).

Formatted: Indent: Left: 0.12 cm, Outline numbered + Level: 4 + Numbering Style: 1, 2, 3, ... + Start at: 1 + Alignment: Left + Aligned at: 4.44 cm + Indent at: 5.08 cm

2212 File National_Fossil_Carbon_Emissions_2023v1.0.xlsx includes the following:

Deleted: 2023v0.1

- 2213 1. Summary
- 2214 2. Territorial country CO₂ emissions from fossil fuels and cement production (1850-2022);
- 2215 3. Consumption country CO₂ emissions from fossil fuels and cement production and emissions transfer from the international trade of goods and services (1990-2020) using CDIAC/UNFCCC data as reference;
- 2216
- 2217 4. Emissions transfers (Consumption minus territorial emissions; 1990-2020);
- 2218 5. Country definitions.

Formatted: Indent: Left: 0.12 cm, Outline numbered + Level: 4 + Numbering Style: 1, 2, 3, ... + Start at: 1 + Alignment: Left + Aligned at: 4.44 cm + Indent at: 5.08 cm

2219 File National_LandUseChange_Carbon_Emissions_2023v1.0.xlsx includes the following:

Deleted: 2023v0.1.xlsx

- 2220 1. Summary
- 2221 2. Territorial country CO₂ emissions from Land Use Change (1850-2022) from three bookkeeping models;

Formatted: Indent: Left: 0.12 cm, Outline numbered + Level: 4 + Numbering Style: 1, 2, 3, ... + Start at: 1 + Alignment: Left + Aligned at: 4.44 cm + Indent at: 5.08 cm

2222 All three spreadsheets are published by the Integrated Carbon Observation System (ICOS) Carbon Portal and
2223 are available at <https://doi.org/10.18160/GCP-2023> (Friedlingstein et al., 2023). National emissions data are also
2224 available on Zenodo (Andrew and Peters, 2022), from the Global Carbon Atlas
2225 (<http://www.globalcarbonatlas.org/>, last access: 9 November 2023) and from Our World in Data
2226 (<https://ourworldindata.org/co2-emissions>, last access: 9 November 2023).

Deleted: 27 September

Deleted: 27 September

Formatted: Default Paragraph Font, Font colour: Black

Formatted: Normal, Centred, Border: Top: (No border), Bottom: (No border), Left: (No border), Right: (No border), Between: (No border), Tab stops: 7.96 cm, Centred + 15.92 cm, Right, Position: Horizontal: Left, Relative to: Column, Vertical: In line, Relative to: Margin, Wrap Around

Formatted: Font colour: Black

2232 **Author contributions**

2233 PF, MO, MWJ, RMA, DCEB, JH, PL, CLQ, ITL, GPP, WP, JP, CSc, and SSi designed the study, conducted the
2234 analysis, and wrote the paper with input from JGC, PCi and RBJ. RMA, GPP and JIK produced the fossil CO₂
2235 emissions and their uncertainties and analysed the emissions data. MH and GMa provided fossil fuel emission
2236 data. JP, TGA, CSc and RAH provided the bookkeeping land-use change emissions with synthesis by JP and
2237 CSc. FJo provided peat drainage emission estimates. SSm and CMP provided the estimates of non-vegetation
2238 CDR fluxes. LBo, MCh, ÖG, NG, TI, TJ, LR, JS, RS, and HiT provided an update of the global ocean
2239 biogeochemical models, TTTC, DF, LG, YI, AJ, GMc, ChR, and JZ provided an update of the ocean fCO₂-data
2240 products, with synthesis on both streams by JH, PL and NMa. SRA, LBa, NRB, MB, MCr, KE, WE, RAF, TGk,
2241 AK, NL, DRM, SN, AO, AMO, TO, MEP, DP, KP, GR, AJS, CSw, ST, BT, EvO, RW, and CWR provided
2242 ocean fCO₂ measurements for the year 2022, with synthesis by DCEB and KMO. PA, DB, SF, JG, HJ, AKJ,
2243 EK, DK, JK, GMe, LM, PM, MO, BP, TLS, QS, HTi, WY, XYua, XYue, and SZ provided an update of the
2244 Dynamic Global Vegetation Models, with synthesis by SSi and MO. HL, RSA, MW, and PCa provided
2245 estimates of land and ocean sinks from Earth System Models, as well as a projection of the atmospheric growth
2246 rate for 2023. FC, ITL, NC, LF, ARJ, FJi, JL, ZJin, ZLiu, YN, CR, DY, and BZ provided an updated
2247 atmospheric inversion, WP, FC, and ITL developed the protocol and produced the synthesis and evaluation of
2248 the atmospheric inversions. RMA provided projections of the 2023 fossil emissions and atmospheric CO₂
2249 growth rate. PL provided the predictions of the 2023 ocean and land sinks. IBMB, LPC, GCH, KKG, TMR, and
2250 GRvdW provided forcing data for land-use change. FT and GG provided data for the land-use change NGHGI
2251 harmonisation. RK provided key atmospheric CO₂ data. EJM and RFK provided the atmospheric oxygen
2252 constraint on surface net carbon sinks. XL, PPT and MWJ provided the historical atmospheric CO₂
2253 concentration and growth rate. MO and NB produced the aerosol diffuse radiative forcing for the DGVMs. IH
2254 provided the climate forcing data for the DGVMs. ER provided the evaluation of the DGVMs. MWJ provided
2255 the emissions prior for use in the inversion systems. XD provided seasonal emissions data for most recent years
2256 for the emission prior. PF, MO and MWJ coordinated the effort, revised all figures, tables, text and numbers to
2257 ensure the update was clear from the 2022 edition and in line with the globalcarbonatlas.org.

Formatted: Default Paragraph Font, Font colour: Black

Formatted: Normal, Centred, Border: Top: (No border),
Bottom: (No border), Left: (No border), Right: (No border),
Between : (No border), Tab stops: 7.96 cm, Centred + 15.92
cm, Right, Position: Horizontal: Left, Relative to: Column,
Vertical: In line, Relative to: Margin, Wrap Around

Formatted: Font colour: Black

2258 **Competing interests.**

2259 At least one of the (co-)authors is a member of the editorial board of Earth System Science Data

2260 **Acknowledgements**

2261 We thank all people and institutions who provided the data used in this global carbon budget 2023 and the Global
2262 Carbon Project members for their input throughout the development of this publication. We thank Nigel Hawtin
2263 for producing Figure 2 and Figure 15. We thank Alex Vermeulen and Hanna Ritchie for respectively hosting the
2264 Global Carbon Budget datasets on the ICOS portal and the Our World in Data website. We thank Ian G. C. Ashton,
2265 Sebastian Brune, Fatemeh Cheginig, Sam Ditkovsky, Christian Ethé, Amanda R. Fay, Lonneke Goddijn-Murphy,
2266 T. Holding, Yawen Kong, Fabrice Lacroix, Yi Liu, Damian Loher, Naiqing Pan, Paridhi Rustogi, Shijie Shu, J.
2267 D. Shutler, Richard Sims, Phillip Townsend, Jing Wang, Andrew J. Watson, and David K. Woolf for their
2268 involvement in the development, use and analysis of the models and data-products used here. We thank Toste
2269 Tanhua, Marcos Fontela, Claire Lo Monaco and Nicolas Metzl who contributed to the provision of surface ocean
2270 CO₂ observations for the year 2022 (see Table S6). We also thank Stephen D. Jones of the Ocean Thematic Centre
2271 of the EU Integrated Carbon Observation System (ICOS) Research Infrastructure, Eugene Burger of NOAA's
2272 Pacific Marine Environmental Laboratory and Alex Kozyr of NOAA's National Centers for Environmental
2273 Information, for their contribution to surface ocean CO₂ data and metadata management. This is PMEL
2274 contribution 5550. We thank the scientists, institutions, and funding agencies responsible for the collection and
2275 quality control of the data in SOCAT as well as the International Ocean Carbon Coordination Project (IOCCP),
2276 the Surface Ocean Lower Atmosphere Study (SOLAS) and the Integrated Marine Biosphere Research (IMBeR)
2277 program for their support. We thank [Nadine Goris](#) and [Lavinia Patara](#) for [support in calculating observational](#)
2278 [ocean evaluation metrics](#). We thank Fortunat Joos, Samar Khatiwala and Timothy DeVries for providing historical
2279 atmospheric and ocean data. [We thank data providers ObsPack GLOBALVIEWplus v8.0 and NRT v8.1 for](#)
2280 [atmospheric CO₂ observations](#). Ingrid T Lujikx and Wouter Peters thank the CarbonTracker Europe team at
2281 Wageningen University, including Remco de Kok, Joram Hooghiem, Linda Kooijmans and Auke van der Woude.
2282 Daniel Kennedy thanks all the scientists, software engineers, and administrators who contributed to the
2283 development of CESM2. Josefine Ghattas thanks the whole ORCHIDEE group. Ian Harris thanks the Japan
2284 Meteorological Agency (JMA) for producing the Japanese 55-year Reanalysis (JRA-55). Reinel Sospedra-
2285 Alfonso thanks Barbara Winter, Woosung Lee, and William J. Merryfield for their contribution to the preparation

Deleted: data providers ObsPack GLOBALVIEWplus v8.0

Deleted: NRT v8.1

Deleted: atmospheric CO₂ observations

Formatted: Default Paragraph Font, Font colour: Black

Formatted: Normal, Centred, Border: Top: (No border), Bottom: (No border), Left: (No border), Right: (No border), Between : (No border), Tab stops: 7.96 cm, Centred + 15.92 cm, Right, Position: Horizontal: Left, Relative to: Column, Vertical: In line, Relative to: Margin, Wrap Around

Formatted: Font colour: Black

2289 and production of CanESM5 runs. Patricia Cadule thanks Olivier Torres, Juliette Mignot, Didier Swingedouw,
2290 and Laurent Bopp for contributions to the IPSL-CM6-LR-ESMCO2 simulations. Yosuke Niwa thanks CSIRO,
2291 EC, EMPA, FMI, IPEN, JMA, LSCE, NCAR, NIES, NILU, NIWA, NOAA, SIO, and TU/NIPR for providing
2292 data for NISMOM-CO2. Zhe Jin thanks Xiangjun Tian, Yilong Wang, Hongqin Zhang, Min Zhao, Tao Wang,
2293 Jinzhi Ding and Shilong Piao for their contributions to the GONGGA inversion system. Bo Zheng thanks Yawen
2294 Kong for running the THU inversion system. Frédéric Chevallier thanks Zoé Lloret who maintained the
2295 atmospheric transport model for the CAMS inversions. Frédéric Chevallier and Thi-Tuyet-Trang Chau thank
2296 Marion Gehlen for her contribution to the CMEMS-LSCE-FFNNv2 product. Lian Fang thanks Paul I. Palmer and
2297 acknowledges ongoing support from the National Centre for Earth Observation. Junjie Liu thanks the Jet
2298 Propulsion Laboratory, California Institute of Technology. Zhiqiang Liu thanks Ning Zeng, Yun Liu, Eugenia
2299 Kalnay, and Gassem Asrar for their contributions to the COLA system. Fei Jiang acknowledges ongoing support
2300 from Frontiers Science Center for Critical Earth Material Cycling, Nanjing University. Andy Jacobson thanks the
2301 team at NOAA GML, Boulder, Colorado, USA, who provided the CarbonTracker CT2022 and CT-NRT.v2023-
2302 3 results from the website at <http://carbontracker.noaa.gov>. Meike Becker and Are Olsen thank Sparebanken Vest
2303 / Agenda Vestlandet for their support for the observations on the Statsraad Lehmkühl. Margot Cronin thanks
2304 Anthony English, Clynt Gregory and Gordon Furey (P&O Maritime Services), Tobias Steinhoff and Aodhan
2305 Fitzgerald (Marine Institute) for their support. Wiley Evans and Katie Pocock thank the Tula Foundation for
2306 funding support. Thanos Gkritzalis and the VLIZ ICOS team are thankful to the crew of the research vessel Simon
2307 Stevin for all the support and help they provide. Data providers Nicolas Metzl and Claire LoMonaco thank the
2308 French Institut National des Sciences de l'Univers (INSU), Institut Polaire français, Paul-Emile Victor(IPEV),
2309 Observatoire des sciences de l'univers Ecce-Terra (OSU at Sorbonne Université), Institut de recherche français
2310 sur les ressources marines (IFREMER), French Oceanographic Fleet (FOF) for the Marion Dufresne data set
2311 (<http://dx.doi.org/10.17600/18001858>). Bronte Tilbrook and Erik van Ooijen thank Australia's Integrated Marine
2312 Observing System (IMOS) for sourcing of CO₂ data. IMOS is enabled by the National Collaborative Research
2313 Infrastructure Strategy (NCRIS). FAOSTAT is funded by FAO member states through their contributions to the
2314 FAO Regular Programme, data contributions by national experts are greatly acknowledged. The views expressed
2315 in this paper are the authors' only and do not necessarily reflect those of FAO. Finally, we thank all funders who
2316 have supported the individual and joint contributions to this work (see details below), as well as the [two](#)
2317 [anonymous](#) reviewers of this manuscript, and the many researchers who have provided feedback.

Deleted: and previous versions

Formatted: Default Paragraph Font, Font colour: Black

Formatted: Normal, Centred, Border: Top: (No border), Bottom: (No border), Left: (No border), Right: (No border), Between : (No border), Tab stops: 7.96 cm, Centred + 15.92 cm, Right, Position: Horizontal: Left, Relative to: Column, Vertical: In line, Relative to: Margin, Wrap Around

Formatted: Font colour: Black

2319 **Financial and computing support**

2320 This research was supported by the following sources of funding: Integrated Marine Observing System (IMOS)
2321 [Australia]; ICOS Flanders [Belgium]; Research Foundation Flanders (grant no. I001821N) [Belgium]; Tula
2322 Foundation [Canada]; Chinese Academy of Science Project for Young Scientists in Basic Research (Grant No.
2323 YSBR-037) [China]; National Key R&D Program of China (Grant No: 2020YFA0607504); National Natural
2324 Science Foundation (grant no. 42141020, 42275128) [China]; National Natural Science Foundation (grant no.
2325 42275128) [China]; National Natural Science Foundation (grant no. 41921005) [China]; Scientific Research Start-
2326 up Funds (grant no. QD2021024C) from Tsinghua Shenzhen International Graduate School [China]; Second
2327 Tibetan Plateau Scientific Expedition and Research Program (Grant: 2022QZKK0101) [China]; Young Elite
2328 Scientists Sponsorship Program by CAST (grant no. YESS20200135) [China]; Copernicus Atmosphere
2329 Monitoring Service, implemented by ECMWF (Grant: CAMS2 55) [EC]; Copernicus Marine Environment
2330 Monitoring Service, implemented by MOi (Grant: CAMS2 55) [EC]; H2020 (Horizon 2020) 4C (grant no.
2331 821003) [European Commission, EC]; H2020 ESM2025 – Earth System Models for the Future (grant no.
2332 101003536) [European Commission, EC]; H2020 EuroSea (grant no. 862626) [EC]; H2020 GEORGE (grant no.
2333 101094716) [EC]; H2020 JERICO-S3 (grant no. 871153) [EC]; ICOS France [France]; Institut de Recherche pour
2334 le Développement (IRD) [France]; Federal Ministry of Education and Research (BMBF) (grant no. 03F0885AL1)
2335 [Germany]; Federal Ministry of Education and Research, collaborative project C-SCOPE (Towards Marine
2336 Carbon Observations 2.0: Socializing, COnnecting, Perfecting and Expanding, project no. 03F0877A) [Germany];
2337 Helmholtz Association ATMO programme [Germany]; Helmholtz Association of German Research Centres
2338 (project MOSES; Modular Observation Solutions for Earth Systems) [Germany]; ICOS (Integrated Carbon
2339 Observation System) Germany [Germany]; Ludwig-Maximilians-University Munich, Department of Geography
2340 [Germany]; Marine Institute [Ireland]; Arctic Challenge for Sustainability phase II project (ArCS-II; grant no. JP-
2341 MXD1420318865) [Japan]; Environment Research and Technology Development Fund (grant no. JP-
2342 MEERF21S20800) [Japan]; Fundamental Research Funds for the Central Universities (Grant No:
2343 090414380031); Global Environmental Research Coordination System, Ministry of the Environment (grant no.
2344 E2252) [Japan]; Japan Meteorological Agency [Japan]; Ministry of Education, Culture, Sports, Science and
2345 Technology, MEXT program for the advanced studies of climate change projection (SENTAN) (grant numbers
2346 JPMXD0722680395, JPMXD0722681344) [Japan]; Ministry of Environment, Environmental Restoration and
2347 Conservation Agency, Environment Research and Technology Development Fund (grant no.

Formatted: Justified, Line spacing: Double

Formatted: Default Paragraph Font, Font colour: Black

Formatted: Normal, Centred, Border: Top: (No border), Bottom: (No border), Left: (No border), Right: (No border), Between : (No border), Tab stops: 7.96 cm, Centred + 15.92 cm, Right, Position: Horizontal: Left, Relative to: Column, Vertical: In line, Relative to: Margin, Wrap Around

Formatted: Font colour: Black

2348 JPMEERF21S20810) [Japan]; [National Institute for Environmental Studies \[Japan\]](#); Research Council of Norway
2349 (N-ICOS-2, grant no. 296012) [Norway]; Swiss National Science Foundation (grant no. 200020-200511)
2350 [Switzerland]; National Centre for Atmospheric Science [UK]; NERC (Natural Environment Research Council)
2351 Independent Research Fellowship (NE/V01417X/1) [UK]; NERC (NE/R016518/1) [UK]; Royal Society (grant
2352 no. RP/R1\191063) [UK]; UK Research and Innovation (UKRI) for Horizon Europe (GreenFeedBack, grant no.
2353 10040851) [UK]; NASA Carbon Monitoring System program (80NSSC21K1059) [USA]; NASA OCO Science
2354 team program (80NM0018F0583) [USA]; National Center for Atmospheric Research (NCAR) cooperative
2355 agreement (NSF No. 1852977) [USA]; National Oceanic and Atmospheric Administration (NOAA) cooperative
2356 agreement (NA22OAR4320151) [USA]; National Science Foundation (NSF- 831361857) [USA]; NOAA
2357 (NA20OAR4320278) [USA]; NOAA Cooperative Agreement, Cooperative Institute for Climate, Ocean, &
2358 Ecosystem Studies (CIOCES; NA20OAR4320271) [USA]; NOAA Cooperative Agreement, Cooperative Institute
2359 for Marine and Atmospheric Studies (CIMAS) / University of Miami (NA20OAR4320472) [USA]; NOAA
2360 Global Ocean Monitoring and Observing Program (grant no. 100018302, 100007298, NA-03-AR4320179)
2361 [USA]; NOAA Ocean Acidification Program [USA]; National Science Foundation (OPP-1922922) [USA]. We
2362 also acknowledge support from the following computing facilities: Adapter Allocation Scheme from the National
2363 Computational Infrastructure (NCI) [Australia]; High-Performance Computing Center (HPCC) of Nanjing
2364 University [China]; GENCI -TGCC (A0130102201, A0130106328, A0140107732 and A0130107403) [France],
2365 CCRT awarded by CEA/DRF (CCRT2023-p24cheva) [France]; HPC cluster Aether at the University of Bremen,
2366 financed by DFG within the scope of the Excellence Initiative [Germany], the State of Baden-Württemberg,
2367 through bwHPC [Germany]; Earth Simulator (ES4) at JAMSTEC [Japan], JAMSTEC's Super Computer system
2368 [Japan], NIES supercomputer system [Japan], NIES (SX-Aurora) and MRI (FUJITSU Server PRIMERGY
2369 CX2550M5) [Japan]; ADA HPC cluster at the University of East Anglia [UK], UK CEDA JASMIN
2370 supercomputer [UK]; Cheyenne NCAR HPC resources managed by CISL (doi:10.5065/D6RX99HX) [USA].

2371

2372

Deleted: ¶

Formatted: Default Paragraph Font, Font colour: Black

Formatted: Normal, Centred, Border: Top: (No border),
Bottom: (No border), Left: (No border), Right: (No border),
Between : (No border), Tab stops: 7.96 cm, Centred + 15.92
cm, Right, Position: Horizontal: Left, Relative to: Column,
Vertical: In line, Relative to: Margin, Wrap Around

Formatted: Font colour: Black

2374 **References**

- 2375 Ahlström, A., Raupach, M. R., Schurgers, G., Smith, B., Arneth, A., Jung, M., Reichstein, M., Canadell, J. G.,
2376 Friedlingstein, P., Jain, A. K., Kato, E., Poulter, B., Sitch, S., Stocker, B. D., Viovy, N., Wang, Y. P., Wiltshire, A., Zaehle,
2377 S., and Zeng, N.: The dominant role of semi-arid ecosystems in the trend and variability of the land CO₂ sink, 348, 895–899,
2378 <https://doi.org/10.1126/science.aaa1668>, 2015.
- 2379 Amador-Jiménez, M., Millner, N., Palmer, C., Pennington, R. T., and Sileci, L.: The Unintended Impact of Colombia's
2380 Covid-19 Lockdown on Forest Fires, *Environ Resource Econ*, 76, 1081–1105, <https://doi.org/10.1007/s10640-020-00501-5>,
2381 2020.
- 2382 Andela, N., Morton, D. C., Giglio, L., Chen, Y., van der Werf, G. R., Kasibhatla, P. S., DeFries, R. S., Collatz, G. J.,
2383 Hantson, S., Kloster, S., Bachelet, D., Forrest, M., Lasslop, G., Li, F., Mangeon, S., Melton, J. R., Yue, C., and Randerson, J.
2384 T.: A human-driven decline in global burned area, *Science*, 356, 1356–1362, <https://doi.org/10.1126/science.aal4108>, 2017.
- 2385 Andrew, R. M.: A comparison of estimates of global carbon dioxide emissions from fossil carbon sources, *Earth Syst. Sci.*
2386 *Data*, 12, 1437–1465, <https://doi.org/10.5194/essd-12-1437-2020>, 2020a.
- 2387 Andrew, R. M.: Timely estimates of India's annual and monthly fossil CO₂ emissions, *Earth Syst. Sci. Data*, 12, 2411–2421,
2388 <https://doi.org/10.5194/essd-12-2411-2020>, 2020b.
- 2389 Andrew, R. M. and Peters, G. P.: The Global Carbon Project's fossil CO₂ emissions dataset (2022v27), [https://doi.org/](https://doi.org/10.5281/zenodo.7215364)
2390 [10.5281/zenodo.7215364](https://doi.org/10.5281/zenodo.7215364), 2022.
- 2391 Angelsen, A. and Kaimowitz, D.: Rethinking the Causes of Deforestation: Lessons from Economic Models, *World Bank*
2392 *Res. Obs.*, 14, 73–98, <https://doi.org/10.1093/wbro/14.1.73>, 1999.
- 2393 Aragão, L. E. O. C., Anderson, L. O., Fonseca, M. G., Rosan, T. M., Vedovato, L. B., Wagner, F. H., Silva, C. V. J., Silva
2394 Junior, C. H. L., Arai, E., Aguiar, A. P., Barlow, J., Berenguer, E., Deeter, M. N., Domingues, L. G., Gatti, L., Gloor, M.,
2395 Malhi, Y., Marengo, J. A., Miller, J. B., Phillips, O. L., and Saatchi, S.: 21st Century drought-related fires counteract the
2396 decline of Amazon deforestation carbon emissions, *Nat Commun*, 9, 536, <https://doi.org/10.1038/s41467-017-02771-y>,
2397 2018.
- 2398 Archer, D., Eby, M., Brovkin, V., Ridgwell, A., Cao, L., Mikolajewicz, U., Caldeira, K., Matsumoto, K., Munhoven, G.,
2399 Montenegro, A., and Tokos, K.: Atmospheric Lifetime of Fossil Fuel Carbon Dioxide, *Annu. Rev. Earth Planet. Sci.*, 37,
2400 117–134, <https://doi.org/10.1146/annurev.earth.031208.100206>, 2009.
- 2401 Arneth, A., Sitch, S., Pongratz, J., Stocker, B. D., Ciais, P., Poulter, B., Bayer, A. D., Bondeau, A., Calle, L., Chini, L. P.,
2402 Gasser, T., Fader, M., Friedlingstein, P., Kato, E., Li, W., Lindeskog, M., Nabel, J. E. M. S., Pugh, T. A. M., Robertson, E.,
2403 Viovy, N., Yue, C., and Zaehle, S.: Historical carbon dioxide emissions caused by land-use changes are possibly larger than
2404 assumed, *Nature Geosci*, 10, 79–84, <https://doi.org/10.1038/ngeo2882>, 2017.
- 2405 Asaadi, A., Arora, V. K., Melton, J. R., and Bartlett, P.: An improved parameterization of leaf area index (LAI) seasonality
2406 in the Canadian Land Surface Scheme (CLASS) and Canadian Terrestrial Ecosystem Model (CTEM) modelling framework,
2407 15, 6885–6907, <https://doi.org/10.5194/bg-15-6885-2018>, 2018.

Formatted: Space Before: 12 pt, After: 12 pt

Deleted: org/record/

Formatted: Default Paragraph Font, Font colour: Black

Formatted: Normal, Centred, Border: Top: (No border),
Bottom: (No border), Left: (No border), Right: (No border),
Between : (No border), Tab stops: 7.96 cm, Centred + 15.92
cm, Right, Position: Horizontal: Left, Relative to: Column,
Vertical: In line, Relative to: Margin, Wrap Around

Formatted: Font colour: Black

- 2409 Aumont, O., Orr, J. C., Monfray, P., Ludwig, W., Amiotte-Suchet, P., and Probst, J.-L.: Riverine-driven interhemispheric
2410 transport of carbon, *Global Biogeochem. Cycles*, 15, 393–405, <https://doi.org/10.1029/1999GB001238>, 2001.
- 2411 Aumont, O., Ethé, C., Tagliabue, A., Bopp, L., and Gehlen, M.: PISCES-v2: an ocean biogeochemical model for carbon and
2412 ecosystem studies, 8, 2465–2513, <https://doi.org/10.5194/gmd-8-2465-2015>, 2015.
- 2413 Baccini, A., Walker, W., Carvalho, L., Farina, M., Sulla-Menashe, D., and Houghton, R. A.: Tropical forests are a net carbon
2414 source based on aboveground measurements of gain and loss, *Science*, 358, 230–234,
2415 <https://doi.org/10.1126/science.aam5962>, 2017.
- 2416 Bakker, D. C. E., Pfeil, B., Landa, C. S., Metzl, N., O'Brien, K. M., Olsen, A., Smith, K., Cosca, C., Harasawa, S., Jones, S.
2417 D., Nakaoka, S., Nojiri, Y., Schuster, U., Steinhoff, T., Sweeney, C., Takahashi, T., Tilbrook, B., Wada, C., Wanninkhof, R.,
2418 Alin, S. R., Balestrini, C. F., Barbero, L., Bates, N. R., Bianchi, A. A., Bonou, F., Boutin, J., Bozec, Y., Burger, E. F., Cai,
2419 W.-J., Castle, R. D., Chen, L., Chierici, M., Currie, K., Evans, W., Featherstone, C., Feely, R. A., Fransson, A., Goyet, C.,
2420 Greenwood, N., Gregor, L., Hankin, S., Hardman-Mountford, N. J., Harlay, J., Hauck, J., Hoppema, M., Humphreys, M. P.,
2421 Hunt, C. W., Huss, B., Ibáñez, J. S. P., Johannessen, T., Keeling, R., Kitidis, V., Körtzinger, A., Kozyr, A., Krasakopoulou,
2422 E., Kuwata, A., Landschützer, P., Lauvset, S. K., Lefèvre, N., Lo Monaco, C., Manke, A., Mathis, J. T., Merlivat, L.,
2423 Millero, F. J., Monteiro, P. M. S., Munro, D. R., Murata, A., Newberger, T., Omar, A. M., Ono, T., Paterson, K., Pearce, D.,
2424 Pierrot, D., Robbins, L. L., Saito, S., Salisbury, J., Schlitzer, R., Schneider, B., Schweitzer, R., Sieger, R., Skjelvan, I.,
2425 Sullivan, K. F., Sutherland, S. C., Sutton, A. J., Tadokoro, K., Telszewski, M., Tuma, M., van Heuven, S. M. A. C.,
2426 Vandemark, D., Ward, B., Watson, A. J., and Xu, S.: A multi-decade record of high-quality CO₂ data in version 3 of the
2427 Surface Ocean CO₂ Atlas (SOCAT), *Earth Syst. Sci. Data*, 8, 383–413, <https://doi.org/10.5194/essd-8-383-2016>, 2016.
- 2428 Bakker, Dorothee C. E.; Alin, Simone R.; Bates, Nicholas; Becker, Meike; Feely, Richard A.; Gkritzalis, Thanos; Jones,
2429 Steve D.; Kozyr, Alex; Lauvset, Siv K.; Metzl, Nicolas; Munro, David R.; Nakaoka, Shin-ichiro; Nojiri, Yukihiro; O'Brien,
2430 Kevin M.; Olsen, Are; Pierrot, Denis; Rehder, Gregor; Steinhoff, Tobias; Sutton, Adrienne J.; Sweeney, Colm; Tilbrook,
2431 Bronte; Wada, Chisato; Wanninkhof, Rik; Akl, John; Barbero, Leticia; Beatty, Cory M.; Berghoff, Carla F.; Bittig, Henry
2432 C.; Bott, Randy; Burger, Eugene F.; Cai, Wei-Jun; Castaño-Primo, Rocío; Corredor, Jorge E.; Cronin, Margot; De Carlo,
2433 Eric H.; DeGrandpre, Michael D.; Dietrich, Colin; Drennan, William M.; Emerson, Steven R.; Enochs, Ian C.; Enyo,
2434 Kazutaka; Epherra, Lucia; Evans, Wiley; Fiedler, Björn; Fontela, Marcos; Frangoulis, Constantin; Gehrung, Martina;
2435 Giannoudi, Louisa; Glockzin, Michael; Hales, Burke; Howden, Stephan D.; Ibáñez, J. Severino P.; Kamb, Linus;
2436 Körtzinger, Arne; Lefèvre, Nathalie; Lo Monaco, Claire; Lutz, Vivian A.; Macovei, Vlad A.; Maenner Jones, Stacy;
2437 Manalang, Dana; Manzello, Derek P.; Metzl, Nicolas; Mickett, John; Millero, Frank J.; Monacci, Natalie M.; Morell, Julio
2438 M.; Musielewicz, Sylvia; Neill, Craig; Newberger, Tim; Newton, Jan; Noakes, Scott; Ólafsdóttir, Sólveig Rósa; Ono,
2439 Tsuneo; Osborne, John; Padín, Xose A.; Paulsen, Melf; Perivoliotis, Leonidas; Petersen, Wilhelm; Petihakis, George;
2440 Plueddemann, Albert J.; Rodriguez, Carmen; Rutgersson, Anna; Sabine, Christopher L.; Salisbury, Joseph E.; Schlitzer,
2441 Reiner; Skjelvan, Ingunn; Stamatakis, Natalia; Sullivan, Kevin F.; Sutherland, Stewart C.; T'Jampens, Michiel; Tadokoro,
2442 Kazuaki; Tanhua, Toste; Telszewski, Maciej; Theetaert, Hannelore; Tomlinson, Michael; Vandemark, Douglas; Velo,
2443 Antón; Voynova, Yoana G.; Weller, Robert A.; Whitehead, Chris; Wimart-Rousseau, Cathy (2023). Surface Ocean CO₂
2444 Atlas Database Version 2023 (SOCATv2023) (NCEI Accession 0278913). [indicate subset used]. NOAA National Centers
2445 for Environmental Information. Dataset. <https://doi.org/10.25921/r7xa-bt92>, 2023.
- 2446 Ballantyne, A. P., Alden, C. B., Miller, J. B., Tans, P. P., and White, J. W. C.: Increase in observed net carbon dioxide
2447 uptake by land and oceans during the past 50 years, *Nature*, 488, 70–72, <https://doi.org/10.1038/nature11299>, 2012.

Formatted: Default Paragraph Font, Font colour: Black

Formatted: Normal, Centred, Border: Top: (No border),
Bottom: (No border), Left: (No border), Right: (No border),
Between : (No border), Tab stops: 7.96 cm, Centred + 15.92
cm, Right, Position: Horizontal: Left, Relative to: Column,
Vertical: In line, Relative to: Margin, Wrap Around

Formatted: Font colour: Black

2448 Ballantyne, A. P., Andres, R., Houghton, R., Stocker, B. D., Wanninkhof, R., Anderegg, W., Cooper, L. A., DeGrandpre,
2449 M., Tans, P. P., Miller, J. B., Alden, C., and White, J. W. C.: Audit of the global carbon budget: estimate errors and their
2450 impact on uptake uncertainty, *Biogeosciences*, 12, 2565–2584, <https://doi.org/10.5194/bg-12-2565-2015>, 2015.

2451 Bastos, A., Hartung, K., Nützel, T. B., Nabel, J. E. M. S., Houghton, R. A., and Pongratz, J.: Comparison of uncertainties in
2452 land-use change fluxes from bookkeeping model parameterisation, 12, 745–762, <https://doi.org/10.5194/esd-12-745-2021>,
2453 2021.

2454 Battle, M. O., Raynor, R., Kesler, S., and Keeling, R.: Technical Note: The impact of industrial activity on the amount of
2455 atmospheric O₂, *Atmospheric Chem. Phys. Discuss.*, 1–17, <https://doi.org/10.5194/acp-2022-765>, 2023.

2456 Beckman, J. and Countryman, A. M.: The Importance of Agriculture in the Economy: Impacts from COVID-19, *Am. J. Agr.*
2457 *Econ.*, 103, 1595–1611, <https://doi.org/10.1111/ajae.12212>, 2021.

2458 Bellenger, H., Bopp, L., Ethé, C., Ho, D., Duvel, J. P., Flavoni, S., Guez, L., Kataoka, T., Perrot, X., Parc, L., and Watanabe,
2459 M.: Sensitivity of the Global Ocean Carbon Sink to the Ocean Skin in a Climate Model, *J. Geophys. Res. Oceans*, 128,
2460 e2022JC019479, <https://doi.org/10.1029/2022JC019479>, 2023.

2461

2462 Bennington, V., Gloege, L., and McKinley, G. A.: Variability in the Global Ocean Carbon Sink From 1959 to 2020 by
2463 Correcting Models with Observations, *Geophys. Res. Lett.*, 49, e2022GL098632, <https://doi.org/10.1029/2022GL098632>,
2464 2022.

2465 Berthet, S., Séférian, R., Bricaud, C., Chevallier, M., Voltaire, A., and Ethé, C.: Evaluation of an Online Grid-Coarsening
2466 Algorithm in a Global Eddy-Admitting Ocean Biogeochemical Model, *J. Adv. Model Earth Sy.*, 11, 1759–1783,
2467 <https://doi.org/10.1029/2019MS001644>, 2019.

2468 [Betts, R. A., Jones, C. D., Knight, J. R., Keeling, R. F., and Kennedy, J. J.: El Niño and a record CO₂ rise, *Nat. Clim.*
2469 *Change*, 6, 806–810, <https://doi.org/10.1038/nclimate3063>, 2016.](#)

2470 Bloom, A. A. and Williams, M.: Constraining ecosystem carbon dynamics in a data-limited world: integrating ecological
2471 “common sense” in a model–data fusion framework, *Biogeosciences*, 12, 1299–1315, [https://doi.org/10.5194/bg-12-1299-](https://doi.org/10.5194/bg-12-1299-2015)
2472 2015, 2015.

2473

2474 Bloom, A. A., Exbrayat, J.-F., van der Velde, I. R., Feng, L., and Williams, M.: The decadal state of the terrestrial carbon
2475 cycle: Global retrievals of terrestrial carbon allocation, pools, and residence times, *Proc. Natl. Acad. Sci.*, 113, 1285–1290,
2476 <https://doi.org/10.1073/pnas.1515160113>, 2016.

2477

2478 Boer, G. J., Smith, D. M., Cassou, C., Doblas-Reyes, F., Danabasoglu, G., Kirtman, B., Kushnir, Y., Kimoto, M., Meehl, G.
2479 A., Msadek, R., Mueller, W. A., Taylor, K. E., Zwiers, F., Rixen, M., Ruprich-Robert, Y., and Eade, R.: The Decadal
2480 Climate Prediction Project (DCPP) contribution to CMIP6, *Geosci. Model Dev.*, 9, 3751–3777, [https://doi.org/10.5194/gmd-](https://doi.org/10.5194/gmd-9-3751-2016)
2481 9-3751-2016, 2016.

2482

2483 Boucher, O., Servonnat, J., Albright, A. L., Aumont, O., Balkanski, Y., Bastrikov, V., Bekki, S., Bonnet, R., Bony, S., Bopp,
2484 L., Braconnot, P., Brockmann, P., Cadule, P., Caubel, A., Cheruy, F., Codron, F., Cozic, A., Cugnet, D., D’Andrea, F.,
2485 Davini, P., de Lavergne, C., Denvil, S., Deshayes, J., Devillers, M., Ducharne, A., Dufresne, J.-L., Dupont, E., Éthé, C.,
2486 Fairhead, L., Falletti, L., Flavoni, S., Foujols, M.-A., Gardoll, S., Gastineau, G., Ghattas, J., Grandpeix, J.-Y., Guenet, B.,

Formatted: Default Paragraph Font, Font colour: Black

Formatted: Normal, Centred, Border: Top: (No border), Bottom: (No border), Left: (No border), Right: (No border), Between : (No border), Tab stops: 7.96 cm, Centred + 15.92 cm, Right, Position: Horizontal: Left, Relative to: Column, Vertical: In line, Relative to: Margin, Wrap Around

Formatted: Font colour: Black

2487 Guez, E., Lionel, Guilyardi, E., Guimberteau, M., Hauglustaine, D., Hourdin, F., Idelkadi, A., Joussaume, S., Kageyama, M.,
2488 Khodri, M., Krinner, G., Lebas, N., Levassasseur, G., Lévy, C., Li, L., Lott, F., Lurton, T., Luysaert, S., Madec, G.,
2489 Madeleine, J.-B., Maignan, F., Marchand, M., Marti, O., Mellul, L., Meurdesoif, Y., Mignot, J., Musat, I., Ottlé, C., Peylin,
2490 P., Planton, Y., Polcher, J., Rio, C., Rochetin, N., Rousset, C., Sepulchre, P., Sima, A., Swingedouw, D., Thiéblemont, R.,
2491 Traore, A. K., Vancoppenolle, M., Vial, J., Vialard, J., Viovy, N., and Vuichard, N.: Presentation and Evaluation of the
2492 IPSL-CM6A-LR Climate Model, *J. Adv. Model. Earth Syst.*, 12, e2019MS002010, <https://doi.org/10.1029/2019MS002010>,
2493 2020.

2494 Bourgeois, T., Goris, N., Schwinger, J., and Tjiputra, J. F.: Stratification constrains future heat and carbon uptake in the
2495 Southern Ocean between 30°S and 55°S, *Nat. Commun.*, 13, 340, <https://doi.org/10.1038/s41467-022-27979-5>, 2022.

2496 Bray, E.: 2017 Minerals Yearbook: Aluminum [Advance Release], Tech. rep., U.S. Geological Survey, <https://d9-wret.s3-us-west-2.amazonaws.com/assets/palladium/production/atoms/files/myb1-2017-alumi.pdf>, 2020.

2498 Brancalion, P. H. S., Broadbent, E. N., de-Miguel, S., Cardil, A., Rosa, M. R., Almeida, C. T., Almeida, D. R. A.,
2499 Chakravarty, S., Zhou, M., Gamarra, J. G. P., Liang, J., Crouzeilles, R., Hérault, B., Aragão, L. E. O. C., Silva, C. A., and
2500 Almeyda-Zambrano, A. M.: Emerging threats linking tropical deforestation and the COVID-19 pandemic, *Perspectives in
2501 Ecology and Conservation*, 18, 243–246, <https://doi.org/10.1016/j.pecon.2020.09.006>, 2020.

2502 Brien, R. J. W., Caldwell, L., Duchesne, L., Voelker, S., Barichivich, J., Baliva, M., Ceccantini, G., Di Filippo, A.,
2503 Helama, S., Locosselli, G. M., Lopez, L., Piovesan, G., Schöngart, J., Villalba, R., and Gloor, E.: Forest carbon sink
2504 neutralized by pervasive growth-lifespan trade-offs, *Nat. Commun.*, 11, 4241, <https://doi.org/10.1038/s41467-020-17966-z>,
2505 2020.

2506 Brien, R. J. W., Phillips, O. L., Feldpausch, T. R., Gloor, E., Baker, T. R., Lloyd, J., Lopez-Gonzalez, G., Monteagudo-
2507 Mendoza, A., Malhi, Y., Lewis, S. L., Vásquez Martínez, R., Alexiades, M., Álvarez Dávila, E., Alvarez-Loayza, P.,
2508 Andrade, A., Aragão, L. E. O. C., Araujo-Murakami, A., Arets, E. J. M. M., Arroyo, L., Aymard C., G. A., Bánki, O. S.,
2509 Baraloto, C., Barroso, J., Bonal, D., Boot, R. G. A., Camargo, J. L. C., Castilho, C. V., Chama, V., Chao, K. J., Chave, J.,
2510 Comiskey, J. A., Cornejo Valverde, F., da Costa, L., de Oliveira, E. A., Di Fiore, A., Erwin, T. L., Fauset, S., Forsthofer, M.,
2511 Galbraith, D. R., Grahame, E. S., Groot, N., Hérault, B., Higuchi, N., Honorio Coronado, E. N., Keeling, H., Killeen, T. J.,
2512 Laurance, W. F., Laurance, S., Licona, J., Magnussen, W. E., Marimon, B. S., Marimon-Junior, B. H., Mendoza, C., Neill,
2513 D. A., Nogueira, E. M., Núñez, P., Pallqui Camacho, N. C., Parada, A., Pardo-Molina, G., Peacock, J., Peña-Claros, M.,
2514 Pickavance, G. C., Pitman, N. C. A., Poorter, L., Prieto, A., Quesada, C. A., Ramirez, F., Ramirez-Angulo, H., Restrepo, Z.,
2515 Roopsind, A., Rudas, A., Salomão, R. P., Schwarz, M., Silva, N., Silva-Espejo, J. E., Silveira, M., Stropp, J., Talbot, J., ter
2516 Steege, H., Teran-Aguilar, J., Terborgh, J., Thomas-Caesar, R., Toledo, M., Torello-Raventos, M., Umetsu, R. K., van der
2517 Heijden, G. M. F., van der Hout, P., Guimarães Vieira, I. C., Vieira, S. A., Vilanova, E., Vos, V. A., and Zagt, R. J.: Long-
2518 term decline of the Amazon carbon sink, *Nature*, 519, 344–348, <https://doi.org/10.1038/nature14283>, 2015.

2519 Bronselaer, B., Winton, M., Russell, J., Sabine, C. L., and Khatiwala, S.: Agreement of CMIP5 Simulated and Observed
2520 Ocean Anthropogenic CO₂ Uptake, *Geophys. Res. Lett.*, 44, 12,298–12,305, <https://doi.org/10.1002/2017GL074435>, 2017.

2521 Bruno, M. and Joos, F.: Terrestrial carbon storage during the past 200 years: A Monte Carlo Analysis of CO₂ data from ice
2522 core and atmospheric measurements, *Global Biogeochem. Cycles*, 11, 111–124, <https://doi.org/10.1029/96GB03611>, 1997.

Formatted: Default Paragraph Font, Font colour: Black

Formatted: Normal, Centred, Border: Top: (No border), Bottom: (No border), Left: (No border), Right: (No border), Between : (No border), Tab stops: 7.96 cm, Centred + 15.92 cm, Right, Position: Horizontal: Left, Relative to: Column, Vertical: In line, Relative to: Margin, Wrap Around

Formatted: Font colour: Black

2523 Burrows, S. M., Maltrud, M., Yang, X., Zhu, Q., Jeffery, N., Shi, X., Ricciuto, D., Wang, S., Bisht, G., Tang, J., Wolfe, J.,
2524 Harrop, B. E., Singh, B., Brent, L., Baldwin, S., Zhou, T., Cameron-Smith, P., Keen, N., Collier, N., Xu, M., Hunke, E. C.,
2525 Elliott, S. M., Turner, A. K., Li, H., Wang, H., Golaz, J.-C., Bond-Lamberty, B., Hoffman, F. M., Riley, W. J., Thornton, P.
2526 E., Calvin, K., and Leung, L. R.: The DOE E3SM v1.1 Biogeochemistry Configuration: Description and Simulated
2527 Ecosystem-Climate Responses to Historical Changes in Forcing, *J. Adv. Model. Earth Syst.*, 12, e2019MS001766,
2528 <https://doi.org/10.1029/2019MS001766>, 2020.

2529 Burton, C., Betts, R., Cardoso, M., Feldpausch, T. R., Harper, A., Jones, C. D., Kelley, D. I., Robertson, E., and Wiltshire,
2530 A.: Representation of fire, land-use change and vegetation dynamics in the Joint UK Land Environment Simulator vn4.9
2531 (JULES), *Geosci. Model Dev.*, 12, 179–193, <https://doi.org/10.5194/gmd-12-179-2019>, 2019.

2532 Burton, C. et al.: Global burned area increasingly explained by climate change, *under review*,
2533 <https://doi.org/10.21203/rs.3.rs-3168150/v1>, 2023.

2534 Bushinsky, S. M., Landschützer, P., Rödenbeck, C., Gray, A. R., Baker, D., Mazloff, M. R., Resplandy, L., Johnson, K. S.,
2535 and Sarmiento, J. L.: Reassessing Southern Ocean Air-Sea CO₂ Flux Estimates With the Addition of Biogeochemical Float
2536 Observations, *Global Biogeochem. Cycles*, 33, 1370–1388, <https://doi.org/10.1029/2019GB006176>, 2019.

2537 Canadell, J. G., Le Quere, C., Raupach, M. R., Field, C. B., Buitenhuis, E. T., Ciais, P., Conway, T. J., Gillett, N. P.,
2538 Houghton, R. A., and Marland, G.: Contributions to accelerating atmospheric CO₂ growth from economic activity, carbon
2539 intensity, and efficiency of natural sinks, *Proceedings of the National Academy of Sciences*, 104, 18866–18870,
2540 <https://doi.org/10.1073/pnas.0702737104>, 2007.

2541 Canadell, J. G., Monteiro, P. M. S., Costa, M. H., Cotrim da Cunha, L., Cox, P. M., Eliseev, A. V., Henson, S., Ishii, M.,
2542 Jaccard, S., Koven, C., Lohila, A., Patra, P. K., Piao, S., Rogelj, J., Syampungani, S., Zaehle, S., and Zickfeld, K.: Global
2543 Carbon and other Biogeochemical Cycles and Feedbacks. In: *Climate Change 2021: The Physical Science Basis*.
2544 Contribution of Working Group I to the Sixth Assessment Report of the Intergovernmental Panel on Climate Change
2545 [Masson-Delmotte, V., P. Zhai, A. Pirani, S. L. Connors, C. Péan, S. Berger, N. Caud, Y. Chen, L. Goldfarb, M. I. Gomis,
2546 M. Huang, K. Leitzell, E. Lonnoy, J.B.R. Matthews, T. K. Maycock, T. Waterfield, O. Yelekçi, R. Yu and B. Zhou (eds.)].
2547 Cambridge University Press, Cambridge, United Kingdom and New York, NY, USA, pp. 673–816, doi:
2548 10.1017/9781009157896.007., 2021.

2549 Cao, Z., Myers, R. J., Lupton, R. C., Duan, H., Sacchi, R., Zhou, N., Reed Miller, T., Cullen, J. M., Ge, Q., and Liu, G.: The
2550 sponge effect and carbon emission mitigation potentials of the global cement cycle, *Nat Commun*, 11, 3777,
2551 <https://doi.org/10.1038/s41467-020-17583-w>, 2020.

2552 Céspedes, J., Sylvester, J. M., Pérez-Marulanda, L., Paz-García, P., Reymondin, L., Khodadadi, M., Tello, J. J., and Castro-
2553 Nunez, A.: Has global deforestation accelerated due to the COVID-19 pandemic?, *J. For. Res.*, 34, 1153–1165,
2554 <https://doi.org/10.1007/s11676-022-01561-7>, 2023.

2555 Chandra, N., Patra, P. K., Niwa, Y., Ito, A., Iida, Y., Goto, D., Morimoto, S., Kondo, M., Takigawa, M., Hajima, T., and
2556 Watanabe, M.: Estimated regional CO₂ flux and uncertainty based on an ensemble of atmospheric CO₂ inversions,
2557 *Atmospheric Chem. Phys.*, 22, 9215–9243, <https://doi.org/10.5194/acp-22-9215-2022>, 2022.

2558 Chatfield, C.: The Holt-Winters Forecasting Procedure, *J. Roy. Stat. Soc. C.*, 27, 264–279, <https://doi.org/10.2307/2347162>,
2559 1978.

Formatted: Default Paragraph Font, Font colour: Black

Formatted: Normal, Centred, Border: Top: (No border),
Bottom: (No border), Left: (No border), Right: (No border),
Between : (No border), Tab stops: 7.96 cm, Centred + 15.92
cm, Right, Position: Horizontal: Left, Relative to: Column,
Vertical: In line, Relative to: Margin, Wrap Around

Formatted: Font colour: Black

- 2560 Chau, T. T. T., Gehlen, M., and Chevallier, F.: A seamless ensemble-based reconstruction of surface ocean $p\text{CO}_2$ and air–sea
 2561 CO_2 fluxes over the global coastal and open oceans, *Biogeosciences*, 19, 1087–1109, [https://doi.org/10.5194/bg-19-1087-](https://doi.org/10.5194/bg-19-1087-2022)
 2562 2022, 2022.
- 2563 Chevallier, F., Fisher, M., Peylin, P., Serrar, S., Bousquet, P., Bréon, F.-M., Chédin, A., and Ciais, P.: Inferring CO_2
 2564 sources and sinks from satellite observations: Method and application to TOVS data, *J. Geophys. Res.*, 110, D24309,
 2565 <https://doi.org/10.1029/2005JD006390>, 2005.
- 2566 Ciais, P., Sabine, C., Bala, G., Bopp, L., Brovkin, V., Canadell, J. G., Chhabra, A., DeFries, R., Galloway, J., Heimann, M.,
 2567 Jones, C., Le Quéré, C., Myneni, R., Piao, S., Thornton, P., Willem, J., Friedlingstein, P., and Munhoven, G.: Carbon and
 2568 Other Biogeochemical Cycles, in *Climate Change 2013: The Physical Science Basis, Contribution of Working Group I to the*
 2569 *Fifth Assessment Report of the Intergovernmental Panel on Climate Change*, edited by: Intergovernmental Panel on Climate
 2570 Change, Cambridge University Press, Cambridge, United Kingdom and New York, NY, USA.
 2571 doi:10.1017/CBO9781107415324.015, 2013.
- 2572 Ciais, P., Tan, J., Wang, X., Roedenbeck, C., Chevallier, F., Piao, S.-L., Moriarty, R., Broquet, G., Le Quéré, C., Canadell, J.
 2573 G., Peng, S., Poulter, B., Liu, Z., and Tans, P.: Five decades of northern land carbon uptake revealed by the interhemispheric
 2574 CO_2 gradient, *Nature*, 568, 221–225, <https://doi.org/10.1038/s41586-019-1078-6>, 2019.
- 2575 Ciais, P., Bastos, A., Chevallier, F., Lauerwald, R., Poulter, B., Canadell, P., Hugelius, G., Jackson, R. B., Jain, A., Jones,
 2576 M., Kondo, M., Luijckx, I. T., Patra, P. K., Peters, W., Pongratz, J., Petrescu, A. M. R., Piao, S., Qiu, C., Von Randow, C.,
 2577 Regnier, P., Saunois, M., Scholes, R., Shvidenko, A., Tian, H., Yang, H., Wang, X., and Zheng, B.: Definitions and methods
 2578 to estimate regional land carbon fluxes for the second phase of the REgional Carbon Cycle Assessment and Processes
 2579 Project (RECCAP-2), *Geosci. Model Dev.*, 15, 1289–1316, <https://doi.org/10.5194/gmd-15-1289-2022>, 2022.
- 2580 Collier, N., Hoffman, F. M., Lawrence, D. M., Keppel-Aleks, G., Koven, C. D., Riley, W. J., Mu, M., and Randerson, J. T.:
 2581 The International Land Model Benchmarking (ILAMB) System: Design, Theory, and Implementation, *J. Adv. Model. Earth*
 2582 *Syst.*, 10, 2731–2754, <https://doi.org/10.1029/2018MS001354>, 2018.
- 2583 Cox, P. M., Pearson, D., Booth, B. B., Friedlingstein, P., Huntingford, C., Jones, C. D., and Luke, C. M.: Sensitivity of
 2584 tropical carbon to climate change constrained by carbon dioxide variability, *Nature*, 494, 341–344,
 2585 <https://doi.org/10.1038/nature11882>, 2013.
- 2586 De Kauwe, M. G., Medlyn, B. E., Zaehle, S., Walker, A. P., Dietze, M. C., Wang, Y.-P., Luo, Y., Jain, A. K., El-Masri, B.,
 2587 Hickler, T., Wärlind, D., Weng, E., Parton, W. J., Thornton, P. E., Wang, S., Prentice, I. C., Asao, S., Smith, B., McCarthy,
 2588 H. R., Iversen, C. M., Hanson, P. J., Warren, J. M., Oren, R., and Norby, R. J.: Where does the carbon go? A model–data
 2589 intercomparison of vegetation carbon allocation and turnover processes at two temperate forest free-air CO_2 enrichment
 sites, *New Phytol.*, 203, 883–899, <https://doi.org/10.1111/nph.12847>, 2014.
- 2591 Delire, C., Séférian, R., Decharme, B., Alkama, R., Calvet, J.-C., Carrer, D., Gibelin, A.-L., Joetzjer, E., Morel, X., Rocher,
 2592 M., and Tzanos, D.: The Global Land Carbon Cycle Simulated With ISBA-CTRIP: Improvements Over the Last Decade, *J.*
 2593 *Adv. Model. Earth Syst.*, 12, e2019MS001886, <https://doi.org/10.1029/2019MS001886>, 2020.
- 2594 Denman, K. L., Brasseur, G., Chidthaisong, A., Ciais, P., Cox, P. M., Dickinson, R. E., Hauglustaine, D., Heinze, C.,
 2595 Holland, E., Jacob, D., Lohmann, U., Ramachandran, S., Leite da Silva Dias, P., Wofsy, S. C., and Zhang, X.: Couplings
 2596 Between Changes in the Climate System and Biogeochemistry, in: *Climate Change 2007: The Physical Science Basis*.

Formatted: Default Paragraph Font, Font colour: Black

Formatted: Normal, Centred, Border: Top: (No border),
 Bottom: (No border), Left: (No border), Right: (No border),
 Between : (No border), Tab stops: 7.96 cm, Centred + 15.92
 cm, Right, Position: Horizontal: Left, Relative to: Column,
 Vertical: In line, Relative to: Margin, Wrap Around

Formatted: Font colour: Black

- 2597 Contribution of Working Group I to the Fourth Assessment Report of the Intergovernmental Panel on Climate Change,
2598 edited by: Solomon, S., Qin, D., Manning, M., Marquis, M., Averyt, K., Tignor, M. M. B., Miller, H. L., and Chen, Z. L.,
2599 Cambridge University Press, Cambridge, UK and New York, USA, 499–587, ISBN: 9780521705967, 2007.
- 2600 Denvil-Sommer, A., Gehlen, M., and Vrac, M.: Observation system simulation experiments in the Atlantic Ocean for
2601 enhanced surface ocean pCO₂ reconstructions, *Ocean Sci.*, 17, 1011–1030, <https://doi.org/10.5194/os-17-1011-2021>, 2021.
- 2602 DeVries, T., Holzer, M., and Primeau, F.: Recent increase in oceanic carbon uptake driven by weaker upper-ocean
2603 overturning, *Nature*, 542, 215–218, <https://doi.org/10.1038/nature21068>, 2017.
- 2604 DeVries, T., Quéré, C. L., Andrews, O., Berthet, S., Hauck, J., Ilyina, T., Landschützer, P., Lenton, A., Lima, I. D., Nowicki,
2605 M., Schwinger, J., and Séférian, R.: Decadal trends in the ocean carbon sink, *PNAS*, 116, 11646–11651,
2606 <https://doi.org/10.1073/pnas.1900371116>, 2019.
- 2607 DeVries, T., Yamamoto, K., Wanninkhof, R., Gruber, N., Hauck, J., Müller, J. D., Bopp, L., Carroll, D., Carter, B., Chau,
2608 T.-T.-T., Doney, S. C., Gehlen, M., Gloege, L., Gregor, L., Henson, S., Kim, J. H., Iida, Y., Ilyina, T., Landschützer, P., Le
2609 Quéré, C., Munro, D., Nissen, C., Patara, L., Pérez, F. F., Resplandy, L., Rodgers, K. B., Schwinger, J., Séférian, R., Sicardi,
2610 V., Terhaar, J., Triñanes, J., Tsujino, H., Watson, A., Yasunaka, S., and Zeng, J.: Magnitude, trends, and variability of the
2611 global ocean carbon sink from 1985–2018, *Glob. Biogeochem. Cycles*, n/a, e2023GB007780,
2612 <https://doi.org/10.1029/2023GB007780>, 2023.
- 2613
- 2614 Forster, P. M., Smith, C. J., Walsh, T., Lamb, W. F., Lamboll, R., Hauser, M., Ribes, A., Rosen, D., Gillett, N., Palmer, M.
2615 D., Rogelj, J., von Schuckmann, K., Seneviratne, S. I., Trewin, B., Zhang, X., Allen, M., Andrew, R., Birt, A., Borger, A.,
2616 Boyer, T., Broersma, J. A., Cheng, L., Dentener, F., Friedlingstein, P., Gutiérrez, J. M., Gütschow, J., Hall, B., Ishii, M.,
2617 Jenkins, S., Lan, X., Lee, J.-Y., Morice, C., Kadow, C., Kennedy, J., Killick, R., Minx, J. C., Naik, V., Peters, G. P., Pirani,
2618 A., Pongratz, J., Schleussner, C.-F., Szopa, S., Thorne, P., Rohde, R., Rojas Corradi, M., Schumacher, D., Vose, R.,
2619 Zickfeld, K., Masson-Delmotte, V., and Zhai, P.: Indicators of Global Climate Change 2022: annual update of large-scale
2620 indicators of the state of the climate system and human influence, *Earth Syst. Sci. Data*, 15, 2295–2327,
2621 <https://doi.org/10.5194/essd-15-2295-2023>, 2023.
- 2622 Doney, S. C., Lima, I., Feely, R. A., Glover, D. M., Lindsay, K., Mahowald, N., Moore, J. K., and Wanninkhof, R.:
2623 Mechanisms governing interannual variability in upper-ocean inorganic carbon system and air–sea CO₂ fluxes: Physical
2624 climate and atmospheric dust, *Deep Sea Research Part II: Topical Studies in Oceanography*, 56, 640–655,
2625 <https://doi.org/10.1016/j.dsr2.2008.12.006>, 2009.
- 2626 Dong, Y., Bakker, D. C. E., Bell, T. G., Huang, B., Landschützer, P., Liss, P. S., and Yang, M.: Update on the Temperature
2627 Corrections of Global Air–Sea CO₂ Flux Estimates, *Glob. Biogeochem. Cycles*, 36, e2022GB007360,
2628 <https://doi.org/10.1029/2022GB007360>, 2022.
- 2629
- 2630 Dou, X., Wang, Y., Ciais, P., Chevallier, F., Davis, S. J., Crippa, M., Janssens-Maenhout, G., Guizzardi, D., Solazzo, E.,
2631 Yan, F., Huo, D., Zheng, B., Zhu, B., Cui, D., Ke, P., Sun, T., Wang, H., Zhang, Q., Gentine, P., Deng, Z., and Liu, Z.: Near-
2632 real-time global gridded daily CO₂ emissions, *The Innovation*, 3, 100182, <https://doi.org/10.1016/j.xinn.2021.100182>, 2022.

Formatted: Default Paragraph Font, Font colour: Black

Formatted: Normal, Centred, Border: Top: (No border),
Bottom: (No border), Left: (No border), Right: (No border),
Between : (No border), Tab stops: 7.96 cm, Centred + 15.92
cm, Right, Position: Horizontal: Left, Relative to: Column,
Vertical: In line, Relative to: Margin, Wrap Around

Formatted: Font colour: Black

2633 Edson, J. B., Jampana, V., Weller, R. A., Bigorre, S. P., Plueddemann, A. J., Fairall, C. W., Miller, S. D., Mahrt, L., Vickers,
2634 D., and Hersbach, H.: On the Exchange of Momentum over the Open Ocean, *J. Phys. Oceanogr.*, 43, 1589–1610,
2635 <https://doi.org/10.1175/JPO-D-12-0173.1>, 2013.

2636 EIA. Short-Term Energy Outlook: September 2023. U.S. Energy Information Administration. Available at:
2637 <http://www.eia.gov/forecasts/steo/outlook.cfm>, last access: 9 November 2023, 2023.

Deleted: 27 September

2638 Erb, K.-H., Kastner, T., Luyssaert, S., Houghton, R. A., Kuemmerle, T., Olofsson, P., and Haberl, H.: Bias in the attribution
2639 of forest carbon sinks, *Nature Clim Change*, 3, 854–856, <https://doi.org/10.1038/nclimate2004>, 2013.

2640 Erb, K.-H., Kastner, T., Plutzer, C., Bais, A. L. S., Carvalhais, N., Fetzel, T., Gingrich, S., Haberl, H., Lauk, C.,
2641 Niederscheider, M., Pongratz, J., Thurner, M., and Luyssaert, S.: Unexpectedly large impact of forest management and
2642 grazing on global vegetation biomass, *Nature*, 553, 73–76, <https://doi.org/10.1038/nature25138>, 2018.

2643 Eskander, S. M. S. U. and Fankhauser, S.: Reduction in greenhouse gas emissions from national climate legislation, *Nat.*
2644 *Clim. Chang.*, 10, 750–756, <https://doi.org/10.1038/s41558-020-0831-z>, 2020.

2645 Etheridge, D. M., Steele, L. P., Langenfelds, R. L., Francey, R. J., Barnola, J.-M., and Morgan, V. I.: Natural and
2646 anthropogenic changes in atmospheric CO₂ over the last 1000 years from air in Antarctic ice and firn, *J. Geophys. Res.*,
2647 101, 4115–4128, <https://doi.org/10.1029/95JD03410>, 1996.

2648 Eyring, V., Bony, S., Meehl, G. A., Senior, C. A., Stevens, B., Stouffer, R. J., and Taylor, K. E.: Overview of the Coupled
2649 Model Intercomparison Project Phase 6 (CMIP6) experimental design and organization, *Geosci. Model Dev.*, 9, 1937–1958,
2650 <https://doi.org/10.5194/gmd-9-1937-2016>, 2016.

2651 FAO, Impact of the Ukraine-Russia conflict on global food security and related matters under the mandate of the Food and
2652 Agriculture Organization of the United Nations (FAO), Hundred and Seventieth Session of the Council,
2653 <https://www.fao.org/3/nj164en/nj164en.pdf>, last access: 9 November 2023, 2023.

Deleted: 27 September

2654 Fay, A. R., Gregor, L., Landschützer, P., McKinley, G. A., Gruber, N., Gehlen, M., Iida, Y., Laruelle, G. G., Rödenbeck, C.,
2655 Roobaert, A., and Zeng, J.: SeaFlux: harmonization of air–sea CO₂ fluxes from surface pCO₂ data products using a
2656 standardized approach, *Earth System Science Data*, 13, 4693–4710, <https://doi.org/10.5194/essd-13-4693-2021>, 2021.

2657 Feng, L., Palmer, P. I., Bösch, H., and Dance, S.: Estimating surface CO₂ fluxes from space-borne CO₂ dry air mole fraction
2658 observations using an ensemble Kalman Filter, *Atmospheric Chem. Phys.*, 9, 2619–2633, <https://doi.org/10.5194/acp-9-2619-2009>, 2009.

2660 Feng, L., Palmer, P. I., Parker, R. J., Deutscher, N. M., Feist, D. G., Kivi, R., Morino, I., and Sussmann, R.: Estimates of
2661 European uptake of CO₂ inferred from GOSAT XCO₂ retrievals: sensitivity to measurement bias inside and outside Europe,
2662 *Atmos. Chem. Phys.*, 16, 1289–1302, <https://doi.org/10.5194/acp-16-1289-2016>, 2016.

2663 Flanagan, D.: 2017 Minerals Yearbook: Copper [Advance Release], Tech. rep., U.S. Geological Survey,
2664 <https://pubs.usgs.gov/myb/vol11/2017/myb1-2017-copper.pdf>, 2021.

Formatted: Default Paragraph Font, Font colour: Black

2665 Friedlingstein, P., Houghton, R. A., Marland, G., Hackler, J., Boden, T. A., Conway, T. J., Canadell, J. G., Raupach, M. R.,
2666 Ciais, P., and Le Quéré, C.: Update on CO₂ emissions, *Nature Geosci.*, 3, 811–812, <https://doi.org/10.1038/ngeo1022>, 2010.

Formatted: Normal, Centred, Border: Top: (No border), Bottom: (No border), Left: (No border), Right: (No border), Between : (No border), Tab stops: 7.96 cm, Centred + 15.92 cm, Right, Position: Horizontal: Left, Relative to: Column, Vertical: In line, Relative to: Margin, Wrap Around

Formatted: Font colour: Black

- 2669 Friedlingstein, P., Andrew, R. M., Rogelj, J., Peters, G. P., Canadell, J. G., Knutti, R., Luderer, G., Raupach, M. R.,
2670 Schaeffer, M., van Vuuren, D. P., and Le Quéré, C.: Persistent growth of CO₂ emissions and implications for reaching
2671 climate targets, *Nature Geosci.*, 7, 709–715, <https://doi.org/10.1038/ngeo2248>, 2014.
- 2672 Friedlingstein, P., Jones, M. W., O’Sullivan, M., Andrew, R. M., Hauck, J., Peters, G. P., Peters, W., Pongratz, J., Sitch, S.,
2673 Le Quéré, C., Bakker, D. C. E., Canadell, J. G., Ciais, P., Jackson, R. B., Anthoni, P., Barbero, L., Bastos, A., Bastrikov, V.,
2674 Becker, M., Bopp, L., Buitenhuis, E., Chandra, N., Chevallier, F., Chini, L. P., Currie, K. I., Feely, R. A., Gehlen, M.,
2675 Gilfillan, D., Gkritzalis, T., Goll, D. S., Gruber, N., Gutekunst, S., Harris, I., Haverd, V., Houghton, R. A., Hurtt, G., Ilyina,
2676 T., Jain, A. K., Joetzjer, E., Kaplan, J. O., Kato, E., Klein Goldewijk, K., Korsbakken, J. I., Landschützer, P., Lauvset, S. K.,
2677 Lefèvre, N., Lenton, A., Lienert, S., Lombardozi, D., Marland, G., McGuire, P. C., Melton, J. R., Metzl, N., Munro, D. R.,
2678 Nabel, J. E. M. S., Nakaoka, S.-I., Neill, C., Omar, A. M., Ono, T., Peregón, A., Pierrot, D., Poulter, B., Rehder, G.,
2679 Resplandy, L., Robertson, E., Rödenbeck, C., Séférian, R., Schwinger, J., Smith, N., Tans, P. P., Tian, H., Tilbrook, B.,
2680 Tubiello, F. N., van der Werf, G. R., Wiltshire, A. J., and Zaehle, S.: Global Carbon Budget 2019, *Earth Syst. Sci. Data*, 11,
2681 1783–1838, <https://doi.org/10.5194/essd-11-1783-2019>, 2019.
- 2682 Friedlingstein, P., O’Sullivan, M., Jones, M. W., Andrew, R. M., Hauck, J., Olsen, A., Peters, G. P., Peters, W., Pongratz, J.,
2683 Sitch, S., Le Quéré, C., Canadell, J. G., Ciais, P., Jackson, R. B., Alin, S., Aragão, L. E. O. C., Armeth, A., Arora, V., Bates,
2684 N. R., Becker, M., Benoit-Cattin, A., Bittig, H. C., Bopp, L., Bultan, S., Chandra, N., Chevallier, F., Chini, L. P., Evans, W.,
2685 Florentie, L., Forster, P. M., Gasser, T., Gehlen, M., Gilfillan, D., Gkritzalis, T., Gregor, L., Gruber, N., Harris, I., Hartung,
2686 K., Haverd, V., Houghton, R. A., Ilyina, T., Jain, A. K., Joetzjer, E., Kadono, K., Kato, E., Kitidis, V., Korsbakken, J. I.,
2687 Landschützer, P., Lefèvre, N., Lenton, A., Lienert, S., Liu, Z., Lombardozi, D., Marland, G., Metzl, N., Munro, D. R.,
2688 Nabel, J. E. M. S., Nakaoka, S.-I., Niwa, Y., O’Brien, K., Ono, T., Palmer, P. I., Pierrot, D., Poulter, B., Resplandy, L.,
2689 Robertson, E., Rödenbeck, C., Schwinger, J., Séférian, R., Skjelvan, I., Smith, A. J. P., Sutton, A. J., Tanhua, T., Tans, P. P.,
2690 Tian, H., Tilbrook, B., van der Werf, G., Vuichard, N., Walker, A. P., Wanninkhof, R., Watson, A. J., Willis, D., Wiltshire,
2691 A. J., Yuan, W., Yue, X., and Zaehle, S.: Global Carbon Budget 2020, *Earth Syst. Sci. Data*, 12, 3269–3340,
2692 <https://doi.org/10.5194/essd-12-3269-2020>, 2020.
- 2693 Friedlingstein, P., Jones, M. W., O’Sullivan, M., Andrew, R. M., Bakker, D. C. E., Hauck, J., Le Quéré, C., Peters, G. P.,
2694 Peters, W., Pongratz, J., Sitch, S., Canadell, J. G., Ciais, P., Jackson, R. B., Alin, S. R., Anthoni, P., Bates, N. R., Becker, M.,
2695 Bellouin, N., Bopp, L., Chau, T. T. T., Chevallier, F., Chini, L. P., Cronin, M., Currie, K. I., Decharme, B., Djeutchouang, L.
2696 M., Dou, X., Evans, W., Feely, R. A., Feng, L., Gasser, T., Gilfillan, D., Gkritzalis, T., Grassi, G., Gregor, L., Gruber, N.,
2697 Gürses, Ö., Harris, I., Houghton, R. A., Hurtt, G. C., Iida, Y., Ilyina, T., Lujikx, I. T., Jain, A., Jones, S. D., Kato, E.,
2698 Kennedy, D., Klein Goldewijk, K., Knauer, J., Korsbakken, J. I., Körtzinger, A., Landschützer, P., Lauvset, S. K., Lefèvre,
2699 N., Lienert, S., Liu, J., Marland, G., McGuire, P. C., Melton, J. R., Munro, D. R., Nabel, J. E. M. S., Nakaoka, S.-I., Niwa,
2700 Y., Ono, T., Pierrot, D., Poulter, B., Rehder, G., Resplandy, L., Robertson, E., Rödenbeck, C., Rosan, T. M., Schwinger, J.,
2701 Schwingshackl, C., Séférian, R., Sutton, A. J., Sweeney, C., Tanhua, T., Tans, P. P., Tian, H., Tilbrook, B., Tubiello, F., van
2702 der Werf, G. R., Vuichard, N., Wada, C., Wanninkhof, R., Watson, A. J., Willis, D., Wiltshire, A. J., Yuan, W., Yue, C.,
2703 Yue, X., Zaehle, S., and Zeng, J.: Global Carbon Budget 2021, *Earth Syst. Sci. Data*, 14, 1917–2005,
2704 <https://doi.org/10.5194/essd-14-1917-2022>, 2022a.
- 2705 Friedlingstein, P. and co-authors of the current study, Supplemental data of the Global Carbon Budget 2023, ICOS-ERIC
2706 Carbon Portal, <https://doi.org/10.18160/GCP-2023>, 2023.
- 2707 Friedlingstein, P., O’Sullivan, M., Jones, M. W., Andrew, R. M., Gregor, L., Hauck, J., Le Quéré, C., Lujikx, I. T., Olsen,
2708 A., Peters, G. P., Peters, W., Pongratz, J., Schwingshackl, C., Sitch, S., Canadell, J. G., Ciais, P., Jackson, R. B., Alin, S. R.,

Formatted: Default Paragraph Font, Font colour: Black

Formatted: Normal, Centred, Border: Top: (No border),
Bottom: (No border), Left: (No border), Right: (No border),
Between : (No border), Tab stops: 7.96 cm, Centred + 15.92
cm, Right, Position: Horizontal: Left, Relative to: Column,
Vertical: In line, Relative to: Margin, Wrap Around

Formatted: Font colour: Black

2709 Alkama, R., Arneth, A., Arora, V. K., Bates, N. R., Becker, M., Bellouin, N., Bittig, H. C., Bopp, L., Chevallier, F., Chini, L.
2710 P., Cronin, M., Evans, W., Falk, S., Feely, R. A., Gasser, T., Gehlen, M., Gkritzalis, T., Gloege, L., Grassi, G., Gruber, N.,
2711 Gürses, Ö., Harris, I., Hefner, M., Houghton, R. A., Hurtt, G. C., Iida, Y., Ilyina, T., Jain, A. K., Jersild, A., Kadono, K.,
2712 Kato, E., Kennedy, D., Klein Goldewijk, K., Knauer, J., Korsbakken, J. I., Landschützer, P., Lefèvre, N., Lindsay, K., Liu,
2713 J., Liu, Z., Marland, G., Mayot, N., McGrath, M. J., Metzl, N., Monacci, N. M., Munro, D. R., Nakaoka, S.-I., Niwa, Y.,
2714 O'Brien, K., Ono, T., Palmer, P. I., Pan, N., Pierrot, D., Pocock, K., Poulter, B., Resplandy, L., Robertson, E., Rödenbeck,
2715 C., Rodriguez, C., Rosan, T. M., Schwinger, J., Séférian, R., Shutler, J. D., Skjelvan, I., Steinhoff, T., Sun, Q., Sutton, A. J.,
2716 Sweeney, C., Takao, S., Tanhua, T., Tans, P. P., Tian, X., Tian, H., Tilbrook, B., Tsujino, H., Tubiello, F., van der Werf, G.
2717 R., Walker, A. P., Wanninkhof, R., Whitehead, C., Willstrand Wranne, A., et al.: Global Carbon Budget 2022, Earth Syst.
2718 Sci. Data, 14, 4811–4900, <https://doi.org/10.5194/essd-14-4811-2022>, 2022b.

2719 Ganzenmüller, R., Bultan, S., Winkler, K., Fuchs, R., Zabel, F., and Pongratz, J.: Land-use change emissions based on high-
2720 resolution activity data substantially lower than previously estimated, Environ. Res. Lett., 17, 064050,
2721 <https://doi.org/10.1088/1748-9326/ac70d8>, 2022.

2722 Gasser, T., Crepin, L., Quilcaille, Y., Houghton, R. A., Ciais, P., and Obersteiner, M.: Historical CO2 emissions from land
2723 use and land cover change and their uncertainty, Biogeosciences, 17, 4075–4101, <https://doi.org/10.5194/bg-17-4075-2020>,
2724 2020.

2725 Gaubert, B., Stephens, B. B., Basu, S., Chevallier, F., Deng, F., Kort, E. A., Patra, P. K., Peters, W., Rödenbeck, C., Saeki,
2726 T., Schimel, D., Van der Laan-Luijckx, I., Wofsy, S., and Yin, Y.: Global atmospheric CO2 inverse models converging on
2727 neutral tropical land exchange, but disagreeing on fossil fuel and atmospheric growth rate, Biogeosciences, 16, 117–134,
2728 <https://doi.org/10.5194/bg-16-117-2019>, 2019.

2729 GCP: The Global Carbon Budget 2007, available at: <http://www.globalcarbonproject.org/carbonbudget/archive.htm>, last
2730 access: 9 November 2023, 2007.

2731 Giglio, L., Schroeder, W., and Justice, C. O.: The collection 6 MODIS active fire detection algorithm and fire products,
2732 Remote Sensing of Environment, 178, 31–41, <https://doi.org/10.1016/j.rse.2016.02.054>, 2016.

2733 Gloege, L., McKinley, G. A., Landschützer, P., Fay, A. R., Frölicher, T. L., Fyfe, J. C., Ilyina, T., Jones, S., Lovenduski, N.
2734 S., Rodgers, K. B., Schlunegger, S., and Takano, Y.: Quantifying Errors in Observationally Based Estimates of Ocean
2735 Carbon Sink Variability, Global Biogeochem. Cy., 35, e2020GB006788, <https://doi.org/10.1029/2020GB006788>, 2021.

2736 Gloege, L., Yan, M., Zheng, T., and McKinley, G. A.: Improved Quantification of Ocean Carbon Uptake by Using Machine
2737 Learning to Merge Global Models and pCO2 Data, J. Adv. Model. Earth Syst., 14, e2021MS002620,
2738 <https://doi.org/10.1029/2021MS002620>, 2022.

2739 Golar, G., Malik, A., Muis, H., Herman, A., Nurudin, N., and Lukman, L.: The social-economic impact of COVID-19
2740 pandemic: implications for potential forest degradation, Heliyon, 6, e05354, <https://doi.org/10.1016/j.heliyon.2020.e05354>,
2741 2020.

2742 Goris, N., Tjiputra, J. F., Olsen, A., Schwinger, J., Lauvset, S. K., and Jeansson, E.: Constraining Projection-Based Estimates
2743 of the Future North Atlantic Carbon Uptake, J. Clim., 31, 3959–3978, <https://doi.org/10.1175/JCLI-D-17-0564.1>, 2018.

2744 Grassi, G., House, J., Kurz, W. A., Cescatti, A., Houghton, R. A., Peters, G. P., Sanz, M. J., Viñas, R. A., Alkama, R.,
2745 Arneth, A., Bondeau, A., Dentener, F., Fader, M., Federici, S., Friedlingstein, P., Jain, A. K., Kato, E., Koven, C. D., Lee,

Deleted: 27 September

Deleted: Gilfillan, D. and Marland, G.: CDIAC-FF: global and national CO2 emissions from fossil fuel combustion and cement manufacture: 1751–2017, 13, 1667–1680, <https://doi.org/10.5194/essd-13-1667-2021>, 2021.

Formatted: Default Paragraph Font, Font colour: Black

Formatted: Normal, Centred, Border: Top: (No border), Bottom: (No border), Left: (No border), Right: (No border), Between : (No border), Tab stops: 7.96 cm, Centred + 15.92 cm, Right, Position: Horizontal: Left, Relative to: Column, Vertical: In line, Relative to: Margin, Wrap Around

Formatted: Font colour: Black

2751 D., Nabel, J. E. M. S., Nassikas, A. A., Perugini, L., Rossi, S., Sitch, S., Viovy, N., Wiltshire, A., and Zaehle, S.:
2752 Reconciling global-model estimates and country reporting of anthropogenic forest CO2 sinks, *Nature Clim Change*, 8, 914–
2753 920, <https://doi.org/10.1038/s41558-018-0283-x>, 2018.

2754 Grassi, G., Stehfest, E., Rogelj, J., van Vuuren, D., Cescatti, A., House, J., Nabuurs, G.-J., Rossi, S., Alkama, R., Viñas, R.
2755 A., Calvin, K., Ceccherini, G., Federici, S., Fujimori, S., Gusti, M., Hasegawa, T., Havlik, P., Humpenöder, F., Korosuo, A.,
2756 Perugini, L., Tubiello, F. N., and Popp, A.: Critical adjustment of land mitigation pathways for assessing countries' climate
2757 progress, *Nat. Clim. Chang.*, 11, 425–434, <https://doi.org/10.1038/s41558-021-01033-6>, 2021.

2758 Grassi, G., Schwingshackl, C., Gasser, T., Houghton, R. A., Sitch, S., Canadell, J. G., Cescatti, A., Ciais, P., Federici, S.,
2759 Friedlingstein, P., Kurz, W. A., Sanz Sanchez, M. J., Abad Viñas, R., Alkama, R., Bultan, S., Ceccherini, G., Falk, S., Kato,
2760 E., Kennedy, D., Knauer, J., Korosuo, A., Melo, J., McGrath, M. J., Nabel, J. E. M. S., Poulter, B., Romanovskaya, A. A.,
2761 Rossi, S., Tian, H., Walker, A. P., Yuan, W., Yue, X., and Pongratz, J.: Harmonising the land-use flux estimates of global
2762 models and national inventories for 2000–2020, *Earth Syst. Sci. Data*, 15, 1093–1114, [https://doi.org/10.5194/essd-15-1093-](https://doi.org/10.5194/essd-15-1093-2023)
2763 2023, 2023.

2764 Gregor, L. and Gruber, N.: OceanSODA-ETHZ: a global gridded data set of the surface ocean carbonate system for seasonal
2765 to decadal studies of ocean acidification, 13, 777–808, <https://doi.org/10.5194/essd-13-777-2021>, 2021.

2766 Gruber, N., Bakker, D. C. E., DeVries, T., Gregor, L., Hauck, J., Landschützer, P., McKinley, G. A., and Müller, J. D.:
2767 Trends and variability in the ocean carbon sink, *Nat. Rev. Earth Environ.*, 4, 119–134, [https://doi.org/10.1038/s43017-022-](https://doi.org/10.1038/s43017-022-00381-x)
2768 00381-x, 2023.

2769 Gruber, N., Clement, D., Carter, B. R., Feely, R. A., van Heuven, S., Hoppema, M., Ishii, M., Key, R. M., Kozyr, A.,
2770 Lauvset, S. K., Lo Monaco, C., Mathis, J. T., Murata, A., Olsen, A., Perez, F. F., Sabine, C. L., Tanhua, T., and Wanninkhof,
2771 R.: The oceanic sink for anthropogenic CO2 from 1994 to 2007, 363, 1193–1199, <https://doi.org/10.1126/science.aau5153>,
2772 2019.

2773 Guan, D., Liu, Z., Geng, Y., Lindner, S., and Hubacek, K.: The gigatonne gap in China's carbon dioxide inventories, *Nature*
2774 *Clim Change*, 2, 672–675, <https://doi.org/10.1038/nclimate1560>, 2012.

2775 Gulev, S. K., Thorne, P. W., Ahn, J., Dentener, F. J., Domingues, C. M., Gerland, S., Gong, D. S., Kaufman, S., Nnamchi,
2776 H. C., Quaas, J., Rivera, J. A., Sathyendranath, S., Smith, S. L., Trewin, B., von Shuckmann, K., and Vose, R. S.: Changing
2777 State of the Climate System. In: *Climate Change 2021: The Physical Science Basis. Contribution of Working Group I to the*
2778 *Sixth Assessment Report of the Intergovernmental Panel on Climate Change* [Masson-Delmotte, V., Zhai, P., Pirani, A.,
2779 Connors, S. L., Péan, C., Berger, S., Caud, N., Chen, Y., Goldfarb, L., Gomis, M. I., Huang, M., Leitzell, K., Lonnoy, E.,
2780 Matthews, J.B.R., Maycock, T.K., Waterfield, T., Yelekçi, O., Yu, R. and Zhou, B. (eds.)]. Cambridge University Press,
2781 Cambridge, United Kingdom and New York, NY, USA, pp. 287–422, doi:10.1017/9781009157896.004, 2021.

2782 Guo, R., Wang, J., Bing, L., Tong, D., Ciais, P., Davis, S. J., Andrew, R. M., Xi, F., and Liu, Z.: Global CO2 uptake by
2783 cement from 1930 to 2019, 13, 1791–1805, <https://doi.org/10.5194/essd-13-1791-2021>, 2021.

2784 Gürses, Ö., Oziel, L., Karakuş, O., Sidorenko, D., Völker, C., Ye, Y., Zeising, M., Butzin, M., and Hauck, J.: Ocean
2785 biogeochemistry in the coupled ocean–sea ice–biogeochemistry model FESOM2.1–REcoM3, *Geosci. Model Dev.*, 16,
2786 4883–4936, <https://doi.org/10.5194/gmd-16-4883-2023>, 2023.

Formatted: Default Paragraph Font, Font colour: Black

Formatted: Normal, Centred, Border: Top: (No border),
Bottom: (No border), Left: (No border), Right: (No border),
Between : (No border), Tab stops: 7.96 cm, Centred + 15.92
cm, Right, Position: Horizontal: Left, Relative to: Column,
Vertical: In line, Relative to: Margin, Wrap Around

Formatted: Font colour: Black

- 2787 Gütschow, J., Jeffery, M. L., Gieseke, R., Gebel, R., Stevens, D., Krapp, M., and Rocha, M.: The PRIMAP-hist national
2788 historical emissions time series, 8, 571–603, <https://doi.org/10.5194/essd-8-571-2016>, 2016.
- 2789 Gütschow, J., and Pflüger, M. (2023): The PRIMAP-hist national historical emissions time series v2.4.2 (1750-2021)
2790 [dataset]. <https://doi.org/10.5281/zenodo.7727475>, 2023.
- 2791 Hall, B. D., Crotwell, A. M., Kitzis, D. R., Mefford, T., Miller, B. R., Schibig, M. F., and Tans, P. P.: Revision of the World
2792 Meteorological Organization Global Atmosphere Watch (WMO/GAW) CO2 calibration scale, 14, 3015–3032,
2793 <https://doi.org/10.5194/amt-14-3015-2021>, 2021.
- 2794 Hansis, E., Davis, S. J., and Pongratz, J.: Relevance of methodological choices for accounting of land use change carbon
2795 fluxes, *Global Biogeochem. Cycles*, 29, 1230–1246, <https://doi.org/10.1002/2014GB004997>, 2015.
- 2796 Hauck, J., Nissen, C., Landschützer, P., Rödenbeck, C., Bushinsky, S., and Olsen, A.: Sparse observations induce large
2797 biases in estimates of the global ocean CO2 sink: an ocean model subsampling experiment, *Philos. Trans. R. Soc. Math.*
2798 *Phys. Eng. Sci.*, 381, 20220063, <https://doi.org/10.1098/rsta.2022.0063>, 2023.
- 2799 Hauck, J., Zeising, M., Le Quéré, C., Gruber, N., Bakker, D. C. E., Bopp, L., Chau, T. T. T., Gürses, Ö., Ilyina, T.,
2800 Landschützer, P., Lenton, A., Resplandy, L., Rödenbeck, C., Schwinger, J., and Séférian, R.: Consistency and Challenges in
2801 the Ocean Carbon Sink Estimate for the Global Carbon Budget, *Front. Mar. Sci.*, 7, 571720,
2802 <https://doi.org/10.3389/fmars.2020.571720>, 2020.
- 2803 Haverd, V., Smith, B., Nieradzki, L., Briggs, P. R., Woodgate, W., Trudinger, C. M., Canadell, J. G., and Cuntz, M.: A new
2804 version of the CABLE land surface model (Subversion revision r4601) incorporating land use and land cover change, woody
2805 vegetation demography, and a novel optimisation-based approach to plant coordination of photosynthesis, *Geosci. Model*
2806 *Dev.*, 11, 2995–3026, <https://doi.org/10.5194/gmd-11-2995-2018>, 2018.
- 2807 Heinke, J., Rolinski, S., and Müller, C.: Modelling the role of livestock grazing in C and N cycling in grasslands with
2808 LPJmL5.0-grazing, *Geosci. Model Dev.*, 16, 2455–2475, <https://doi.org/10.5194/gmd-16-2455-2023>, 2023.
- 2809 [Hefner, M., Marland, G., Boden, T., Andres, R.: Global, Regional, and National Fossil-Fuel CO2 Emissions: 1751-2020](#)
2810 [CDIAC-FF \[dataset\], available at: <https://energy.appstate.edu/cdiac-appstate/data-products>, last access: 9 November 2023,](#)
2811 [2023.](#)
- 2812 Hickler, T., Smith, B., Prentice, I. C., Mjöfors, K., Miller, P., Ameth, A., and Sykes, M. T.: CO2 fertilization in temperate
2813 FACE experiments not representative of boreal and tropical forests, *Glob. Change Biol.*, 14, 1531–1542,
2814 <https://doi.org/10.1111/j.1365-2486.2008.01598.x>, 2008.
- 2815 Hoesly, R. M., Smith, S. J., Feng, L., Klimont, Z., Janssens-Maenhout, G., Pitkanen, T., Seibert, J. J., Vu, L., Andres, R. J.,
2816 Bolt, R. M., Bond, T. C., Dawidowski, L., Kholod, N., Kurokawa, J., Li, M., Liu, L., Lu, Z., Moura, M. C. P., O'Rourke, P.
2817 R., and Zhang, Q.: Historical (1750–2014) anthropogenic emissions of reactive gases and aerosols from the Community
2818 Emissions Data System (CEDS), *Geosci. Model Dev.*, 11, 369–408, <https://doi.org/10.5194/gmd-11-369-2018>, 2018.
- 2819 Hong, C., Burney, J. A., Pongratz, J., Nabel, J. E. M. S., Mueller, N. D., Jackson, R. B., and Davis, S. J.: Global and regional
2820 drivers of land-use emissions in 1961–2017, *Nature*, 589, 554–561, <https://doi.org/10.1038/s41586-020-03138-y>, 2021.

Formatted: English (UK)

Formatted: Default Paragraph Font, Font colour: Black

Formatted: Normal, Centred, Border: Top: (No border),
Bottom: (No border), Left: (No border), Right: (No border),
Between : (No border), Tab stops: 7.96 cm, Centred + 15.92
cm, Right, Position: Horizontal: Left, Relative to: Column,
Vertical: In line, Relative to: Margin, Wrap Around

Formatted: Font colour: Black

- 2821 Holding, T., Ashton, I. G., Shutler, J. D., Land, P. E., Nightingale, P. D., Rees, A. P., Brown, I., Piolle, J.-F., Kock, A.,
2822 Bange, H. W., Woolf, D. K., Goddijn-Murphy, L., Pereira, R., Paul, F., Girard-Ardhuin, F., Chapron, B., Rehder, G.,
2823 Ardhuin, F., and Donlon, C. J.: The FluxEngine air-sea gas flux toolbox: simplified interface and extensions for in situ
2824 analyses and multiple sparingly soluble gases, *Ocean Sci.*, 15, 1707–1728, <https://doi.org/10.5194/os-15-1707-2019>, 2019.
- 2825 Houghton, R. A. and Castanho, A.: Annual emissions of carbon from land use, land-use change, and forestry from 1850 to
2826 2020, *Earth Syst. Sci. Data*, 15, 2025–2054, <https://doi.org/10.5194/essd-15-2025-2023>, 2023.
- 2827 Houghton, R. A., House, J. I., Pongratz, J., van der Werf, G. R., DeFries, R. S., Hansen, M. C., Le Quéré, C., and
2828 Ramankutty, N.: Carbon emissions from land use and land-cover change, *Biogeosciences*, 9, 5125–5142,
2829 <https://doi.org/10.5194/bg-9-5125-2012>, 2012.
- 2830 [Huang, B., Thorne, P. W., Banzon, V. F., Boyer, T., Chepurin, G., Lawrimore, J. H., Menne, M. J., Smith, T. M., Vose, R.](#)
2831 [S., and Zhang, H.-M.: NOAA Extended Reconstructed Sea Surface Temperature \(ERSST\), Version 5,](#)
2832 <https://doi.org/10.7289/V5T72FNM.2017>.
- 2833 Hubau, W., Lewis, S.L., Phillips, O.L., Affum-Baffoe, K., Beekman, H., Cuni-Sanchez, A., Daniels, A.K., Ewango, C.E.N.,
2834 Fauset, S., Mukinzi, J.M., Sheil, D., Sonké, B., Sullivan, M.J.P., Sunderland, T.C.H., Taedoumg, H., Thomas, S.C., White,
2835 L.J.T., Abernethy, K.A., Adu-Bredu, S., Amani, C.A., Baker, T.R., Banin, L.F., Baya, F., Begne, S.K., Bennett, A.C.,
2836 Benedet, F., Bitariho, R., Bocko, Y.E., Boeckx, P., Boundja, P., Brienen, R.J.W., Brncic, T., Chezeaux, E., Chuyong, G.B.,
2837 Clark, C.J., Collins, M., Comiskey, J.A., Coomes, D.A., Dargie, G.C., de Haulleville, T., Kamdem, M.N.D., Doucet, J.-L.,
2838 Esquivel-Muelbert, A., Feldpausch, T.R., Fofanah, A., Foli, E.G., Gilpin, M., Gloor, E., Gonmadje, C., Gourlet-Fleury, S.,
2839 Hall, J.S., Hamilton, A.C., Harris, D.J., Hart, T.B., Hockemba, M.B.N., Hladik, A., Ifo, S.A., Jeffery, K.J., Jucker, T.,
2840 Yakusu, E.K., Kearsley, E., Kenfack, D., Koch, A., Leal, M.E., Levesley, A., Lindsell, J.A., Lisingo, J., Lopez-Gonzalez, G.,
2841 Lovett, J.C., Makana, J.-R., Malhi, Y., Marshall, A.R., Martin, J., Martin, E.H., Mbayu, F.M., Medjibe, V.P., Mihindou, V.,
2842 Mitchard, E.T.A., Moore, S., Munishi, P.K.T., Bengone, N.N., Ojo, L., Ondo, F.E., Peh, K.S.-H., Pickavance, G.C., Poulsen,
2843 A.D., Poulsen, J.R., Qie, L., Reitsma, J., Rovero, F., Swaine, M.D., Talbot, J., Taplin, J., Taylor, D.M., Thomas, D.W.,
2844 Toirambe, B., Mukendi, J.T., Tuagben, D., Umunay, P.M., van der Heijden, G.M.F., Verbeeck, H., Vleminckx, J., Willcock,
2845 S., Wöll, H., Woods, J.T., Zemagho, L.: Asynchronous carbon sink saturation in African and Amazonian tropical forests,
2846 *Nature*, 579, 80–87, <https://doi.org/10.1038/s41586-020-2035-0>, 2020.
- 2847 Humphrey, V., Zscheischler, J., Ciais, P., Gudmundsson, L., Sitch, S., and Seneviratne, S. I.: Sensitivity of atmospheric CO₂
2848 growth rate to observed changes in terrestrial water storage, *Nature*, 560, 628–631, <https://doi.org/10.1038/s41586-018->
2849 0424-4, 2018.
- 2850 Humphrey, V., Berg, A., Ciais, P., Gentile, P., Jung, M., Reichstein, M., Seneviratne, S. I., and Frankenberg, C.: Soil
2851 moisture-atmosphere feedback dominates land carbon uptake variability, *Nature*, 592, 65–69,
2852 <https://doi.org/10.1038/s41586-021-03325-5>, 2021.
- 2853 Huntzinger, D. N., Michalak, A. M., Schwalm, C., Ciais, P., King, A. W., Fang, Y., Schaefer, K., Wei, Y., Cook, R. B.,
2854 Fisher, J. B., Hayes, D., Huang, M., Ito, A., Jain, A. K., Lei, H., Lu, C., Maignan, F., Mao, J., Parazoo, N., Peng, S., Poulter,
2855 B., Ricciuto, D., Shi, X., Tian, H., Wang, W., Zeng, N., and Zhao, F.: Uncertainty in the response of terrestrial carbon sink to
2856 environmental drivers undermines carbon-climate feedback predictions, *Sci Rep*, 7, 4765, <https://doi.org/10.1038/s41598->
2857 017-03818-2, 2017.

Formatted: Default Paragraph Font, Font colour: Black

Formatted: Normal, Centred, Border: Top: (No border),
Bottom: (No border), Left: (No border), Right: (No border),
Between : (No border), Tab stops: 7.96 cm, Centred + 15.92
cm, Right, Position: Horizontal: Left, Relative to: Column,
Vertical: In line, Relative to: Margin, Wrap Around

Formatted: Font colour: Black

2858 Iida, Y., Takatani, Y., Kojima, A., and Ishii, M.: Global trends of ocean CO₂ sink and ocean acidification: an observation-
2859 based reconstruction of surface ocean inorganic carbon variables, *J Oceanogr*, 77, 323–358, [https://doi.org/10.1007/s10872-](https://doi.org/10.1007/s10872-020-00571-5)
2860 020-00571-5, 2021.

2861 Ilyina, T., Li, H., Spring, A., Müller, W. A., Bopp, L., Chikamoto, M. O., Danabasoglu, G., Dobrynin, M., Dunne, J.,
2862 Fransner, F., Friedlingstein, P., Lee, W., Lovenduski, N. S., Merryfield, W. J., Mignot, J., Park, J. Y., Séférian, R., Sospedra-
2863 Alfonso, R., Watanabe, M., and Yeager, S.: Predictable Variations of the Carbon Sinks and Atmospheric CO₂ Growth in a
2864 Multi-Model Framework, *Geophys. Res. Lett.*, 48, e2020GL090695, <https://doi.org/10.1029/2020GL090695>, 2021.

2865 IMF: International Monetary Fund: World Economic Outlook, available at: <http://www.imf.org>, last access: [9 November](#)
2866 2023, [2023](#).

Deleted: 27 September

Deleted: 2022

2867 IPCC: Annex II: Glossary [Möller, V, J.B.R. Matthews, R. van Diemen, C. Méndez, S. Semenov, J.S. Fuglestedt, A.
2868 Reisinger (eds.)]. In: *Climate Change 2022: Impacts, Adaptation, and Vulnerability. Contribution of Working Group II to the*
2869 *Sixth Assessment Report of the Intergovernmental Panel on Climate Change* [H.-O. Pörtner, D.C. Roberts, M. Tignor, E.S.
2870 Poloczanska, K. Mintenbeck, A. Alegria, M. Craig, S. Langsdorf, S. Löschke, V. Möller, A. Okem, B. Rama (eds.)], in:
2871 *Climate Change 2022 – Impacts, Adaptation and Vulnerability: Working Group II Contribution to the Sixth Assessment*
2872 *Report of the Intergovernmental Panel on Climate Change* [Möller, V, J.B.R. Matthews, R. van Diemen, C. Méndez, S.
2873 Semenov, J.S. Fuglestedt, A. Reisinger (eds.)], Cambridge University Press, Cambridge, UK and New York, NY, 2897–
2874 2930, <https://doi.org/10.1017/9781009325844.029>, 2023.

2875 Ito, A. and Inatomi, M.: Use of a process-based model for assessing the methane budgets of global terrestrial ecosystems and
2876 evaluation of uncertainty, *9*, 759–773, <https://doi.org/10.5194/bg-9-759-2012>, 2012.

2877 Jackson, R. B., Canadell, J. G., Le Quéré, C., Andrew, R. M., Korsbakken, J. I., Peters, G. P., and Nakicenovic, N.:
2878 Reaching peak emissions, *Nature Clim Change*, 6, 7–10, <https://doi.org/10.1038/nclimate2892>, 2016.

2879 Jackson, R. B., Le Quéré, C., Andrew, R. M., Canadell, J. G., Korsbakken, J. I., Liu, Z., Peters, G. P., and Zheng, B.: Global
2880 energy growth is outpacing decarbonization, *Environ. Res. Lett.*, 13, 120401, <https://doi.org/10.1088/1748-9326/aaf303>,
2881 2018.

2882 Jackson, R. B., Friedlingstein, P., Andrew, R. M., Canadell, J. G., Le Quéré, C., and Peters, G. P.: Persistent fossil fuel
2883 growth threatens the Paris Agreement and planetary health, *Environ. Res. Lett.*, 14, 121001, [https://doi.org/10.1088/1748-](https://doi.org/10.1088/1748-9326/ab57b3)
2884 9326/ab57b3, 2019.

2885 Jackson, R. B., Friedlingstein, P., Quéré, C. L., Abernethy, S., Andrew, R. M., Canadell, J. G., Ciais, P., Davis, S. J., Deng,
2886 Z., Liu, Z., Korsbakken, J. I., and Peters, G. P.: Global fossil carbon emissions rebound near pre-COVID-19 levels, *Environ.*
2887 *Res. Lett.*, 17, 031001, <https://doi.org/10.1088/1748-9326/ac55b6>, 2022.

2888 Jacobson, A. R., Schuldt, K. N., Tans, P., Arlyn Andrews, Miller, J. B., Oda, T., Mund, J., Weir, B., Ott, L., Aalto, T.,
2889 Abshire, J. B., Aikin, K., Aoki, S., Apadula, F., Arnold, S., Baier, B., Bartyzel, J., Beyersdorf, A., Biermann, T., Biraud, S.
2890 C., Boenisch, H., Brailsford, G., Brand, W. A., Chen, G., Huilin Chen, Lukasz Chmura, Clark, S., Colomb, A., Commane,
2891 R., Conil, S., Couret, C., Cox, A., Cristofanelli, P., Cuevas, E., Curcoll, R., Daube, B., Davis, K. J., De Wekker, S., Coletta,
2892 J. D., Delmotte, M., DiGangi, E., DiGangi, J. P., Di Sarra, A. G., Dlugokencky, E., Elkins, J. W., Emmenegger, L., Shuangxi
2893 Fang, Fischer, M. L., Forster, G., Frumau, A., Galkowski, M., Gatti, L. V., Gehrlein, T., Gerbig, C., Francois Gheusi, Gloor,

Formatted: Default Paragraph Font, Font colour: Black

Formatted: Normal, Centred, Border: Top: (No border),
Bottom: (No border), Left: (No border), Right: (No border),
Between : (No border), Tab stops: 7.96 cm, Centred + 15.92
cm, Right, Position: Horizontal: Left, Relative to: Column,
Vertical: In line, Relative to: Margin, Wrap Around

Formatted: Font colour: Black

- 2896 E., Gomez-Trueba, V., Goto, D., Griffiths, T., Hammer, S., Hanson, C., Haszpra, L., Hatakka, J., Heimann, M., Heliasz, M.,
2897 Hensen, A., Hermansen, O., Hints, E., Holst, J., Ivakhov, V., Jaffe, D. A., Jordan, A., Joubert, W., Karion, A., Kawa, S. R.,
2898 Kazan, V., Keeling, R. F., Keronen, P., Kneuer, T., Kolari, P., Kateřina Kominková, Kort, E., Kozlova, E., Krummel, P.,
2899 Kubistin, D., Labuschagne, C., Lam, D. H. Y., Lan, X., Langenfelds, R. L., Laurent, O., Laurila, T., Lauvaux, T., Lavric, J.,
2900 Law, B. E., Lee, J., Lee, O. S. M., Lehner, I., Lehtinen, K., Leppert, R., et al.: CarbonTracker CT2022,
2901 <https://doi.org/10.25925/Z1GJ-3254>, 2023a.
- 2902 Jacobson, A. R., Schuldt, K. N., Tans, P., Arlyn Andrews, Miller, J. B., Oda, T., Mund, J., Weir, B., Ott, L., Aalto, T.,
2903 Abshire, J. B., Aikin, K., Aoki, S., Apadula, F., Arnold, S., Baier, B., Bartyzel, J., Beyersdorf, A., Biermann, T., Biraud, S.
2904 C., Boenisch, H., Brailsford, G., Brand, W. A., Chen, G., Huilin Chen, Lukasz Chmura, Clark, S., Colomb, A., Commane,
2905 R., Comil, S., Couret, C., Cox, A., Cristofanelli, P., Cuevas, E., Curcoll, R., Daube, B., Davis, K. J., De Wekker, S., Coletta,
2906 J. D., Delmotte, M., DiGangi, E., DiGangi, J. P., Di Sarra, A. G., Dlugokencky, E., Elkins, J. W., Emmenegger, L., Shuangxi
2907 Fang, Fischer, M. L., Forster, G., Frumau, A., Galkowski, M., Gatti, L. V., Gehrlein, T., Gerbig, C., Francois Gheusi, Gloor,
2908 E., Gomez-Trueba, V., Goto, D., Griffiths, T., Hammer, S., Hanson, C., Haszpra, L., Hatakka, J., Heimann, M., Heliasz, M.,
2909 Hensen, A., Hermansen, O., Hints, E., Holst, J., Ivakhov, V., Jaffe, D. A., Jordan, A., Joubert, W., Karion, A., Kawa, S. R.,
2910 Kazan, V., Keeling, R. F., Keronen, P., Kneuer, T., Kolari, P., Kateřina Kominková, Kort, E., Kozlova, E., Krummel, P.,
2911 Kubistin, D., Labuschagne, C., Lam, D. H. Y., Lan, X., Langenfelds, R. L., Laurent, O., Laurila, T., Lauvaux, T., Lavric, J.,
2912 Law, B. E., Lee, J., Lee, O. S. M., Lehner, I., Lehtinen, K., Leppert, R., et al.: CarbonTracker CT-NRT.v2023-3,
2913 <https://doi.org/10.25925/7TAF-J322>, 2023b.
- 2914 Janssens-Maenhout, G., Crippa, M., Guizzardi, D., Muntean, M., Schaaf, E., Dentener, F., Bergamaschi, P., Pagliari, V.,
2915 Olivier, J. G. J., Peters, J. A. H. W., van Aardenne, J. A., Monni, S., Doering, U., Petrescu, A. M. R., Solazzo, E., and
2916 Oreggioni, G. D.: EDGAR v4.3.2 Global Atlas of the three major greenhouse gas emissions for the period 1970–2012, *Earth*
2917 *Syst. Sci. Data*, 11, 959–1002, <https://doi.org/10.5194/essd-11-959-2019>, 2019.
- 2918 Jean-Michel, L., Eric, G., Romain, B.-B., Gilles, G., Angélique, M., Marie, D., Clément, B., Mathieu, H., Olivier, L. G.,
2919 Charly, R., Tony, C., Charles-Emmanuel, T., Florent, G., Giovanni, R., Mounir, B., Yann, D., and Pierre-Yves, L. T.: The
2920 Copernicus Global 1/12° Oceanic and Sea Ice GLORYS12 Reanalysis, *Front. Earth Sci.*, 9, 2021.
- 2921 Jiang, F., Ju, W., He, W., Wu, M., Wang, H., Wang, J., Jia, M., Feng, S., Zhang, L., and Chen, J. M.: A 10-year global
2922 monthly averaged terrestrial net ecosystem exchange dataset inferred from the ACOS GOSAT v9 XCO2 retrievals
2923 (GCAS2021), *Earth Syst. Sci. Data*, 14, 3013–3037, <https://doi.org/10.5194/essd-14-3013-2022>, 2022.
- 2924 Jiang, F., Wang, H., Chen, J. M., Ju, W., Tian, X., Feng, S., Li, G., Chen, Z., Zhang, S., Lu, X., Liu, J., Wang, H., Wang, J.,
2925 He, W., and Wu, M.: Regional CO2 fluxes from 2010 to 2015 inferred from GOSAT XCO2 retrievals using a new version
2926 of the Global Carbon Assimilation System, *Atmospheric Chem. Phys.*, 21, 1963–1985, [https://doi.org/10.5194/acp-21-1963-](https://doi.org/10.5194/acp-21-1963-2021)
2927 2021, 2021.
- 2928
2929 Jin, Z., Wang, T., Zhang, H., Wang, Y., Ding, J., and Tian, X.: Constraint of satellite CO2 retrieval on the global carbon
2930 cycle from a Chinese atmospheric inversion system, *Sci. China Earth Sci.*, 66, 609–618, [https://doi.org/10.1007/s11430-022-](https://doi.org/10.1007/s11430-022-1036-7)
2931 1036-7, 2023.
- 2932 Joos, F. and Spahni, R.: Rates of change in natural and anthropogenic radiative forcing over the past 20,000 years,
2933 *Proceedings of the National Academy of Sciences*, 105, 1425–1430, <https://doi.org/10.1073/pnas.0707386105>, 2008.

Formatted: Default Paragraph Font, Font colour: Black

Formatted: Normal, Centred, Border: Top: (No border), Bottom: (No border), Left: (No border), Right: (No border), Between : (No border), Tab stops: 7.96 cm, Centred + 15.92 cm, Right, Position: Horizontal: Left, Relative to: Column, Vertical: In line, Relative to: Margin, Wrap Around

Formatted: Font colour: Black

2934 Jones, C. D., Hickman, J. E., Rumbold, S. T., Walton, J., Lamboll, R. D., Skeie, R. B., Fiedler, S., Forster, P. M., Rogelj, J.,
 2935 Abe, M., Botzet, M., Calvin, K., Cassou, C., Cole, J. N. S., Davini, P., Deushi, M., Dix, M., Fyfe, J. C., Gillett, N. P., Ilyina,
 2936 T., Kawamiya, M., Kelley, M., Kharin, S., Koshiro, T., Li, H., Mackallah, C., Müller, W. A., Nabat, P., van Noije, T., Nolan,
 2937 P., Ohgaito, R., Olivié, D., Oshima, N., Parodi, J., Reerink, T. J., Ren, L., Romanou, A., Séférian, R., Tang, Y., Timmreck,
 2938 C., Tjiputra, J., Tourigny, E., Tsigaridis, K., Wang, H., Wu, M., Wyser, K., Yang, S., Yang, Y., and Ziehn, T.: The Climate
 2939 Response to Emissions Reductions Due to COVID-19: Initial Results From CovidMIP, *Geophys. Res. Lett.*, 48,
 2940 e2020GL091883, <https://doi.org/10.1029/2020GL091883>, 2021a.

2941

2942 Jones, M. W., Abatzoglou, J. T., Veraverbeke, S., Andela, N., Lasslop, G., Forkel, M., Smith, A. J. P., Burton, C., Betts, R.
 2943 A., van der Werf, G. R., Sitch, S., Canadell, J. G., Santín, C., Kolden, C., Doerr, S. H., and Le Quéré, C.: Global and
 2944 Regional Trends and Drivers of Fire Under Climate Change, *Rev. Geophys.*, 60, e2020RG000726,
 2945 <https://doi.org/10.1029/2020RG000726>, 2022.

2946 Jones, M. W., Andrew, R. M., Peters, G. P., Janssens-Maenhout, G., De-Gol, A. J., Ciais, P., Patra, P. K., Chevallier, F., and
 2947 Le Quéré, C.: Gridded fossil CO₂ emissions and related O₂ combustion consistent with national inventories 1959–2018, *Sci*
 2948 *Data*, 8, 2, <https://doi.org/10.1038/s41597-020-00779-6>, 2021b.

2949 Jones, M. W., Andrew, R. M., Peters, G. P., Janssens-Maenhout, G., De-Gol, A. J., Dou, X., Liu, Z., Pickers, P., Ciais, P.,
 2950 Patra, P. K., Chevallier, F., and Le Quéré, C.: Gridded fossil CO₂ emissions and related O₂ combustion consistent with
 2951 national inventories 1959-2022, Zenodo [dataset], <https://doi.org/10.5281/zenodo.8386803>, 2023.

2952 Jung, M., Reichstein, M., Schwalm, C. R., Huntingford, C., Sitch, S., Ahlström, A., Arneth, A., Camps-Valls, G., Ciais, P.,
 2953 Friedlingstein, P., Gans, F., Ichii, K., Jain, A. K., Kato, E., Papale, D., Poulter, B., Raduly, B., Rödenbeck, C., Tramontana,
 2954 G., Viovy, N., Wang, Y.-P., Weber, U., Zaehle, S., and Zeng, N.: Compensatory water effects link yearly global land CO₂
 2955 sink changes to temperature, *Nature*, 541, 516–520, <https://doi.org/10.1038/nature20780>, 2017.

2956 Kaiser, J. W., Heil, A., Andreae, M. O., Benedetti, A., Chubarova, N., Jones, L., Morcrette, J.-J., Razinger, M., Schultz, M.
 2957 G., Suttie, M., and van der Werf, G. R.: Biomass burning emissions estimated with a global fire assimilation system based
 2958 on observed fire radiative power, *Biogeosciences*, 9, 527–554, <https://doi.org/10.5194/bg-9-527-2012>, 2012.

2959 Kato, E., Kinoshita, T., Ito, A., Kawamiya, M., and Yamagata, Y.: Evaluation of spatially explicit emission scenario of land-
 2960 use change and biomass burning using a process-based biogeochemical model, *J. Land Use Sci.*, 8, 104–122,
 2961 <https://doi.org/10.1080/1747423X.2011.628705>, 2013.

2962 Kawasaki, T., Hasumi, H., and Tanaka, Y.: Role of tide-induced vertical mixing in the deep Pacific Ocean circulation, *J.*
 2963 *Oceanogr.*, 77, 173–184, <https://doi.org/10.1007/s10872-020-00584-0>, 2021.

2964 Keeley, J. E. and Pausas, J. G.: Distinguishing disturbance from perturbations in fire-prone ecosystems, *Int. J. Wildland Fire*,
 2965 28, 282–287, <https://doi.org/10.1071/WF18203>, 2019.

2966 Keeling, C. D., Bacastow, R. B., Bainbridge, A. E., Ekdahl, C. A., Guenther, P. R., Waterman, L. S., and Chin, J. F. S.:
 2967 Atmospheric carbon dioxide variations at Mauna Loa Observatory, Hawaii, *Tellus A.*, 28, 538–551,
 2968 <https://doi.org/10.1111/j.2153-3490.1976.tb00701.x>, 1976.

Formatted: Default Paragraph Font, Font colour: Black

Formatted: Normal, Centred, Border: Top: (No border),
 Bottom: (No border), Left: (No border), Right: (No border),
 Between : (No border), Tab stops: 7.96 cm, Centred + 15.92
 cm, Right, Position: Horizontal: Left, Relative to: Column,
 Vertical: In line, Relative to: Margin, Wrap Around

Formatted: Font colour: Black

2969 Keeling, R. F., Manning, A. C., Paplawsky, W. J., and Cox, A. C.: On the long-term stability of reference gases for
 2970 atmospheric O₂/N₂ and CO₂ measurements, *Tellus B Chem. Phys. Meteorol.*, 59, 3–14, <https://doi.org/10.1111/j.1600->
 2971 [0889.2006.00196.x](https://doi.org/10.1111/j.1600-0889.2006.00196.x), 2007.

2972
 2973 [Keeling, R. F. and Manning, A. C.: 5.15 - Studies of Recent Changes in Atmospheric O₂ Content, in: *Treatise on*
 2974 *Geochemistry \(Second Edition\)*, edited by: Holland, H. D. and Turekian, K. K., Elsevier, Oxford, 385–404,
 2975 <https://doi.org/10.1016/B978-0-08-095975-7.00420-4>, 2014.](#)

2976 Keppeler, L. and Landschützer, P.: Regional Wind Variability Modulates the Southern Ocean Carbon Sink, *Sci Rep*, 9, 7384,
 2977 <https://doi.org/10.1038/s41598-019-43826-y>, 2019.

2978 Khatiwala, S., Primeau, F., and Hall, T.: Reconstruction of the history of anthropogenic CO₂ concentrations in the ocean,
 2979 *Nature*, 462, 346–349, <https://doi.org/10.1038/nature08526>, 2009.

2980 Khatiwala, S., Tanhua, T., Mikaloff Fletcher, S., Gerber, M., Doney, S. C., Graven, H. D., Gruber, N., McKinley, G. A.,
 2981 Murata, A., Rios, A. F., and Sabine, C. L.: Global ocean storage of anthropogenic carbon, *Biogeosciences*, 10, 2169–2191,
 2982 <https://doi.org/10.5194/bg-10-2169-2013>, 2013.

2983 Kong, Y., Zheng, B., Zhang, Q., and He, K.: Global and regional carbon budget for 2015–2020 inferred from OCO-2 based
 2984 on an ensemble Kalman filter coupled with GEOS-Chem, *Atmospheric Chem. Phys.*, 22, 10769–10788,
 2985 <https://doi.org/10.5194/acp-22-10769-2022>, 2022.

2986 Korsbakken, J. I., Peters, G. P., and Andrew, R. M.: Uncertainties around reductions in China’s coal use and CO₂ emissions,
 2987 *Nature Clim Change*, 6, 687–690, <https://doi.org/10.1038/nclimate2963>, 2016.

2988 Krinner, G., Viovy, N., de Noblet-Ducoudré, N., Ogée, J., Polcher, J., Friedlingstein, P., Ciais, P., Sitch, S., and Prentice, I.
 2989 C.: A dynamic global vegetation model for studies of the coupled atmosphere-biosphere system: DVGCM for coupled climate
 2990 studies, *Global Biogeochem. Cycles*, 19, GB1015, <https://doi.org/10.1029/2003GB002199>, 2005.

2991 Lacroix, F., Ilyina, T., and Hartmann, J.: Oceanic CO₂ outgassing and biological production hotspots induced by pre-
 2992 industrial river loads of nutrients and carbon in a global modeling approach, *Biogeosciences*, 17, 55–88,
 2993 <https://doi.org/10.5194/bg-17-55-2020>, 2020.

2994 Lacroix, F., Ilyina, T., Mathis, M., Laruelle, G. G., and Regnier, P.: Historical increases in land-derived nutrient inputs may
 2995 alleviate effects of a changing physical climate on the oceanic carbon cycle, *Glob Change Biol*, 27, 5491–5513,
 2996 <https://doi.org/10.1111/gcb.15822>, 2021.

2997 [Lamboll, R. D., Nicholls, Z. R. J., Smith, C. J., Kikstra, J. S., Byers, E., and Rogelj, J.: Assessing the size and uncertainty of](#)
 2998 [remaining carbon budgets](https://doi.org/10.1038/s41558-023-01848-5), *Nat. Clim. Change*, <https://doi.org/10.1038/s41558-023-01848-5>, 2023.

2999 Lan, X., Tans, P. and K.W. Thoning: Trends in globally-averaged CO₂ determined from NOAA Global Monitoring
 3000 Laboratory measurements, Version 2023-09. National Oceanic and Atmospheric Administration, Global Monitoring
 3001 Laboratory (NOAA/GML), available at: <https://gml.noaa.gov/ccgg/trends/global.html>, last access: 9 November 2023, 2023.

Deleted: 27 September

Formatted: Default Paragraph Font, Font colour: Black

Formatted: Normal, Centred, Border: Top: (No border), Bottom: (No border), Left: (No border), Right: (No border), Between : (No border), Tab stops: 7.96 cm, Centred + 15.92 cm, Right, Position: Horizontal: Left, Relative to: Column, Vertical: In line, Relative to: Margin, Wrap Around

Formatted: Font colour: Black

3003 Landschützer, P., Gruber, N., Haumann, F. A., Rödenbeck, C., Bakker, D. C. E., van Heuven, S., Hoppema, M., Metzl, N.,
3004 Sweeney, C., Takahashi, T., Tilbrook, B., and Wanninkhof, R.: The reinvigoration of the Southern Ocean carbon sink,
3005 Science, 349, 1221–1224, <https://doi.org/10.1126/science.aab2620>, 2015.

3006 Landschützer, P., Gruber, N., and Bakker, D. C. E.: Decadal variations and trends of the global ocean carbon sink: decadal
3007 air-sea CO₂ flux variability, *Global Biogeochem. Cycles*, 30, 1396–1417, <https://doi.org/10.1002/2015GB005359>, 2016.

3008 Law, R. M., Ziehn, T., Matear, R. J., Lenton, A., Chamberlain, M. A., Stevens, L. E., Wang, Y.-P., Srbinovsky, J., Bi, D.,
3009 Yan, H., and Vohralik, P. F.: The carbon cycle in the Australian Community Climate and Earth System Simulator
3010 (ACCESS-ESM1) – Part 1: Model description and pre-industrial simulation, *Geosci. Model Dev.*, 10, 2567–2590,
3011 <https://doi.org/10.5194/gmd-10-2567-2017>, 2017.

3012 Lawrence, D. M., Fisher, R. A., Koven, C. D., Oleson, K. W., Swenson, S. C., Bonan, G., Collier, N., Ghimire, B., van
3013 Kampenhout, L., Kennedy, D., Kluzek, E., Lawrence, P. J., Li, F., Li, H., Lombardozzi, D., Riley, W. J., Sacks, W. J., Shi,
3014 M., Vertenstein, M., Wieder, W. R., Xu, C., Ali, A. A., Badger, A. M., Bisht, G., van den Broeke, M., Brunke, M. A., Burns,
3015 S. P., Buzan, J., Clark, M., Craig, A., Dahlin, K., Drewniak, B., Fisher, J. B., Flanner, M., Fox, A. M., Gentine, P., Hoffman,
3016 F., Keppel-Aleks, G., Knox, R., Kumar, S., Lenaerts, J., Leung, L. R., Lipscomb, W. H., Lu, Y., Pandey, A., Pelletier, J. D.,
3017 Perket, J., Randerson, J. T., Ricciuto, D. M., Sanderson, B. M., Slater, A., Subin, Z. M., Tang, J., Thomas, R. Q., Val Martin,
3018 M., and Zeng, X.: The Community Land Model Version 5: Description of New Features, Benchmarking, and Impact of
3019 Forcing Uncertainty, *J. Adv. Model Earth. Sy.*, 11, 4245–4287, <https://doi.org/10.1029/2018MS001583>, 2019.

3020 Le Quéré, C., Rödenbeck, C., Buitenhuis, E. T., Conway, T. J., Langenfelds, R., Gomez, A., Labuschagne, C., Ramonet, M.,
3021 Nakazawa, T., Metzl, N., Gillett, N., and Heimann, M.: Saturation of the Southern Ocean CO₂ Sink Due to Recent Climate
3022 Change, *Science*, 316, 1735–1738, <https://doi.org/10.1126/science.1136188>, 2007.

3023 Le Quéré, C., Raupach, M. R., Canadell, J. G., Marland, G., Bopp, L., Ciais, P., Conway, T. J., Doney, S. C., Feely, R. A.,
3024 Foster, P., Friedlingstein, P., Gurney, K., Houghton, R. A., House, J. I., Huntingford, C., Levy, P. E., Lomas, M. R., Majkut,
3025 J., Metzl, N., Ometto, J. P., Peters, G. P., Prentice, I. C., Randerson, J. T., Running, S. W., Sarmiento, J. L., Schuster, U.,
3026 Sitch, S., Takahashi, T., Viovy, N., van der Werf, G. R., and Woodward, F. I.: Trends in the sources and sinks of carbon
3027 dioxide, *Nature Geosci.*, 2, 831–836, <https://doi.org/10.1038/ngeo689>, 2009.

3028 Le Quéré, C., Andres, R. J., Boden, T., Conway, T., Houghton, R. A., House, J. I., Marland, G., Peters, G. P., van der Werf,
3029 G. R., Ahlström, A., Andrew, R. M., Bopp, L., Canadell, J. G., Ciais, P., Doney, S. C., Enright, C., Friedlingstein, P.,
3030 Huntingford, C., Jain, A. K., Jourdain, C., Kato, E., Keeling, R. F., Klein Goldewijk, K., Levis, S., Levy, P., Lomas, M.,
3031 Poulter, B., Raupach, M. R., Schwinger, J., Sitch, S., Stocker, B. D., Viovy, N., Zaehle, S., and Zeng, N.: The global carbon
3032 budget 1959–2011, *Earth Syst. Sci. Data*, 5, 165–185, <https://doi.org/10.5194/essd-5-165-2013>, 2013.

3033 Le Quéré, C., Peters, G. P., Andres, R. J., Andrew, R. M., Boden, T. A., Ciais, P., Friedlingstein, P., Houghton, R. A.,
3034 Marland, G., Moriarty, R., Sitch, S., Tans, P., Armeth, A., Arvanitis, A., Bakker, D. C. E., Bopp, L., Canadell, J. G., Chini, L.
3035 P., Doney, S. C., Harper, A., Harris, I., House, J. I., Jain, A. K., Jones, S. D., Kato, E., Keeling, R. F., Klein Goldewijk, K.,
3036 Körtzinger, A., Koven, C., Lefèvre, N., Maignan, F., Omar, A., Ono, T., Park, G.-H., Pfeil, B., Poulter, B., Raupach, M. R.,
3037 Regnier, P., Rödenbeck, C., Saito, S., Schwinger, J., Segsneider, J., Stocker, B. D., Takahashi, T., Tilbrook, B., van
3038 Heuven, S., Viovy, N., Wanninkhof, R., Wiltshire, A., and Zaehle, S.: Global carbon budget 2013, *Earth Syst. Sci. Data*, 6,
3039 235–263, <https://doi.org/10.5194/essd-6-235-2014>, 2014.

Formatted: Default Paragraph Font, Font colour: Black

Formatted: Normal, Centred, Border: Top: (No border),
Bottom: (No border), Left: (No border), Right: (No border),
Between : (No border), Tab stops: 7.96 cm, Centred + 15.92
cm, Right, Position: Horizontal: Left, Relative to: Column,
Vertical: In line, Relative to: Margin, Wrap Around

Formatted: Font colour: Black

- 3040 Le Quéré, C., Moriarty, R., Andrew, R. M., Peters, G. P., Ciais, P., Friedlingstein, P., Jones, S. D., Sitch, S., Tans, P.,
3041 Armeth, A., Boden, T. A., Bopp, L., Bozec, Y., Canadell, J. G., Chini, L. P., Chevallier, F., Cosca, C. E., Harris, I.,
3042 Hoppema, M., Houghton, R. A., House, J. I., Jain, A. K., Johannessen, T., Kato, E., Keeling, R. F., Kitidis, V., Klein
3043 Goldewijk, K., Koven, C., Landa, C. S., Landschützer, P., Lenton, A., Lima, I. D., Marland, G., Mathis, J. T., Metzl, N.,
3044 Nojiri, Y., Olsen, A., Ono, T., Peng, S., Peters, W., Pfeil, B., Poulter, B., Raupach, M. R., Regnier, P., Rödenbeck, C., Saito,
3045 S., Salisbury, J. E., Schuster, U., Schwinger, J., Séférian, R., Segsneider, J., Steinhoff, T., Stocker, B. D., Sutton, A. J.,
3046 Takahashi, T., Tilbrook, B., van der Werf, G. R., Viovy, N., Wang, Y.-P., Wanninkhof, R., Wiltshire, A., and Zeng, N.:
3047 Global carbon budget 2014, *Earth Syst. Sci. Data*, 7, 47–85, <https://doi.org/10.5194/essd-7-47-2015>, 2015a.
- 3048 Le Quéré, C., Moriarty, R., Andrew, R. M., Canadell, J. G., Sitch, S., Korsbakken, J. I., Friedlingstein, P., Peters, G. P.,
3049 Andres, R. J., Boden, T. A., Houghton, R. A., House, J. I., Keeling, R. F., Tans, P., Armeth, A., Bakker, D. C. E., Barbero,
3050 L., Bopp, L., Chang, J., Chevallier, F., Chini, L. P., Ciais, P., Fader, M., Feely, R. A., Gkritzalis, T., Harris, I., Hauck, J.,
3051 Ilyina, T., Jain, A. K., Kato, E., Kitidis, V., Klein Goldewijk, K., Koven, C., Landschützer, P., Lauvset, S. K., Lefèvre, N.,
3052 Lenton, A., Lima, I. D., Metzl, N., Millero, F., Munro, D. R., Murata, A., Nabel, J. E. M. S., Nakaoka, S., Nojiri, Y.,
3053 O'Brien, K., Olsen, A., Ono, T., Pérez, F. F., Pfeil, B., Pierrot, D., Poulter, B., Rehder, G., Rödenbeck, C., Saito, S.,
3054 Schuster, U., Schwinger, J., Séférian, R., Steinhoff, T., Stocker, B. D., Sutton, A. J., Takahashi, T., Tilbrook, B., van der
3055 Laan-Luijkx, I. T., van der Werf, G. R., van Heuven, S., Vandemark, D., Viovy, N., Wiltshire, A., Zaehe, S., and Zeng, N.:
3056 Global Carbon Budget 2015, *Earth Syst. Sci. Data*, 7, 349–396, <https://doi.org/10.5194/essd-7-349-2015>, 2015b.
- 3057 Le Quéré, C., Andrew, R. M., Canadell, J. G., Sitch, S., Korsbakken, J. I., Peters, G. P., Manning, A. C., Boden, T. A., Tans,
3058 P. P., Houghton, R. A., Keeling, R. F., Alin, S., Andrews, O. D., Anthoni, P., Barbero, L., Bopp, L., Chevallier, F., Chini, L.
3059 P., Ciais, P., Currie, K., Delire, C., Doney, S. C., Friedlingstein, P., Gkritzalis, T., Harris, I., Hauck, J., Haverd, V.,
3060 Hoppema, M., Klein Goldewijk, K., Jain, A. K., Kato, E., Körtzinger, A., Landschützer, P., Lefèvre, N., Lenton, A., Lienert,
3061 S., Lombardozi, D., Melton, J. R., Metzl, N., Millero, F., Monteiro, P. M. S., Munro, D. R., Nabel, J. E. M. S., Nakaoka, S.,
3062 O'Brien, K., Olsen, A., Omar, A. M., Ono, T., Pierrot, D., Poulter, B., Rödenbeck, C., Salisbury, J., Schuster, U., Schwinger,
3063 J., Séférian, R., Skjelvan, I., Stocker, B. D., Sutton, A. J., Takahashi, T., Tian, H., Tilbrook, B., van der Laan-Luijkx, I. T.,
3064 van der Werf, G. R., Viovy, N., Walker, A. P., Wiltshire, A. J., and Zaehe, S.: Global Carbon Budget 2016, *Earth Syst. Sci.*
3065 *Data*, 8, 605–649, <https://doi.org/10.5194/essd-8-605-2016>, 2016.
- 3066 Le Quéré, C., Andrew, R. M., Friedlingstein, P., Sitch, S., Pongratz, J., Manning, A. C., Korsbakken, J. I., Peters, G. P.,
3067 Canadell, J. G., Jackson, R. B., Boden, T. A., Tans, P. P., Andrews, O. D., Arora, V. K., Bakker, D. C. E., Barbero, L.,
3068 Becker, M., Betts, R. A., Bopp, L., Chevallier, F., Chini, L. P., Ciais, P., Cosca, C. E., Cross, J., Currie, K., Gasser, T.,
3069 Harris, I., Hauck, J., Haverd, V., Houghton, R. A., Hunt, C. W., Hurtt, G., Ilyina, T., Jain, A. K., Kato, E., Kautz, M.,
3070 Keeling, R. F., Klein Goldewijk, K., Körtzinger, A., Landschützer, P., Lefèvre, N., Lenton, A., Lienert, S., Lima, I.,
3071 Lombardozi, D., Metzl, N., Millero, F., Monteiro, P. M. S., Munro, D. R., Nabel, J. E. M. S., Nakaoka, S., Nojiri, Y., Padin,
3072 X. A., Peregón, A., Pfeil, B., Pierrot, D., Poulter, B., Rehder, G., Reimer, J., Rödenbeck, C., Schwinger, J., Séférian, R.,
3073 Skjelvan, I., Stocker, B. D., Tian, H., Tilbrook, B., Tubiello, F. N., van der Laan-Luijkx, I. T., van der Werf, G. R., van
3074 Heuven, S., Viovy, N., Vuichard, N., Walker, A. P., Watson, A. J., Wiltshire, A. J., Zaehe, S., and Zhu, D.: Global Carbon
3075 Budget 2017, *Earth Syst. Sci. Data*, 10, 405–448, <https://doi.org/10.5194/essd-10-405-2018>, 2018a.
- 3076 Le Quéré, C., Andrew, R. M., Friedlingstein, P., Sitch, S., Hauck, J., Pongratz, J., Pickers, P. A., Korsbakken, J. I., Peters, G.
3077 P., Canadell, J. G., Armeth, A., Arora, V. K., Barbero, L., Bastos, A., Bopp, L., Chevallier, F., Chini, L. P., Ciais, P., Doney,
3078 S. C., Gkritzalis, T., Goll, D. S., Harris, I., Haverd, V., Hoffman, F. M., Hoppema, M., Houghton, R. A., Hurtt, G., Ilyina, T.,
3079 Jain, A. K., Johannessen, T., Jones, C. D., Kato, E., Keeling, R. F., Klein Goldewijk, K., Landschützer, P., Lefèvre, N.,

Formatted: Default Paragraph Font, Font colour: Black

Formatted: Normal, Centred, Border: Top: (No border),
Bottom: (No border), Left: (No border), Right: (No border),
Between : (No border), Tab stops: 7.96 cm, Centred + 15.92
cm, Right, Position: Horizontal: Left, Relative to: Column,
Vertical: In line, Relative to: Margin, Wrap Around

Formatted: Font colour: Black

3080 Lienert, S., Liu, Z., Lombardozzi, D., Metzl, N., Munro, D. R., Nabel, J. E. M. S., Nakaoka, S., Neill, C., Olsen, A., Ono, T.,
3081 Patra, P., Peregon, A., Peters, W., Peylin, P., Pfeil, B., Pierrot, D., Poulter, B., Rehder, G., Resplandy, L., Robertson, E.,
3082 Rocher, M., Rödenbeck, C., Schuster, U., Schwinger, J., Séférian, R., Skjelvan, I., Steinhoff, T., Sutton, A., Tans, P. P.,
3083 Tian, H., Tilbrook, B., Tubiello, F. N., van der Laan-Luijkx, I. T., van der Werf, G. R., Viovy, N., Walker, A. P., Wiltshire,
3084 A. J., Wright, R., Zaehle, S., and Zheng, B.: Global Carbon Budget 2018, *Earth Syst. Sci. Data*, 10, 2141–2194,
3085 <https://doi.org/10.5194/essd-10-2141-2018>, 2018b.

3086 Le Quéré, C., Korsbakken, J. I., Wilson, C., Tosun, J., Andrew, R., Andres, R. J., Canadell, J. G., Jordan, A., Peters, G. P.,
3087 and van Vuuren, D. P.: Drivers of declining CO₂ emissions in 18 developed economies, *Nat. Clim. Chang.*, 9, 213–217,
3088 <https://doi.org/10.1038/s41558-019-0419-7>, 2019.

3089 Le Quéré, C., Peters, G. P., Friedlingstein, P., Andrew, R. M., Canadell, J. G., Davis, S. J., Jackson, R. B., and Jones, M. W.:
3090 Fossil CO₂ emissions in the post-COVID-19 era, *Nat. Clim. Chang.*, 11, 197–199, [https://doi.org/10.1038/s41558-021-](https://doi.org/10.1038/s41558-021-01001-0)
3091 [01001-0](https://doi.org/10.1038/s41558-021-01001-0), 2021.

3092 Levitus, S., Antonov, J. I., Boyer, T. P., Baranova, O. K., Garcia, H. E., Locarnini, R. A., Mishonov, A. V., Reagan, J. R.,
3093 Seidov, D., Yarosh, E. S., and Zweng, M. M.: World ocean heat content and thermosteric sea level change (0–2000 m),
3094 1955–2010, *Geophys. Res. Lett.*, 39, <https://doi.org/10.1029/2012GL051106>, 2012.

3095

3096 Li, H., Ilyina, T., Müller, W. A., and Sienz, F.: Decadal predictions of the North Atlantic CO₂ uptake, *Nat. Commun.*, 7,
3097 11076, <https://doi.org/10.1038/ncomms11076>, 2016.

3098

3099 Li, H., Ilyina, T., Müller, W. A., and Landschützer, P.: Predicting the variable ocean carbon sink, *Sci. Adv.*, 5, eaav6471,
3100 <https://doi.org/10.1126/sciadv.aav6471>, 2019.

3101

3102 Li, H., Ilyina, T., Loughran, T., Spring, A., and Pongratz, J.: Reconstructions and predictions of the global carbon budget
3103 with an emission-driven Earth system model, *Earth Syst. Dyn.*, 14, 101–119, <https://doi.org/10.5194/esd-14-101-2023>, 2023.

3104 Li, W., Ciais, P., Peng, S., Yue, C., Wang, Y., Thurner, M., Saatchi, S. S., Armeth, A., Avitabile, V., Carvalhais, N., Harper,
3105 A. B., Kato, E., Koven, C., Liu, Y. Y., Nabel, J. E. M. S., Pan, Y., Pongratz, J., Poulter, B., Pugh, T. A. M., Santoro, M.,
3106 Sitch, S., Stocker, B. D., Viovy, N., Wiltshire, A., Yousefpour, R., and Zaehle, S.: Land-use and land-cover change carbon
3107 emissions between 1901 and 2012 constrained by biomass observations, *Biogeosciences*, 14, 5053–5067,
3108 <https://doi.org/10.5194/bg-14-5053-2017>, 2017.

3109 Liao, E., Resplandy, L., Liu, J., and Bowman, K. W.: Amplification of the Ocean Carbon Sink During El Niños: Role of
3110 Poleward Ekman Transport and Influence on Atmospheric CO₂, *Global Biogeochem. Cy.*, 34, e2020GB006574,
3111 <https://doi.org/10.1029/2020GB006574>, 2020.

3112 Lienert, S. and Joos, F.: A Bayesian ensemble data assimilation to constrain model parameters and land-use carbon
3113 emissions, *Biogeosciences*, 15, 2909–2930, <https://doi.org/10.5194/bg-15-2909-2018>, 2018.

3114 Liu, J., Baskaran, L., Bowman, K., Schimel, D., Bloom, A. A., Parazoo, N. C., Oda, T., Carroll, D., Menemenlis, D., Joiner,
3115 J., Commane, R., Daube, B., Gatti, L. V., McKain, K., Miller, J., Stephens, B. B., Sweeney, C., and Wofsy, S.: Carbon
3116 Monitoring System Flux Net Biosphere Exchange 2020 (CMS-Flux NBE 2020), 13, 299–330, [https://doi.org/10.5194/essd-](https://doi.org/10.5194/essd-13-299-2021)
3117 [13-299-2021](https://doi.org/10.5194/essd-13-299-2021), 2021.

Formatted: Default Paragraph Font, Font colour: Black

Formatted: Normal, Centred, Border: Top: (No border),
Bottom: (No border), Left: (No border), Right: (No border),
Between : (No border), Tab stops: 7.96 cm, Centred + 15.92
cm, Right, Position: Horizontal: Left, Relative to: Column,
Vertical: In line, Relative to: Margin, Wrap Around

Formatted: Font colour: Black

- 3118 Liu, Z., Guan, D., Wei, W., Davis, S. J., Ciais, P., Bai, J., Peng, S., Zhang, Q., Hubacek, K., Marland, G., Andres, R. J.,
 3119 Crawford-Brown, D., Lin, J., Zhao, H., Hong, C., Boden, T. A., Feng, K., Peters, G. P., Xi, F., Liu, J., Li, Y., Zhao, Y.,
 3120 Zeng, N., and He, K.: Reduced carbon emission estimates from fossil fuel combustion and cement production in China,
 3121 *Nature*, 524, 335–338, <https://doi.org/10.1038/nature14677>, 2015.
- 3122 Liu, Z., Zeng, N., Liu, Y., Kalnay, E., Asrar, G., Wu, B., Cai, Q., Liu, D., and Han, P.: Improving the joint estimation of
 3123 CO₂ and surface carbon fluxes using a constrained ensemble Kalman filter in COLA (v1.0), *Geosci. Model Dev.*, 15, 5511–
 3124 5528, <https://doi.org/10.5194/gmd-15-5511-2022>, 2022.
- 3125
- 3126 Lovenduski, N. S., Bonan, G. B., Yeager, S. G., Lindsay, K., and Lombardozzi, D. L.: High predictability of terrestrial
 3127 carbon fluxes from an initialized decadal prediction system, *Environ. Res. Lett.*, 14, 124074, <https://doi.org/10.1088/1748-9326/ab5c55>, 2019a.
- 3128
- 3129
- 3130 Lovenduski, N. S., Yeager, S. G., Lindsay, K., and Long, M. C.: Predicting near-term variability in ocean carbon uptake,
 3131 *Earth Syst. Dyn.*, 10, 45–57, <https://doi.org/10.5194/esd-10-45-2019>, 2019b.
- 3132
- 3133 Lutz, F., Herzfeld, T., Heinke, J., Rolinski, S., Schaphoff, S., von Bloh, W., Stoorvogel, J. J., and Müller, C.: Simulating the
 3134 effect of tillage practices with the global ecosystem model LPJmL (version 5.0-tillage), *Geosci. Model Dev.*, 12, 2419–2440,
<https://doi.org/10.5194/gmd-12-2419-2019>, 2019.
- 3135
- 3136 Ma, L., Hurtt, G., Ott, L., Sahajpal, R., Fisk, J., Lamb, R., Tang, H., Flanagan, S., Chini, L., Chatterjee, A., and Sullivan, J.:
 3137 Global evaluation of the Ecosystem Demography model (ED v3.0), *Geosci. Model Dev.*, 15, 1971–1994,
<https://doi.org/10.5194/gmd-15-1971-2022>, 2022.
- 3138
- 3139 Magi, B. I., Rabin, S., Shevliakova, E., and Pacala, S.: Separating agricultural and non-agricultural fire seasonality at
 3140 regional scales, *Biogeosciences*, 9, 3003–3012, <https://doi.org/10.5194/bg-9-3003-2012>, 2012.
- 3141
- 3142 Masarie, K. A. and Tans, P. P.: Extension and integration of atmospheric carbon dioxide data into a globally consistent
 measurement record, *J. Geophys. Res.*, 100, 11593, <https://doi.org/10.1029/95JD00859>, 1995.
- 3143
- 3144 Mather, A. S.: The transition from deforestation to reforestation in Europe, in: *Agricultural technologies and tropical*
 3145 *deforestation* (eds. Angelsen, A.; Kaimowitz, D.), CABI in association with centre for international Forestry Research, 35–
 52, 2001.
- 3146
- 3147 Mauritsen, T., Bader, J., Becker, T., Behrens, J., Bittner, M., Brokopf, R., Brovkin, V., Claussen, M., Crueger, T., Esch, M.,
 Fast, I., Fiedler, S., Fläschner, D., Gayler, V., Giorgetta, M., Goll, D. S., Haak, H., Hagemann, S., Hedemann, C.,
 3148 Hohenegger, C., Ilyina, T., Jahns, T., Jimenez-de-la-Cuesta, D., Jungclaus, J., Kleinen, T., Kloster, S., Kracher, D., Kinne,
 3149 S., Kleberg, D., Lasslop, G., Kornbluh, L., Marotzke, J., Matei, D., Meraner, K., Mikolajewicz, U., Modali, K., Möbis, B.,
 3150 Müller, W. A., Nabel, J. E. M. S., Nam, C. C. W., Notz, D., Nyawira, S.-S., Paulsen, H., Peters, K., Pincus, R., Pohlmann,
 3151 H., Pongratz, J., Popp, M., Raddatz, T. J., Rast, S., Redler, R., Reick, C. H., Rohrschneider, T., Schemann, V., Schmidt, H.,
 3152 Schnur, R., Schulzweida, U., Six, K. D., Stein, L., Stemmler, I., Stevens, B., von Storch, J.-S., Tian, F., Voigt, A., Vrese, P.,
 3153 Wieners, K.-H., Wilkenskjaeld, S., Winkler, A., and Roeckner, E.: Developments in the MPI-M Earth System Model version
 3154 1.2 (MPI-ESM1.2) and Its Response to Increasing CO₂, *J. Adv. Model Earth Sy.*, 11, 998–1038,
 3155 <https://doi.org/10.1029/2018MS001400>, 2019.

Formatted: Default Paragraph Font, Font colour: Black

Formatted: Normal, Centred, Border: Top: (No border),
 Bottom: (No border), Left: (No border), Right: (No border),
 Between : (No border), Tab stops: 7.96 cm, Centred + 15.92
 cm, Right, Position: Horizontal: Left, Relative to: Column,
 Vertical: In line, Relative to: Margin, Wrap Around

Formatted: Font colour: Black

3156 McGrath, M. J., Luysaert, S., Meyfroidt, P., Kaplan, J. O., Bürgi, M., Chen, Y., Erb, K., Gimmi, U., McInerney, D., Naudts,
3157 K., Otto, J., Pasztor, F., Ryder, J., Schelhaas, M.-J., and Valade, A.: Reconstructing European forest management from 1600
3158 to 2010, *12*, 4291–4316, <https://doi.org/10.5194/bg-12-4291-2015>, 2015.

3159 McKinley, G. A., Fay, A. R., Eddebbbar, Y. A., Gloege, L., and Lovenduski, N. S.: External Forcing Explains Recent
3160 Decadal Variability of the Ocean Carbon Sink, *AGU Advances*, *1*, e2019AV000149,
3161 <https://doi.org/10.1029/2019AV000149>, 2020.

3162 McKinley, G. A., Fay, A. R., Lovenduski, N. S., and Pilcher, D. J.: Natural Variability and Anthropogenic Trends in the
3163 Ocean Carbon Sink, *Annu. Rev. Mar. Sci.*, *9*, 125–150, <https://doi.org/10.1146/annurev-marine-010816-060529>, 2017.

3164 Meiyappan, P., Jain, A. K., and House, J. I.: Increased influence of nitrogen limitation on CO₂ emissions from future land
3165 use and land use change, *Global Biogeochem. Cycles*, *29*, 1524–1548, <https://doi.org/10.1002/2015GB005086>, 2015.

3166 Melton, J. R., Arora, V. K., Wisemig-Cojoc, E., Seiler, C., Fortier, M., Chan, E., and Teckentrup, L.: CLASSIC v1.0: the
3167 open-source community successor to the Canadian Land Surface Scheme (CLASS) and the Canadian Terrestrial Ecosystem
3168 Model (CTEM) – Part 1: Model framework and site-level performance, *Geosci. Model Dev.*, *13*, 2825–2850,
3169 <https://doi.org/10.5194/gmd-13-2825-2020>, 2020.

3170 Mercado, L. M., Bellouin, N., Sitch, S., Boucher, O., Huntingford, C., Wild, M., and Cox, P. M.: Impact of changes in
3171 diffuse radiation on the global land carbon sink, *Nature*, *458*, 1014–1017, <https://doi.org/10.1038/nature07949>, 2009.

3172 Merchant, C. J., Embury, O., Bulgin, C. E., Block, T., Corlett, G. K., Fiedler, E., Good, S. A., Mittaz, J., Rayner, N. A.,
3173 Berry, D., Eastwood, S., Taylor, M., Tsushima, Y., Waterfall, A., Wilson, R., and Donlon, C.: Satellite-based time-series of
3174 sea-surface temperature since 1981 for climate applications, *Sci. Data*, *6*, 223, <https://doi.org/10.1038/s41597-019-0236-x>,
3175 2019.

3176 Moorcroft, P. R., Hurtt, G. C., and Pacala, S. W.: A Method for Scaling Vegetation Dynamics: The Ecosystem Demography
3177 Model (ed), *Ecol. Monogr.*, *71*, 557–586, [https://doi.org/10.1890/0012-9615\(2001\)071\[0557:AMFSVD\]2.0.CO;2](https://doi.org/10.1890/0012-9615(2001)071[0557:AMFSVD]2.0.CO;2), 2001.

3178 Müller, J. D., Gruber, N., Carter, B., Feely, R., Ishii, M., Lange, N., Lauvset, S. K., Murata, A., Olsen, A., Pérez, F. F.,
3179 Sabine, C., Tanhua, T., Wanninkhof, R., and Zhu, D.: Decadal Trends in the Oceanic Storage of Anthropogenic Carbon
3180 From 1994 to 2014, *AGU Adv.*, *4*, e2023AV000875, <https://doi.org/10.1029/2023AV000875>, 2023.

3181 Nakano, H., Tsujino, H., Hirabara, M., Yasuda, T., Motoi, T., Ishii, M., and Yamanaka, G.: Uptake mechanism of
3182 anthropogenic CO₂ in the Kuroshio Extension region in an ocean general circulation model, *J. Oceanogr.*, *67*, 765–783,
3183 <https://doi.org/10.1007/s10872-011-0075-7>, 2011.

3184 NCEP: National Centers for Environmental Prediction. ONI Index. Cold & Warm Episodes by Season, available at:
3185 https://origin.cpc.ncep.noaa.gov/products/analysis_monitoring/ensostuff/ONI_v5.php, last access: 9 November 2023, 2023.

3186 Niu, G.-Y., Yang, Z.-L., Mitchell, K. E., Chen, F., Ek, M. B., Barlage, M., Kumar, A., Manning, K., Niyogi, D., Rosero, E.,
3187 Tewari, M., and Xia, Y.: The community Noah land surface model with multiparameterization options (Noah-MP): 1. Model
3188 description and evaluation with local-scale measurements, *J. Geophys. Res. Atmospheres*, *116*,
3189 <https://doi.org/10.1029/2010JD015139>, 2011.

Deleted: 27 September

Formatted: Default Paragraph Font, Font colour: Black

Formatted: Normal, Centred, Border: Top: (No border), Bottom: (No border), Left: (No border), Right: (No border), Between : (No border), Tab stops: 7.96 cm, Centred + 15.92 cm, Right, Position: Horizontal: Left, Relative to: Column, Vertical: In line, Relative to: Margin, Wrap Around

Formatted: Font colour: Black

- 3191 Niwa, Y., Ishijima, K., Ito, A., and Iida, Y.: Toward a long-term atmospheric CO₂ inversion for elucidating natural carbon
 3192 fluxes: technical notes of NISMON-CO₂ v2021.1, *Prog. Earth Planet Sci.*, 9, 42, [https://doi.org/10.1186/s40645-022-00502-](https://doi.org/10.1186/s40645-022-00502-6)
 3193 6, 2022.
- 3194 Niwa, Y., Langenfelds, R., Krummel, P., Loh, Zoc, Worthy, Doug, Hatakka, Juha, Aalto, Tuula, Ramonet, Michel,
 3195 Delmotte, Marc, Schmidt, Martina, Gheusi, Francois, Mihalopoulos, N., Morgui, J.A., Andrews, Arlyn, Dlugokencky, Ed,
 3196 Lee, John, Sweeney, Colm, Thoning, Kirk, Tans, Pieter, De Wekker, Stephan, Fischer, Marc L., Jaffé, Dan, McKain,
 3197 Kathryn, Viner, Brian, Miller, John B., Karion, Anna, Miller, Charles, Sloop, Christopher D., Saito, Kazuyuki, Aoki, Shuji,
 3198 Morimoto, Shinji, Goto, Daisuke, Steinbacher, Martin, Myhre, Cathrine Lund, Hermanssen, Ove, Stephens, Britton, Keeling,
 3199 Ralph, Afshar, Sara, Paplawsky, Bill, Cox, Adam, Walker, Stephen, Schuldt, Kenneth, Mukai, Hitoshi, Machida, Toshinobu,
 3200 Sasakawa, Motoki, Nomura, Shohei, Ito, Akihiko, Iida, Yosuke, and Jones, Matthew W.: Long-term global CO₂ fluxes
 3201 estimated by NICAM-based Inverse Simulation for Monitoring CO₂ (NISMON-CO₂) (ver.2022.1), National Institute for
 3202 Environmental Studies Japan [dataset], <https://doi.org/10.17595/20201127.001>, 2020.
- 3203 Obermeier, W. A., Nabel, J. E. M. S., Loughran, T., Hartung, K., Bastos, A., Havermann, F., Anthoni, P., Arneth, A., Goll,
 3204 D. S., Lienert, S., Lombardozi, D., Luyssaert, S., McGuire, P. C., Melton, J. R., Poulter, B., Sitch, S., Sullivan, M. O., Tian,
 3205 H., Walker, A. P., Wiltshire, A. J., Zaehle, S., and Pongratz, J.: Modelled land use and land cover change emissions – a
 3206 spatio-temporal comparison of different approaches, *12*, 635–670, <https://doi.org/10.5194/esd-12-635-2021>, 2021.
- 3207 O'Rourke, P. R., Smith, S. J., Mott, A., Ahsan, H., McDuffie, E. E., Crippa, M., Klimont, Z., McDonald, B., Wang, S.,
 3208 Nicholson, M. B., Feng, L., and Hoesly, R. M.: CEDS v_2021_04_21 Release Emission Data,
 3209 <https://doi.org/10.5281/zenodo.4741285>, 2021.
- 3210 O'Sullivan, M., Zhang, Y., Bellouin, N., Harris, I., Mercado, L. M., Sitch, S., Ciaia, P., and Friedlingstein, P.: Aerosol–light
 3211 interactions reduce the carbon budget imbalance, *Environ. Res. Lett.*, 16, 124072, <https://doi.org/10.1088/1748-9326/ac3b77>,
 3212 2021.
- 3213 O'Sullivan, M., Friedlingstein, P., Sitch, S., Anthoni, P., Arneth, A., Arora, V. K., Bastrikov, V., Delire, C., Goll, D. S., Jain,
 3214 A., Kato, E., Kennedy, D., Knauer, J., Lienert, S., Lombardozi, D., McGuire, P. C., Melton, J. R., Nabel, J. E. M. S.,
 3215 Pongratz, J., Poulter, B., Séférian, R., Tian, H., Vuichard, N., Walker, A. P., Yuan, W., Yue, X., and Zaehle, S.: Process-
 3216 oriented analysis of dominant sources of uncertainty in the land carbon sink, *Nat. Commun.*, 13, 4781,
 3217 <https://doi.org/10.1038/s41467-022-32416-8>, 2022.
- 3218 O'Sullivan, M., Spracklen, D. V., Batterman, S. A., Arnold, S. R., Gloor, M., and Buermann, W.: Have Synergies Between
 3219 Nitrogen Deposition and Atmospheric CO₂ Driven the Recent Enhancement of the Terrestrial Carbon Sink?, *Glob.*
 3220 *Biogeochem. Cycles*, 33, 163–180, <https://doi.org/10.1029/2018GB005922>, 2019.
- 3221 Palmer, P. I., Feng, L., Baker, D., Chevallier, F., Bösch, H., and Somkuti, P.: Net carbon emissions from African biosphere
 3222 dominate pan-tropical atmospheric CO₂ signal, *Nat Commun*, 10, 3344, <https://doi.org/10.1038/s41467-019-11097-w>, 2019.
- 3223 Pan, Y., Birdsey, R. A., Fang, J., Houghton, R., Kauppi, P. E., Kurz, W. A., Phillips, O. L., Shvidenko, A., Lewis, S. L.,
 3224 Canadell, J. G., Ciaia, P., Jackson, R. B., Pacala, S. W., McGuire, A. D., Piao, S., Rautiainen, A., Sitch, S., and Hayes, D.: A
 3225 Large and Persistent Carbon Sink in the World's Forests, *Science*, 333, 988–993, <https://doi.org/10.1126/science.1201609>,
 3226 2011.

Formatted: Default Paragraph Font, Font colour: Black

Formatted: Normal, Centred, Border: Top: (No border), Bottom: (No border), Left: (No border), Right: (No border), Between : (No border), Tab stops: 7.96 cm, Centred + 15.92 cm, Right, Position: Horizontal: Left, Relative to: Column, Vertical: In line, Relative to: Margin, Wrap Around

Formatted: Font colour: Black

- 3227 Pendrill, F., Persson, U. M., Godar, J., Kastner, T., Moran, D., Schmidt, S., and Wood, R.: Agricultural and forestry trade
 3228 drives large share of tropical deforestation emissions, *Global Environmental Change*, 56, 1–10,
 3229 <https://doi.org/10.1016/j.gloenvcha.2019.03.002>, 2019.
- 3230 Peters, G. P., Minx, J. C., Weber, C. L., and Edenhofer, O.: Growth in emission transfers via international trade from 1990 to
 3231 2008, *Proceedings of the National Academy of Sciences*, 108, 8903–8908, <https://doi.org/10.1073/pnas.1006388108>, 2011a.
- 3232 Peters, G. P., Marland, G., Le Quéré, C., Boden, T., Canadell, J. G., and Raupach, M. R.: Rapid growth in CO2 emissions
 3233 after the 2008–2009 global financial crisis, *Nature Clim Change*, 2, 2–4, <https://doi.org/10.1038/nclimate1332>, 2012a.
- 3234 Peters, G. P., Andrew, R. M., Boden, T., Canadell, J. G., Ciais, P., Le Quéré, C., Marland, G., Raupach, M. R., and Wilson,
 3235 C.: The challenge to keep global warming below 2 °C, *Nature Clim Change*, 3, 4–6, <https://doi.org/10.1038/nclimate1783>,
 3236 2013.
- 3237 Peters, G. P., Le Quéré, C., Andrew, R. M., Canadell, J. G., Friedlingstein, P., Ilyina, T., Jackson, R. B., Joos, F.,
 3238 Korsbakken, J. I., McKinley, G. A., Sitch, S., and Tans, P.: Towards real-time verification of CO2 emissions, *Nature Clim*
 3239 *Change*, 7, 848–850, <https://doi.org/10.1038/s41558-017-0013-9>, 2017.
- 3240 Peters, G. P., Andrew, R. M., Canadell, J. G., Friedlingstein, P., Jackson, R. B., Korsbakken, J. I., Le Quéré, C., and
 3241 Pregon, A.: Carbon dioxide emissions continue to grow amidst slowly emerging climate policies, *Nat. Clim. Chang.*, 10, 3–
 3242 6, <https://doi.org/10.1038/s41558-019-0659-6>, 2020.
- 3243 Peters, W., Miller, J. B., Whitaker, J., Denning, A. S., Hirsch, A., Krol, M. C., Zupanski, D., Bruhwiler, L., and Tans, P. P.:
 3244 An ensemble data assimilation system to estimate CO2 surface fluxes from atmospheric trace gas observations, *J. Geophys.*
 3245 *Res. Atmospheres*, 110, <https://doi.org/10.1029/2005JD006157>, 2005.
- 3246 Peters W, Woude Avd, Luijckx I, Joetzer E, Lafont S, Loubet B, Herig-Coimbra P, Loustau D, Koren G, Ciais P, Ramonet
 3247 M, Xu Y, Bastos A, Sitch S, Kneuer T, Tubistin D, De Kok R, Botia S. Temperature extremes of 2022 reduced carbon
 3248 uptake by forests in Europe. [doi:10.21203/rs.3.rs-2841861/v1](https://doi.org/10.21203/rs.3.rs-2841861/v1). PPR:PPR653515, 2023.
- 3249 Petrescu, A. M. R., Peters, G. P., Janssens-Maenhout, G., Ciais, P., Tubiello, F. N., Grassi, G., Nabuurs, G.-J., Leip, A.,
 3250 Carmona-Garcia, G., Winiwarter, W., Höglund-Isaksson, L., Günther, D., Solazzo, E., Kiesow, A., Bastos, A., Pongratz, J.,
 3251 Nabel, J. E. M. S., Conchedda, G., Pilli, R., Andrew, R. M., Schelhaas, M.-J., and Dolman, A. J.: European anthropogenic
 3252 AFOLU greenhouse gas emissions: a review and benchmark data, *Earth Syst. Sci. Data*, 12, 961–1001,
 3253 <https://doi.org/10.5194/essd-12-961-2020>, 2020.
- 3254 Pfeil, B., Olsen, A., Bakker, D. C. E., Hankin, S., Koyuk, H., Kozyr, A., Malczyk, J., Manke, A., Metzl, N., Sabine, C. L.,
 3255 Akl, J., Alin, S. R., Bates, N., Bellerby, R. G. J., Borges, A., Boutin, J., Brown, P. J., Cai, W.-J., Chavez, F. P., Chen, A.,
 3256 Cosca, C., Fassbender, A. J., Feely, R. A., González-Dávila, M., Goyet, C., Hales, B., Hardman-Mountford, N., Heinze, C.,
 3257 Hood, M., Hoppema, M., Hunt, C. W., Hydes, D., Ishii, M., Johannessen, T., Jones, S. D., Key, R. M., Körtzinger, A.,
 3258 Landschützer, P., Lauvset, S. K., Lefèvre, N., Lenton, A., Lourantou, A., Merlivat, L., Midorikawa, T., Mintrop, L.,
 3259 Miyazaki, C., Murata, A., Nakadate, A., Nakano, Y., Nakaoka, S., Nojiri, Y., Omar, A. M., Padin, X. A., Park, G.-H.,
 3260 Paterson, K., Perez, F. F., Pierrot, D., Poisson, A., Ríos, A. F., Santana-Casiano, J. M., Salisbury, J., Sarma, V. V. S. S.,
 3261 Schlitzer, R., Schneider, B., Schuster, U., Sieger, R., Skjelvan, I., Steinhoff, T., Suzuki, T., Takahashi, T., Tedesco, K.,
 3262 Telszewski, M., Thomas, H., Tilbrook, B., Tjiputra, J., Vandemark, D., Veness, T., Wanninkhof, R., Watson, A. J., Weiss,

Formatted: Default Paragraph Font, Font colour: Black

Formatted: Normal, Centred, Border: Top: (No border), Bottom: (No border), Left: (No border), Right: (No border), Between : (No border), Tab stops: 7.96 cm, Centred + 15.92 cm, Right, Position: Horizontal: Left, Relative to: Column, Vertical: In line, Relative to: Margin, Wrap Around

Formatted: Font colour: Black

3263 R., Wong, C. S., and Yoshikawa-Inoue, H.: A uniform, quality controlled Surface Ocean CO₂ Atlas (SOCAT), *Earth Syst.*
3264 *Sci. Data*, 5, 125–143, <https://doi.org/10.5194/essd-5-125-2013>, 2013.

3265 Piao, S., Ciais, P., Friedlingstein, P., de Noblet-Ducoudré, N., Cadule, P., Viovy, N., and Wang, T.: Spatiotemporal patterns
3266 of terrestrial carbon cycle during the 20th century, *Global Biogeochem. Cy.*, 23, GB4026,
3267 <https://doi.org/10.1029/2008GB003339>, 2009.

3268 Piao, S., Huang, M., Liu, Z., Wang, X., Ciais, P., Canadell, J. G., Wang, K., Bastos, A., Friedlingstein, P., Houghton, R. A.,
3269 Le Quéré, C., Liu, Y., Myneni, R. B., Peng, S., Pongratz, J., Sitch, S., Yan, T., Wang, Y., Zhu, Z., Wu, D., and Wang, T.:
3270 Lower land-use emissions responsible for increased net land carbon sink during the slow warming period, *Nature Geosci.*, 11,
3271 739–743, <https://doi.org/10.1038/s41561-018-0204-7>, 2018.

3272 Pongratz, J., Reick, C. H., Houghton, R. A., and House, J. I.: Terminology as a key uncertainty in net land use and land
3273 cover change carbon flux estimates, *Earth Syst. Dynam.*, 5, 177–195, <https://doi.org/10.5194/esd-5-177-2014>, 2014.

3274 Poulter, B., [Bastos, A.](#), [Canadell, J.](#), [Ciais, P.](#), [Gruber, N.](#), [Hauck, J.](#), [Jackson, R.](#), [Ishii, M.](#), [Müller, J.](#), [Patra, P.](#), and [Tian, H.](#):
3275 [Inventorying Earth's Land and Ocean Greenhouse Gases. Eos. 103](#), <https://doi.org/10.1029/2022EO179084>, 2022.

3276 [Poulter, B.](#), Frank, D. C., Hodson, E. L., and Zimmermann, N. E.: Impacts of land cover and climate data selection on
3277 understanding terrestrial carbon dynamics and the CO₂ airborne fraction, *Biogeosciences*, 8, 2027–2036,
3278 <https://doi.org/10.5194/bg-8-2027-2011>, 2011.

3279 Poulter, B., Freeborn, P. H., Jolly, W. M., and Varner, J. M.: COVID-19 lockdowns drive decline in active fires in
3280 southeastern United States, *PNAS*, 118, e2105666118, <https://doi.org/10.1073/pnas.2105666118>, 2021.

3281 Powis, C. M., Smith, S. M., Minx, J. C., and Gasser, T.: Quantifying global carbon dioxide removal deployment, *Environ.*
3282 *Res. Lett.*, 18, 024022, <https://doi.org/10.1088/1748-9326/acb450>, 2023.

3283 Prentice, I. C., Farquhar, G. D., Fasham, M. J. R., Goulden, M. L., Heimann, M., Jaramillo, V. J., Khashgi, H. S., Le Quéré,
3284 C., Scholes, R. J., and Wallace, D. W. R.: The Carbon Cycle and Atmospheric Carbon Dioxide, in *Climate Change 2001:*
3285 *The Scientific Basis. Contribution of Working Group I to the Third Assessment Report of the Intergovernmental Panel on*
3286 *Climate Change*, edited by: Houghton, J. T., Ding, Y., Griggs, D. J., Noguér, M., van der Linden, P. J., Dai, X., Maskell, K.,
3287 and Johnson, C. A., Cambridge University Press, Cambridge, United Kingdom and New York, NY, USA, 183–237, ISBN:
3288 978-0521014953, 2001.

3289 Price, J. T. and Warren, R.: Literature Review of the Potential of “Blue Carbon” Activities to Reduce Emissions, available
3290 at: [https://avoid-net-uk.cc.ic.ac.uk/wp-content/uploads/delightful-downloads/2016/03/Literature-review-of-the-potential-of-](https://avoid-net-uk.cc.ic.ac.uk/wp-content/uploads/delightful-downloads/2016/03/Literature-review-of-the-potential-of-blue-carbon-activities-to-reduce-emissions-AVOID2-WPE2.pdf)
3291 [blue-carbon-activities-to-reduce-emissions-AVOID2-WPE2.pdf](https://avoid-net-uk.cc.ic.ac.uk/wp-content/uploads/delightful-downloads/2016/03/Literature-review-of-the-potential-of-blue-carbon-activities-to-reduce-emissions-AVOID2-WPE2.pdf), last access: [9 November](#) 2023, 2016.

3292 Qin, Y., Xiao, X., Wigneron, J.-P., Ciais, P., Brandt, M., Fan, L., Li, X., Crowell, S., Wu, X., Doughty, R., Zhang, Y., Liu,
3293 F., Sitch, S., and Moore, B.: Carbon loss from forest degradation exceeds that from deforestation in the Brazilian Amazon,
3294 *Nat. Clim. Chang.*, 11, 442–448, <https://doi.org/10.1038/s41558-021-01026-5>, 2021.

3295 Randerson, J. T., Chen, Y., van der Werf, G. R., Rogers, B. M., and Morton, D. C.: Global burned area and biomass burning
3296 emissions from small fires: BURNED AREA FROM SMALL FIRES, *J. Geophys. Res. Biogeosciences*, 117, n/a-n/a,
3297 <https://doi.org/10.1029/2012JG002128>, 2012.

Deleted: 27 September

Formatted: Default Paragraph Font, Font colour: Black

Formatted: Normal, Centred, Border: Top: (No border), Bottom: (No border), Left: (No border), Right: (No border), Between : (No border), Tab stops: 7.96 cm, Centred + 15.92 cm, Right, Position: Horizontal: Left, Relative to: Column, Vertical: In line, Relative to: Margin, Wrap Around

Formatted: Font colour: Black

3299 Raupach, M. R., Marland, G., Ciais, P., Le Quere, C., Canadell, J. G., Klepper, G., and Field, C. B.: Global and regional
3300 drivers of accelerating CO₂ emissions, *Proceedings of the National Academy of Sciences*, 104, 10288–10293,
3301 <https://doi.org/10.1073/pnas.0700609104>, 2007.

3302 Regnier, P., Resplandy, L., Najjar, R. G., and Ciais, P.: The land-to-ocean loops of the global carbon cycle, *Nature*, 603,
3303 401–410, <https://doi.org/10.1038/s41586-021-04339-9>, 2022.

3304 Reick, C. H., Gayler, V., Goll, D., Hagemann, S., Heidkamp, M., Nabel, J. E. M. S., Raddatz, T., Roeckner, E., Schnur, R.,
3305 110 and Wilkenskjeld, S.: JSBACH 3 – The land component of the MPI Earth System Model: documentation of version 3.2,
3306 available at: <https://doi.org/10.17617/2.3279802>, 2021.

3307 Remaud, M., Chevallier, F., Cozic, A., Lin, X., and Bousquet, P.: On the impact of recent developments of the LMDz
3308 atmospheric general circulation model on the simulation of CO₂ transport, 11, 4489, [https://doi.org/10.5194/gmd-11-4489-](https://doi.org/10.5194/gmd-11-4489-2018)
3309 2018, 2018.

3310 Resplandy, L., Keeling, R. F., Rödenbeck, C., Stephens, B. B., Khatiwala, S., Rodgers, K. B., Long, M. C., Bopp, L., and
3311 Tans, P. P.: Revision of global carbon fluxes based on a reassessment of oceanic and riverine carbon transport, *Nature*
3312 *Geosci*, 11, 504–509, <https://doi.org/10.1038/s41561-018-0151-3>, 2018.

3313 Rodenbeck, C., Houweling, S., Gloor, M., and Heimann, M.: CO₂ flux history 1982–2001 inferred from atmospheric data
3314 using a global inversion of atmospheric transport, *Atmos Chem Phys*, 3, 1919–1964, 2003.

3315 Rödenbeck, C., Bakker, D. C. E., Metzl, N., Olsen, A., Sabine, C., Cassar, N., Reum, F., Keeling, R. F., and Heimann, M.:
3316 Interannual sea–air CO₂ flux variability from an observation-driven ocean mixed-layer scheme, 11, 4599–4613,
3317 <https://doi.org/10.5194/bg-11-4599-2014>, 2014.

3318 Rödenbeck, C., Zaehle, S., Keeling, R., and Heimann, M.: History of El Niño impacts on the global carbon cycle 1957–
3319 2017: a quantification from atmospheric CO₂ data, 373, 20170303, <https://doi.org/10.1098/rstb.2017.0303>, 2018.

3320 Rödenbeck, C., DeVries, T., Hauck, J., Le Quéré, C., and Keeling, R. F.: Data-based estimates of interannual sea–air CO₂
3321 flux variations 1957–2020 and their relation to environmental drivers, *Biogeosciences*, 19, 2627–2652,
3322 <https://doi.org/10.5194/bg-19-2627-2022>, 2022.

3323 Rosan, T. M., Klein Goldewijk, K., Ganzenmüller, R., O’Sullivan, M., Pongratz, J., Mercado, L. M., Aragao, L. E. O. C.,
3324 Heinrich, V., Randow, C. V., Wiltshire, A., Tubiello, F. N., Bastos, A., Friedlingstein, P., and Sitch, S.: A multi-data
3325 assessment of land use and land cover emissions from Brazil during 2000–2019, *Environ. Res. Lett.*, 16, 074004,
3326 <https://doi.org/10.1088/1748-9326/ac08c3>, 2021.

3327 Sakamoto, K., H. Nakano, S. Urakawa, T. Toyoda, Y. Kawakami, H. Tsujino, G. Yamanaka, 2023: Reference manual for the
3328 Meteorological Research Institute Community Ocean Model version 5 (MRI.COMv5), Technical Reports of the
3329 Meteorological Research Institute, No.87, <https://doi.org/10.11483/mritechrepo.87>.

3330 Sarma, V. V. S. S., Sridevi, B., Metzl, N., Patra, P. K., Lachkar, Z., Chakraborty, K., Goyet, C., Levy, M., Mehari, M., and
3331 Chandra, N.: Air-Sea Fluxes of CO₂ in the Indian Ocean Between 1985 and 2018: A Synthesis Based on Observation-Based
3332 Surface CO₂, Hindcast and Atmospheric Inversion Models, *Glob. Biogeochem. Cycles*, 37, e2023GB007694,
3333 <https://doi.org/10.1029/2023GB007694>, 2023.

Formatted: Default Paragraph Font, Font colour: Black

Formatted: Normal, Centred, Border: Top: (No border), Bottom: (No border), Left: (No border), Right: (No border), Between : (No border), Tab stops: 7.96 cm, Centred + 15.92 cm, Right, Position: Horizontal: Left, Relative to: Column, Vertical: In line, Relative to: Margin, Wrap Around

Formatted: Font colour: Black

- 3334 Schaphoff, S., von Bloh, W., Rammig, A., Thonicke, K., Biemans, H., Forkel, M., Gerten, D., Heinke, J., Jägermeyr, J.,
 3335 Knauer, J., Langerwisch, F., Lucht, W., Müller, C., Rolinski, S., and Waha, K.: LPJmL4 – a dynamic global vegetation
 3336 model with managed land – Part I: Model description, *Geosci. Model Dev.*, 11, 1343–1375, [https://doi.org/10.5194/gmd-11-](https://doi.org/10.5194/gmd-11-1343-2018)
 3337 1343-2018, 2018.
- 3338 Schimel, D., Alves, D., Enting, I. G., Heimann, M., Joos, F., Raynaud, D., Wigley, T., Prater, M., Derwent, R., Ehhalt, D.,
 3339 Fraser, P., Sanhueza, E., Zhou, X., Jonas, P., Charlson, R., Rodhe, H., Sadasivan, S., Shine, K. P., Fouquart, Y.,
 3340 Ramaswamy, V., Solomon, S., Srinivasan, J., Albritton, D., Derwent, R., Isaksen, I., Lal, M., and Wuebbles, D.: Radiative
 3341 Forcing of Climate Change, in: *Climate Change 1995: The Science of Climate Change, Contribution of Working Group I to*
 3342 *the Second Assessment Report of the Intergovernmental Panel on Climate Change* [Houghton, J. T., Meira Rillo, L. G.,
 3343 Callander, B. A., Harris, N., Kattenberg, A., and Maskell, K. (eds.)], Cambridge University Press, Cambridge, United
 3344 Kingdom and New York, NY, USA, ISBN: 978-0521559621, 1995.
- 3345 Schimel, D., Stephens, B. B., and Fisher, J. B.: Effect of increasing CO₂ on the terrestrial carbon cycle, *Proc Natl Acad Sci*
 3346 *USA*, 112, 436–441, <https://doi.org/10.1073/pnas.1407302112>, 2015.
- 3347 Schuh, A. E., Jacobson, A. R., Basu, S., Weir, B., Baker, D., Bowman, K., Chevallier, F., Crowell, S., Davis, K. J., Deng, F.,
 3348 Denning, S., Feng, L., Jones, D., Liu, J., and Palmer, P. I.: Quantifying the Impact of Atmospheric Transport Uncertainty on
 3349 CO₂ Surface Flux Estimates, *Global Biogeochem. Cycles*, 33, 484–500, <https://doi.org/10.1029/2018GB006086>, 2019.
- 3350 Schwinger, J., Goris, N., Tjiputra, J. F., Kriest, I., Bentsen, M., Bethke, I., Ilicak, M., Assmann, K. M., and Heinze, C.:
 3351 Evaluation of NorESM-OC (versions 1 and 1.2), the ocean carbon-cycle stand-alone configuration of the Norwegian Earth
 3352 System Model (NorESM1), *Geosci. Model Dev.*, 9, 2589–2622, <https://doi.org/10.5194/gmd-9-2589-2016>, 2016.
- 3353 Schwingshackl, C., Obermeier, W. A., Bultan, S., Grassi, G., Canadell, J. G., Friedlingstein, P., Gasser, T., Houghton, R. A.,
 3354 Kurz, W. A., Sitch, S., and Pongratz, J.: Differences in land-based mitigation estimates reconciled by separating natural and
 3355 land-use CO₂ fluxes at the country level, *One Earth*, 5, 1367–1376, <https://doi.org/10.1016/j.oneear.2022.11.009>, 2022.
- 3356 Séférian, R., Nabat, P., Michou, M., Saint-Martin, D., Voldoire, A., Colin, J., Decharme, B., Delire, C., Berthet, S.,
 3357 Chevallier, M., Sénési, S., Franchisteguy, L., Vial, J., Mallet, M., Joetzjer, E., Geoffroy, O., Guérémy, J.-F., Moine, M.-P.,
 3358 Msadek, R., Ribes, A., Rocher, M., Rochrig, R., Salas-y-Méla, D., Sanchez, E., Terray, L., Valcke, S., Waldman, R.,
 3359 Aumont, O., Bopp, L., Deshayes, J., Éthé, C., and Madec, G.: Evaluation of CNRM Earth System Model, CNRM-ESM2-1:
 3360 Role of Earth System Processes in Present-Day and Future Climate, *Journal of Advances in Modeling Earth Systems*, 11,
 3361 4182–4227, <https://doi.org/10.1029/2019MS001791>, 2019.
- 3362 Seiler, C., Melton, J. R., Arora, V. K., Sitch, S., Friedlingstein, P., Anthoni, P., Goll, D., Jain, A. K., Joetzjer, E., Lienert, S.,
 3363 Lombardozi, D., Luyssaert, S., Nabel, J. E. M. S., Tian, H., Vuichard, N., Walker, A. P., Yuan, W., and Zaehle, S.: Are
 3364 Terrestrial Biosphere Models Fit for Simulating the Global Land Carbon Sink?, *J. Adv. Model. Earth Syst.*, 14,
 3365 e2021MS002946, <https://doi.org/10.1029/2021MS002946>, 2022.
- 3366 Sellar, A. A., Jones, C. G., Mulcahy, J. P., Tang, Y., Yool, A., Wiltshire, A., O'Connor, F. M., Stringer, M., Hill, R.,
 3367 Palmieri, J., Woodward, S., Mora, L., Kuhlbrodt, T., Rumbold, S. T., Kelley, D. I., Ellis, R., Johnson, C. E., Walton, J.,
 3368 Abraham, N. L., Andrews, M. B., Andrews, T., Archibald, A. T., Berthou, S., Burke, E., Blockley, E., Carslaw, K., Dalvi,
 3369 M., Edwards, J., Folberth, G. A., Gedney, N., Griffiths, P. T., Harper, A. B., Hendry, M. A., Hewitt, A. J., Johnson, B.,
 3370 Jones, A., Jones, C. D., Keeble, J., Liddicoat, S., Morgenstern, O., Parker, R. J., Predoi, V., Robertson, E., Siahhaan, A.,

Formatted: Default Paragraph Font, Font colour: Black

Formatted: Normal, Centred, Border: Top: (No border), Bottom: (No border), Left: (No border), Right: (No border), Between : (No border), Tab stops: 7.96 cm, Centred + 15.92 cm, Right, Position: Horizontal: Left, Relative to: Column, Vertical: In line, Relative to: Margin, Wrap Around

Formatted: Font colour: Black

- 3371 Smith, R. S., Swaminathan, R., Woodhouse, M. T., Zeng, G., and Zerroukat, M.: UKESM1: Description and Evaluation of
3372 the U.K. Earth System Model, *J. Adv. Model. Earth Syst.*, 11, 4513–4558, <https://doi.org/10.1029/2019MS001739>, 2019.
- 3373 Shu, S., Jain, A. K., Koven, C. D., and Mishra, U.: Estimation of Permafrost SOC Stock and Turnover Time Using a Land
3374 Surface Model With Vertical Heterogeneity of Permafrost Soils, *Global Biogeochem. Cy.*, 34, e2020GB006585,
3375 <https://doi.org/10.1029/2020GB006585>, 2020.
- 3376 Shutler, J. D., Land, P. E., Piolle, J.-F., Woolf, D. K., Goddijn-Murphy, L., Paul, F., Girard-Arduin, F., Chapron, B., and
3377 Donlon, C. J.: FluxEngine: A Flexible Processing System for Calculating Atmosphere–Ocean Carbon Dioxide Gas Fluxes
3378 and Climatologies, *J. Atmospheric Ocean. Technol.*, 33, 741–756, <https://doi.org/10.1175/JTECH-D-14-00204.1>, 2016.
- 3379 Sitch, S., Huntingford, C., Gedney, N., Levy, P. E., Lomas, M., Piao, S. L., Betts, R., Ciais, P., Cox, P., Friedlingstein, P.,
3380 Jones, C. D., Prentice, I. C., and Woodward, F. I.: Evaluation of the terrestrial carbon cycle, future plant geography and
3381 climate-carbon cycle feedbacks using five Dynamic Global Vegetation Models (DGVMs): Uncertainty In Land Carbon
3382 Cycle Feedbacks, *Glob. Change Biol.*, 14, 2015–2039, <https://doi.org/10.1111/j.1365-2486.2008.01626.x>, 2008.
- 3383 Smallman, T. L., Milodowski, D. T., Neto, E. S., Koren, G., Ometto, J., and Williams, M.: Parameter uncertainty dominates
3384 C-cycle forecast errors over most of Brazil for the 21st century, *Earth Syst. Dyn.*, 12, 1191–1237,
3385 <https://doi.org/10.5194/esd-12-1191-2021>, 2021.
- 3386 Smith, B., Wårlind, D., Arneth, A., Hickler, T., Leadley, P., Siltberg, J., and Zaehle, S.: Implications of incorporating N
3387 cycling and N limitations on primary production in an individual-based dynamic vegetation model, *Biogeosciences*, 11,
3388 2027–2054, <https://doi.org/10.5194/bg-11-2027-2014>, 2014.
- 3389 Smith, S., Geden, O., Nemet, G., Gidden, M., Lamb, W., Powis, C., Bellamy, R., Callaghan, M., Cowie, A., Cox, E. and
3390 Fuss, S., 2023. The State of Carbon Dioxide Removal–1st Edition, <http://dx.doi.org/10.17605/OSF.IO/W3B4Z>, 2023.
- 3391 Sospedra-Alfonso, R., Merryfield, W. J., Boer, G. J., Kharin, V. V., Lee, W.-S., Seiler, C., and Christian, J. R.: Decadal
3392 climate predictions with the Canadian Earth System Model version 5 (CanESM5), *Geosci. Model Dev.*, 14, 6863–6891,
3393 <https://doi.org/10.5194/gmd-14-6863-2021>, 2021.
- 3394 Stephens, B. B., Gurney, K. R., Tans, P. P., Sweeney, C., Peters, W., Bruhwiler, L., Ciais, P., Ramonet, M., Bousquet, P.,
3395 Nakazawa, T., Aoki, S., Machida, T., Inoue, G., Vinnichenko, N., Lloyd, J., Jordan, A., Heimann, M., Shibistova, O.,
3396 Langenfelds, R. L., Steele, L. P., Francey, R. J., and Denning, A. S.: Weak Northern and Strong Tropical Land Carbon
3397 Uptake from Vertical Profiles of Atmospheric CO₂, *Science*, 316, 1732–1735, <https://doi.org/10.1126/science.1137004>,
3398 2007.
- 3399 Stephens, B. B., Keeling, R. F., Heimann, M., Six, K. D., Murnane, R., and Caldeira, K.: Testing global ocean carbon cycle
3400 models using measurements of atmospheric O₂ and CO₂ concentration, *Glob. Biogeochem. Cycles*, 12, 213–230,
3401 <https://doi.org/10.1029/97GB03500>, 1998.
- 3402 Stocker, T., Qin, D., and Plattner, G.-K.: Climate Change 2013: The Physical Science Basis. Contribution of Working Group
3403 I to the Fifth Assessment Report of the Intergovernmental Panel on Climate Change [Intergovernmental Panel on Climate
3404 Change (eds.)], Cambridge University Press, Cambridge, ISBN: 9789291691388, 2013.

Formatted: Default Paragraph Font, Font colour: Black

Formatted: Normal, Centred, Border: Top: (No border),
Bottom: (No border), Left: (No border), Right: (No border),
Between : (No border), Tab stops: 7.96 cm, Centred + 15.92
cm, Right, Position: Horizontal: Left, Relative to: Column,
Vertical: In line, Relative to: Margin, Wrap Around

Formatted: Font colour: Black

3405 Swart, N. C., Cole, J. N. S., Kharin, V. V., Lazare, M., Scinocca, J. F., Gillett, N. P., Anstey, J., Arora, V., Christian, J. R.,
3406 Hanna, S., Jiao, Y., Lee, W. G., Majaess, F., Saenko, O. A., Seiler, C., Seinen, C., Shao, A., Sigmund, M., Solheim, L., von
3407 Salzen, K., Yang, D., and Winter, B.: The Canadian Earth System Model version 5 (CanESM5.0.3), *Geosci. Model Dev.*, 12,
3408 4823–4873, <https://doi.org/10.5194/gmd-12-4823-2019>, 2019.

3409 SX Coal: Monthly coal consumption estimates, <http://www.sxcoal.com/>, last access: 9 November 2023, 2022.

Deleted: 27 September

3410 Takahashi, T., Sutherland, S. C., Wanninkhof, R., Sweeney, C., Feely, R. A., Chipman, D. W., Hales, B., Friederich, G.,
3411 Chavez, F., Sabine, C., Watson, A., Bakker, D. C. E., Schuster, U., Metzl, N., Yoshikawa-Inoue, H., Ishii, M., Midorikawa,
3412 T., Nojiri, Y., Körtzinger, A., Steinhoff, T., Hoppema, M., Olafsson, J., Arnarson, T. S., Tilbrook, B., Johannessen, T.,
3413 Olsen, A., Bellerby, R., Wong, C. S., Delille, B., Bates, N. R., and de Baar, H. J. W.: Climatological mean and decadal
3414 change in surface ocean pCO₂, and net sea–air CO₂ flux over the global oceans, *Deep Sea Research Part II: Topical Studies*
3415 *in Oceanography*, 56, 554–577, <https://doi.org/10.1016/j.dsr2.2008.12.009>, 2009.

3416 Terhaar, J., Frölicher, T. L., and Joos, F.: Southern Ocean anthropogenic carbon sink constrained by sea surface salinity, *Sci.*
3417 *Adv.*, 7, eabd5964, <https://doi.org/10.1126/sciadv.abd5964>, 2021.

3418 Terhaar, J., Frölicher, T. L., and Joos, F.: Observation-constrained estimates of the global ocean carbon sink from Earth
3419 system models, *Biogeosciences*, 19, 4431–4457, <https://doi.org/10.5194/bg-19-4431-2022>, 2022.

3420 Tian, H., Xu, X., Lu, C., Liu, M., Ren, W., Chen, G., Melillo, J., and Liu, J.: Net exchanges of CO₂, CH₄, and N₂O between
3421 China's terrestrial ecosystems and the atmosphere and their contributions to global climate warming, *J. Geophys. Res.*
3422 *Biogeosciences*, 116, G02011, <https://doi.org/10.1029/2010JG001393>, 2011.

3423 Tian, H., Chen, G., Lu, C., Xu, X., Hayes, D. J., Ren, W., Pan, S., Huntzinger, D. N., and Wofsy, S. C.: North American
3424 terrestrial CO₂ uptake largely offset by CH₄ and N₂O emissions: toward a full accounting of the greenhouse gas budget,
3425 *Climatic Change*, 129, 413–426, <https://doi.org/10.1007/s10584-014-1072-9>, 2015.

3426 Tubiello, F. N., Conchedda, G., Wanner, N., Federici, S., Rossi, S., and Grassi, G.: Carbon emissions and removals from
3427 forests: new estimates, 1990–2020, *Earth Syst. Sci. Data*, 13, 1681–1691, <https://doi.org/10.5194/essd-13-1681-2021>, 2021.

3428 Tuck, C.: 2022 Mineral Commodity Summary: Iron Ore, Tech. rep., U.S. Geological Survey,
3429 <https://pubs.usgs.gov/periodicals/mcs2022/mcs2022-iron-ore.pdf>, 2022.

3430 UNFCCC: Synthesis report for the technical assessment component of the first global stocktake, available at:
3431 <https://unfccc.int/documents/461466>, last access: 9 November 2023, 2022.

Deleted: 27 September

3432 Urakawa, L. S., Tsujino, H., Nakano, H., Sakamoto, K., Yamanaka, G., and Toyoda, T.: The sensitivity of a depth-
3433 coordinate model to diapycnal mixing induced by practical implementations of the isopycnal tracer diffusion scheme, *Ocean*
3434 *Model.*, 154, 101693, <https://doi.org/10.1016/j.ocemod.2020.101693>, 2020.

3435 Vale, M. M., Berenguer, E., Argollo de Menezes, M., Viveiros de Castro, E. B., Pugliese de Siqueira, L., and Portela, R. de
3436 C. Q.: The COVID-19 pandemic as an opportunity to weaken environmental protection in Brazil, *Biological Conservation*,
3437 255, 108994, <https://doi.org/10.1016/j.biocon.2021.108994>, 2021.

Formatted: Default Paragraph Font, Font colour: Black

Formatted: Normal, Centred, Border: Top: (No border),
Bottom: (No border), Left: (No border), Right: (No border),
Between : (No border), Tab stops: 7.96 cm, Centred + 15.92
cm, Right, Position: Horizontal: Left, Relative to: Column,
Vertical: In line, Relative to: Margin, Wrap Around

Formatted: Font colour: Black

3440 van der Laan-Luijkx, I. T., van der Velde, I. R., van der Veen, E., Tsuruta, A., Stanislawska, K., Babenhausheide, A.,
3441 Zhang, H. F., Liu, Y., He, W., Chen, H., Masarie, K. A., Krol, M. C., and Peters, W.: The CarbonTracker Data Assimilation
3442 Shell (CTDAS) v1.0: implementation and global carbon balance 2001–2015, *Geosci. Model Dev.*, 10, 2785–2800,
3443 <https://doi.org/10.5194/gmd-10-2785-2017>, 2017.

3444 van der Velde, I. R., van der Werf, G. R., Houweling, S., Maasakkers, J. D., Borsdorff, T., Landgraf, J., Tol, P., van
3445 Kempen, T. A., van Hees, R., Hoogeveen, R., Veeffkind, J. P., and Aben, I.: Vast CO₂ release from Australian fires in 2019–
3446 2020 constrained by satellite, *Nature*, 597, 366–369, <https://doi.org/10.1038/s41586-021-03712-y>, 2021.

3447 van der Werf, G. R., Randerson, J. T., Giglio, L., Collatz, G. J., Mu, M., Kasibhatla, P. S., Morton, D. C., DeFries, R. S., Jin,
3448 Y., and van Leeuwen, T. T.: Global fire emissions and the contribution of deforestation, savanna, forest, agricultural, and
3449 peat fires (1997–2009), *Atmospheric Chem. Phys.*, 10, 11707–11735, <https://doi.org/10.5194/acp-10-11707-2010>, 2010.

3450 van der Werf, G. R., Randerson, J. T., Giglio, L., van Leeuwen, T. T., Chen, Y., Rogers, B. M., Mu, M., van Marle, M. J. E.,
3451 Morton, D. C., Collatz, G. J., Yokelson, R. J., and Kasibhatla, P. S.: Global fire emissions estimates during 1997–2016,
3452 *Earth Syst. Sci. Data*, 9, 697–720, <https://doi.org/10.5194/essd-9-697-2017>, 2017.

3453 van Wees, D., van der Werf, G. R., Randerson, J. T., Andela, N., Chen, Y., and Morton, D. C.: The role of fire in global
3454 forest loss dynamics, *Glob. Change Biol.*, 27, 2377–2391, <https://doi.org/10.1111/gcb.15591>, 2021.

3455 von Bloh, W., Schaphoff, S., Müller, C., Rolinski, S., Waha, K., and Zaehle, S.: Implementing the nitrogen cycle into the
3456 dynamic global vegetation, hydrology, and crop growth model LPJmL (version 5.0), *Geosci. Model Dev.*, 11, 2789–2812,
3457 <https://doi.org/10.5194/gmd-11-2789-2018>, 2018.

3458 Vaittinada Ayar, P., Bopp, L., Christian, J. R., Ilyina, T., Krasting, J. P., Séférian, R., Tsujino, H., Watanabe, M., Yool, A.,
3459 and Tjiputra, J.: Contrasting projections of the ENSO-driven CO₂ flux variability in the equatorial Pacific under high-
3460 warming scenario, *Earth Syst. Dynam.*, 13, 1097–1118, <https://doi.org/10.5194/esd-13-1097-2022>, 2022.

3461 Vuichard, N., Messina, P., Luyssaert, S., Guenet, B., Zaehle, S., Ghattas, J., Bastrikov, V., and Peylin, P.: Accounting for
3462 carbon and nitrogen interactions in the global terrestrial ecosystem model ORCHIDEE (trunk version, rev 4999): multi-scale
3463 evaluation of gross primary production, *Geosci. Model Dev.*, 12, 4751–4779, <https://doi.org/10.5194/gmd-12-4751-2019>,
3464 2019.

3465 Walker, A. P., Quaife, T., Bodegom, P. M., De Kauwe, M. G., Keenan, T. F., Joiner, J., Lomas, M. R., MacBean, N., Xu, C.,
3466 Yang, X., and Woodward, F. I.: The impact of alternative trait-scaling hypotheses for the maximum photosynthetic
3467 carboxylation rate (V_{cmax}) on global gross primary production, *New Phytol.*, 215, 1370–1386,
3468 <https://doi.org/10.1111/nph.14623>, 2017.

3469 Walker, A. P., De Kauwe, M. G., Bastos, A., Belmecheri, S., Georgiou, K., Keeling, R. F., McMahon, S. M., Medlyn, B. E.,
3470 Moore, D. J. P., Norby, R. J., Zaehle, S., Anderson-Teixeira, K. J., Battipaglia, G., Brienens, R. J. W., Cabugao, K. G.,
3471 Cailleret, M., Campbell, E., Canadell, J. G., Ciais, P., Craig, M. E., Ellsworth, D. S., Farquhar, G. D., Faticchi, S., Fisher, J.
3472 B., Frank, D. C., Graven, H., Gu, L., Haverd, V., Heilman, K., Heimann, M., Hungate, B. A., Iversen, C. M., Joos, F., Jiang,
3473 M., Keenan, T. F., Knauer, J., Körner, C., Leshyk, V. O., Leuzinger, S., Liu, Y., MacBean, N., Malhi, Y., McVicar, T. R.,
3474 Penuelas, J., Pongratz, J., Powell, A. S., Riutta, T., Sabot, M. E. B., Schleucher, J., Sitch, S., Smith, W. K., Sulman, B.,
3475 Taylor, B., Terrer, C., Torn, M. S., Treseder, K. K., Trugman, A. T., Trumbore, S. E., van Mantgem, P. J., Voelker, S. L.,

Formatted: Default Paragraph Font, Font colour: Black

Formatted: Normal, Centred, Border: Top: (No border),
Bottom: (No border), Left: (No border), Right: (No border),
Between : (No border), Tab stops: 7.96 cm, Centred + 15.92
cm, Right, Position: Horizontal: Left, Relative to: Column,
Vertical: In line, Relative to: Margin, Wrap Around

Formatted: Font colour: Black

- 3476 Whelan, M. E., and Zuidema, P. A.: Integrating the evidence for a terrestrial carbon sink caused by increasing atmospheric
3477 CO₂, *New Phytol.*, 229, 2413–2445, <https://doi.org/10.1111/nph.16866>, 2021.
- 3478 Watanabe, M., Tatebe, H., Koyama, H., Hajima, T., Watanabe, M., and Kawamiya, M.: Importance of El Niño
3479 reproducibility for reconstructing historical CO₂ flux variations in the equatorial Pacific, *Ocean Sci.*, 16, 1431–1442,
3480 <https://doi.org/10.5194/os-16-1431-2020>, 2020.
- 3481 Watson, A. J., Schuster, U., Shutler, J. D., Holding, T., Ashton, I. G. C., Landschützer, P., Woolf, D. K., and Goddijn-
3482 Murphy, L.: Revised estimates of ocean-atmosphere CO₂ flux are consistent with ocean carbon inventory, *Nat Commun*, 11,
3483 4422, <https://doi.org/10.1038/s41467-020-18203-3>, 2020.
- 3484 Watson, R. T., Rohde, H., Oeschger, H., and Siegenthaler, U.: Greenhouse Gases and Aerosols, in: *Climate Change: The*
3485 *IPCC Scientific Assessment. Intergovernmental Panel on Climate Change (IPCC)*, edited by: Houghton, J. T., Jenkins, G. J.,
3486 and Ephraums, J. J., Cambridge University Press, Cambridge, ISBN: 978-0521403603, 1990.
- 3487 Wenzel, S., Cox, P. M., Eyring, V., and Friedlingstein, P.: Projected land photosynthesis constrained by changes in the
3488 seasonal cycle of atmospheric CO₂, *Nature*, 538, 499–501, <https://doi.org/10.1038/nature19772>, 2016.
- 3489 Wilkenskjeld, S., Kloster, S., Pongratz, J., Raddatz, T., and Reick, C. H.: Comparing the influence of net and gross
3490 anthropogenic land-use and land-cover changes on the carbon cycle in the MPI-ESM, *Biogeosciences*, 11, 4817–4828,
3491 <https://doi.org/10.5194/bg-11-4817-2014>, 2014.
- 3492 Wiltshire, A. J., Burke, E. J., Chadburn, S. E., Jones, C. D., Cox, P. M., Davies-Barnard, T., Friedlingstein, P., Harper, A. B.,
3493 Liddicoat, S., Sitch, S., and Zaehle, S.: JULES-CN: a coupled terrestrial carbon–nitrogen scheme (JULES vn5.1), 14, 2161–
3494 2186, <https://doi.org/10.5194/gmd-14-2161-2021>, 2021.
- 3495 Winkler, K., Yang, H., Ganzenmüller, R., Fuchs, R., Ceccherini, G., Duveiller, G., Grassi, G., Pongratz, J., Bastos, A.,
3496 Shvidenko, A., Araza, A., Herold, M., Wigneron, J.-P., and Ciais, P.: Changes in land use and management led to a decline
3497 in Eastern Europe’s terrestrial carbon sink, *Commun. Earth Environ.*, 4, 1–14, <https://doi.org/10.1038/s43247-023-00893-4>,
3498 2023.
- 3499 Woodward, F. I. and Lomas, M. R.: Vegetation dynamics – simulating responses to climatic change, *Biol. Rev.*, 79, 643–
3500 670, <https://doi.org/10.1017/S1464793103006419>, 2004.
- 3501 Wright, R. M., Le Quéré, C., Buitenhuis, E., Pitois, S., and Gibbons, M. J.: Role of jellyfish in the plankton ecosystem
3502 revealed using a global ocean biogeochemical model, 18, 1291–1320, <https://doi.org/10.5194/bg-18-1291-2021>, 2021.
- 3503 Wunder, S., Kaimowitz, D., Jensen, S., and Feder, S.: Coronavirus, macroeconomy, and forests: What likely impacts?, *For.*
3504 *Policy Econ.*, 131, 102536, <https://doi.org/10.1016/j.forpol.2021.102536>, 2021.
- 3505 Xi, F., Davis, S. J., Ciais, P., Crawford-Brown, D., Guan, D., Pade, C., Shi, T., Syddall, M., Lv, J., Ji, L., Bing, L., Wang, J.,
3506 Wei, W., Yang, K.-H., Lagerblad, B., Galan, I., Andrade, C., Zhang, Y., and Liu, Z.: Substantial global carbon uptake by
3507 cement carbonation, *Nature Geosci*, 9, 880–883, <https://doi.org/10.1038/ngeo2840>, 2016.
- 3508 Xia, J., Chen, Y., Liang, S., Liu, D., and Yuan, W.: Global simulations of carbon allocation coefficients for deciduous
3509 vegetation types, *Tellus B*, 67, 28016, <https://doi.org/10.3402/tellusb.v67.28016>, 2015.

Formatted: Default Paragraph Font, Font colour: Black

Formatted: Normal, Centred, Border: Top: (No border), Bottom: (No border), Left: (No border), Right: (No border), Between : (No border), Tab stops: 7.96 cm, Centred + 15.92 cm, Right, Position: Horizontal: Left, Relative to: Column, Vertical: In line, Relative to: Margin, Wrap Around

Formatted: Font colour: Black

3510 Yang, D., Liu, Y., Feng, L., Wang, J., Yao, L., Cai, Z., Zhu, S., Lu, N., and Lyu, D.: The First Global Carbon Dioxide Flux
3511 Map Derived from TanSat Measurements, *Adv. Atmospheric Sci.*, 38, 1433–1443, [https://doi.org/10.1007/s00376-021-](https://doi.org/10.1007/s00376-021-1179-7)
3512 1179-7, 2021.

3513 Yang, X., Thornton, P., Ricciuto, D., Wang, Y., and Hoffman, F.: Global evaluation of terrestrial biogeochemistry in the
3514 Energy Exascale Earth System Model (E3SM) and the role of the phosphorus cycle in the historical terrestrial carbon
3515 balance, *Biogeosciences*, 20, 2813–2836, <https://doi.org/10.5194/bg-20-2813-2023>, 2023.

3516 Yu, Z., Ciais, P., Piao, S., Houghton, R. A., Lu, C., Tian, H., Agathokleous, E., Kattel, G. R., Sitch, S., Goll, D., Yue, X.,
3517 Walker, A., Friedlingstein, P., Jain, A. K., Liu, S., and Zhou, G.: Forest expansion dominates China’s land carbon sink since
3518 1980, *Nat. Commun.*, 13, 5374, <https://doi.org/10.1038/s41467-022-32961-2>, 2022.

3519 Yue, X. and Unger, N.: The Yale Interactive terrestrial Biosphere model version 1.0: description, evaluation and
3520 implementation into NASA GISS ModelE2, *Geosci. Model Dev.*, 8, 2399–2417, <https://doi.org/10.5194/gmd-8-2399-2015>,
3521 2015.

3522 Yuan, W., Liu, D., Dong, W., Liu, S., Zhou, G., Yu, G., Zhao, T., Feng, J., Ma, Z., Chen, J., Chen, Y., Chen, S., Han, S.,
3523 Huang, J., Li, L., Liu, H., Liu, S., Ma, M., Wang, Y., Xia, J., Xu, W., Zhang, Q., Zhao, X., and Zhao, L.: Multiyear
3524 precipitation reduction strongly decreases carbon uptake over northern China, *J. Geophys. Res.-Biogeo.*, 119, 881–896,
3525 <https://doi.org/10.1002/2014JG002608>, 2014.

3526 Yue, C., Ciais, P., Zhu, D., Wang, T., Peng, S. S., and Piao, S. L.: How have past fire disturbances contributed to the current
3527 carbon balance of boreal ecosystems?, *Biogeosciences*, 13, 675–690, <https://doi.org/10.5194/bg-13-675-2016>, 2016.

3528 Zaehle, S. and Friend, A. D.: Carbon and nitrogen cycle dynamics in the O-CN land surface model: 1. Model description,
3529 site-scale evaluation, and sensitivity to parameter estimates: Site-scale evaluation of a C-N model, *Global Biogeochem.*
3530 *Cycles*, 24, GB1005, <https://doi.org/10.1029/2009GB003521>, 2010.

3531 Zaehle, S., Ciais, P., Friend, A. D., and Prieur, V.: Carbon benefits of anthropogenic reactive nitrogen offset by nitrous oxide
3532 emissions, *Nature Geosci.*, 4, 601–605, <https://doi.org/10.1038/ngeo1207>, 2011.

3533 Zaehle, S., Medlyn, B. E., De Kauwe, M. G., Walker, A. P., Dietze, M. C., Hickler, T., Luo, Y., Wang, Y.-P., El-Masri, B.,
3534 Thornton, P., Jain, A., Wang, S., Warlind, D., Weng, E., Parton, W., Iversen, C. M., Gallet-Budynek, A., McCarthy, H.,
3535 Finzi, A., Hanson, P. J., Prentice, I. C., Oren, R., and Norby, R. J.: Evaluation of 11 terrestrial carbon–nitrogen cycle models
3536 against observations from two temperate Free-Air CO₂ Enrichment studies, *New Phytol.*, 202, 803–822,
3537 <https://doi.org/10.1111/nph.12697>, 2014.

3538 Zeng, J., Iida, Y., Matsunaga, T., and Shirai, T.: Surface ocean CO₂ concentration and air-sea flux estimate by machine
3539 learning with modelled variable trends, *Front. Mar. Sci.*, 9, <https://doi.org/10.3389/fmars.2022.989233>, 2022.

3540 Zheng, B., Ciais, P., Chevallier, F., Chuvieco, E., Chen, Y., and Yang, H.: Increasing forest fire emissions despite the
3541 decline in global burned area, *Sci. Adv.*, 7, eabh2646, <https://doi.org/10.1126/sciadv.abh2646>, 2021.

3542 Zou, Y., Wang, Y., Ke, Z., Tian, H., Yang, J., and Liu, Y.: Development of a REgion-Specific Ecosystem Feedback Fire
3543 (RESFire) Model in the Community Earth System Model, *J. Adv. Model. Earth Syst.*, 11, 417–445,
3544 <https://doi.org/10.1029/2018MS001368>, 2019.

Formatted: Default Paragraph Font, Font colour: Black

Formatted: Normal, Centred, Border: Top: (No border), Bottom: (No border), Left: (No border), Right: (No border), Between : (No border), Tab stops: 7.96 cm, Centred + 15.92 cm, Right, Position: Horizontal: Left, Relative to: Column, Vertical: In line, Relative to: Margin, Wrap Around

Formatted: Font colour: Black

3545 Zscheischler, J., Mahecha, M. D., Avitabile, V., Calle, L., Carvalhais, N., Ciais, P., Gans, F., Gruber, N., Hartmann, J.,
3546 Herold, M., Ichii, K., Jung, M., Landschützer, P., Laruelle, G. G., Lauerwald, R., Papale, D., Peylin, P., Poulter, B., Ray, D.,
3547 Regnier, P., Rödenbeck, C., Roman-Cuesta, R. M., Schwalm, C., Tramontana, G., Tyukavina, A., Valentini, R., van der
3548 Werf, G., West, T. O., Wolf, J. E., and Reichstein, M.: Reviews and syntheses: An empirical spatiotemporal description of
3549 the global surface–atmosphere carbon fluxes: opportunities and data limitations, *Biogeosciences*, 14, 3685–3703,
3550 <https://doi.org/10.5194/bg-14-3685-2017>.

Formatted: Space Before: 12 pt, After: 12 pt

Deleted: <https://doi.org/10.5194/bg-14-3685-2017.2017>.

Formatted: Font: 10 pt, Bold

Formatted: Default Paragraph Font, Font colour: Black

Formatted: Normal, Centred, Border: Top: (No border), Bottom: (No border), Left: (No border), Right: (No border), Between : (No border), Tab stops: 7.96 cm, Centred + 15.92 cm, Right, Position: Horizontal: Left, Relative to: Column, Vertical: In line, Relative to: Margin, Wrap Around

Formatted: Font colour: Black

3552

Tables

Unit 1	Unit 2	Conversion	Source
GtC (gigatonnes of carbon)	ppm (parts per million) (a)	2.124 (b)	Ballantyne et al. (2012)
GtC (gigatonnes of carbon)	PgC (petagrams of carbon)		1 SI unit conversion
GtCO ₂ (gigatonnes of carbon dioxide)	GtC (gigatonnes of carbon)	3.664	44.01/12.011 in mass equivalent
GtC (gigatonnes of carbon)	MtC (megatonnes of carbon)	1000	SI unit conversion
(a) Measurements of atmospheric CO ₂ concentration have units of dry-air mole fraction. 'ppm' is an abbreviation for micromole/mol, dry air.			
(b) The use of a factor of 2.124 assumes that all the atmosphere is well mixed within one year. In reality, only the troposphere is well mixed and the growth rate of CO ₂ concentration in the less well-mixed stratosphere is not measured by sites from the NOAA network. Using a factor of 2.124 makes the approximation that the growth rate of CO ₂ concentration in the stratosphere equals that of the troposphere on a yearly basis.			

Table 1. Factors used to convert carbon in various units (by convention, Unit 1 = Unit 2 × conversion).

3554

3555

3556

Deleted: ¶

Page Break

Deleted: ¶

Formatted Table

Formatted: Default Paragraph Font, Font colour: Black

Formatted: Normal, Centred, Border: Top: (No border), Bottom: (No border), Left: (No border), Right: (No border), Between : (No border), Tab stops: 7.96 cm, Centred + 15.92 cm, Right, Position: Horizontal: Left, Relative to: Column, Vertical: In line, Relative to: Margin, Wrap Around

Formatted: Font colour: Black

Component	Primary reference
Global fossil CO2 emissions (EFOS), total and by fuel type	Updated from Andrew and Peters (2022)
National territorial fossil CO2 emissions (EFOS)	Gillfillan and Marland (2021), UNFCCC (2022)
National consumption-based fossil CO2 emissions (EFOS) by country (consumption)	Peters et al. (2011a) updated as described in this paper
Net land-use change flux (ELUC)	This paper (see Table 4 for individual model references).
Growth rate in atmospheric CO2 concentration (GATM)	Lan et al. (2023)
Ocean and land CO2 sinks (SOCEAN and SLAND)	This paper (see Table 4 for individual model and data products references).

Formatted Table

Formatted Table

3563
3564
3565

Table 2. How to cite the individual components of the global carbon budget presented here.

Formatted: Default Paragraph Font, Font colour: Black

Formatted: Normal, Centred, Border: Top: (No border), Bottom: (No border), Left: (No border), Right: (No border), Between : (No border), Tab stops: 7.96 cm, Centred + 15.92 cm, Right, Position: Horizontal: Left, Relative to: Column, Vertical: In line, Relative to: Margin, Wrap Around

Formatted: Font colour: Black

Publication year	Fossil fuel emissions		LUC emissions	Reservoirs			Other changes
	Global	Country (territorial)		Atmosphere	Ocean	Land	
2019 Friedlingstein et al. (2019) GCB2019	Global emissions calculated as sum of all countries plus bunkers, rather than taken directly from CDIAC.		Average of two bookkeeping models; use of 15 DGVMs	Use of three atmospheric inversions	Based on nine models	Based on 16 models	
2020 Friedlingstein et al. (2020) GCB2020	Cement carbonation now included in the EFOS estimate, reducing EFOS by about 0.2GtC yr ⁻¹ for the last decade	India's emissions from Andrew (2020: India); Corrections to Netherland Antilles and Aruba and Soviet emissions before 1950 as per Andrew (2020: CO ₂); China's coal emissions in 2019 derived from official statistics, emissions now shown for EU27 instead of EU28. Projection for 2020 based on assessment of four approaches.	Average of three bookkeeping models; use of 17 DGVMs. Estimate of gross land use sources and sinks provided	Use of six atmospheric inversions	Based on nine models. River flux revised and partitioned NH, Tropics, SH	Based on 17 models	
2021 Friedlingstein et al. (2022a) GCB2021	Projections are no longer an assessment of four approaches.	Official data included for a number of additional countries, new estimates for South Korea, added emissions from lime	ELUC estimate compared to the estimates adopted in national GHG inventories (NGHGI)		Average of means of eight models and means of seven data-products. Current year prediction of SOCEAN using a feed-forward	Current year prediction of SLAND using a feed-forward neural network method	

Formatted: Default Paragraph Font, Font colour: Black

Formatted: Normal, Centred, Border: Top: (No border), Bottom: (No border), Left: (No border), Right: (No border), Between : (No border), Tab stops: 7.96 cm, Centred + 15.92 cm, Right, Position: Horizontal: Left, Relative to: Column, Vertical: In line, Relative to: Margin, Wrap Around

Formatted: Font colour: Black

		production in China.			neural network method		
2022			ELUC provided at country level. Revised components decomposition of ELUC fluxes. Revision of LUC maps for Brazil. New datasets for peat drainage.	Use of nine atmospheric inversions	Average of means of ten models and means of seven data-products	Based on 16 models. Revision of LUC maps for Brazil.	
Friedlingstein et al. (2022) GCB2022							
2023			Refined components decomposition of ELUC. Revision of LUC maps for Indonesia. Use of updated peat drainage estimates.	Use of 14 atmospheric inversions. Additional use of 4 Earth System Models to estimate current year CO2	Additional use of 4 Earth System Models and atmospheric oxygen method to assess SOCEAN. Regional distribution of river flux adjustment revised.	Based on 20 models. Additional use of 4 Earth System Models and atmospheric oxygen method to assess the net atmosphere-land flux.	Inclusion of an estimate of Carbon Dioxide Removal (CDR)
This study							

3570 **Table 3.** Main methodological changes in the global carbon budget since 2019. Methodological changes
3571 introduced in one year are kept for the following years unless noted. Empty cells mean there were no
3572 methodological changes introduced that year. Table S8 lists methodological changes from the first global carbon
3573 budget publication up to 2018.

3574

3575

Formatted: Default Paragraph Font, Font colour: Black

Formatted: Normal, Centred, Border: Top: (No border), Bottom: (No border), Left: (No border), Right: (No border), Between : (No border), Tab stops: 7.96 cm, Centred + 15.92 cm, Right, Position: Horizontal: Left, Relative to: Column, Vertical: In line, Relative to: Margin, Wrap Around

Formatted: Font colour: Black

Model/data name	Reference	Change from Global Carbon Budget 2022 (Friedlingstein et al., 2022b)
Bookkeeping models for land-use change emissions		
BLUE	Hansis et al. (2015)	No change to model, but simulations performed with LUH2-GCB2023 forcing. Update in added peat drainage emissions.
H&C2023	Houghton and Castanho (2023)	H&C2023 replaces the formerly used H&N2017 model. Minor bug fix in fuel harvest estimates. Update in added peat drainage emissions.
OSCAR	Gasser et al. (2020)	No change to model, but land-use forcing changed to LUH2-GCB2023 and FRA2020 (extrapolated to 2022). Constraining based on GCB2022 data for SLAND over 1960-2021. Update in added peat drainage emissions.
Dynamic global vegetation models		
CABLE-POP	Haverd et al. (2018)	Improved representation of nitrogen retranslocation and plant uptake, minor bug fixes, parameter changes
CLASSIC	Melton et al. (2020), Asaadi et al. (2018)	Bug fixes, correct allocation of leaves after summer solstice for latitudes higher than 45°N, improved phenology for several PFTs
CLM5.0	Lawrence et al. (2019)	No change.
DLEM	Tian et al. (2011, 2015)	No change.
EDv3	Moorcroft et al. (2001), Ma et al. (2022)	New this year.
ELM	Yang et al.(2023), Burrows et al.(2020)	New this year.
IBIS	Yuan et al. (2014)	Changes in parameterisation and new module of soil nitrogen dynamics (Ma et al., 2022)
ISAM	Jain et al. (2013), Meiyappan et al. (2015), Shu et al. (2020)	Vertically resolved soil biogeochemistry (carbon and nitrogen) module, following Shu et al. (2020),
ISBA-CTrip	Delire et al. (2020)	No change.
JSBACH	Mauritsen et al. (2019), Reick et al. (2021)	No change.
JULES-ES	Wiltshire et al. (2021), Sellar et al. (2019), Burton et al. (2019)	Minor bug fixes. (Using JULES v6.3, suite u-co002)
LPJ-GUESS	Smith et al. (2014)	Minor bug fixes.

Formatted: Default Paragraph Font, Font colour: Black

Formatted: Normal, Centred, Border: Top: (No border), Bottom: (No border), Left: (No border), Right: (No border), Between : (No border), Tab stops: 7.96 cm, Centred + 15.92 cm, Right, Position: Horizontal: Left, Relative to: Column, Vertical: In line, Relative to: Margin, Wrap Around

Formatted: Font colour: Black

LPJml	Schaphoff et al., 2018, von Bloh et al., 2018, Lutz et al., 2019 (tillage), Heinke et al., 2023 (livestock grazing)	New this year.
LPJwsl	Poulter et al. (2011) (d)	No change.
LPX-Bern	Lienert and Joos (2018)	No change.
OCN	Zaehle and Friend (2010), Zaehle et al. (2011)	Minor bug fixes
ORCHIDEEv3	Krinner et al. (2005), Zaehle and Friend (2010), Vuichard et al. (2019)	Small update for leaf senescence (ORCHIDEE - V3; revision 8119)
SDGVM	Woodward and Lomas (2004), Walker et al. (2017)	implement gross land-use transitions, tracking of carbon from wood & crop harvest, and tracking of primary & secondary vegetation .
VISIT	Ito and Inatomi (2012), Kato et al. (2013)	No change.
YIBs	Yue and Unger (2015)	Inclusion of process-based water cycle from Noah-MP (Niu et al., 2011)
Intermediate complexity land carbon cycle model		
CARDAMOM	Bloom et al. (2016), Smallman et al. (2021)	New this year
Global ocean biogeochemistry models		
NEMO3.6-PISCESv2-gas (CNRM)	Berthet et al. (2019), Séférian et al. (2019)	No change.
FESOM-2.1-REcoM2	Gürses et al. (2023)	No change
NEMO-PISCES (IPSL)	Aumont et al. (2015)	No change.
MOM6-COBALT (Princeton)	Liao et al. (2020)	No change
MRI-ESM2-2	Nakano et al. (2011)	The ocean model has been updated to MRI.COMv5 (Sakamoto et al. 2023). The distribution of background vertical diffusivity is changed to the one proposed by Kawasaki et al. (2021). Model was spun-up with a preindustrial xCO2 of 278 ppm.
MICOM-HAMOCC (NorESM-OCv1.2)	Schwinger et al. (2016)	No change.
NEMO-PlankTOM12	Wright et al. (2021)	Minor bug fixes, switch to ERA5 forcing, salinity restoring

Deleted: to track

Deleted: to track

Deleted: .

Formatted: Default Paragraph Font, Font colour: Black

Formatted: Normal, Centred, Border: Top: (No border), Bottom: (No border), Left: (No border), Right: (No border), Between : (No border), Tab stops: 7.96 cm, Centred + 15.92 cm, Right, Position: Horizontal: Left, Relative to: Column, Vertical: In line, Relative to: Margin, Wrap Around

Formatted: Font colour: Black

CESM-ETHZ	Doney et al. (2009)	Model was spun-up with a preindustrial xCO ₂ of 278 ppm.
MPIOM-HAMOC6	Lacroix et al. (2021)	No change.
ACCESS (CSIRO)	Law et al. (2017)	Minor bug fixes, extended spinup since last participation 2020.
fCO₂-products		
CMEMS-LSCE-FFNNv2	Chau et al. (2022)	Update to SOCATv2023 measurements and time period 1985-2022. The mapping approach by Chau et al (2022) has been upgraded by increasing spatial resolution from 1° to 0.25°.
JMA-MLR	Iida et al. (2021)	Updated to SOCATv2023
LDEO-HPD	Gloege et al. (2022), Bennington et al. (2022)	Updated with SOCATv2023. Updated with current GCB2023 models and extending back in time using Bennington et al. (2022) method.
MPI-SOMFFN	Landschützer et al. (2016)	update to SOCATv2023. Since GCB2022, fluxes cover open ocean and coastal domains as well as the Arctic Ocean extension.
NIES-ML3	Zeng et al. (2022)	New this year
OS-ETHZ-GRaCER	Gregor et al. (2021)	Updated to SOCATv2023
Jena-MLS	Rödenbeck et al. (2014, 2022)	update to SOCATv2023 measurements, time period extended to 1957-2022
UOEx-Watson	Watson et al. (2020)	Updated to SOCAT v2023. fCO ₂ (sw) corrected to CCI SST v2.1 (Merchant et al. 2019) instead of OI SST v2.1. Updated interpolation datasets to CCI SST v2.1, CMEMS SSS and MLD (Jean-Michel et al. 2021). Monthly cool skin difference calculated using NOAA COARE 3.5 (Edson et al. 2013). CO ₂ flux computed using FluxEngine (Holding et al., 2019; Shutler et al., 2016).
Atmospheric inversions		
Jena CarboScope	Rödenbeck et al. (2003, 2018)	Extension to 2022, re-addition of a 2.5-year relaxation term.
CAMS	Chevallier et al. (2005), Remaud et al. (2018)	Increase of the 3D resolution (4.5 times more 3D cells than the previous submission); extension to year 2022; update of the prior fluxes.
CarbonTracker Europe (CTE)	van der Laan-Luijckx et al. (2017)	Extension to 2022, update of prior fluxes.
NISMON-CO ₂	Niwa et al. (2020, 2022)	Prior terrestrial fluxes include minor fluxes (BVOC and CH ₄) in addition to GPP, RE and LUC.
CT-NOAA	Peters et al. (2005), Jacobson et al. (2023a, 2023b)	New this year.
CMS-Flux	Liu et al. (2021)	Update of OCO-2 observations and prior fluxes.

Formatted: Default Paragraph Font, Font colour: Black

Formatted: Normal, Centred, Border: Top: (No border), Bottom: (No border), Left: (No border), Right: (No border), Between : (No border), Tab stops: 7.96 cm, Centred + 15.92 cm, Right, Position: Horizontal: Left, Relative to: Column, Vertical: In line, Relative to: Margin, Wrap Around

Formatted: Font colour: Black

CAMS-Satellite	Chevallier et al. (2005), Remaud et al. (2018)	Increase of the 3D resolution, extension to year 2022 and the first months of 2023; removal of the pre-OCO-2 period (2010-2014 with GOSAT); update of the prior fluxes.
GONGGA	Jin et al. (2023)	Update of OCO-2 observations and prior fluxes.
THU	Kong et al. (2022)	Updates to the OCO-2 product and the fossil fuel data.
COLA	Liu et al. (2022)	New this year.
GCASv2	Jiang et al. (2021, 2022)	New this year.
UoE in-situ	Feng et al. (2009), Feng et al. (2016), Palmer et al. (2019)	Update of the inversion system by using new version of GEOS-Chem
IAPCAS	Feng et al. (2016), Yang et al. (2021)	New this year.
MIROC4-ACTM	Chandra et al. (2022)	New this year
Earth System Models		
CanESM5	Swart et al. (2019), Sospedra-Alfonso et al. (2021)	New this year.
IPSL-CM6a-CO2-LR	Boucher et al. (2020)	New this year.
MIROC-ES2L	Watanabe et al. (2020)	New this year.
MPI-ESM1-2-LR	Mauritsen et al. (2019), Li et al. (2023)	New this year.

3583

3584 **Table 4.** References for the process models, bookkeeping models, ocean data products, and atmospheric
3585 inversions. All models and products are updated with new data to the end of year 2022, and the atmospheric
3586 forcing for the DGVMs has been updated as described in Section C.2.2 and C.4.1.

3587

Formatted: Font: Times New Roman, Not Bold

Formatted: Default Paragraph Font, Font colour: Black

Formatted: Normal, Centred, Border: Top: (No border), Bottom: (No border), Left: (No border), Right: (No border), Between : (No border), Tab stops: 7.96 cm, Centred + 15.92 cm, Right, Position: Horizontal: Left, Relative to: Column, Vertical: In line, Relative to: Margin, Wrap Around

Formatted: Font colour: Black

	1960s	1970s	1980s	1990s	2000s	2013-2022	2022
Bookkeeping (BK) Net flux (1a)	1.5±0.7	1.3±0.7	1.4±0.7	1.6±0.7	1.4±0.7	1.3±0.7	1.2±0.7
BK - deforestation (total)	1.7 [1.3,2.1]	1.6 [1.2,1.9]	1.7 [1.3,2.1]	1.9 [1.6,2.2]	2 [1.6,2.4]	1.9 [1.5,2.4]	1.9 [1.4,2.5]
BK - forest regrowth (total)	-0.8 [-1.1,-0.6]	-0.9 [-1.1,-0.7]	-0.9 [-1.1,-0.7]	-1 [-1.2,-0.7]	-1.1 [-1.3,-0.8]	-1.3 [-1.5,-0.9]	-1.3 [-1.6,-1]
Land-use change emissions (ELUC)							
BK - other transitions	0.4 [0.3,0.4]	0.2 [0.1,0.3]	0.2 [0.2,0.3]	0.1 [0,0.2]	0.1 [0,0.2]	0.1 [0,0.3]	0.1 [0,0.2]
BK - peat drainage & peat fires	0.2 [0.1,0.2]	0.2 [0.1,0.2]	0.2 [0.2,0.3]	0.3 [0.3,0.3]	0.3 [0.2,0.3]	0.3 [0.3,0.3]	0.2 [0.2,0.3]
BK - wood harvest & forest management	0.2 [-0.2,0.6]	0.2 [-0.2,0.6]	0.2 [-0.2,0.6]	0.2 [-0.1,0.6]	0.2 [-0.1,0.6]	0.2 [0,0.6]	0.2 [0,0.7]
DGVMs-net flux (1b)	1.5±0.5	1.3±0.5	1.6±0.6	1.8±0.6	1.8±0.7	1.7±0.6	1.7±0.6
Terrestrial sink (SLAND)							
Residual sink from global budget (E _{FOS} +E _{ELUC(1a)} -G _{ATM} -G _{OCEAN}) (2a)	1.7±0.8	1.8±0.8	1.7±0.9	2.7±0.9	2.9±0.9	2.9±0.9	3.7±1
DGVMs (2b)	1.3±0.5	2±0.7	1.9±0.8	2.5±0.6	2.9±0.7	3.3±0.8	3.8±0.8
Net land fluxes (SLAND-ELUC)							
GCB2023 Budget (2b-1a)	-0.2±0.8	0.8±1	0.5±1	0.9±0.9	1.4±1	2.1±1.1	2.6±1.1
Atmospheric O ₂	---	---	---	1.2±1	1.1±1.1	1.1±1.3	-
DGVMs-net (2b-1b)	-0.2±0.4	0.7±0.7	0.3±0.6	0.7±0.5	1.1±0.4	1.7±0.6	2.1±0.6
Inversions*	- [-,-]	- [-,-]	0.5 [0.4,0.6] (2)	0.9 [0.6,1.3] (3)	1.3 [0.7,2] (4)	1.6 [0.5,2.3] (8)	2.7 [1.4-3.8] (13)
ESMs	---	---	0.6 [0.1,1]	1.7 [1.3,2]	2 [1.4,2.7]	2.4 [1.8,3.3]	3.9 [2.8-5.5]

3589

3590 *Estimates are adjusted for the pre-industrial influence of river fluxes, for the cement carbonation sink, and
3591 adjusted to common E_{FOS} (Sect. 2.7). The ranges given include varying numbers (in parentheses) of inversions
3592 in each decade (Table S4).

3593 **Table 5.** Comparison of results from the bookkeeping method and budget residuals with results from the
3594 DGVMs, as well as additional estimates from atmospheric oxygen, atmospheric inversions and Earth System
3595 Models (ESMs) for different periods, the last decade, and the last year available. All values are in GtCyr⁻¹. See
3596 Figure 7 for explanation of the bookkeeping component fluxes. The DGVM uncertainties represent ±1σ of the
3597 decadal or annual (for 2022) estimates from the individual DGVMs: for the inverse systems the mean and range
3598 of available results is given. All values are rounded to the nearest 0.1 GtC and therefore columns do not
3599 necessarily add to zero.

3600

3601

3602

Deleted: <object>

Formatted: Default Paragraph Font, Font colour: Black

Formatted: Normal, Centred, Border: Top: (No border), Bottom: (No border), Left: (No border), Right: (No border), Between : (No border), Tab stops: 7.96 cm, Centred + 15.92 cm, Right, Position: Horizontal: Left, Relative to: Column, Vertical: In line, Relative to: Margin, Wrap Around

Formatted: Font colour: Black

Product	1960s	1970s	1980s	1990s	2000s	2013-2022	2022
$f\text{CO}_2$ -products	---	---	---	2.3 [2,2.9]	2.4 [2.2,2.7]	3.1 [2.6,3.3]	3.1 [2.5,3.3]
GOBMs	1 ± 0.3	1.2 ± 0.3	1.7 ± 0.3	2 ± 0.3	2.1 ± 0.4	2.6 ± 0.4	2.5 ± 0.4
GCB2023 Budget	1.1 ± 0.4	1.4 ± 0.4	1.9 ± 0.4	2.1 ± 0.4	2.3 ± 0.4	2.8 ± 0.4	2.8 ± 0.4
Atmospheric O_2	---	---	---	2 ± 0.7	2.6 ± 0.6	3.3 ± 0.6	-
Inversions	- [-,-]	- [-,-]	1.7 [1.6,1.8] (2)	2.2 [1.9,2.5] (3)	2.4 [1.8,3.1] (4)	3 [2.4,4.1] (8)	3 [2.2-4.2] (13)
ESMs	---	---	1.6 [0.7,2.4]	1.8 [1.1,2.5]	2.1 [1.5,2.8]	2.6 [2.2,3.4]	2.7 [2.3-3.5]

Product	1960s	1970s	1980s
$f\text{CO}_2$ -products	---	---	---
GOBMs	1 ± 0.3	1.2 ± 0.3	1.7 ± 0.3
GCB2023 Budget	1.1 ± 0.4	1.4 ± 0.4	1.9 ± 0.4
Atmospheric O_2	---	---	---
Inversions	- [-,-]	- [-,-]	1 [1] (2)
ESMs	---	---	1 [1] (0)

Deleted:

Formatted: Subscript

Formatted: Subscript

Formatted: Superscript

3605
3606 **Table 6:** Comparison of results for the ocean sink from the $f\text{CO}_2$ -products, from global ocean biogeochemistry
3607 models (GOBMs), the best estimate for GCB2023 as calculated from $f\text{CO}_2$ -products and GOBMs that is used in
3608 the budget Table 7, as well as additional estimates from atmospheric oxygen, atmospheric inversions and Earth
3609 System Models (ESMs) for different periods, the last decade, and the last year available. All values are in
3610 GtCyr^{-1} . Uncertainties represent $\pm 1\sigma$ of the estimates from the GOBMs ($N>10$) and range of ensemble members
3611 is given for ensembles with $N<10$ ($f\text{CO}_2$ -products, inversions, ESMs). The uncertainty of the GCB2023 budget
3612 estimate is based on expert judgement (Section 2 and Supplementary S1 to S4) and for oxygen it is the standard
3613 deviation of a Monte Carlo ensemble (Section 2.8).

Formatted: Default Paragraph Font, Font colour: Black

Formatted: Normal, Centred, Border: Top: (No border), Bottom: (No border), Left: (No border), Right: (No border), Between : (No border), Tab stops: 7.96 cm, Centred + 15.92 cm, Right, Position: Horizontal: Left, Relative to: Column, Vertical: In line, Relative to: Margin, Wrap Around

Formatted: Font colour: Black

		1960s	1970s	1980s	1990s	2000s	2013-2022	2022	2023 (Projection)
Total emissions (EFOS + ELUC)	Fossil CO2 emissions (EFOS) ¹	3±0.2	4.7±0.2	5.5±0.3	6.4±0.3	7.8±0.4	9.6±0.5	9.9±0.5	10.1±0.5
	Land-use change emissions (ELUC)	1.5±0.7	1.3±0.7	1.4±0.7	1.6±0.7	1.4±0.7	1.3±0.7	1.2±0.7	1.1±0.7
	Total emissions	4.6±0.7	6±0.7	6.9±0.8	7.9±0.8	9.2±0.8	10.9±0.8	11.1±0.9	11.2±0.9
Partitioning	Growth rate in atmos CO2 (GATM)	1.7±0.07	2.8±0.07	3.4±0.02	3.1±0.02	4±0.02	5.2±0.02	4.6±0.2	5.1±0.4
	Ocean sink (SOCEAN)	1.1±0.4	1.4±0.4	1.9±0.4	2.1±0.4	2.3±0.4	2.8±0.4	2.8±0.4	2.9±0.6
	Terrestrial sink (SLAND)	1.3±0.5	2±0.7	1.9±0.8	2.5±0.6	2.9±0.7	3.3±0.8	3.8±0.8	2.9±1.2
Budget imbalance	BIM=EFOS+ELUC-(GATM+SOCEAN+SLAND)	0.4	-0.2	-0.2	0.2	0	-0.4	-0.1	0.3

¹Fossil emissions excluding the cement carbonation sink amount to 3±0.2 GtC/yr, 4.7±0.2 GtC/yr, 5.5±0.3 GtC/yr, 6.4±0.3 GtC/yr, 7.8±0.4 GtC/yr, 9.6±0.5 GtC/yr, and 9.8±0.5 GtC/yr for the decades 1960s to 2010s respectively and to 10.2±0.5 GtC/yr for 2022, and 10.3±0.5 GtC/yr for 2023.

3616

3617

3618

3619

3620

3621

3622

3623

Table 7: Decadal mean in the five components of the anthropogenic CO2 budget for different periods, and last year available. All values are in GtC yr⁻¹, and uncertainties are reported as ±1σ. Fossil CO2 emissions include cement carbonation. The table also shows the budget imbalance (BIM), which provides a measure of the discrepancies among the nearly independent estimates. A positive imbalance means the emissions are overestimated and/or the sinks are too small. All values are rounded to the nearest 0.1 GtC and therefore columns do not necessarily add to zero.

		1960s
Total emissions (EFOS + ELUC)	Fossil CO2 emissions (EFOS) ¹	3±0.2
	Land-use change emissions (ELUC)	1.5±0.7
	Total emissions	4.6±0.7
Partitioning	Growth rate in atmos CO2 (GATM)	1.7±0.07
	Ocean sink (SOCEAN)	1.1±0.4
	Terrestrial sink (SLAND)	1.3±0.5
Budget imbalance	BIM=EFOS+ELUC-(GATM+SOCEAN+SLAND)	0.4

¹Fossil emissions excluding the cement carbonation sink amount to 3±0.2 GtC/yr, 4.7±0.2 GtC/yr, 5.5±0.3 GtC/yr, 6.4±0.3 GtC/yr, 7.8±0.4 GtC/yr, 9.6±0.5 GtC/yr, and 9.8±0.5 GtC/yr for the decades 1960s to 2010s respectively and to 10.2±0.5 GtC/yr for 2022, and 10.3±0.5 GtC/yr for 2023.

Deleted:

Formatted: Superscript

Formatted: Default Paragraph Font, Font colour: Black

Formatted: Normal, Centred, Border: Top: (No border), Bottom: (No border), Left: (No border), Right: (No border), Between: (No border), Tab stops: 7.96 cm, Centred + 15.92 cm, Right, Position: Horizontal: Left, Relative to: Column, Vertical: In line, Relative to: Margin, Wrap Around

Formatted: Font colour: Black

	1750-2022	1850-2014	1850-2022	1960-2022	1850-2023	
Emissions	Fossil CO2 emissions (EFOS)	480±25	400±20	475±25	395±20	485±25
	Land-use change emissions (ELUC)	250±75	210±65	220±65	90±45	220±65
	Total emissions	730±80	610±65	695±70	485±50	705±70
Partitioning	Growth rate in atmos CO2 (GATM)	300±5	235±5	280±5	215±5	285±5
	Ocean sink (SOCEAN)	190±40	155±30	180±35	125±25	180±35
	Terrestrial sink (SLAND)	245±60	200±50	225±55	150±35	225±55
Budget imbalance	BIM=EFOS+ELUC-(GATM+SOCEAN+SLAND)	-5	20	15	-5	15

Table 8. Cumulative CO₂ for different time periods in gigatonnes of carbon (GtC). Fossil CO₂ emissions include cement carbonation. The budget imbalance (B_{IM}) provides a measure of the discrepancies among the nearly independent estimates. All values are rounded to the nearest 5 GtC and therefore columns do not necessarily add to zero. Uncertainties are reported as follows: EFOS is 5% of cumulative emissions; ELUC prior to 1959 is 1σ spread from the DGVMs, ELUC post-1959 is $0.7 \times \text{number of years}$ (where 0.7 GtC/yr is the uncertainty on the annual ELUC flux estimate); G_{ATM} uncertainty is held constant at 5 GtC for all time periods; SOCEAN uncertainty is 20% of the cumulative sink (20% relates to the annual uncertainty of 0.4 GtC/yr, which is ~20% of the current ocean sink); and SLAND is the 1σ spread from the DGVMs estimates.

	Fossil CO2 emissions (EFOS)
Emissions	Land-use change emissions (ELUC);
	Total emissions
	Growth rate in atmos CO2 (GATM)
Partitioning	Ocean sink (SOCEAN)
	Terrestrial sink (SLAND)
Budget imbalance	BIM=EFOS+ELUC-(GATM+SOCEAN

Deleted:

Deleted: 1σ

Deleted: 1σ

Formatted: Default Paragraph Font, Font colour: Black

Formatted: Normal, Centred, Border: Top: (No border), Bottom: (No border), Left: (No border), Right: (No border), Between : (No border), Tab stops: 7.96 cm, Centred + 15.92 cm, Right, Position: Horizontal: Left, Relative to: Column, Vertical: In line, Relative to: Margin, Wrap Around

Formatted: Font colour: Black

3638

	2003-2012	2013-2022
ELUC from bookkeeping estimates (from Table 5)	1.4	1.3
SLAND on non-intact forest from DGVMs	1.9	2.0
ELUC subtract SLAND on non-intact forests	-0.5	-0.8
National Greenhouse Gas Inventories	-0.4	-0.7

Formatted Table

3639 **Table 9:** Translation of global carbon cycle models' land flux definitions to the definition of the LULUCF net
3640 flux used in national Greenhouse Gas Inventories reported to UNFCCC. See Sec. C.2.3 and Table S9 for detail
3641 on methodology and comparison to other datasets. Units are GtC yr⁻¹.

Formatted: Superscript

3642

Formatted: Default Paragraph Font, Font colour: Black

Formatted: Normal, Centred, Border: Top: (No border), Bottom: (No border), Left: (No border), Right: (No border), Between : (No border), Tab stops: 7.96 cm, Centred + 15.92 cm, Right, Position: Horizontal: Left, Relative to: Column, Vertical: In line, Relative to: Margin, Wrap Around

Formatted: Font colour: Black

Source of uncertainty	Time scale (years)	Location	Evidence
Fossil CO2 emissions (EFOS; Section 2.1)			
energy statistics	annual to decadal	global, but mainly China & major developing countries	(Korsbakken et al., 2016, Guan et al., 2012)
carbon content of coal	annual to decadal	global, but mainly China & major developing countries	(Liu et al., 2015)
system boundary	annual to decadal	all countries	(Andrew, 2020a)
Net land-use change flux (ELUC; section 2.2)			
land-cover and land-use change statistics	continuous	global; in particular tropics	(Houghton et al., 2012, Gasser et al., 2020, Ganzenmüller et al., 2022, Yu et al. 2022)
sub-grid-scale transitions	annual to decadal	global	(Wilkenskjeld et al., 2014)
vegetation biomass	annual to decadal	global; in particular tropics	(Houghton et al., 2012, Bastos et al., 2021)
forest degradation (fire, selective logging)	annual to decadal	tropics	(Aragão et al., 2018, Qin et al., 2021)
wood and crop harvest	annual to decadal	global; SE Asia	(Arneeth et al., 2017, Erb et al., 2018)
peat burning	multi-decadal trend	global	(van der Werf et al., 2010, 2017)
loss of additional sink capacity	multi-decadal trend	global	(Pongratz et al, 2014, Gasser et al, 2020; Obermeier et al., 2021)
Atmospheric growth rate (GATM; section 2.4) no demonstrated uncertainties larger than ± 0.3 GtC yr⁻¹. The uncertainties in GATM have been estimated as ± 0.2 GtC yr⁻¹, although the conversion of the growth rate into a global annual flux assuming instantaneous mixing throughout the atmosphere introduces additional errors that have not yet been quantified.			
Ocean sink (SOCEAN; section 2.5)			
sparsity in surface fCO2 observations	mean, decadal variability and trend	global, in particular southern hemisphere	(Gloeger et al., 2021, Denvil-Sommer et al., 2021, Hauck et al., 2023)

Formatted Table

Formatted: French

Formatted Table

Formatted: French

Formatted: French

Formatted: French

Formatted: French

Formatted: French

Formatted Table

Formatted: French

Formatted: Default Paragraph Font, Font colour: Black

Formatted: Normal, Centred, Border: Top: (No border), Bottom: (No border), Left: (No border), Right: (No border), Between : (No border), Tab stops: 7.96 cm, Centred + 15.92 cm, Right, Position: Horizontal: Left, Relative to: Column, Vertical: In line, Relative to: Margin, Wrap Around

Formatted: Font colour: Black

riverine carbon outgassing and its anthropogenic perturbation	annual to decadal	global, in particular partitioning between Tropics and South	(Aumont et al., 2001, Lacroix et al., 2020, Cris et al., 2022)
Models underestimate interior ocean anthropogenic carbon storage	annual to decadal	global	(Friedlingstein et al., 2021, this study, DeVries et al., 2023, see also Terhaar et al., 2022)
near-surface temperature and salinity gradients	mean on all time-scales	global	(Watson et al., 2020, Dong et al., 2022, Bellenger et al., 2023)
Land sink (SLAND; section 2.6)			
strength of CO2 fertilisation	multi-decadal trend	global	(Wenzel et al., 2016; Walker et al., 2021)
response to variability in temperature and rainfall	annual to decadal	global; in particular tropics	(Cox et al., 2013; Jung et al., 2017; Humphrey et al., 2018; 2021)
nutrient limitation and supply	annual to decadal	global	(Zaehle et al., 2014)
carbon allocation and tissue turnover rates	annual to decadal	global	(De Kauwe et al., 2014; O'Sullivan et al., 2022)
tree mortality	annual	global in particular tropics	(Hubau et al., 2021; Brienen et al., 2020)
response to diffuse radiation	annual	global	(Mercado et al., 2009; O'Sullivan et al., 2021)

Formatted: French

Formatted: French

Formatted: French

Formatted: French

Formatted: French

Formatted: French

Formatted: French

3647

3648 **Table 10.** Major known sources of uncertainties in each component of the Global Carbon Budget, defined as
 3649 input data or processes that have a demonstrated effect of at least $\pm 0.3 \text{ GtC yr}^{-1}$.

Formatted: Superscript

3650

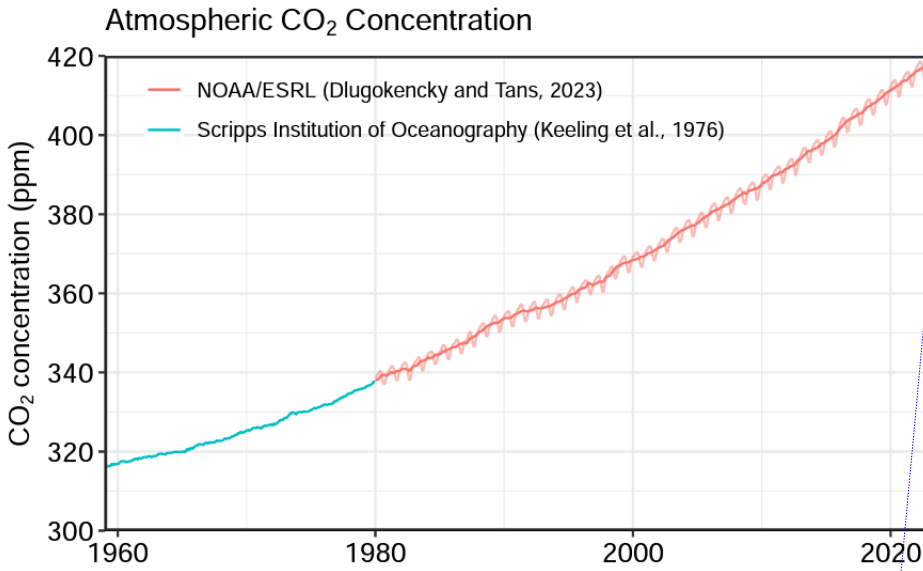
3651

Formatted: Default Paragraph Font, Font colour: Black

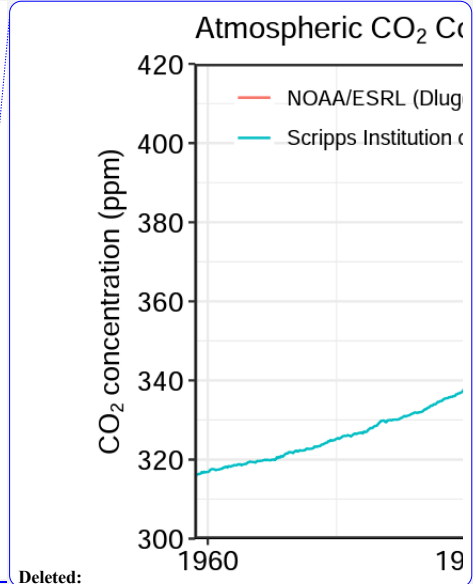
Formatted: Normal, Centred, Border: Top: (No border), Bottom: (No border), Left: (No border), Right: (No border), Between : (No border), Tab stops: 7.96 cm, Centred + 15.92 cm, Right, Position: Horizontal: Left, Relative to: Column, Vertical: In line, Relative to: Margin, Wrap Around

Formatted: Font colour: Black

3653 **Figures and Captions**



Formatted: Indent: Left: 0 cm, First line: 0 cm



3654
3655 **Figure 1.** Surface average atmospheric CO₂ concentration (ppm). Since 1980, monthly data are from
3656 NOAA/GML (Lan et al., 2023) and are based on an average of direct atmospheric CO₂ measurements from
3657 multiple stations in the marine boundary layer (Masarie and Tans, 1995). The 1958-1979 monthly data are from
3658 the Scripps Institution of Oceanography, based on an average of direct atmospheric CO₂ measurements from the
3659 Mauna Loa and South Pole stations (Keeling et al., 1976). To account for the difference of mean CO₂ and
3660 seasonality between the NOAA/GML and the Scripps station networks used here, the Scripps surface average
3661 (from two stations) was de-seasonalised and adjusted to match the NOAA/GML surface average (from multiple
3662 stations) by adding the mean difference of 0.667 ppm, calculated here from overlapping data during 1980-2012.

Deleted:

Formatted: Font: Not Bold

Formatted: Heading 2

3663

3664

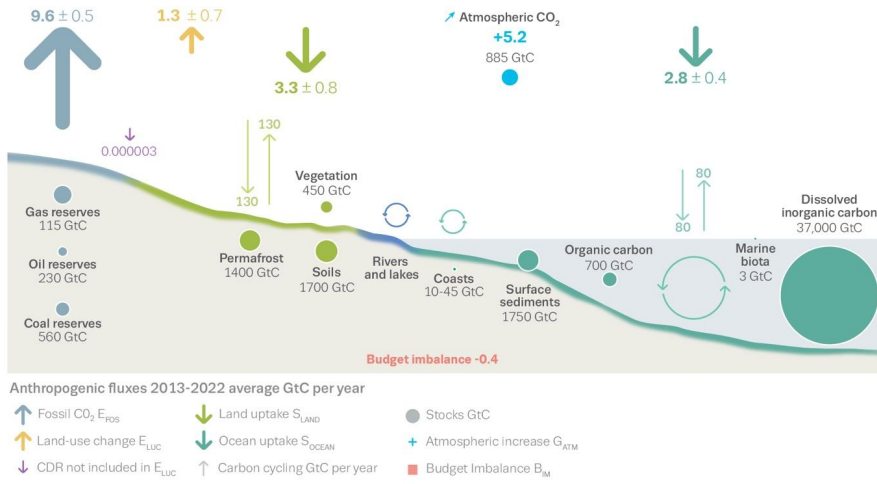
Formatted: Font: Not Bold

Formatted: Default Paragraph Font, Font colour: Black

Formatted: Normal, Centred, Border: Top: (No border), Bottom: (No border), Left: (No border), Right: (No border), Between : (No border), Tab stops: 7.96 cm, Centred + 15.92 cm, Right, Position: Horizontal: Left, Relative to: Column, Vertical: In line, Relative to: Margin, Wrap Around

Formatted: Font colour: Black

The global carbon cycle



3666
3667

3668 **Figure 2.** Schematic representation of the overall perturbation of the global carbon cycle caused by
 3669 anthropogenic activities, averaged globally for the decade 2013-2022. See legends for the corresponding arrows.
 3670 [Fluxes estimates and their 1 standard deviation uncertainty are as reported in Table 7.](#) The uncertainty in the
 3671 atmospheric CO₂ growth rate is very small (± 0.02 GtC yr⁻¹) and is neglected for the figure. The anthropogenic
 3672 perturbation occurs on top of an active carbon cycle, with fluxes and stocks represented in the background and
 3673 taken from Canadell et al. (2021) for all numbers, except for the carbon stocks in coasts which is from a
 3674 literature review of coastal marine sediments (Price and Warren, 2016). [Fluxes are in GtC yr⁻¹ and reservoirs in](#)
 3675 [GtC.](#)

- Formatted: Font: Not Bold
- Formatted: Heading 2
- Deleted: and units.
- Formatted: Font: Not Bold
- Formatted: Font: Not Bold, Superscript
- Formatted: Font: Not Bold
- Formatted: Font: Not Bold

3676

Deleted: ¶
 Page Break
 ¶ [12]

- Formatted: Default Paragraph Font, Font colour: Black
- Formatted: Normal, Centred, Border: Top: (No border), Bottom: (No border), Left: (No border), Right: (No border), Between : (No border), Tab stops: 7.96 cm, Centred + 15.92 cm, Right, Position: Horizontal: Left, Relative to: Column, Vertical: In line, Relative to: Margin, Wrap Around
- Formatted: Font colour: Black

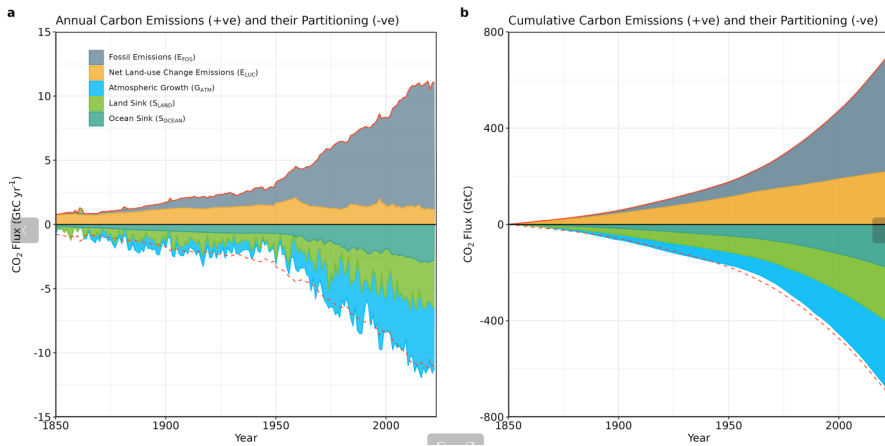


Figure 3. Combined components of the global carbon budget as a function of time, for fossil CO_2 emissions (E_{FOS} , including a small sink from cement carbonation; grey) and emissions from land-use change (E_{LUC} ; brown), as well as their partitioning among the atmosphere (G_{ATM} ; cyan), ocean (S_{OCEAN} ; blue), and land (S_{LAND} ; green). Panel (a) shows annual estimates of each flux (in GtC yr^{-1}) and panel (b) the cumulative flux (the sum of all prior annual fluxes, in GtC) since the year 1850. The partitioning is based on nearly independent estimates from observations (for G_{ATM}) and from process model ensembles constrained by data (for S_{OCEAN} and S_{LAND}) and does not exactly add up to the sum of the emissions, resulting in a budget imbalance (B_{IM}) which is represented by the difference between the bottom red line (mirroring total emissions) and the sum of carbon fluxes in the ocean, land, and atmosphere reservoirs. All data are in GtC yr^{-1} (panel a) and GtC (panel b). The E_{FOS} estimate is based on a mosaic of different datasets and has an uncertainty of $\pm 5\%$ ($\pm 1\sigma$). The E_{LUC} estimate is from three bookkeeping models (Table 4) with uncertainty of $\pm 0.7 \text{ GtC yr}^{-1}$. The G_{ATM} estimates prior to 1959 are from Joos and Spahni (2008) with uncertainties equivalent to about $\pm 0.1\text{--}0.15 \text{ GtC yr}^{-1}$ and from Lan et al. (2023) since 1959 with uncertainties of about $\pm 0.07 \text{ GtC yr}^{-1}$ during 1959–1979 and $\pm 0.02 \text{ GtC yr}^{-1}$ since 1980. The S_{OCEAN} estimate is the average from Khatiwala et al. (2013) and DeVries (2014) with uncertainty of about $\pm 30\%$ prior to 1959, and the average of an ensemble of models and an ensemble of $f\text{CO}_2$ -products (Table 4) with uncertainties of about $\pm 0.4 \text{ GtC yr}^{-1}$ since 1959. The S_{LAND} estimate is the average of an ensemble of models (Table 4) with uncertainties of about $\pm 1 \text{ GtC yr}^{-1}$. See the text for more details of each component and their uncertainties.

Formatted: Heading 2

Formatted ... [13]

Formatted ... [14]

Formatted ... [15]

Formatted: Font: Not Bold

Formatted: Font: Not Bold

Formatted ... [16]

Formatted ... [17]

Formatted ... [18]

Deleted: ,

Formatted ... [19]

Formatted ... [20]

Formatted ... [21]

Formatted ... [22]

Formatted ... [23]

Formatted ... [24]

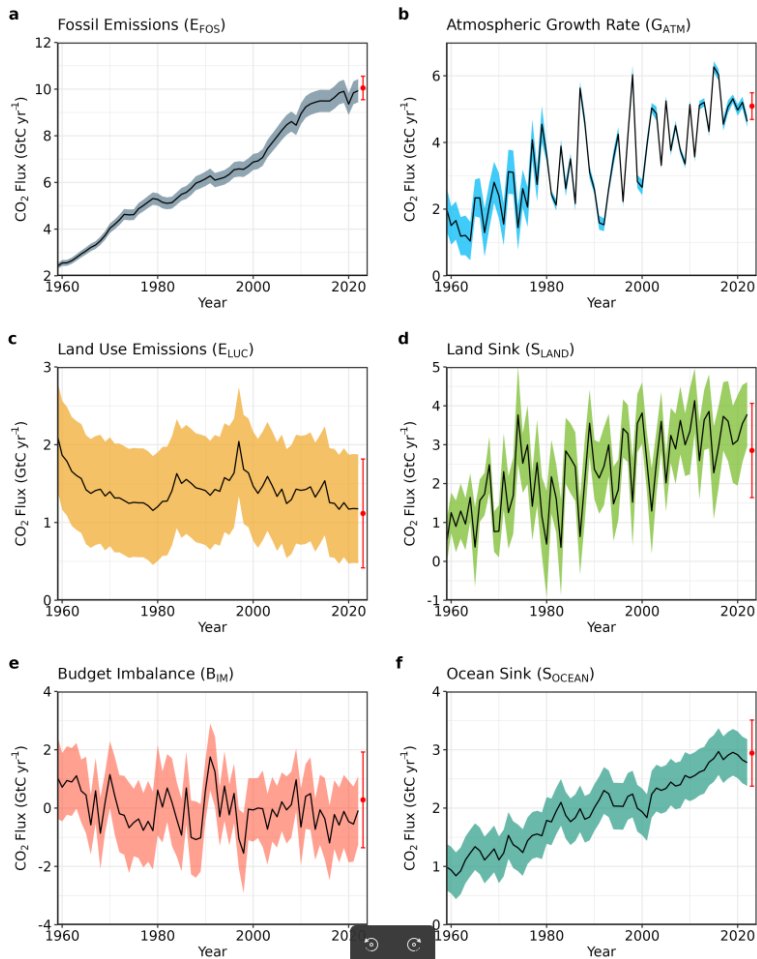
Formatted ... [25]

Formatted ... [26]

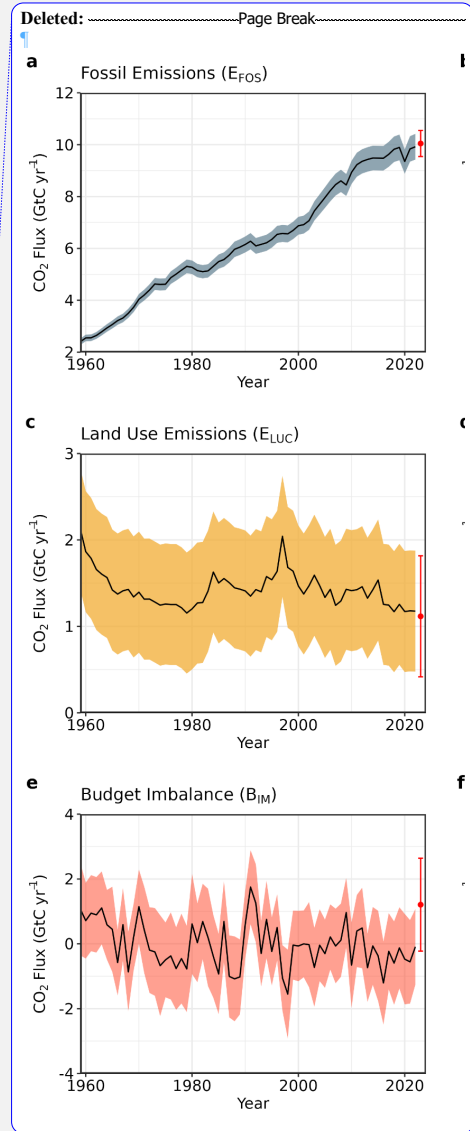
Formatted: Default Paragraph Font, Font colour: Black

Formatted: Normal, Centred, Border: Top: (No border), Bottom: (No border), Left: (No border), Right: (No border), Between: (No border), Tab stops: 7.96 cm, Centred + 15.92 cm, Right, Position: Horizontal: Left, Relative to: Column, Vertical: In line, Relative to: Margin, Wrap Around

Formatted: Font colour: Black



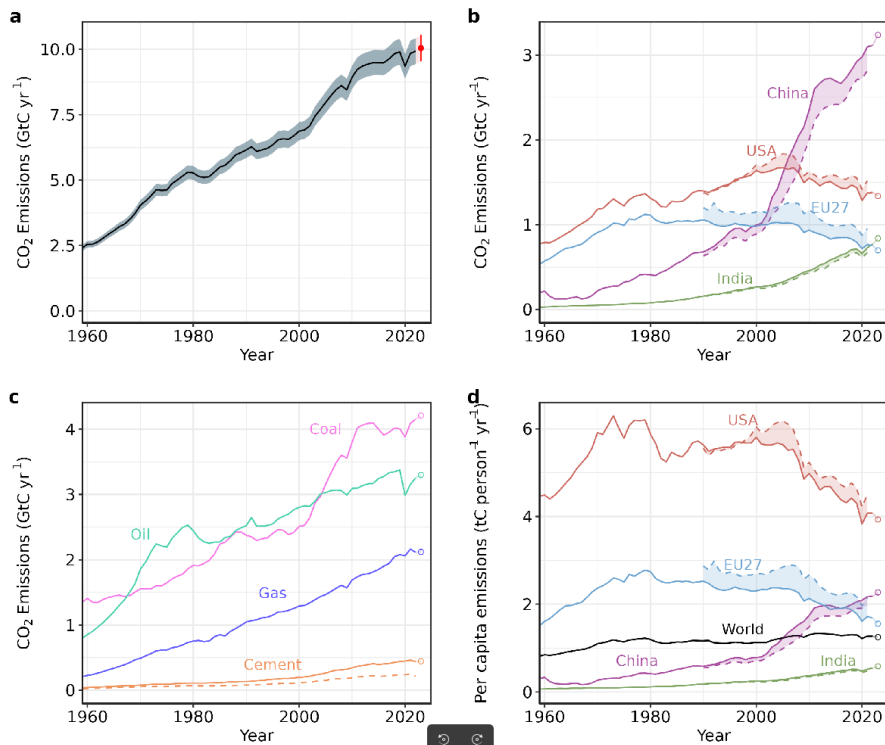
3707
3708 **Figure 4.** Components of the global carbon budget and their uncertainties as a function of time, presented
3709 individually for (a) fossil CO₂ and cement carbonation emissions (E_{FOS}), (b) growth rate in atmospheric CO₂
3710 concentration (G_{ATM}), (c) emissions from land-use change (E_{LUC}), (d) the land CO₂ sink (S_{LAND}), (e) the ocean
3711 CO₂ sink (S_{OCEAN}), (f) the budget imbalance that is not accounted for by the other terms. Positive values of
3712 S_{LAND} and S_{OCEAN} represent a flux from the atmosphere to land or the ocean. All data are in GtC yr⁻¹ with the
3713 uncertainty bounds representing ± 1 standard deviation in shaded colour. Data sources are as in Figure 3. The red
3714 dots indicate our projections for the year 2023 and the red error bars the uncertainty in the projections (see
3715 methods).



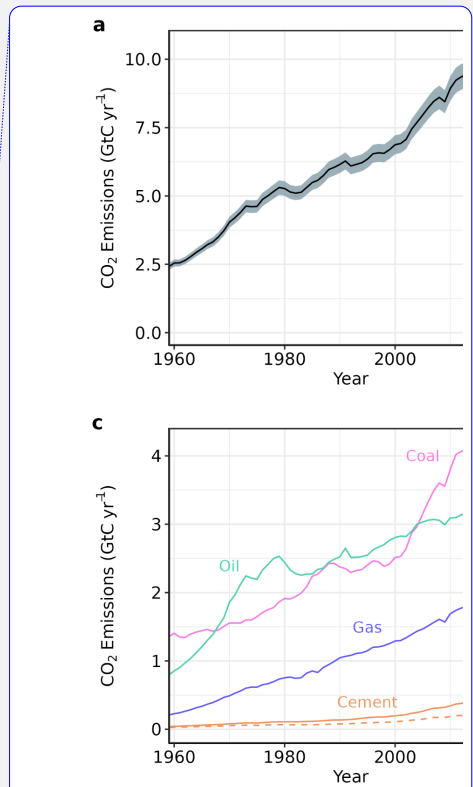
Formatted: Default Paragraph Font, Font colour: Black

Formatted: Normal, Centred, Border: Top: (No border), Bottom: (No border), Left: (No border), Right: (No border), Between: (No border), Tab stops: 7.96 cm, Centred + 15.92 cm, Right, Position: Horizontal: Left, Relative to: Column, Vertical: In line, Relative to: Margin, Wrap Around

Formatted: Font colour: Black

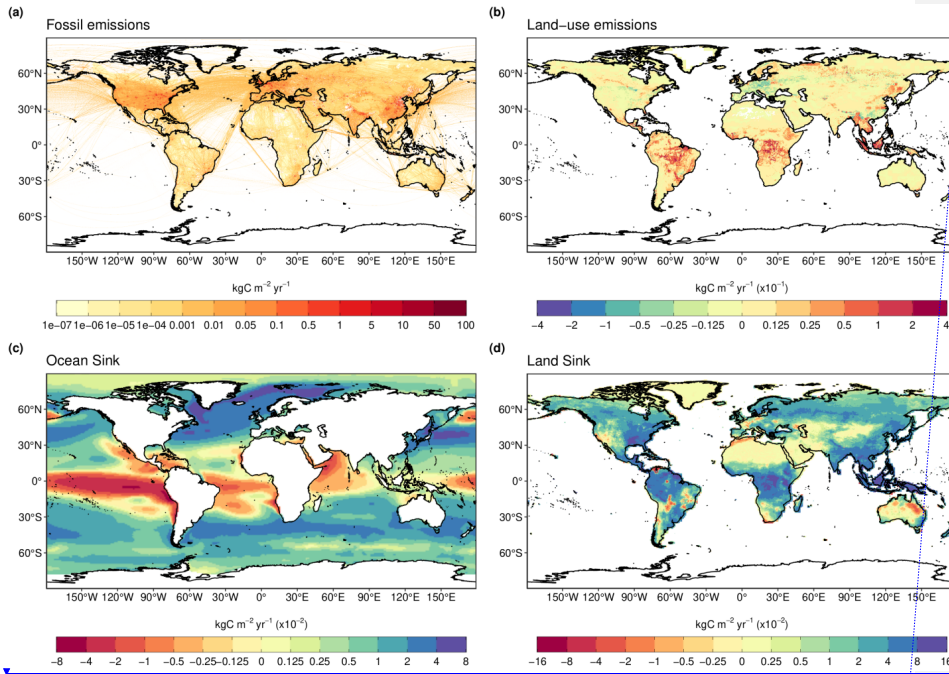


3719 **Figure 5.** Fossil CO₂ emissions for (a) the globe, including an uncertainty of $\pm 5\%$ (grey shading) and a
 3720 projection through the year 2023 (red dot and uncertainty range), (b) territorial (solid lines) and consumption
 3721 (dashed lines) emissions for the top three country emitters (USA, China, India) and for the European Union
 3722 (EU27), (c) global emissions by fuel type, including coal, oil, gas, and cement, and cement minus cement
 3723 carbonation (dashed), and (d) per-capita emissions the world and for the large emitters as in panel (b). Territorial
 3724 emissions are primarily from a draft update of Gilfillan and Marland (2021) except for national data for Annex I
 3725 countries for 1990-2021, which are reported to the UNFCCC as detailed in the text, as well as some
 3726 improvements in individual countries, and extrapolated forward to 2022 using data from Energy Institute.
 3727 Consumption-based emissions are updated from Peters et al. (2011a). See Section 2.1 and Supplement S.1 for
 3728 details of the calculations and data sources.

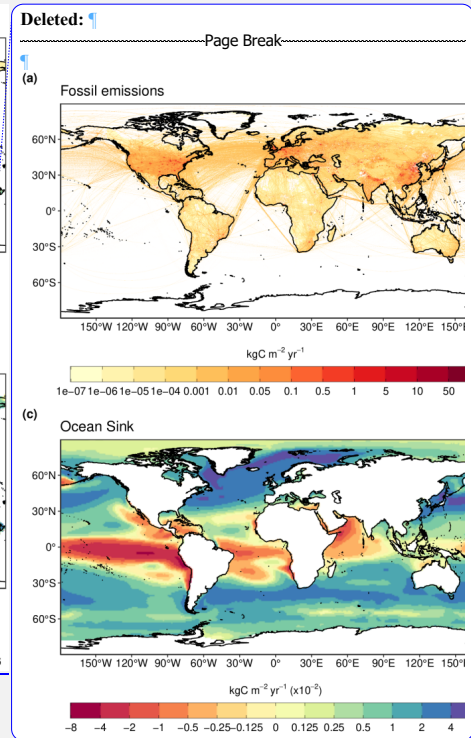


Deleted:
Formatted: Font: Not Bold
Formatted: Heading 2

Formatted: Default Paragraph Font, Font colour: Black
Formatted: Normal, Centred, Border: Top: (No border), Bottom: (No border), Left: (No border), Right: (No border), Between : (No border), Tab stops: 7.96 cm, Centred + 15.92 cm, Right, Position: Horizontal: Left, Relative to: Column, Vertical: In line, Relative to: Margin, Wrap Around
Formatted: Font colour: Black



3731 **Figure 6.** The 2013-2022 decadal mean components of the global carbon budget, presented for (a) fossil CO₂
 3732 emissions (E_{FOS}), (b) land-use change emissions (E_{LUC}), (c) the ocean CO₂ sink (S_{OCEAN}), and (d) the land CO₂
 3733 sink (S_{LAND}). Positive values for E_{FOS} and E_{LUC} represent a flux to the atmosphere, whereas positive values of
 3734 S_{OCEAN} and S_{LAND} represent a flux from the atmosphere to the ocean or the land (carbon sink). In all panels,
 3735 yellow/red colours represent a source (flux from the land/ocean to the atmosphere), green/blue colours represent
 3736 a sink (flux from the atmosphere into the land/ocean). All units are in $\text{kgC m}^{-2} \text{yr}^{-1}$. Note the different scales in
 3737 each panel. E_{FOS} data shown is from GCP-GridFEDv2023. and does not include cement carbonation. The E_{LUC}
 3738 map shows the average E_{LUC} from the three bookkeeping models plus emissions from peat drainage and peat
 3739 fires. Gridded E_{LUC} estimates for H&C2023 and OSCAR are derived by spatially distributing their national data
 3740 based on the spatial patterns of BLUE gross fluxes in each country (see Schwingshackl et al., 2022, for more
 3741 details about the methodology). S_{OCEAN} data shown is the average of GOBMs and data-products means, using
 3742 GOBMs simulation A, no adjustment for bias and drift applied to the gridded fields (see Section 2.5). S_{LAND} data
 3743 shown is the average of the DGVMs for simulation S2 (see Section 2.6).
 3744
 3745



Formatted: Font: Not Bold

Formatted: Heading 2

Deleted: .

Formatted: Font: Not Bold

Formatted: Default Paragraph Font, Font colour: Black

Formatted: Normal, Centred, Border: Top: (No border), Bottom: (No border), Left: (No border), Right: (No border), Between : (No border), Tab stops: 7.96 cm, Centred + 15.92 cm, Right, Position: Horizontal: Left, Relative to: Column, Vertical: In line, Relative to: Margin, Wrap Around

Formatted: Font colour: Black

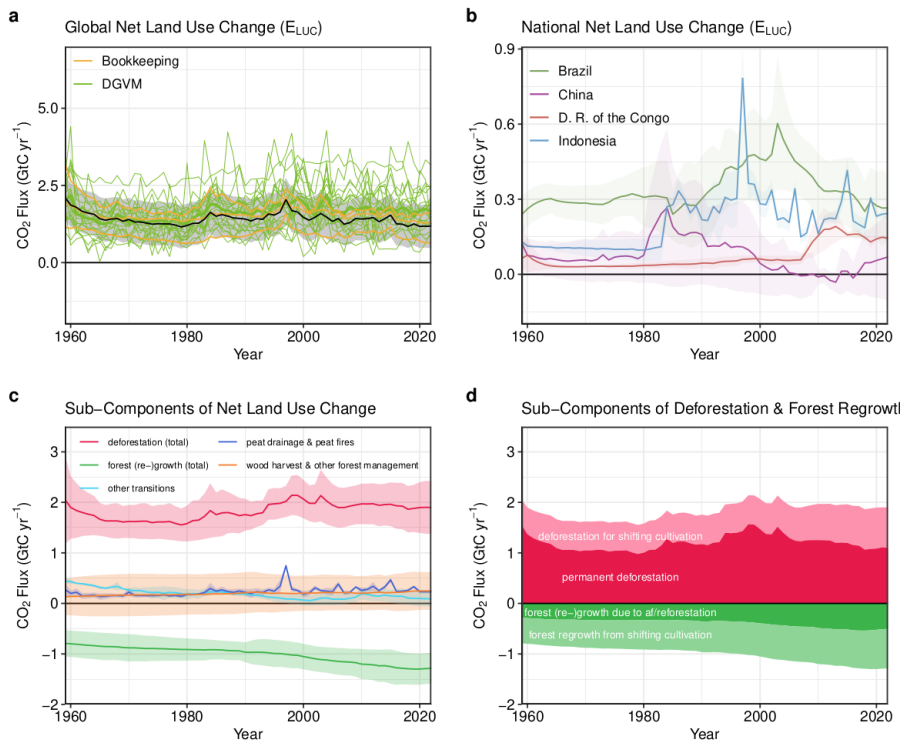
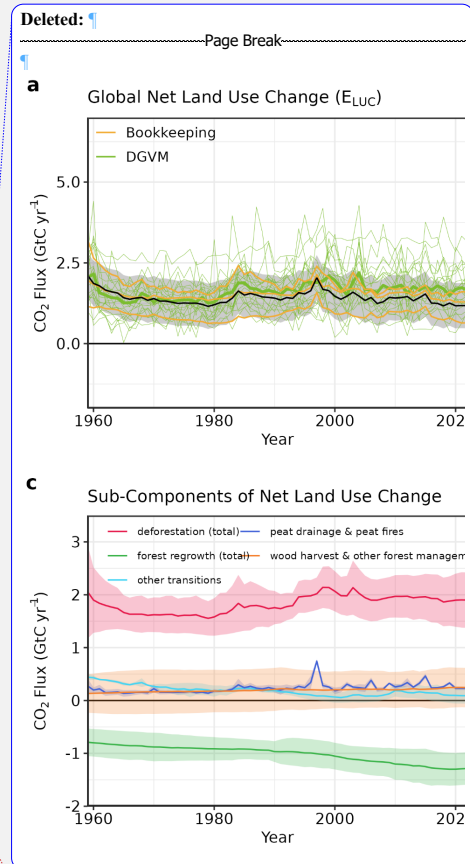


Figure 7. Net CO₂ exchanges between the atmosphere and the terrestrial biosphere related to land use change.

(a) Net CO₂ emissions from land-use change (E_{LUC}) with estimates from the three bookkeeping models (yellow lines) and the budget estimate (black with $\pm 1\sigma$ uncertainty), which is the average of the three bookkeeping models. Estimates from individual DGVMs (narrow green lines) and the DGVM ensemble mean (thick green line) are also shown. (b) Net CO₂ emissions from land-use change from the four countries with largest cumulative emissions since 1959. Values shown are the average of the three bookkeeping models, with shaded regions as $\pm 1\sigma$ uncertainty. (c) Sub-components of E_{LUC}: (i) emissions from deforestation (including permanent deforestation and deforestation in shifting cultivation cycles), (ii) emissions from peat drainage & peat fires, (iii) removals from forest (re-)growth (including forest (re-)growth due to afforestation and reforestation and forest regrowth in shifting cultivation cycles), (iv) fluxes from wood harvest and other forest management (comprising slash and product decay following wood harvest, regrowth after wood harvest, and fire suppression), and (v) emissions and removals related to other land-use transitions. The sum of the five components is E_{LUC} shown in panel (a). (d) Sub-components of 'deforestation (total)' and of 'forest (re-)growth (total)': (i) deforestation in shifting cultivation cycles, (ii) permanent deforestation, (iii) forest (re-)growth due to afforestation and/or reforestation, and (iv) forest regrowth in shifting cultivation cycles.



Formatted: Font: Not Bold

Formatted: Heading 2

Formatted: Default Paragraph Font, Font colour: Black

Formatted: Normal, Centred, Border: Top: (No border), Bottom: (No border), Left: (No border), Right: (No border), Between: (No border), Tab stops: 7.96 cm, Centred + 15.92 cm, Right, Position: Horizontal: Left, Relative to: Column, Vertical: In line, Relative to: Margin, Wrap Around

Formatted: Font colour: Black

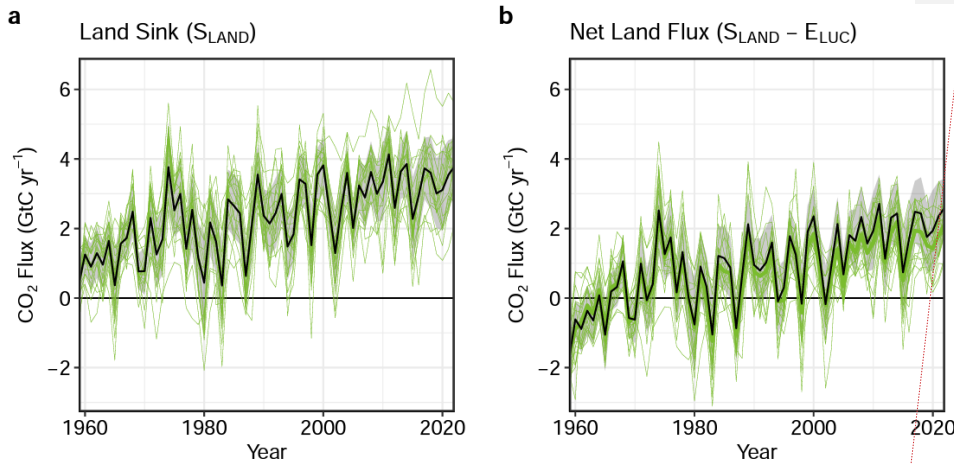
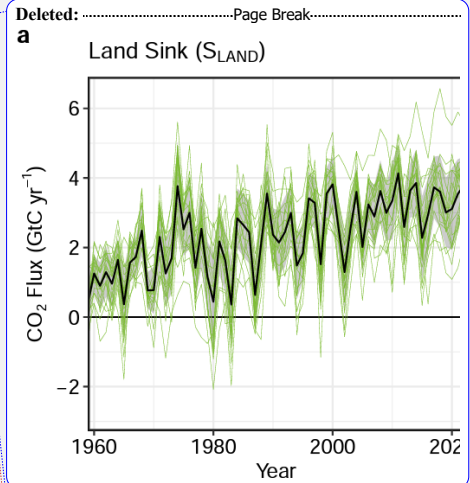


Figure 8. (a) The land CO₂ sink (S_{LAND}) estimated by individual DGVMs (green), as well as the budget estimate (black with $\pm 1\sigma$ uncertainty), which is the average of all DGVMs. (b) Net atmosphere-land CO₂ fluxes ($S_{LAND} - E_{LUC}$). The budget estimate of the net land flux (black with $\pm 1\sigma$ uncertainty) combines the DGVM estimate of S_{LAND} from panel (a) with the bookkeeping estimate of E_{LUC} from Figure 7a. Uncertainties are similarly propagated in quadrature. DGVMs also provide estimates of E_{LUC} (see Figure 7a), which can be combined with their own estimates of the land sink. Hence panel (b) also includes an estimate for the net land flux for individual DGVMs (thin green lines) and their multi-model mean (thick green line).

Formatted: Font: Not Bold



Deleted: : Page Break

Formatted: Font: Not Bold

Deleted:

Formatted: Font: 10 pt

Deleted: : Page Break

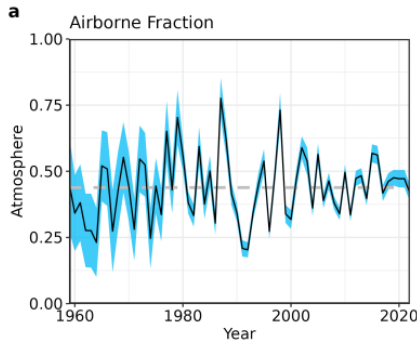
<object>

Formatted: Default Paragraph Font, Font colour: Black

Formatted: Normal, Centred, Border: Top: (No border), Bottom: (No border), Left: (No border), Right: (No border), Between: (No border), Tab stops: 7.96 cm, Centred + 15.92 cm, Right, Position: Horizontal: Left, Relative to: Column, Vertical: In line, Relative to: Margin, Wrap Around

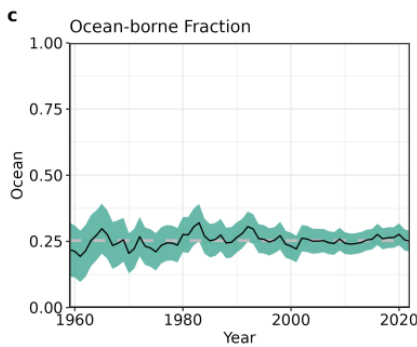
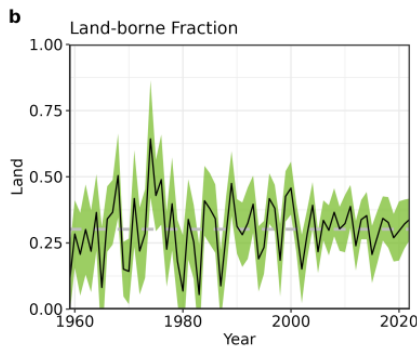
Formatted: Font colour: Black

3788



Formatted: Font: Not Bold

Formatted: Indent: Left: 0 cm



Formatted: Font: Bold

3833 **Figure 9.** The partitioning of total anthropogenic CO₂ emissions ($E_{FOS} + E_{LUC}$) across (a) the atmosphere
3834 (airborne fraction), (b) land (land-borne fraction), and (c) ocean (ocean-borne fraction). Black lines represent the
3835 central estimate, and the coloured shading represents the uncertainty. The grey dashed lines represent the long-
3836 term average of the airborne (44%), land-borne (30%) and ocean-borne (25%) fractions during 1960-2022 (with
3837 a B_{IM} of 1%).

Formatted: Font: Not Bold

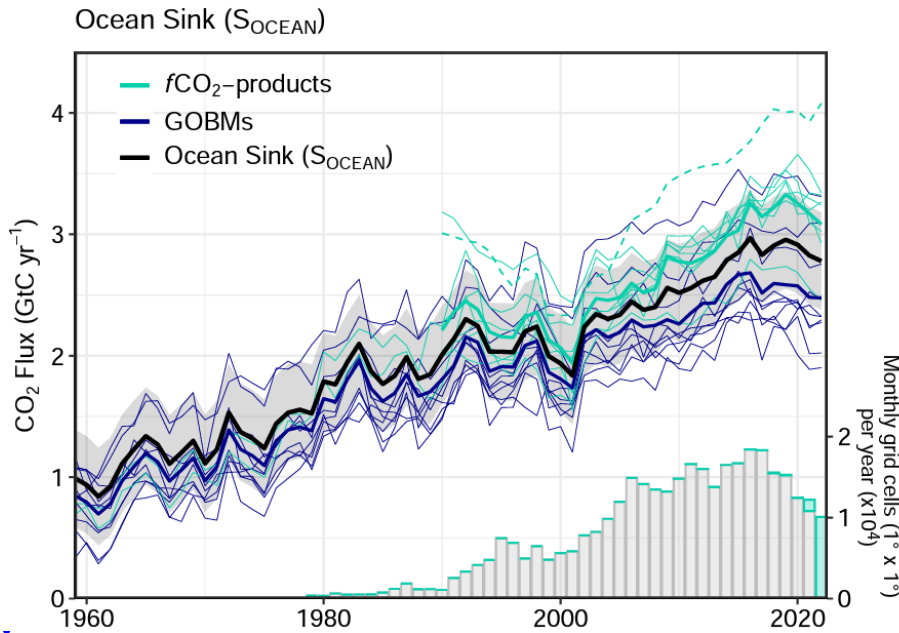
Formatted: Font: Not Bold, Subscript

Formatted: Font: Not Bold

Formatted: Default Paragraph Font, Font colour: Black

Formatted: Normal, Centred, Border: Top: (No border),
Bottom: (No border), Left: (No border), Right: (No border),
Between : (No border), Tab stops: 7.96 cm, Centred + 15.92
cm, Right, Position: Horizontal: Left, Relative to: Column,
Vertical: In line, Relative to: Margin, Wrap Around

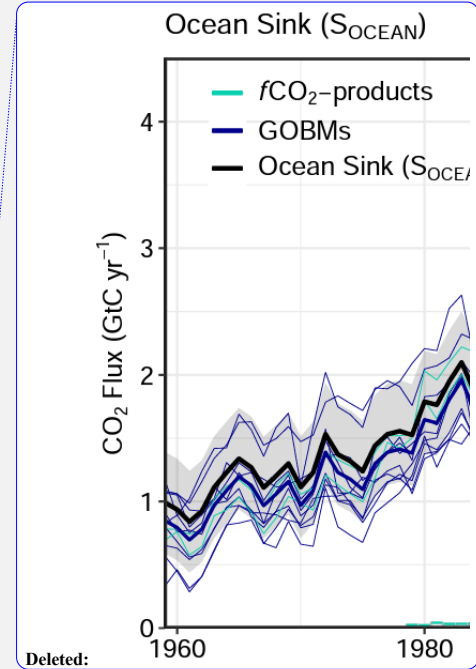
Formatted: Font colour: Black



3839

3840 **Figure 10.** Comparison of the anthropogenic atmosphere-ocean CO₂ flux showing the budget values of S_{OCEAN}
 3841 (black; with the uncertainty in grey shading), individual ocean models (royal blue), and the ocean fCO_2 -products
 3842 (cyan; with Watson et al. (2020) in dashed line as not used for ensemble mean). Only one fCO_2 -product (Jena-
 3843 MLS) extends back to 1959 (Rödenbeck et al., 2022). The fCO_2 -products were adjusted for the pre-industrial
 3844 ocean source of CO₂ from river input to the ocean, by subtracting a source of 0.65 GtC yr⁻¹ to make them
 3845 comparable to S_{OCEAN} (see Section 2.5). Bar-plot in the lower right illustrates the number of fCO_2 observations
 3846 in the SOCAT v2023 database (Bakker et al., 2023). Grey bars indicate the number of data points in SOCAT
 3847 v2022, and coloured bars the newly added observations in v2023.

3848



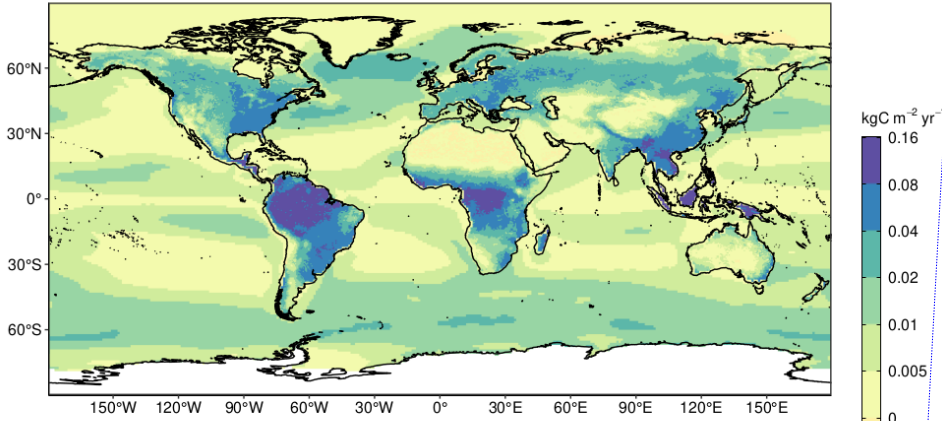
Deleted:

Formatted: Default Paragraph Font, Font colour: Black

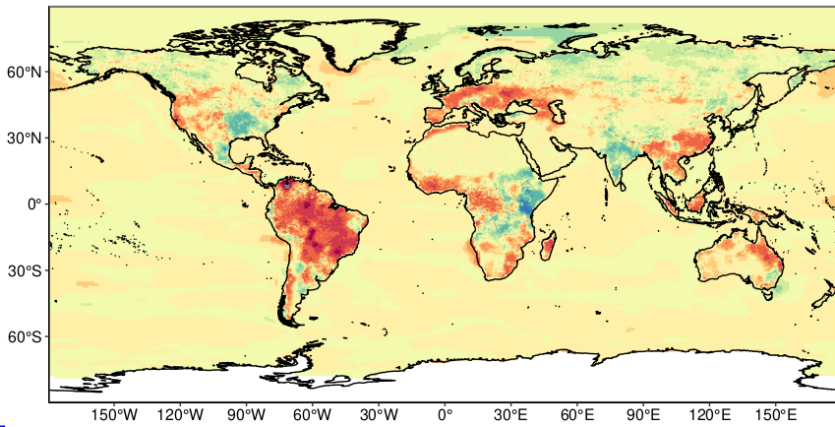
Formatted: Normal, Centred, Border: Top: (No border),
 Bottom: (No border), Left: (No border), Right: (No border),
 Between : (No border), Tab stops: 7.96 cm, Centred + 15.92
 cm, Right, Position: Horizontal: Left, Relative to: Column,
 Vertical: In line, Relative to: Margin, Wrap Around

Formatted: Font colour: Black

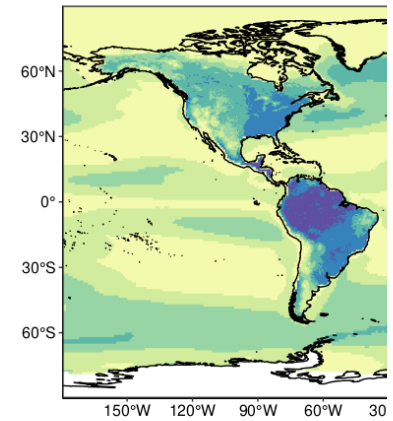
a CO₂ effect



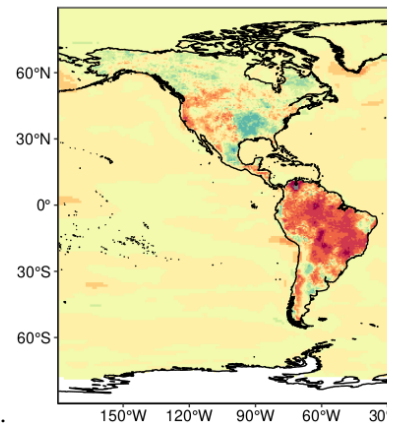
b Climate effect



a CO₂ effect



b Climate effect



Deleted:

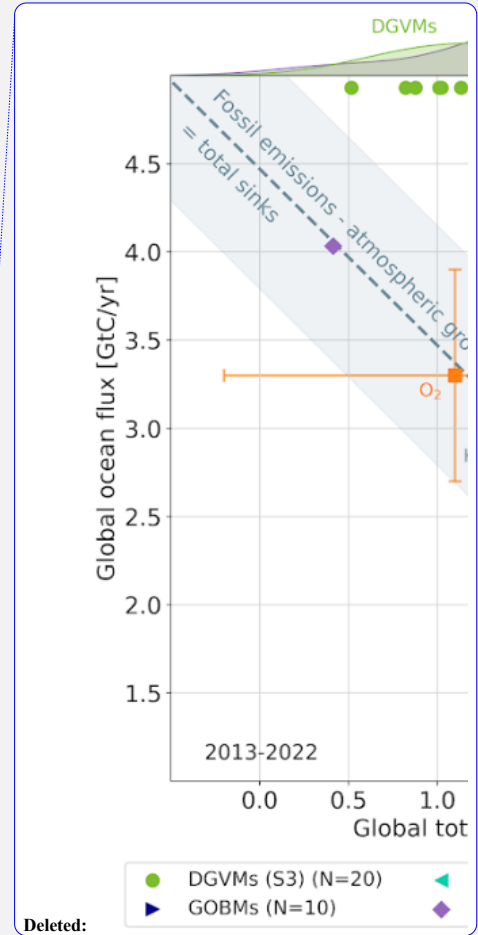
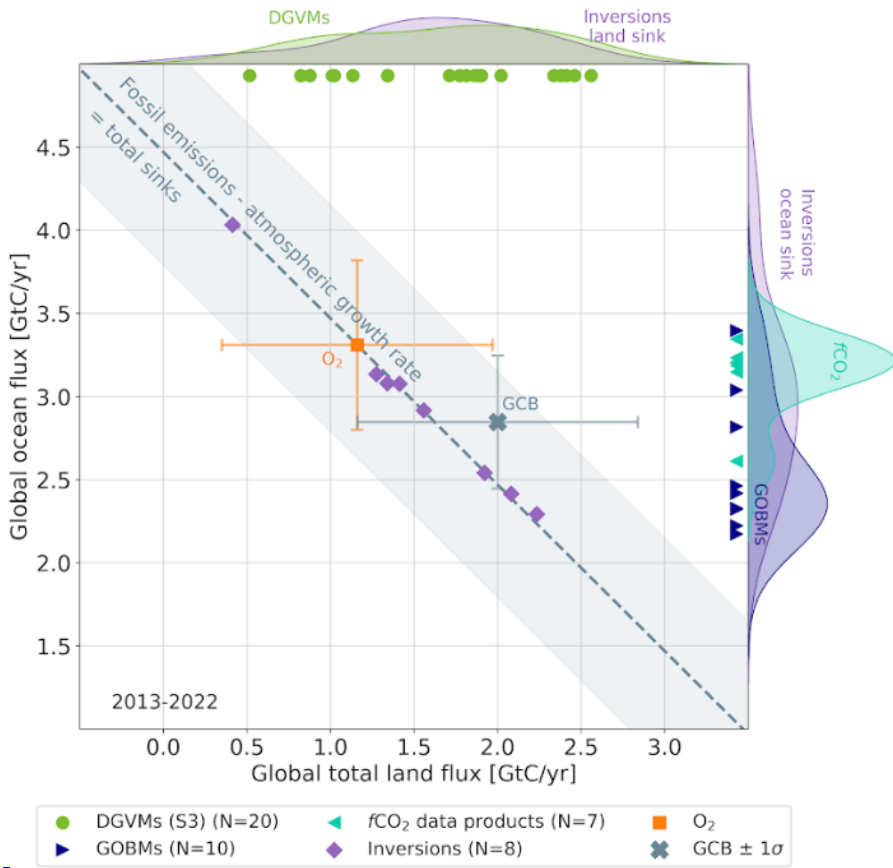
Figure 11. Attribution of the atmosphere-ocean (S_{OCEAN}) and atmosphere-land (S_{LAND}) CO₂ fluxes to (a) increasing atmospheric CO₂ concentrations and (b) changes in climate, averaged over the previous decade 2013-2022. All data shown is from the processed-based GOBMs and DGVMs. Note that the sum of ocean CO₂ and climate effects shown here will not equal the ocean sink shown in Figure 6 which includes the fCO_2 -products. See Supplement S.3.2 and S.4.1 for attribution methodology. Units are in kgC m⁻² yr⁻¹ (note the non-linear colour scale).

Formatted: Font: Bold

Formatted: Default Paragraph Font, Font colour: Black

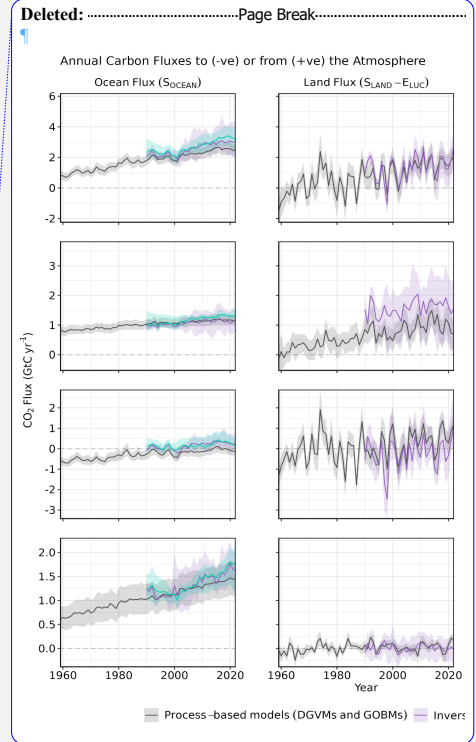
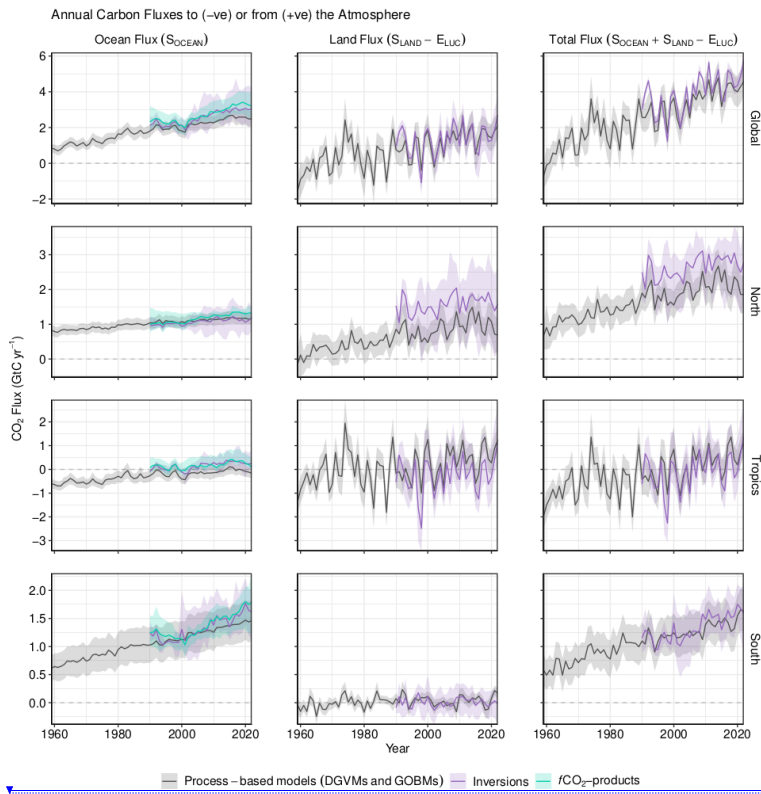
Formatted: Normal, Centred, Border: Top: (No border), Bottom: (No border), Left: (No border), Right: (No border), Between: (No border), Tab stops: 7.96 cm, Centred + 15.92 cm, Right, Position: Horizontal: Left, Relative to: Column, Vertical: In line, Relative to: Margin, Wrap Around

Formatted: Font colour: Black



3859
 3860 **Figure 12.** The 2013-2022 decadal mean [global](#) net atmosphere-ocean and atmosphere-land fluxes derived from
 3861 the ocean models and $f\text{CO}_2$ products (y-axis, right and left pointing blue triangles respectively), and from the
 3862 DGVMs (x-axis, green symbols), and the same fluxes estimated from the [atmospheric](#) inversions (purple
 3863 symbols). The shaded distributions show the densities of the ensembles of individual estimates. The grey central
 3864 cross is the mean ($\pm 1\sigma$) of S_{OCEAN} and ($S_{\text{LAND}} - E_{\text{LUC}}$) as assessed in this budget. The grey diagonal line
 3865 represents the [constraint on the](#) global land + ocean net flux, i.e. global fossil fuel emissions minus the
 3866 atmospheric growth rate from this budget ($E_{\text{FOS}} - G_{\text{ATM}}$). The orange [cross](#) represents the [same global net](#)
 3867 [atmosphere-ocean and atmosphere-land fluxes](#) as estimated from the atmospheric O_2 constraint ($\pm 1\sigma$ for each of
 3868 the fluxes although caution is needed to interpret these error bars, since solutions outside the grey band are
 3869 unlikely, as outside of the 1σ uncertainty). Positive values are CO_2 sinks. Note that the inverse estimates have
 3870 been scaled for a minor difference between E_{FOS} and GridFEDv2023.1 (Jones et al., 2023).

- Deleted: square
- Deleted: sink
- Deleted: .
- Formatted: Font: Bold
- Formatted: Default Paragraph Font, Font colour: Black
- Formatted: Normal, Centred, Border: Top: (No border), Bottom: (No border), Left: (No border), Right: (No border), Between: (No border), Tab stops: 7.96 cm, Centred + 15.92 cm, Right, Position: Horizontal: Left, Relative to: Column, Vertical: In line, Relative to: Margin, Wrap Around
- Formatted: Font colour: Black



3875

Formatted: Default Paragraph Font, Font colour: Black

Formatted: Normal, Centred, Border: Top: (No border), Bottom: (No border), Left: (No border), Right: (No border), Between : (No border), Tab stops: 7.96 cm, Centred + 15.92 cm, Right, Position: Horizontal: Left, Relative to: Column, Vertical: In line, Relative to: Margin, Wrap Around

Formatted: Font colour: Black

3879 **Figure 13.** CO₂ fluxes between the atmosphere and the Earth's surface separated between land and oceans,
3880 globally and in three latitude bands. The ocean flux is S_{OCEAN} and the land flux is the net atmosphere-land fluxes
3881 from the DGVMs. The latitude bands are (top row) global, (2nd row) north (>30°N), (3rd row) tropics (30°S-
3882 30°N), and (bottom row) south (<30°S), and over ocean (left column), land (middle column), and total (right
3883 column). Estimates are shown for: process-based models (DGVMs for land, GOBMs for oceans); inversion
3884 systems (land and ocean); and $f\text{CO}_2$ -products (ocean only). Positive values are CO₂ sinks. Mean estimates from
3885 the combination of the process models for the land and oceans are shown (black line) with $\pm 1\sigma$ of the model
3886 ensemble (grey shading). For the total uncertainty in the process-based estimate of the total sink, uncertainties
3887 are summed in quadrature. Mean estimates from the atmospheric inversions are shown (purple lines) with their
3888 full spread (purple shading). Mean estimates from the $f\text{CO}_2$ -products are shown for the ocean domain (light blue
3889 lines) with full model spread (light blue shading). The global S_{OCEAN} (upper left) and the sum of S_{OCEAN} in all
3890 three regions represents the anthropogenic atmosphere-to-ocean flux based on the assumption that the
3891 preindustrial ocean sink was 0 GtC yr⁻¹ when riverine fluxes are not considered. This assumption does not hold
3892 at the regional level, where preindustrial fluxes can be significantly different from zero. Hence, the regional
3893 panels for S_{OCEAN} represent a combination of natural and anthropogenic fluxes. Bias-correction and area-
3894 weighting were only applied to global S_{OCEAN} ; hence the sum of the regions is slightly different from the global
3895 estimate (<0.05 GtC yr⁻¹).

Formatted: Font: Bold

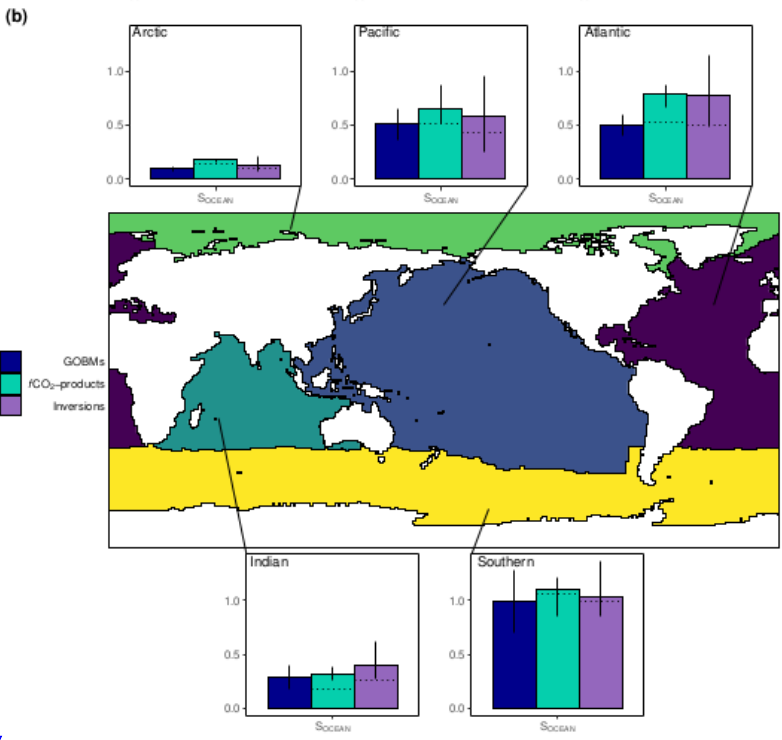
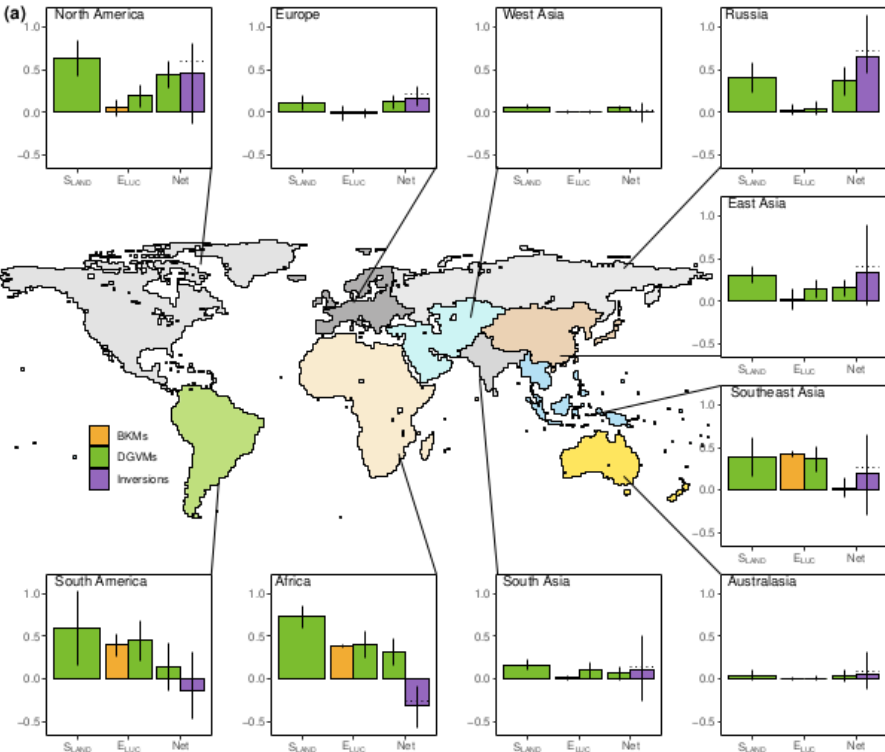
Deleted: standard deviation (1σ)

Formatted: Font: Bold

Formatted: Default Paragraph Font, Font colour: Black

Formatted: Normal, Centred, Border: Top: (No border), Bottom: (No border), Left: (No border), Right: (No border), Between : (No border), Tab stops: 7.96 cm, Centred + 15.92 cm, Right, Position: Horizontal: Left, Relative to: Column, Vertical: In line, Relative to: Margin, Wrap Around

Formatted: Font colour: Black



Deleted:Page Break..... [27]

Formatted: Default Paragraph Font, Font colour: Black
 Formatted: Normal, Centred, Border: Top: (No border), Bottom: (No border), Left: (No border), Right: (No border), Between : (No border), Tab stops: 7.96 cm, Centred + 15.92 cm, Right, Position: Horizontal: Left, Relative to: Column, Vertical: In line, Relative to: Margin, Wrap Around
 Formatted: Font colour: Black

3903 **Figure 14.** Decadal mean (a) land and (b) ocean fluxes for RECCAP-2 regions over 2013-2022. For land fluxes,
3904 S_{LAND} is estimated by the DGVMs (green bars), with the error bar as $\pm 1\sigma$ spread among models. A positive
3905 S_{LAND} is a net transfer of carbon from the atmosphere to the land. E_{LUC} fluxes are shown for both DGVMs
3906 (green) and bookkeeping models (orange), again with the uncertainty calculated as the $\pm 1\sigma$ spread. Note, a
3907 positive E_{LUC} flux indicates a loss of carbon from the land. The net land flux is shown for both DGVMs (green)
3908 and atmospheric inversions (purple), including the full model spread for inversions. The net ocean sink (S_{OCEAN})
3909 is estimated by GOBMs (royal blue), fCO_2 -products (cyan), and atmospheric inversions (purple). Uncertainty is
3910 estimated as the $\pm 1\sigma$ spread for GOBMs, and the full model spread for the other two products. The dotted lines
3911 show the fCO_2 -products and inversion results without river flux adjustment. Positive values are CO_2 sinks.

Formatted: Font: Bold

Formatted: Default Paragraph Font, Font colour: Black

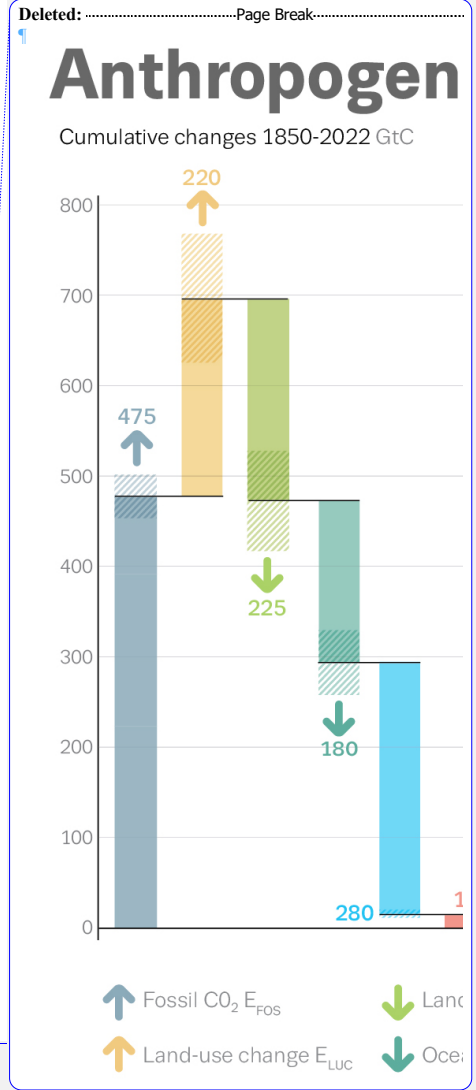
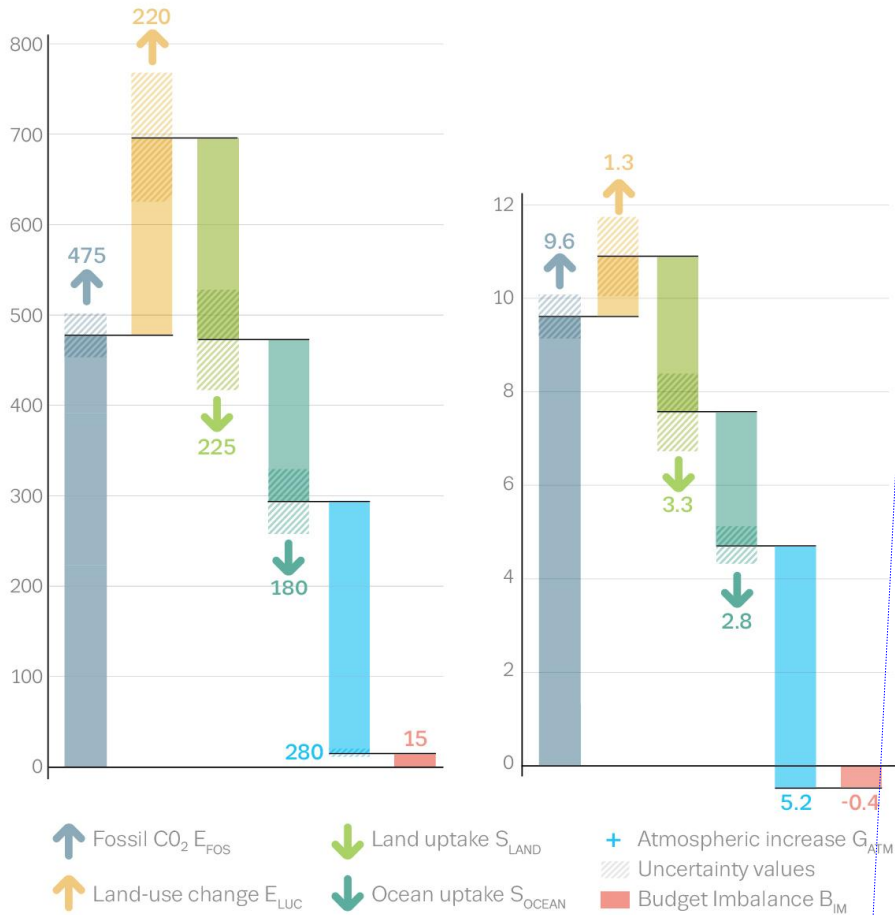
Formatted: Normal, Centred, Border: Top: (No border), Bottom: (No border), Left: (No border), Right: (No border), Between : (No border), Tab stops: 7.96 cm, Centred + 15.92 cm, Right, Position: Horizontal: Left, Relative to: Column, Vertical: In line, Relative to: Margin, Wrap Around

Formatted: Font colour: Black

Anthropogenic carbon flows

Cumulative changes 1850-2022 GtC

Mean fluxes 2013-2022 GtC per year



3912

3913 **Figure 15.** Cumulative changes over the 1850-2022 period (left) and average fluxes over the 2013-2022 period
 3914 (right) for the anthropogenic perturbation of the global carbon cycle. See the caption of Figure 3 for key
 3915 information and the methods in text for full details.

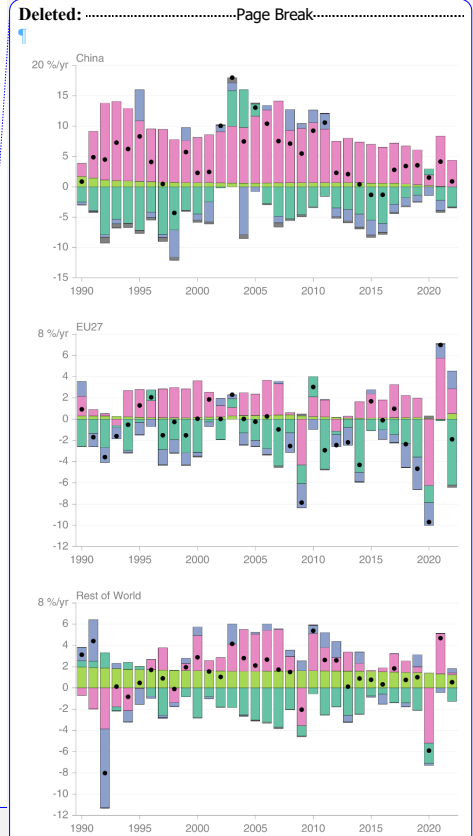
Formatted: Font: Not Bold

Formatted: Heading 2

Formatted: Default Paragraph Font, Font colour: Black

Formatted: Normal, Centred, Border: Top: (No border), Bottom: (No border), Left: (No border), Right: (No border), Between : (No border), Tab stops: 7.96 cm, Centred + 15.92 cm, Right, Position: Horizontal: Left, Relative to: Column, Vertical: In line, Relative to: Margin, Wrap Around

Formatted: Font colour: Black



3919

3920 **Figure 16.** Kaya decomposition of the main drivers of fossil CO₂ emissions, considering population, GDP per
 3921 person, Energy per GDP, and CO₂ emissions per energy, for China (top left), USA (top right), EU27 (middle
 3922 left), India (middle right), Rest of the World (bottom left), and World (bottom right). Black dots are the annual
 3923 fossil CO₂ emissions growth rate, coloured bars are the contributions from the different drivers to this growth
 3924 rate. A general trend is that population and GDP growth put upward pressure on emissions (positive values),
 3925 while energy per GDP and, more recently, CO₂ emissions per energy put downward pressure on emissions
 3926 (negative values). Both the COVID-19 induced drop during 2020 and the recovery in 2021 led to a stark contrast
 3927 to previous years, with different drivers in each region. The EU27 had strong Energy/GDP improvements in
 3928 2022.

Formatted: Font: Not Bold
 Formatted: Heading 2
 Deleted: .
 Deleted: ,
 Formatted: Font: Not Bold
 Formatted: Font: Not Bold
 Deleted: .
 Deleted: changes
 Formatted: Font: Not Bold
 Formatted: Font: Not Bold
 Deleted: ¶

Formatted: Default Paragraph Font, Font colour: Black
 Formatted
 Formatted: Font colour: Black

Page 1: [1] Formatted **Friedlingstein, Pierre** **12/11/2023 15:12:00**

Normal, Centred, Border: Top: (No border), Bottom: (No border), Left: (No border), Right: (No border),
Between : (No border), Tab stops: 7.96 cm, Centred + 15.92 cm, Right, Position: Horizontal: Left, Relative to:
Column, Vertical: In line, Relative to:

Page 1: [2] Deleted **Friedlingstein, Pierre** **12/11/2023 15:12:00**

▼

Page 1: [2] Deleted **Friedlingstein, Pierre** **12/11/2023 15:12:00**

▼

Page 1: [2] Deleted **Friedlingstein, Pierre** **12/11/2023 15:12:00**

▼

Page 1: [2] Deleted **Friedlingstein, Pierre** **12/11/2023 15:12:00**

▼

Page 1: [2] Deleted **Friedlingstein, Pierre** **12/11/2023 15:12:00**

▼

Page 1: [2] Deleted **Friedlingstein, Pierre** **12/11/2023 15:12:00**

▼

Page 1: [2] Deleted **Friedlingstein, Pierre** **12/11/2023 15:12:00**

▼

Page 1: [2] Deleted **Friedlingstein, Pierre** **12/11/2023 15:12:00**

▼

Page 1: [2] Deleted **Friedlingstein, Pierre** **12/11/2023 15:12:00**

▼.....
Page 1: [2] Deleted **Friedlingstein, Pierre** **12/11/2023 15:12:00**

▼.....
Page 1: [2] Deleted **Friedlingstein, Pierre** **12/11/2023 15:12:00**

▼.....
Page 1: [2] Deleted **Friedlingstein, Pierre** **12/11/2023 15:12:00**

▼.....
Page 1: [2] Deleted **Friedlingstein, Pierre** **12/11/2023 15:12:00**

▼.....
Page 1: [2] Deleted **Friedlingstein, Pierre** **12/11/2023 15:12:00**

▼.....
Page 1: [2] Deleted **Friedlingstein, Pierre** **12/11/2023 15:12:00**

▼.....
Page 1: [2] Deleted **Friedlingstein, Pierre** **12/11/2023 15:12:00**

▼.....
Page 1: [2] Deleted **Friedlingstein, Pierre** **12/11/2023 15:12:00**

▼.....
Page 1: [2] Deleted **Friedlingstein, Pierre** **12/11/2023 15:12:00**

▼.....
Page 1: [2] Deleted **Friedlingstein, Pierre** **12/11/2023 15:12:00**

▼.....

Page 1: [2] Deleted	Friedlingstein, Pierre	12/11/2023 15:12:00
---------------------	------------------------	---------------------

▼.....

Page 1: [2] Deleted	Friedlingstein, Pierre	12/11/2023 15:12:00
---------------------	------------------------	---------------------

▼.....

Page 1: [2] Deleted	Friedlingstein, Pierre	12/11/2023 15:12:00
---------------------	------------------------	---------------------

▼.....

Page 1: [2] Deleted	Friedlingstein, Pierre	12/11/2023 15:12:00
---------------------	------------------------	---------------------

▼.....

Page 1: [2] Deleted	Friedlingstein, Pierre	12/11/2023 15:12:00
---------------------	------------------------	---------------------

▼.....

Page 1: [2] Deleted	Friedlingstein, Pierre	12/11/2023 15:12:00
---------------------	------------------------	---------------------

▼.....

Page 1: [2] Deleted	Friedlingstein, Pierre	12/11/2023 15:12:00
---------------------	------------------------	---------------------

▼.....

Page 1: [2] Deleted	Friedlingstein, Pierre	12/11/2023 15:12:00
---------------------	------------------------	---------------------

▼.....

Page 1: [2] Deleted	Friedlingstein, Pierre	12/11/2023 15:12:00
---------------------	------------------------	---------------------

▼.....

Page 1: [2] Deleted	Friedlingstein, Pierre	12/11/2023 15:12:00
---------------------	------------------------	---------------------

▼.....
Page 1: [2] Deleted Friedlingstein, Pierre 12/11/2023 15:12:00

▼.....
Page 1: [2] Deleted Friedlingstein, Pierre 12/11/2023 15:12:00

▼.....
Page 1: [2] Deleted Friedlingstein, Pierre 12/11/2023 15:12:00

▼.....
Page 1: [2] Deleted Friedlingstein, Pierre 12/11/2023 15:12:00

▼.....
Page 1: [2] Deleted Friedlingstein, Pierre 12/11/2023 15:12:00

▼.....
Page 1: [2] Deleted Friedlingstein, Pierre 12/11/2023 15:12:00

▼.....
Page 1: [2] Deleted Friedlingstein, Pierre 12/11/2023 15:12:00

▼.....
Page 1: [2] Deleted Friedlingstein, Pierre 12/11/2023 15:12:00

▼.....
Page 1: [2] Deleted Friedlingstein, Pierre 12/11/2023 15:12:00

▼.....
Page 1: [2] Deleted Friedlingstein, Pierre 12/11/2023 15:12:00

▼.....
Page 1: [2] Deleted Friedlingstein, Pierre 12/11/2023 15:12:00

▼.....
Page 1: [2] Deleted Friedlingstein, Pierre 12/11/2023 15:12:00

▼.....
Page 1: [2] Deleted Friedlingstein, Pierre 12/11/2023 15:12:00

▼.....
Page 1: [2] Deleted Friedlingstein, Pierre 12/11/2023 15:12:00

▼.....
Page 1: [2] Deleted Friedlingstein, Pierre 12/11/2023 15:12:00

▼.....
Page 1: [2] Deleted Friedlingstein, Pierre 12/11/2023 15:12:00

▼.....
Page 1: [2] Deleted Friedlingstein, Pierre 12/11/2023 15:12:00

▼.....
Page 1: [2] Deleted Friedlingstein, Pierre 12/11/2023 15:12:00

▼.....
Page 1: [2] Deleted Friedlingstein, Pierre 12/11/2023 15:12:00

▼.....
Page 1: [2] Deleted Friedlingstein, Pierre 12/11/2023 15:12:00

▼.....
Page 1: [2] Deleted **Friedlingstein, Pierre** **12/11/2023 15:12:00**

▼.....
Page 1: [2] Deleted **Friedlingstein, Pierre** **12/11/2023 15:12:00**

▼.....
Page 1: [2] Deleted **Friedlingstein, Pierre** **12/11/2023 15:12:00**

▼.....
Page 1: [2] Deleted **Friedlingstein, Pierre** **12/11/2023 15:12:00**

▼.....
Page 1: [2] Deleted **Friedlingstein, Pierre** **12/11/2023 15:12:00**

▼.....
Page 1: [2] Deleted **Friedlingstein, Pierre** **12/11/2023 15:12:00**

▼.....
Page 1: [2] Deleted **Friedlingstein, Pierre** **12/11/2023 15:12:00**

▼.....
Page 1: [2] Deleted **Friedlingstein, Pierre** **12/11/2023 15:12:00**

▼.....
Page 1: [2] Deleted **Friedlingstein, Pierre** **12/11/2023 15:12:00**

▼.....
Page 1: [2] Deleted **Friedlingstein, Pierre** **12/11/2023 15:12:00**

▼.....
Page 1: [2] Deleted **Friedlingstein, Pierre** **12/11/2023 15:12:00**

▼.....
Page 1: [2] Deleted **Friedlingstein, Pierre** **12/11/2023 15:12:00**

▼.....
Page 1: [2] Deleted **Friedlingstein, Pierre** **12/11/2023 15:12:00**

▼.....
Page 1: [2] Deleted **Friedlingstein, Pierre** **12/11/2023 15:12:00**

▼.....
Page 1: [2] Deleted **Friedlingstein, Pierre** **12/11/2023 15:12:00**

▼.....
Page 1: [2] Deleted **Friedlingstein, Pierre** **12/11/2023 15:12:00**

▼.....
Page 1: [2] Deleted **Friedlingstein, Pierre** **12/11/2023 15:12:00**

▼.....
Page 1: [2] Deleted **Friedlingstein, Pierre** **12/11/2023 15:12:00**

▼.....
Page 1: [2] Deleted **Friedlingstein, Pierre** **12/11/2023 15:12:00**

▼.....
Page 1: [2] Deleted **Friedlingstein, Pierre** **12/11/2023 15:12:00**

▼.....

Page 1: [2] Deleted	Friedlingstein, Pierre	12/11/2023 15:12:00
---------------------	------------------------	---------------------

▼.....

Page 1: [2] Deleted	Friedlingstein, Pierre	12/11/2023 15:12:00
---------------------	------------------------	---------------------

▼.....

Page 1: [2] Deleted	Friedlingstein, Pierre	12/11/2023 15:12:00
---------------------	------------------------	---------------------

▼.....

Page 24: [3] Deleted	Friedlingstein, Pierre	12/11/2023 15:12:00
----------------------	------------------------	---------------------

▼.....

Page 24: [3] Deleted	Friedlingstein, Pierre	12/11/2023 15:12:00
----------------------	------------------------	---------------------

▼.....

Page 24: [3] Deleted	Friedlingstein, Pierre	12/11/2023 15:12:00
----------------------	------------------------	---------------------

▼.....

Page 24: [3] Deleted	Friedlingstein, Pierre	12/11/2023 15:12:00
----------------------	------------------------	---------------------

▼.....

Page 24: [3] Deleted	Friedlingstein, Pierre	12/11/2023 15:12:00
----------------------	------------------------	---------------------

▼.....

Page 24: [4] Deleted	Friedlingstein, Pierre	12/11/2023 15:12:00
----------------------	------------------------	---------------------

▼.....

Page 24: [4] Deleted	Friedlingstein, Pierre	12/11/2023 15:12:00
----------------------	------------------------	---------------------

▼.....
Page 24: [4] Deleted **Friedlingstein, Pierre** **12/11/2023 15:12:00**

▼.....
Page 24: [4] Deleted **Friedlingstein, Pierre** **12/11/2023 15:12:00**

▼.....
Page 24: [5] Deleted **Friedlingstein, Pierre** **12/11/2023 15:12:00**

▼.....
Page 24: [5] Deleted **Friedlingstein, Pierre** **12/11/2023 15:12:00**

▼.....
Page 24: [5] Deleted **Friedlingstein, Pierre** **12/11/2023 15:12:00**

▼.....
Page 24: [5] Deleted **Friedlingstein, Pierre** **12/11/2023 15:12:00**

▼.....
Page 24: [5] Deleted **Friedlingstein, Pierre** **12/11/2023 15:12:00**

▼.....
Page 24: [5] Deleted **Friedlingstein, Pierre** **12/11/2023 15:12:00**

▼.....
Page 24: [5] Deleted **Friedlingstein, Pierre** **12/11/2023 15:12:00**

▼.....
Page 24: [5] Deleted **Friedlingstein, Pierre** **12/11/2023 15:12:00**

▼.....

Page 24: [5] Deleted	Friedlingstein, Pierre	12/11/2023 15:12:00
----------------------	------------------------	---------------------

▼.....

Page 24: [5] Deleted	Friedlingstein, Pierre	12/11/2023 15:12:00
----------------------	------------------------	---------------------

▼.....

Page 24: [5] Deleted	Friedlingstein, Pierre	12/11/2023 15:12:00
----------------------	------------------------	---------------------

▼.....

Page 24: [5] Deleted	Friedlingstein, Pierre	12/11/2023 15:12:00
----------------------	------------------------	---------------------

▼.....

Page 24: [5] Deleted	Friedlingstein, Pierre	12/11/2023 15:12:00
----------------------	------------------------	---------------------

▼.....

Page 24: [5] Deleted	Friedlingstein, Pierre	12/11/2023 15:12:00
----------------------	------------------------	---------------------

▼.....

Page 24: [5] Deleted	Friedlingstein, Pierre	12/11/2023 15:12:00
----------------------	------------------------	---------------------

▼.....

Page 24: [5] Deleted	Friedlingstein, Pierre	12/11/2023 15:12:00
----------------------	------------------------	---------------------

▼.....

Page 24: [6] Deleted	Friedlingstein, Pierre	12/11/2023 15:12:00
----------------------	------------------------	---------------------

▼.....

Page 24: [6] Deleted	Friedlingstein, Pierre	12/11/2023 15:12:00
----------------------	------------------------	---------------------

▼.....

Page 24: [6] Deleted	Friedlingstein, Pierre	12/11/2023 15:12:00
----------------------	------------------------	---------------------

▼.....

Page 24: [6] Deleted	Friedlingstein, Pierre	12/11/2023 15:12:00
----------------------	------------------------	---------------------

▼.....

Page 24: [6] Deleted	Friedlingstein, Pierre	12/11/2023 15:12:00
----------------------	------------------------	---------------------

▼.....

Page 24: [6] Deleted	Friedlingstein, Pierre	12/11/2023 15:12:00
----------------------	------------------------	---------------------

▼.....

Page 24: [6] Deleted	Friedlingstein, Pierre	12/11/2023 15:12:00
----------------------	------------------------	---------------------

▼.....

Page 24: [7] Deleted	Friedlingstein, Pierre	12/11/2023 15:12:00
----------------------	------------------------	---------------------

▼.....

Page 24: [7] Deleted	Friedlingstein, Pierre	12/11/2023 15:12:00
----------------------	------------------------	---------------------

▼.....

Page 24: [7] Deleted	Friedlingstein, Pierre	12/11/2023 15:12:00
----------------------	------------------------	---------------------

▼.....

Page 24: [7] Deleted	Friedlingstein, Pierre	12/11/2023 15:12:00
----------------------	------------------------	---------------------

▼.....

Page 24: [7] Deleted	Friedlingstein, Pierre	12/11/2023 15:12:00
----------------------	------------------------	---------------------

▼.....
Page 24: [7] Deleted **Friedlingstein, Pierre** **12/11/2023 15:12:00**

▼.....
Page 24: [8] Deleted **Friedlingstein, Pierre** **12/11/2023 15:12:00**

▼.....
Page 24: [8] Deleted **Friedlingstein, Pierre** **12/11/2023 15:12:00**

▼.....
Page 24: [8] Deleted **Friedlingstein, Pierre** **12/11/2023 15:12:00**

▼.....
Page 24: [8] Deleted **Friedlingstein, Pierre** **12/11/2023 15:12:00**

▼.....
Page 24: [8] Deleted **Friedlingstein, Pierre** **12/11/2023 15:12:00**

▼.....
Page 24: [8] Deleted **Friedlingstein, Pierre** **12/11/2023 15:12:00**

▼.....
Page 1: [9] Formatted **Friedlingstein, Pierre** **12/11/2023 15:12:00**

Normal, Centred, Border: Top: (No border), Bottom: (No border), Left: (No border), Right: (No border),
Between : (No border), Tab stops: 7.96 cm, Centred + 15.92 cm, Right, Position: Horizontal: Left, Relative to:
Column, Vertical: In line, Relative to:

▼.....
Page 42: [10] Formatted **Friedlingstein, Pierre** **12/11/2023 15:12:00**

Indent: Left: 0 cm, First line: 0 cm, Outline numbered + Level: 3 + Numbering Style: 1, 2, 3, ... + Start at: 1 +
Alignment: Left + Aligned at: 0 cm + Indent at: 1.27 cm

Page 42: [11] Deleted **Friedlingstein, Pierre** **12/11/2023 15:12:00**

Page 106: [12] Deleted **Friedlingstein, Pierre** **12/11/2023 15:12:00**

Page 107: [13] Formatted **Friedlingstein, Pierre** **12/11/2023 15:12:00**

Font: Not Bold

Page 107: [13] Formatted **Friedlingstein, Pierre** **12/11/2023 15:12:00**

Font: Not Bold

Page 107: [13] Formatted **Friedlingstein, Pierre** **12/11/2023 15:12:00**

Font: Not Bold

Page 107: [14] Formatted **Friedlingstein, Pierre** **12/11/2023 15:12:00**

Font: Not Bold, Subscript

Page 107: [14] Formatted **Friedlingstein, Pierre** **12/11/2023 15:12:00**

Font: Not Bold, Subscript

Page 107: [14] Formatted **Friedlingstein, Pierre** **12/11/2023 15:12:00**

Font: Not Bold, Subscript

Page 107: [14] Formatted **Friedlingstein, Pierre** **12/11/2023 15:12:00**

Font: Not Bold, Subscript

Page 107: [15] Formatted Friedlingstein, Pierre 12/11/2023 15:12:00

Font: Not Bold, Subscript

Page 107: [15] Formatted Friedlingstein, Pierre 12/11/2023 15:12:00

Font: Not Bold, Subscript

Page 107: [15] Formatted Friedlingstein, Pierre 12/11/2023 15:12:00

Font: Not Bold, Subscript

Page 107: [15] Formatted Friedlingstein, Pierre 12/11/2023 15:12:00

Font: Not Bold, Subscript

Page 107: [15] Formatted Friedlingstein, Pierre 12/11/2023 15:12:00

Font: Not Bold, Subscript

Page 107: [15] Formatted Friedlingstein, Pierre 12/11/2023 15:12:00

Font: Not Bold, Subscript

Page 107: [16] Formatted Friedlingstein, Pierre 12/11/2023 15:12:00

Font: Not Bold, Subscript

Page 107: [16] Formatted Friedlingstein, Pierre 12/11/2023 15:12:00

Font: Not Bold, Subscript

Page 107: [16] Formatted Friedlingstein, Pierre 12/11/2023 15:12:00

Font: Not Bold, Subscript

Page 107: [16] Formatted Friedlingstein, Pierre 12/11/2023 15:12:00

Font: Not Bold, Subscript

Page 107: [16] Formatted Friedlingstein, Pierre 12/11/2023 15:12:00

Font: Not Bold, Subscript

Page 107: [16] Formatted Friedlingstein, Pierre 12/11/2023 15:12:00

Font: Not Bold, Subscript

Page 107: [17] Formatted Friedlingstein, Pierre 12/11/2023 15:12:00

Font: Not Bold, Subscript

Page 107: [17] Formatted Friedlingstein, Pierre 12/11/2023 15:12:00

Font: Not Bold, Subscript

Page 107: [18] Formatted Friedlingstein, Pierre 12/11/2023 15:12:00

Font: Not Bold, Superscript

Page 107: [18] Formatted Friedlingstein, Pierre 12/11/2023 15:12:00

Font: Not Bold, Superscript

Page 107: [19] Formatted Friedlingstein, Pierre 12/11/2023 15:12:00

Font: Not Bold, Subscript

Page 107: [19] Formatted Friedlingstein, Pierre 12/11/2023 15:12:00

Font: Not Bold, Subscript

Page 107: [20] Formatted Friedlingstein, Pierre 12/11/2023 15:12:00

Font: Not Bold

Page 107: [20] Formatted Friedlingstein, Pierre 12/11/2023 15:12:00

Font: Not Bold

Page 107: [20] Formatted Friedlingstein, Pierre 12/11/2023 15:12:00

Font: Not Bold

Page 107: [21] Formatted Friedlingstein, Pierre 12/11/2023 15:12:00

Font: Not Bold, Superscript

Page 107: [21] Formatted Friedlingstein, Pierre 12/11/2023 15:12:00

Font: Not Bold, Superscript

Page 107: [21] Formatted Friedlingstein, Pierre 12/11/2023 15:12:00

Font: Not Bold, Superscript

Page 107: [21] Formatted Friedlingstein, Pierre 12/11/2023 15:12:00

Font: Not Bold, Superscript

Page 107: [22] Formatted Friedlingstein, Pierre 12/11/2023 15:12:00

Font: Not Bold, Superscript

Page 107: [22] Formatted Friedlingstein, Pierre 12/11/2023 15:12:00

Font: Not Bold, Superscript

Page 107: [22] Formatted Friedlingstein, Pierre 12/11/2023 15:12:00

Font: Not Bold, Superscript

Page 107: [22] Formatted Friedlingstein, Pierre 12/11/2023 15:12:00

Font: Not Bold, Superscript

Page 107: [23] Formatted Friedlingstein, Pierre 12/11/2023 15:12:00

Font: Not Bold, Subscript

Page 107: [23] Formatted Friedlingstein, Pierre 12/11/2023 15:12:00

Font: Not Bold, Subscript

Page 107: [24] Formatted Friedlingstein, Pierre 12/11/2023 15:12:00

Font: Not Bold, Subscript

Page 107: [24] Formatted Friedlingstein, Pierre 12/11/2023 15:12:00

Font: Not Bold, Subscript

Page 107: [25] Formatted Friedlingstein, Pierre 12/11/2023 15:12:00

Font: Not Bold, Superscript

Page 107: [25] Formatted Friedlingstein, Pierre 12/11/2023 15:12:00

Font: Not Bold, Superscript

Page 107: [25] Formatted Friedlingstein, Pierre 12/11/2023 15:12:00

Font: Not Bold, Superscript

Page 107: [25] Formatted Friedlingstein, Pierre 12/11/2023 15:12:00

Font: Not Bold, Superscript

Page 107: [26] Formatted Friedlingstein, Pierre 12/11/2023 15:12:00

Font: Not Bold, Superscript

Page 107: [26] Formatted Friedlingstein, Pierre 12/11/2023 15:12:00

Font: Not Bold, Superscript

Page 119: [27] Deleted Friedlingstein, Pierre 12/11/2023 15:12:00

Page 1: [28] Formatted Friedlingstein, Pierre 12/11/2023 15:12:00

Normal, Centred, Border: Top: (No border), Bottom: (No border), Left: (No border), Right: (No border),
Between : (No border), Tab stops: 7.96 cm, Centred + 15.92 cm, Right, Position: Horizontal: Left, Relative to:
Column, Vertical: In line, Relative to: